OPTICAL REMOTE SENSING OF COLOURED DISSOLVED ORGANIC MATTER (CDOM) FOR BETTER ESTIMATION OF DISSOLVED ORGANIC CARBON (DOC) IN SOUTH-EAST QUEENSLAND WATER RESERVOIRS

A Thesis submitted by

Haider Ismael Abdulkadhum Al-Rubaay

For the award of

Doctor of Philosophy

2020

ABSTRACT

Australian inland water-bodies play a great role in the carbon cycle at the regional level and contribute effectively through the carbon exchange between their surface and the atmosphere. This carbon enters the aquatic system from terrestrial sources such as soil or it is generated within the water body itself through the primary production of phytoplankton or from organic matter. It is converted into dissolved organic carbon (DOC) which constitutes about 90% of the dissolved carbon in the aquatic system. Increasing the DOC levels in the water affects the water quality and ecosystem functioning. Remote sensing methods allow DOC to be monitored with a minimum of time, effort and cost. DOC has no colour and remote sensing cannot determine it directly, however, the coloured portion of the dissolved organic matter (CDOM) can be used as a proxy to estimate its amount and its concentration in the aquatic environment. But, remote sensing measurements of DOC can only be done if there is a good relationship between CDOM absorption and DOC concentration. This good relationship does not necessarily exist over many of the water-bodies because CDOM concentration varies both spatially and temporally according to its sources. This weak relationship was observed in the study area South East Queensland (SEQ) as reviewed in this thesis. Therefore, the researcher investigated different ways to improve the characterisation of this relationship in the study area to get a better estimation of DOC based on using remotely sensed CDOM concentrations.

The researcher sampled 11 discrete water bodies in South East Queensland (SEQ), then examined if there was a correlation between CDOM absorption coefficient and DOC but, the overall results showed a weakly positive correlation relationship among all reservoirs. The reason for this poor relationship is attributed to the potential impacts of the allochthonous source on the inputs DOC to water derived from the surrounding areas. Different estimation enhancement approaches were investigated by including both CDOM absorption and its slope in multiple linear regressions which relatively improved the estimation of DOC concentration and assisted in obtaining a better understanding of this relationship.

Then, another investigation was done by fractionating CDOM into its major groups of humic and non-humic substances and measuring their absorption spectra and DOC contents separately. Solid-phase extraction (SPE) technique was used as a chemical separation method. The investigation in the relationship between CDOM fractions and DOC confirmed different relationships such as not all DOC in CDOM can be chromophoric.

Furthermore, the CDOM absorption spectrum shape is a proxy of CDOM composition in water. Therefore, it is important that CDOM absorption spectrum curve be clear, clean and free from any errors if possible (systematic or random) to give better estimation results. But, the most important is using the correct fitting model that characterizes the CDOM absorption spectrum accurately. Some fitting models can lead to a loss in and not fully capture all the information provided by CDOM absorption curve. The CDOM spectral decomposition technique was used to provide better and additional information about CDOM pool and dynamics from the absorption spectrum curve that was done by using the algebraic method of the linear, nonlinear and Gaussian decomposition approaches. The final results of using CDOM spectral decomposition were useful and helpful for giving a good explanation to the relationship between CDOM absorption and DOC concentration on the one hand and between CDOM absorption and its sources on the other. Also, the advantage of using the multi-exponential model is convenient for optical modelling and remote sensing applications.

Finally, the researcher examined how CDOM sources (allochthonous and autochthonous) in SEQ affect the optical properties and on the remote sensing reflectance by separating CDOM into its major groups of humic and non-humic and modelling them. ECOLIGHT® simulation used first to simulate subsurface irradiance reflectance ($\mathrm{R}(0-)$) curves under the conditions found in SEQ waterbodies. The aim to show the contribution of other water components (phytoplankton and tripton) of different concentrations as well as CDOM-SIOPs (specific inherent optical properties) on the water reflectance. ECOLIGHT® has a unique ability to isolate changes in the reflectance due to SIOPs or spectral variability. On the other hand, $\mathrm{R}(0-)$ modelled using a developed semi-analytical bio-optical model. A multi-components bio-optical

model developed in this work by using and inserting SIOPs of CDOM fractions. The retrieving results of CDOM from water reflectance much better when using CDOM fractions SIOPs which reflected positively on estimating DOC.

The study concluded that the estimation of DOC concentrations from water's colour is more complex and the accuracy factor is limited, due to the confounding effects of water components and sources in addition to the poor performance of the standard models and algorithms. Also, CDOM fractions are participating in CDOM absorption spectrum shape which can give us good information and can be used to estimate DOC. The results of the spectral decomposition showed that SEQ water bodies tend to be dominated by humic acid due to the high ratio of HA compared to FA. Another finding, the calculated slope values of the study area were superior to the calculated slope values of Kirk for the Australian inland waters when they used in CDOM decomposition model to characterize the relationship with DOC. While Suwannee River slope values were not applicable within Australian inland waters when it used in CDOM decomposition model.

CERTIFICATION OF THESIS

This Thesis is entirely the work of **Haider Ismael Abdulkadhum Al-Rubaay** except where otherwise acknowledged. The work is original and has not previously been submitted for any other award, except where acknowledged.

Principal Supervisor: *Dr Glenn Campbell*

Associate Supervisor: *Dr Erin Hestir*

Student and supervisors signatures of endorsement are held at the University.

ACKNOWLEDGMENT

Firstly, I would like to express my sincere gratitude to my advisors' ***Dr Glenn Campbell*** and ***Dr Erin Hestir*** for their continuous support during my PhD study, for their patience, motivation, and immense knowledge. Their guidance helped me throughout this work and presenting this thesis.

I want to thank my study sponsor the ***Iraqi Ministry of Higher Education and Scientific Research***, that gave me financial support until finishing my study. Also, special thanks to the ***Commonwealth Scientific and Industrial Research Organisation (CSIRO)*** for giving me a Postgraduate Studentship to assist me in fulfilling the work experience component of my university studies.

My sincere thanks also go to ***Dr Tim J Malthus*** from CSIRO's Ocean and Atmosphere Business Unit (Brisbane), ***Ms Janet Anstee*** from CSIRO's Oceans and Atmosphere Flagship (Canberra), ***Dr Hannelie Botha*** from CSIRO's Oceans and Atmosphere Flagship (Canberra), ***Dr David Beale*** from CSIRO's Land and Water (Brisbane), ***Mr David Blondeau-Patissier*** from CSIRO's Ocean and Atmosphere (Brisbane), ***Ms Heidi Franklin*** when she was working at CSIRO's Ocean and Atmosphere (Brisbane) who they gave me the opportunity to join their team as an intern and provided me with the necessary support in this work. Special thanks to ***Dr Friederike Susette Ederhard*** from Faculty of Health, Engineering and Sciences (USQ) who offered me the fundamental support during my work in the USQ water laboratory. Without their precious support, it would not be possible to conduct this research.

Words cannot express how grateful I am to ***my family***: my parents and to my brothers and sisters for supporting me spiritually throughout writing this thesis and my life in general.

In the end, I would like an express appreciation to my beloved wife ***Naam Al-Helli*** who spent sleepless nights with and was always my support in the moments when there was no one to answer my queries, and to my wonderful children ***Karar***, ***Farah***, ***Ahmad*** and ***Nasam*** for their endless love.

Haider Al-Rubaay

TABLE OF CONTENTS

LIST OF FIGURES

LIST OF TABLES

SYMBOLS AND ABBREVIATIONS

I. Abbreviations

Abbreviation	Expansion
ANOVA	Analysis of variance
AOPs	Apparent optical properties
CDOM	Coloured dissolved organic matter
CE	Cellulose esters filter
Chl-a	Chlorophyll a
CSIRO	Commonwealth Scientific and Industrial Research Organisation
DDW	Deionized distilled water
DEM	Double exponential model
DIW	Deionized water
DOC	Dissolved organic carbon
DOM	Dissolved organic matter
FA	Fulvic acid
GF/F	Glass fibre filter
GRG	Generalized reduced gradient techniques
H_2SO_4	Sulfuric acid
HA	Humic acid
HCl	Hydrochloric acid
HPI	Hydrophilic
HPIA	Hydrophilic acid
HPIB	Hydrophilic base
HPIN	Hydrophilic neutral
HPO	Hydrophobic
HPOA	Hydrophobic acid
HPOB	Hydrophobic base
HPON	Hydrophobic Neutral
HS	Humic substances
IDL	Interactive Data Language
IHSS	International humic substances society
IOPs	Inherent optical properties

LLSR	Linear least-squares regression
MAPE	Mean Absolute Percentage Error
MeOH	Methanol
MERIS	MEdium Resolution Imaging Spectrometer
MIM	Matrix inversion method
NaOH	Sodium hydroxide
NAP	Non-algal particulate matter
NHS	Non-humic substances
NLLSR	Nonlinear least square regression
NOM	Natural organic matter
NRMSE	Normalized Root Mean Square Error
PC	Polycarbonate filter
POM	Particulate organic matter
PTFE	Polytetrafluoroethylene or best known (TEFLON)
RMSE	Root means square errors
RTE	Radiative transfer equation
SCT	Separation Column Technique
SEM	Simple exponential model
SEQ	South East Queensland
SIOPs	Specific inherent optical properties
SPE	Solid-phase extraction
SRFA	Suwannee River fulvic acid
SWE_NOM	Suwannee River Natural Organic Matter
SSE	Sum of squared error
TR	Tripton
TSS	Total suspended solids
UV	Ultraviolet

II. Symbols list

Symbol	Description	Unit
a	absorption coefficient	m^{-1}
a^*	Specific absorption coefficients	$m^2.mg^{-1}$
a^*_{CDOM}	CDOM specific absorption coefficients	-
$a^*_{DOC}(\lambda_o)$	*DOC-normalized absorption coefficients of CDOM at a reference wavelength*	$m^2.mg^{-1}$
$a_{CDOM}(\lambda)$	*CDOM* absorption coefficient	m^{-1}
$a_{CDOM}(\lambda_o)$	*CDOM* absorption coefficient at a reference wavelength	m^{-1}
S	Spectral slope	-
R(0-)	Subsurface irradiance reflectance	-
λ	Wavelength	nm
λ_o	Reference wavelength	nm
A	Spectral absorbance	-
OD	Optical density	-
l	Cuvette path length	m
K	Correction parameter in exponential CDOM absorption model (offset)	m^{-1}
C	Substance concentration	$mg.L^{-1}$
τ	Kendall's correlation coefficient (tau)	-
ρ	Statistical significance	-
R^2	Correlation coefficient	-
$Adj.-R^2$	Adjusted correlation coefficient	-
β	Model regression coefficient	-
α	Intercept	-
X^2	Chi-square	-
D_m	Degrees of freedom of the model	-
D_e	Degrees of freedom of the error	-
c	Total attenuation coefficient	m^{-1}
b	Total scattering coefficient	m^{-1}
VSF or β	Volume scattering function	-
ϕ	phytoplankton	-
b_f	Forward scattering coefficient	m^{-1}
b_b	Backward scattering coefficient	m^{-1}

L	Radiance	$Wm^{-2}sr^{-1}nm^{-1}$
Φ	Radiant flux	Watt
E	Irradiance	W/m^2
E_u	Upward irradiance	W/m^2
E_d	Downward irradiance	W/m^2
K	Diffuse attenuation coefficient	m^{-1}
K_d	Diffuse attenuation coefficient of downward irradiance	m^{-1}
z_{att}	The attenuation depth	m
I	Radiant intensity	$W.sr^{-1}$
R_{rs}	Remote sensing reflectance	sr^{-1}
r_{rs}	Remote sensing ratio	-
ω_b	*backscattering albedo*	

Chapter 1

Introduction and Hypothesis

1.1 General Overview and Background

The optical remote sensing of inland and coastal waters is used to study, monitor and derive the basic water components through the observation of the spectrum of the water leaving radiation. These water components participate directly in the interactions with solar radiation in that they absorb or scatter photons (Jerlov 1968; Bukata et al. 1995). Natural waters have four primary groups of optically active water components: the water itself, chlorophyll (Chl) and other photosynthetic pigments, suspended and non-algal particulate matter (NAP), and coloured dissolved organic matter (CDOM) (Jerlov 1968; Gordon et al. 1988; Defoin-Platel & Chami 2007; Keith et al. 2014). They affect water quality and have a significant role in the aquatic ecosystem.

The aquatic ecosystem is a critical component of the global environment and plays an essential role in the global carbon cycle and climate change through the exchange of heat and water with the atmosphere (Tranvik et al. 2009). The amount and type of some of these water components can be measured directly from remote sensing, and the others can be derived indirectly (Dekker & Hestir 2012). Therefore, improving the estimation accuracy and understanding the relationships for the effective water components and their origin is the focus of many researchers such as Bricaud et al. (1981); Vodacek et al. (1997); Laanen (2007); Brando et al. (2008); Mannino et al. (2008); Das et al. (2017).

The organic substances are one of the important parameters that influence water quality and change its physicochemical properties (Boyle et al. 2009). They are a broad range of heterogeneous organic compounds that correlate directly and indirectly with most of the water quality parameters such as turbidity, suspended solids, pH, temperature, nitrogen and dissolved oxygen (Findlay & Sinsabaugh 2003; Shen et al. 2015). Organic matter contains carbon and releases it into the water by various chemical, physical, and biological processes (Keith et al. 2014). More than 90% of the released organic carbon in the water is in the dissolved form (Mishra et al. 2017).

Most of the organic matter in inland water bodies is generally in the dissolved form and called dissolved organic matter (DOM) (Kutser et al. 2005). DOM, in general, can be expressed in terms of their two major groups which are; the humic substances that are comprised of so-called hydrophobic components (HPO) and the non-humic substances that comprised of the hydrophilic components (HPI) (Ratpukdi et al. 2009; Matilainen et al. 2010; Mostofa et al. 2013; Hansell & Carlson 2014; Ibrahim & Aziz 2014). These groups can be further subdivided into three different classes each; called acid, base and neutral, which have various chemical groups such as humic and fulvic acids, hydrocarbons, carbohydrates and protein (Croue et al. 2000; Marhaba et al. 2003; Ratpukdi et al. 2009). Humic substances, especially humic and fulvic acids are the largest fractions that account for 65-75% of DOM and responsible for determining the physicochemical and optical properties of DOM (Bricaud et al. 1981; Pettit 2004; Mostofa et al. 2013).

Measuring and monitoring dissolved organic carbon (DOC) in water is important for different reasons; it is an essential factor in the aquatic carbon cycle linked to vital activities of the waterbody and surrounding it (Hedges 1992; Hansell & Carlson 2014). DOC is produced within the aquatic ecosystem from the decomposition of plants and organisms in water (Keith et al. 2014). Additionally, it enters the aquatic ecosystem from terrestrial sources that washed into the water such as soil and plants leaves, or from absorbing carbon dioxide from the atmosphere at the water's surface and converting it into dissolved carbon (Jaffé et al. 2008).

Coloured dissolved organic matter (CDOM) is considered the optically measurable component of the DOM for remote sensing applications and has been used as an indicator to estimate DOC in the aquatic system (Mannino et al. 2008; Fichot & Benner 2011). This estimation requires a robust relationship between CDOM and DOC, but because of seasonal changes and local variability that impact on the relationship between CDOM and DOC and cause errors in the estimation (Hestir et al. 2015) it is likely to be more complicated to be able to estimate the DOC concentration remotely for inland waters, as opposed to coastal and open ocean areas (Song et al. 2017; Shao et al. 2019). Optical complexity and the errors in calculating CDOM absorption may appear in inland water areas because CDOM absorption cannot be sufficiently discriminated at some wavelengths from phytoplankton pigment absorption (e.g. Chlorophyll-a) (Matsuoka et al. 2013; Pagano et al. 2014).

Estimating water component concentrations usually requires developing a model, which is a mathematical combination of a relationship between the inherent optical properties (IOPs) (properties of the medium that are independent of the incident illumination) and the apparent optical properties (AOPs) (depend on IOPs and the geometry (direction) of the incident and reflected light field) at different wavelengths (Jerlov 1968; Gordon 2002). Figure (1-1) shows a scheme for the interpretation of optical remote sensing to obtain representative spectra of colour water components and conversely. These estimating models differ according to the depth of water, target component and the geographical zone (Bartley et al. 2012). As well, models should be maximally sensitive to changes in the concentration of the target

component and are minimally sensitive to the changes in the concentration of other components present in water. Hence, it is an important point to look for a fast, inexpensive, and accurate way in water monitoring to make a relevant contribution in large-scale areas.

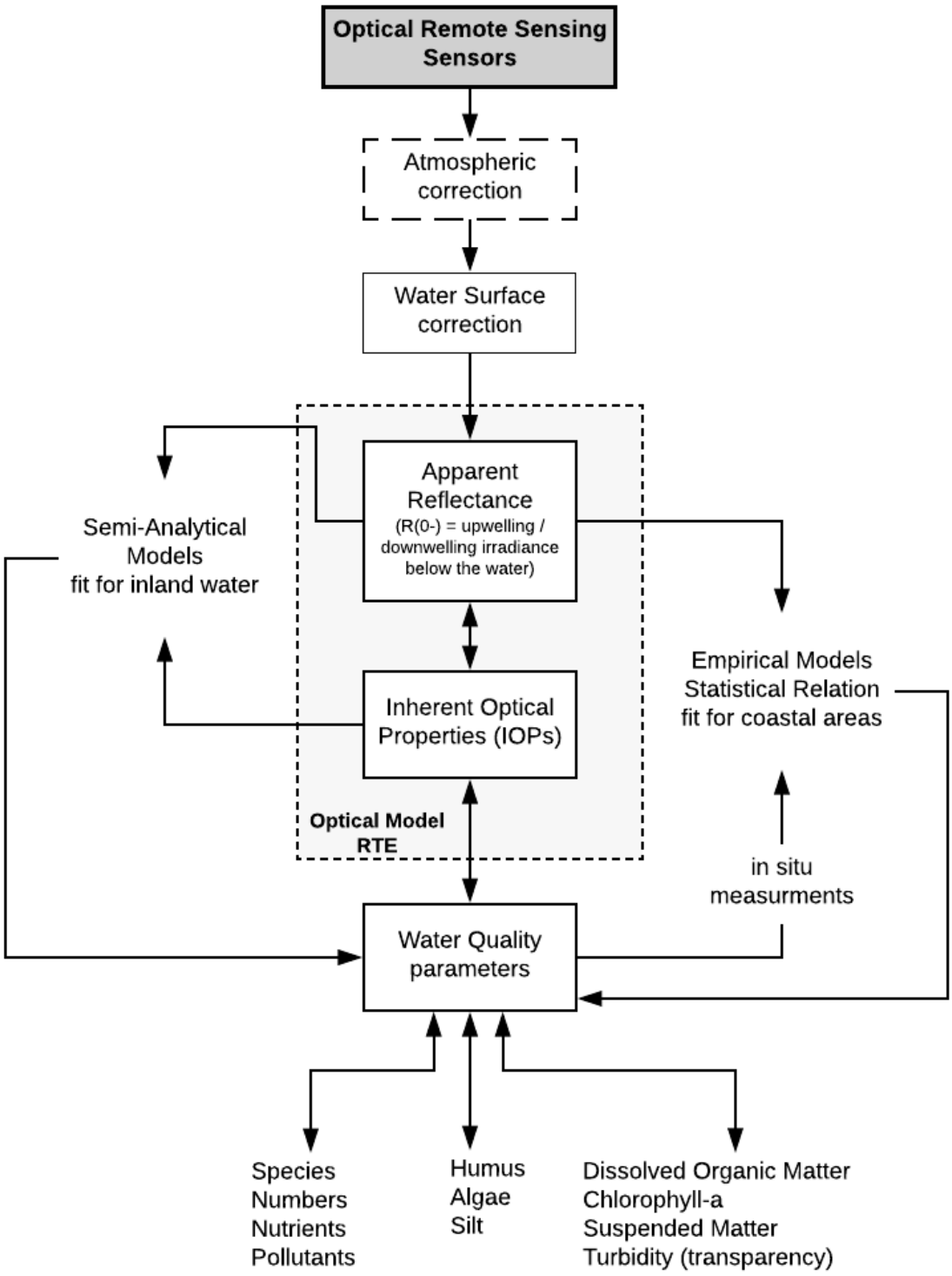

Figure 1-1: Scheme to Interpret Optical Remote Sensing Steps for Water Applications

Thus, using remote sensing techniques could present the opportunities in water monitoring due to its ability and possibilities to collect the largest amount of data for large areas quickly and inexpensively (Sabins 2007; Cazenave et al. 2016). So, remote sensing may be able use CDOM to trace inputs of the water-bodies to predict concentrations, molecular weight, sources, nine types of these DOM components such as (amino acids, humic and fulvic acids and carbohydrates) and estimate DOC concentration.

1.2 The issue that will be addressed by this work

Most DOC has no colour, and remote sensing cannot determine it directly, however the coloured portion, CDOM can be used as a proxy to estimate the amount of DOC concentration in the aquatic environment (Vodacek et al. 1997; Aiken & Moore 2000; Keith et al. 2014; Vantrepotte et al. 2015). But, remote sensing measurements of DOC can only be done if there is a good relationship between CDOM absorption and DOC concentration (Roesler & Culbertson 2016). This good relationship does not necessarily exist over most of the water-bodies because CDOM concentration varies both spatially and temporally according to its sources. Some studies (Matsuoka et al. 2012; Hestir et al. 2015) showed that it is not simple and easy to estimate DOC concentration in the near-surface layer using satellite data, due to the complexity of this relationship. Therefore, finding ways to improve the characterisation of this relationship for wide areas is worthwhile. Finally, improving CDOM retrieval accuracy is one of the problems in aquatic remote sensing, not only because CDOM is of interest itself as a variable, but also because it improves the retrieval of other parameters of interest such as chlorophyll-a that are often confounded by the presence of CDOM. Thus, the key of good estimation from satellite data is a better understanding of the bio-optical properties using both IOPs and AOPs and determination of the error sources which results from the influences of these local variables.

1.3 Description of the study area

The general location of the study area and the investigated reservoirs will be given. Subsequently, the hydrological and ecological characteristics of the selected area will be described to show why this area is suitable as a study area for the purposes of this present thesis.

The study area covered the South-East Queensland region (SEQ) and part of Darling Downs region with a total area about 29835 km^2. SEQ region stretches 240 km from Noosa in the north to the Gold Coast in the south and from the Ocean in the east to Toowoomba in the west (which is simultaneously considered part of the Darling Downs region), and it covers 22420 km^2 area. Some surrounding regions of SEQ were included in this study also which are Warwick, Crow's Nest, Cambooya and Clifton and they are part of Darling Downs region. Figure (1-2) shows the study area map.

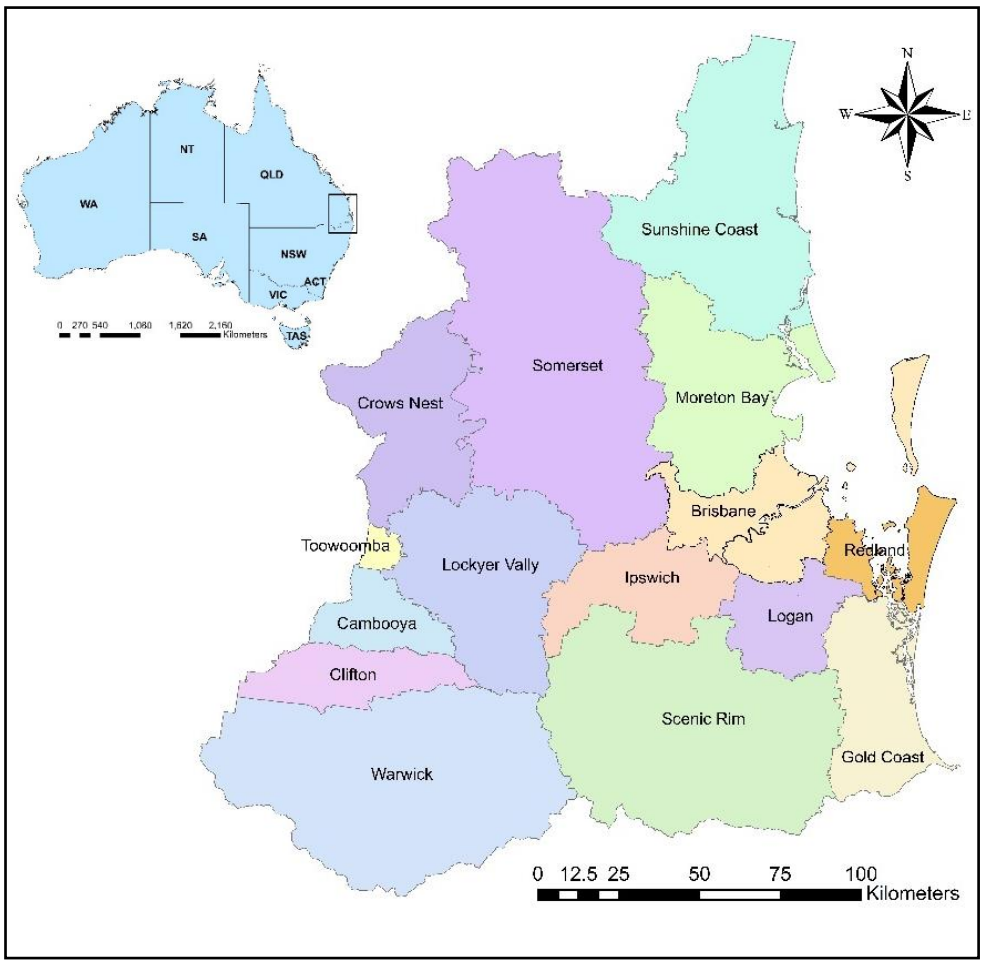

Figure 1-2: The Study Area Map (South-East Queensland Region and Part of Darling Downs Region)

The Darling Downs is a farming region with some industrial and mining activities (Queensland 2014). As for SEQ region, it hosts a diverse range of ecosystems: farms, lakes and reservoirs, rivers, mountains, bushland, coastal areas and urban areas. Water reservoirs in these regions are highly variable in types and concentrations of water constituents caused by natural environmental and human activities. They are a diverse mixture of different types of particulate and dissolved matter (Cottingham et al. 2010; Lyons 2012). A combination of some important factors places SEQ region under increasing water stress. These factors range from the agricultural activity to the rapid economic and population growth because it is the fastest-growing Australian region with 71% of all Queensland's population (Department of Infrastructure Local Government and Planning 2017). But, the most significant factors are the natural environmental conditions and climate patterns affecting the region. Frequent floods in the study area adversely affect their water-bodies and their water quality, especially potable water supply reservoirs (CSIRO and Bureau of Meteorology 2015).

Much of the soil surrounding water reservoirs in these regions loaded with a high amount of humic and non-humic substances and the intensive agriculture has exacerbated soil erosion (Cottingham et al. 2010). Also, land clearing for grazing has led to high levels of organic sediment and nutrients washed into the lakes and reservoirs (Cottingham et al. 2010). Figure (1-3) shows the study area's land-use map.

All the factors mentioned above adds tremendous amounts of organic substances as an external source for the study area reservoirs causing a significant environmental consequence affecting both the availability of water and water quality across the regions. These organic substances can be a pollution source when discharging a large amount of them into these reservoirs (Harrison 2001). When they increase, the number of decomposers increases and grow rapidly so as to deplete the water oxygen and hence, will affect the aquatic organisms and increase the amount of DOC (Mostofa et al. 2013; Vantrepotte et al. 2015). Therefore, the increase and variability in these substances in the major water catchments is considered as one of the fundamental issues of water quality, especially in Australian regions and it affects the stability of CDOM-DOC relationships.

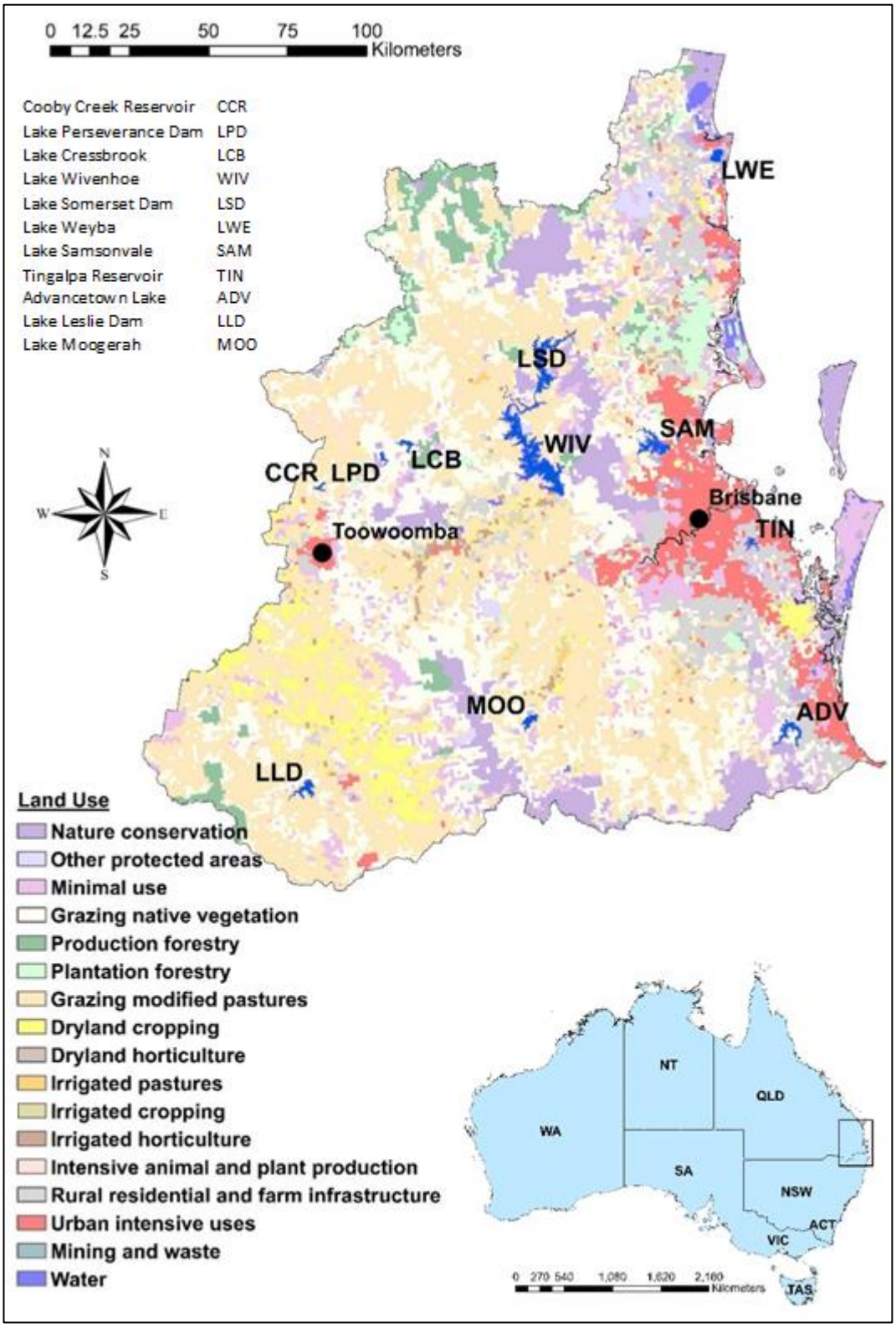

Figure 1-3: Study Area Land-use Map (Queensland 2017)

1.4 Research aims

The aim of this thesis is to examine whether CDOM (hydrophobic (humic and fulvic acids) and hydrophilic) fractions' absorption coefficients can be used for large scale DOC concentration estimation in reservoirs that are subject to heavy impacts from surrounding areas and human activities. Additionally, the thesis seeks to discover whether using the CDOM fractions improve the retrieval and estimation accuracy of the concentration of CDOM/DOC from remote sensing spectra in case II water-bodies. This thesis hypothesises that these CDOM fractions could provide further details about the sources of DOC that influence the distribution and the relationship between CDOM and DOC when no, or weak correlation is observed between total $a_{CDOM}(\lambda_o)$ and DOC concentration.

To meet the aim of this work, it is necessary to first examine how the fractionated CDOM components relate to the DOC concentration in the selected study area reservoirs. Then, it is necessary to study how the sources of CDOM can affect its optical properties and hence the total remote sensing reflectance.

1.5 Research questions

According to the addressed problems and the research aim, a significant question can be as follows:

"Can the estimation of dissolved organic carbon DOC within inland water reservoirs be improved by using different approaches to the remote sensing of CDOM concentrations?"

From this major question arises a number of specific questions this research will also address:

1. *"How do the sources of organic matter (allochthonous and autochthonous) affect the optical properties of CDOM and the remote sensing reflectance?"*

2. *"Does separating CDOM into its major groups of humic and non-humic and modelling them separately prior to input them to the optical model improve CDOM and then DOC estimation?"*

1.6 Research objectives

In order to achieve research aims and answering research questions, a list of research objectives have been summarised as below:

1. *To sample SEQ reservoirs and determine the variation in the CDOM composition, spectral absorption and CDOM spatial changes.*

2. *To examine the regional relationship between the total DOC with CDOM absorption spectra and with CDOM fractions*.

3. *To evaluate the potential of decomposing the measured CDOM absorption spectrum for the purpose of obtaining a better correlation estimation with DOC that can be used as an alternative to the single exponential model in DOC estimation algorithms.*

4. *To parameterize and assess the contribution of the various water components beside CDOM major fractions on the simulated and modelled water reflectance spectra.*

5. *To compare the expected errors occurring when using the simple CDOM model as opposed to a more complex CDOM multi-component model as part of a DOC retrieval algorithm.*

This work was performed in South-East Queensland inland water bodies and attempts to use the full potential of the optical model by improving the input parameterisation. If possible, the estimation of dissolved organic carbon (DOC) concentration will be improved through parametrisation using CDOM fractions instead of total CDOM. Figure (1-4) summarise the research methodology and objectives.

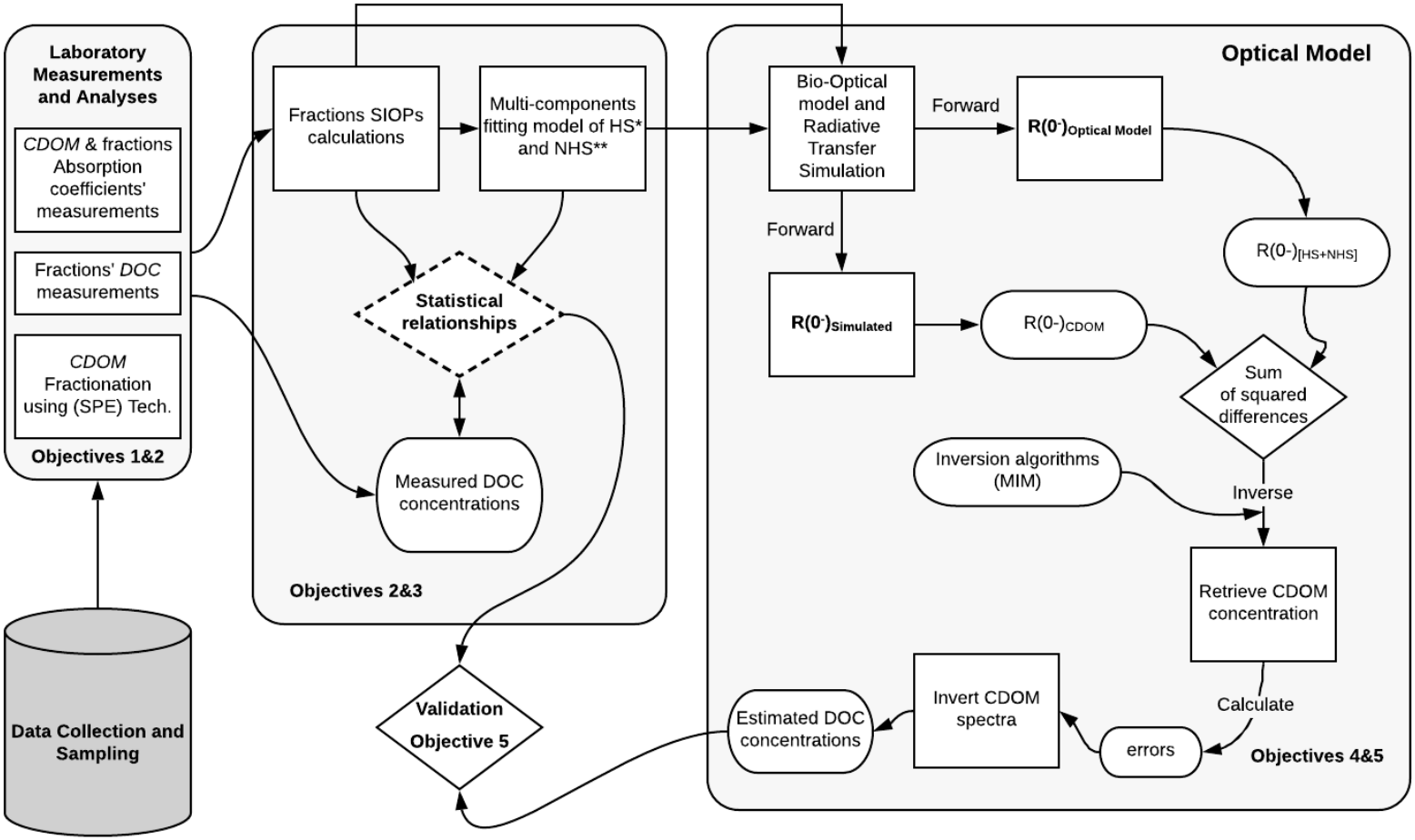

*: (HS) Humic Substances (Hydrophobic part of CDOM).
**: (NHS) Non-Humic Substances (Hydrophilic part of CDOM).

Figure 1-4: Schematic Overview of The Research Methodology and Objectives

1.7 Thesis outlines

This thesis is organised in six chapters, Figure (1-5) summarises the chapters' sequences. **Chapter One** reviews an introduction to the research problem, aims, questions and objectives of this thesis. **Chapter Two** describes the measurements and the methodology for sampling study area locations to achieve objective (1) and part of objective (2). It will explain in detail sampling and fieldwork procedures, laboratory measurements, and measuring the absorbance and DOC concentrations.

The beginning of **Chapter Three** provides the essential information to understand theoretical concepts about organic substances and their fractions and to know how these fractions influence the aquatic ecosystem and the optical measurements. After that, it reviews the isolation techniques to extract CDOM fractions and measuring its absorption. Also, it discusses the absorption behaviour of CDOM's fractions isolated from study area samples. This chapter is essential and important to accomplish objective (2), and it is a preparation for subsequent objectives.

Examining whether DOC estimation may be improved or not by using multi-component absorption spectrum modelling discusses in **Chapter Four**. This chapter addresses objective (3) and to give a better description of the relationship between CDOM absorption coefficient and DOC concentration. It investigates a way to improve the optical corresponds between the measured and modelled CDOM absorption spectra by separating it into its two major components' groups by using spectral decomposition method.

To achieve objectives (4) and (5), **Chapter Five** explains the radiative transfer equation (RTE), which describes the interaction between light and water surface after giving a presentation about water optical properties. Then, it presents the optical modelling approaches of the existing CDOM absorption modelling forms that were proposed by Gordon et al. (1975), Bricaud et al. (1981), Lee et al. (2004) Mannino et al. (2008), Fichot and Benner (2011) and Vantrepotte et al. (2015) that they performed to retrieve CDOM and other water components.

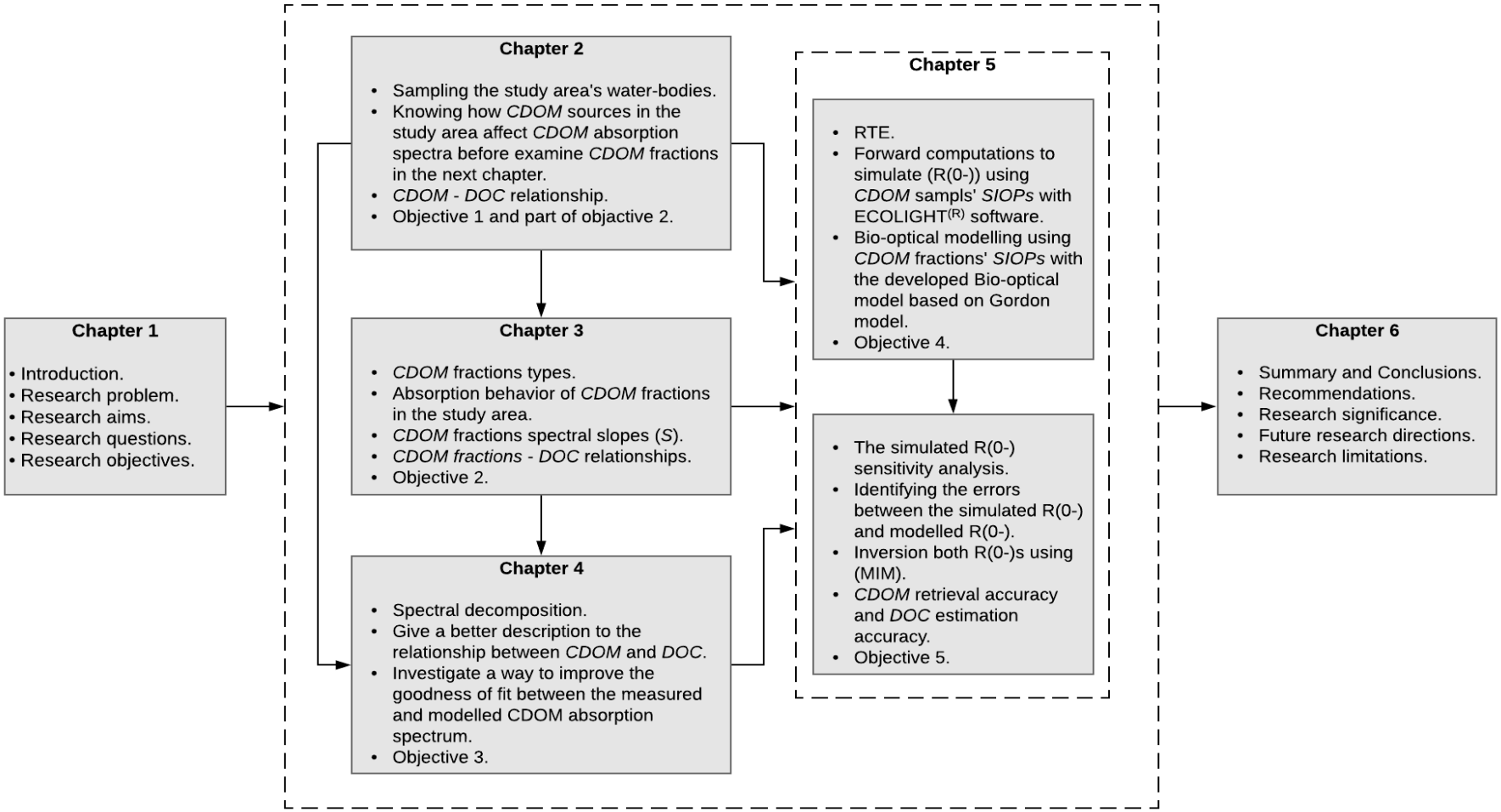

Figure 1-5: Flowchart Shows the Sequence Chapters of This Thesis

As well as it specifically tests the developed hypothesis of this research which is based on using a multi-component absorption modelling to obtain a robust estimation of DOC.

ECOLIGHT® software simulation results of water reflectance based on radiative transfer equation are illustrated in this chapter too. The inputs in this chapter are from Chapters Three and Four and also the available published data for the study area. Additionally, bio-optical modelling results of water reflectance using the developed model of CDOM fractions are examined in this chapter. Then, the obtained results from both simulation and bio-optical modelling are tested in this chapter. Chapter Five ends with inverting water reflectance from both forward approaches by using matrix inversion method to determine the best results and quantifying the expected errors between both models.

Finally, **Chapter Six** is a conclusion of the main findings and results of all previous chapters and discusses if this research achieved the answers to the research questions. It offers suggestions for future research. Also, it demonstrates the limitations of this study and identifies any further improvements in the future. Finally, it describes what the contribution this work makes to the body of knowledge.

Chapter 2

Sampling SEQ Inland Water-bodies for Determining the Variation in CDOM Composition

2.1 Introduction

Before commencing with the investigation into the results of the sampled water-bodies, it is important to assist in understanding and explain the optical properties of CDOM in aquatic environments to the reader. Section (I) presents CDOM physical and chemical properties and also it illustrates synthesis and molecular structure. In addition, it reviews the relationship between CDOM and the other aquatic substances parameters, especially the dissolved organic carbon. Furthermore, it reviews the spatial variation of CDOM sources that influence its optical properties and observed from remote sensing data.

Section (II) in this chapter presents the measurement's methodology and discuss the results of sampling selected SEQ water-bodies after giving an introduction to the

study area with an overview of relevant literature. At the end of this chapter, it presents the discussion and results.

Section I:

2.2 Organic Matter in Natural Waters

Organic material in water is considered the major source and pathway of organic carbon in the aquatic system (Steinberg 2003). It comprises live organisms such as plants and animals, remnants of organisms, dead organisms yet to decompose, and organic compounds resulting from the decomposition processes (Vinebrooke & Leavitt 1998). Additionally, the water could contain industrial and chemical organic compounds such as industrial oils, remnants of irrigation pesticides and other organic compounds. A large amount of organic material in water is considered as an indicator of the extent of contamination of the water and affects the organisms living in the water by lowering the available oxygen and increasing dissolved organic carbon (Osburn & Bianchi 2016). In addition, it makes the water unusable for human consumption and it could be identified as a source of organic pollution (Harrison 2001). The most important fraction and the major form of the organic matter is the dissolved organic matter that can play a significant role in the aquatic system.

2.3 General View of Dissolved Organic Matter and Its Optically Measurable Component

DOM can be defined as the materials that consist of carbon atoms and have the ability to pass through a given GF/F* filter below 0.45 μm (Bukata et al. 1995; Chavez et al. 1995a), but 0.22 μm is also common especially for remote sensing applications (Ogawa & Tanoue 2003; Mostofa et al. 2009), it will be adopted in this thesis. DOM is brown, and when being in high concentration, it tints the water yellowish-brown (Zsolnay 2003). The increase in DOM concentrations in water negatively affects the aquatic ecosystem. At the same time, the aquatic DOM pool identified as a major reservoir of organic carbon. DOM can interact with many different elements because

* **GF/F filter:** glass fibre filter is manufactured from 100% borosilicate glass; it combines fast flow rate with high loading capacity. Type GF grade F filter is used for filtering extremely fine precipitates *Glass Fiber Filter, filter paper and Membrane Solutions*, 2018, https://www.membrane-solutions.com/glass_fiber_disc_membrane.htm>.

it is an important biochemical buffer and consists of a weak acid (McKnight et al. 1993).

Coloured dissolved organic matter is considered the optically measurable component of DOM in waterbodies for remote sensing applications. It is also used as an indicator of DOC measurements in the aquatic system (Mannino et al. 2008; Fichot & Benner 2011). According to literature, CDOM also known as Chromophoric Dissolved Organic Matter (Hoge et al. 1995; Fichot & Benner 2012; Nelson & Siegel 2013; Jacobsson 2014) or Yellow Substance (Carder, K. L. et al. 1989; Laanen 2007), Gilvin (Kirk 2011) or Gelbstoff (Aiken & Moore 2000). In this thesis, the term CDOM is used as it is the most commonly used name adopted in many recent studies like Ferrari and Dowell (1998); Brando et al. (2008); Mannino et al. (2008) and many others.

CDOM strongly absorbs short wavelengths of light that ranging from (200-329 nm) in the ultraviolet region to (330-495 nm) in the blue region and tends to zero with increasing wavelength (Bricaud et al. 1981; Green, Sarah A & Blough, Neil V 1994; Hoge et al. 1995; Zhang et al. 2009). Pure water absorbs longer wavelengths (> 620 nm) (Hoge et al. 1995) so non-turbid water (clear water) with little or no CDOM appears blue and the colour of the water will range through green, yellow and brown as CDOM concentration rises.

Thus, monitoring CDOM concentration periodically can give an indication of the water status especially in case-II* waters (Strömbeck et al. 2003; Zhang, M. et al. 2014), and it is important to look for a fast, accurate and inexpensive way to monitor it in water. For that reason, remote sensing is the optimum technique to measure these water quality parameters and its behaviour with other water components that have an influence on the aquatic ecosystem and its surrounding environment.

* **Case II waters**: this term is called for the coastal and inland waters (water reservoirs, lakes and rivers) where their optical properties are quite complex than **Case I waters** (open ocean) because of their optical properties not only depend on the phytoplankton concentration but it also controlled by other water components like mineral particles, suspended sediments and CDOM.

2.4 CDOM and Its Relationship with DOC in Natural Waters and The Global Carbon Cycle

DOM is the largest reservoir of the organic carbon in the aquatic system (Vantrepotte et al. 2015) and plays a major role in its nutrient system (Findlay & Sinsabaugh 2003; Anesio et al. 2004; Judd et al. 2006). Carbon dioxide is absorbed from the atmosphere at the water's surface and converted into dissolved carbon. It then converts by primary production by phytoplankton into dissolved organic carbon which constitutes about 90% of the dissolved carbon in the aquatic system as shown in Figure (2-1) (Jaffé et al. 2008). In addition, DOC enters the aquatic system from a terrestrial source such as soil.

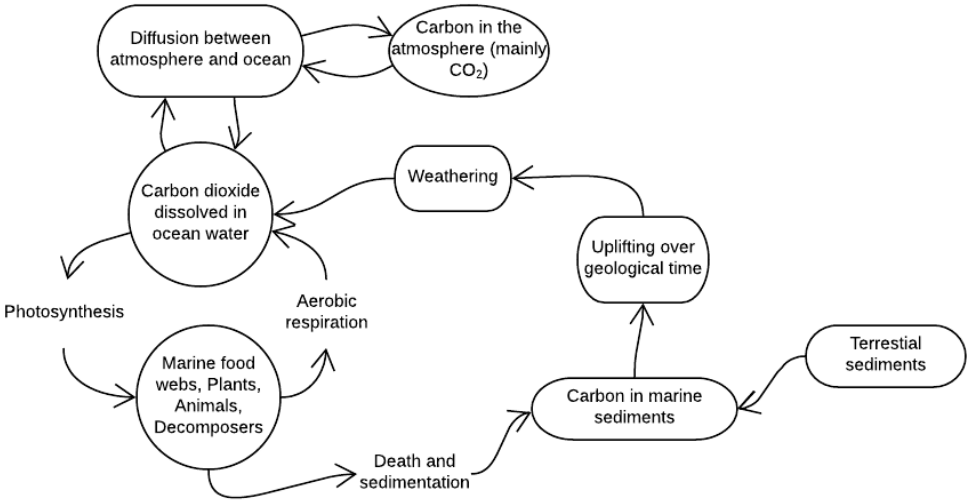

Figure 2-1: Schematic Representation of The Aquatic Carbon Cycle (Jaffé et al. 2008)

Tranvik et al. (2009) showed that the aquatic system provides the largest flux of reduced carbon from land to ocean as the result of organic matter in water as shown in Figure (2-2).

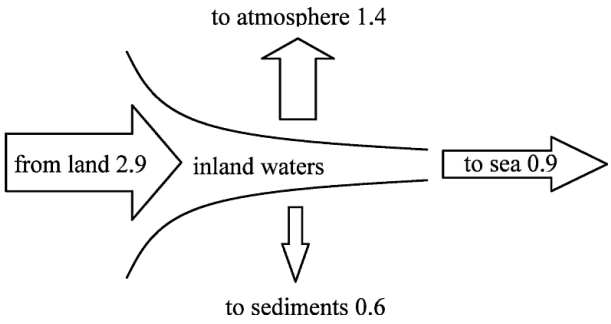

Figure 2-2: Revision of The Hypothesis of The Transport Of Dissolved Organic Carbon (Tranvik et al. 2009). Revised values are explained in the figure represent annual transport of carbon in units (Pg, 10^{15} g)

The carbon exchange between reservoirs and the atmosphere occurs because of various chemical, physical, geological, and biological processes. The decomposition of plants and organisms into the water transforms the organic matter into carbon dioxide (Keith et al. 2014). Therefore, coloured DOM is the portion of the DOC pool that absorbs light in both the ultraviolet and visible ranges and it is controlled by local independent processes (Kirk 2011). As a result, coloured DOM is generally used as an indicator or a tracer value of DOC and it is the optically measurable portion of DOC included in many water monitoring programs (Fichot & Benner 2011).

2.5 Flow, Sources and Sinks of CDOM in Australian Inland Fresh Waters

Terrestrial and aquatic sources and sinks contribute to the observed distribution of CDOM in water-bodies (Jerlov 1968; Bricaud et al. 1983; Carder et al. 1989). Organic matter influence the aquatic system from different external sources such as catchment runoff (drainage basin), point-source discharges, and sediments (Chen et al. 2004; Wells & Boehme 2008). Also, it is naturally produced and generated within the aquatic ecosystem from the decomposition of the remains of organisms in the aquatic environment, or via the biological production (phytoplankton, zooplankton, microbial) as shown in Figure (2-3) (Philp 1981).

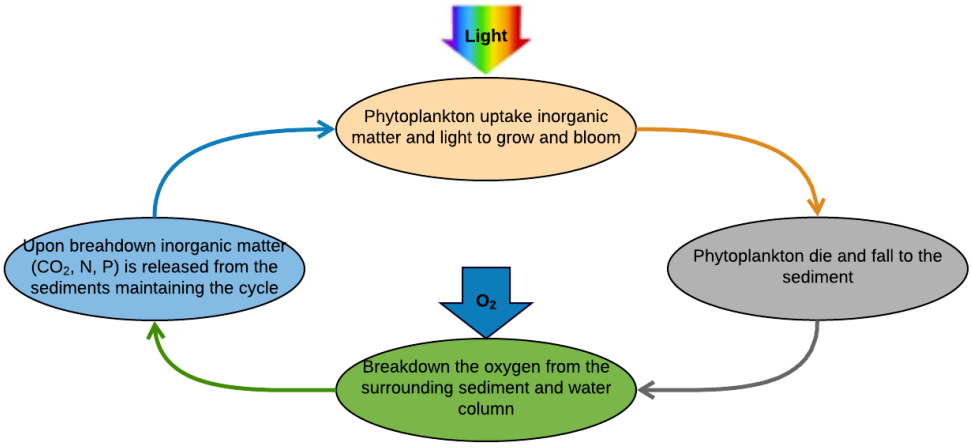

Figure 2-3: Internal Cycle of Organic Matter Production (Philp 1981)

In natural water bodies, CDOM consists of a heterogeneous mixture of numerous compounds originated from two major sources (Thurman 1985):

1. **Allochthonous Natural Organic Matter (NOM):** which is the organic substances that originate from the terrestrial materials and imported to the aquatic ecosystem from outside it. These materials consist of soil, plants (or leaves), root exudates and animal residues that fall or are washed into the water and are composed largely of humic substances* (Wershaw 1999). In Eastern Australian inland waters, Table (2-1) shows the five most common species of terrestrial materials.

Table 2-1: The Percentage of Allochthonous NOM Material in Eastern Australian Inland Freshwaters (Australia state of the environment 2011)

Material	Leaves	Bark	Wood	Soil	Litter and other material
Percentage	46%	16%	9%	24%	5%

Allochthonous NOM is dominant in inland waters and it possibly forms the largest proportion in these waters (lakes and rivers) when compared to the ocean waters.

2. **Autochthonous NOM:** which are the organic substances that formed in the aquatic ecosystem within the water itself derived from algae or phytoplankton. It is generally observed at the upper layers of the water body (epilimnion) compared with the deeper layers (hypolimnion) due to the accumulation of dissolved organic carbon significantly (Padisák et al. 1997).

In case II waters often, the major source of DOC/CDOM portions is the allochthonous NOM, which is the major source of organic acids in water (humic and fulvic acids) that is from outside the water system and affect CDOM properties (Laanen 2007).

* **Humic Substances:** are the broad class of NOM, constitute a large reservoir of organic C and N and characterized as being coloured with high molecular weight .

2.6 Dissolved Organic Carbon Content of Australian Inland Water Bodies

There are about 149,000 water bodies in Australia, many of them are exposed to a series of long periods of relatively low flow or drought conditions, interspersed with intense periods of rainfall leading to flash floods (Dekker & Hestir 2012). These floods cause large fluxes of soil, salts, plants, dead animals' residue and contaminants which can lead to changes in the ecosystem of these water bodies and their physical and chemical properties. Dissolved organic carbon comprises the major component in most Australian inland water bodies and it is reflecting the degree of organic matter pollution in these water bodies. It ranges from about 0.3 mg/L in McMinns Borefield (North Territory) and some unpolluted and non-productive freshwaters to 13.3 mg/L in the Jandakot Mround (West Australia), as shown in Figure (2-4) (Campbell et al. 1992b, 1992a; ANZECC/ARMCANZ 2000; Kirk 2011; Dekker & Hestir 2012; Hestir et al. 2015).

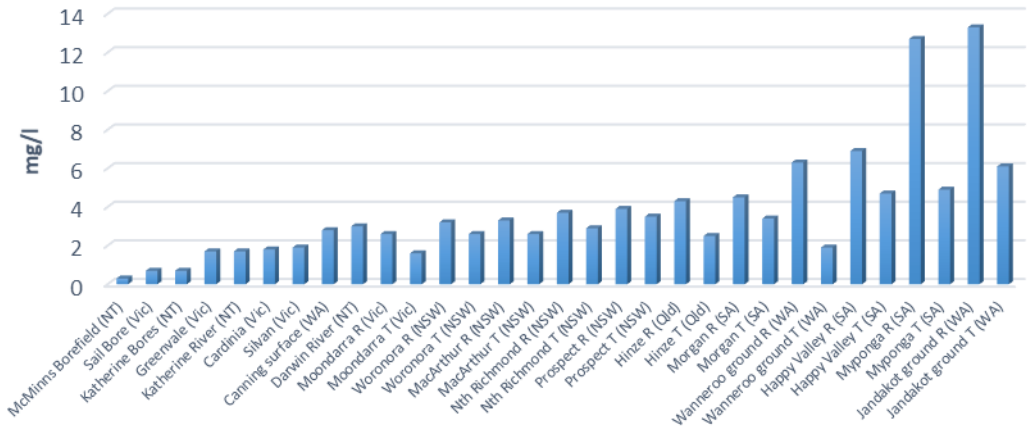

Figure 2-4: Some DOC Levels in Australian Fresh waters

However, some values of DOC that are higher than 10 mg/L have been found in some low pH lakes (CSIRO and Bureau of Meteorology 2015). The average concentration of DOC in these fresh waters from depths of 0-300 m is 1.5 mg/L. The highest values of DOC found in some waters were within an industrial fields area, especially the Murray-Darling basin zone and in South East Queensland (SEQ), Figure (2-5).

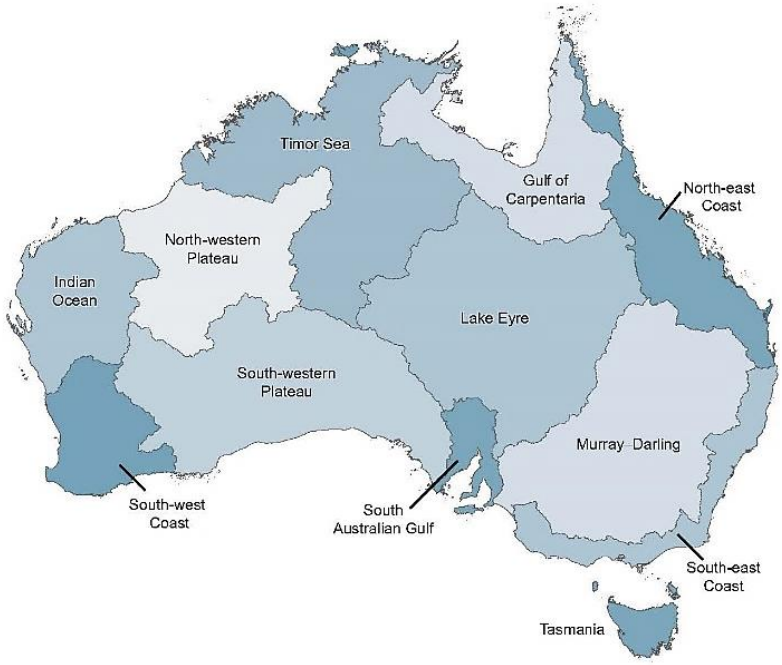

Figure 2-5: Australia's 12 Basin Zones

2.7 Spatial and Temporal Variability of CDOM in Remote Sensing Data for DOC Estimation

In order to invert reliably the remotely sensed water colour to obtain the concentration of optically significant material, it is important to determine CDOM distribution and its effect on water colour. CDOM concentration levels can vary both spatially and temporally depending on the size of the waterbody and types of the terrestrial community that deposit organic material into it. It is possible to do measurements of DOC concentration from optical remote sensing only if there is a good relationship between CDOM absorption and DOC concentration. Some studies (Matsuoka et al. 2012; Hestir et al. 2015) showed that it is possible to measure DOC concentration using remote sensing technique optically, but this technique may not be simple due to many factors that related to CDOM sources and to the seasonal variations.

Conservative behaviour (e.g. the distribution, variability and chemical behaviour) of DOC is necessary to be able to measure DOC remotely to allow for the development of a robust algorithm (Tanaka et al. 2016). Thus, the seasonal changes should not

affect the relationship between CDOM and DOC. However, some researchers (Mannino et al. 2008; Fichot & Benner 2011; Shao et al. 2015; Vantrepotte et al. 2015) explain if the relationship between CDOM and DOC changed seasonally, it is necessary to change the algorithm accordingly and the model used to derive the DOC concentration needs to be modified. Nevertheless, the development of a better algorithm will allow an accurate measurement of CDOM using satellite data.

Section II:

2.8 Study Sites Description

In South East Queensland, 11 reservoirs sampled with a total of 47 sampling stations. The study reservoirs were chosen in different sizes, different catchment properties, different sources, various uses and almost different climate zones (subtropical and temperate zones) reservoirs in SEQ. The selected reservoirs in the study area are shown in Figure (2-6).

Most of these reservoirs except Lake Weyba, which is a natural salt-water lake, are modified environments either created from enlargement of natural lakes or were created in river valleys using artificial barriers. These reservoirs are important for human consumption as a source of potable water supply and irrigation or using it for recreation and flood control. The sources of these reservoirs make a significant contribution in the physical and optical properties of the water components and concentration of dissolved organic matter. That effect is reflected clearly in water colour of the reservoir. Therefore, information about water quality monitoring of these reservoirs is very important especially during flood seasons (Cottingham et al. 2010).

Figure 2-6: Map of The Selected Study Sites in This Work in SEQ.

A brief overview of the study sites reservoirs, major geographic parameters of the sites, its purposes and importance is summarised in Table (2-2) (Sunwater 2005; Committee 2011).

Table 2-2: Selected Study Sites Reservoirs Geographic Properties

Reservoir Name	Site Name	year	Purpose(s)	Water source(s)	Catchment (km^2)	Max depth (m)	Surface area (10^3m^2)	Storage capacity (10^3m^3)
Cooby Creek Reservoir	CCR	1942	• Potable water supply	• Cooby Creek • Rainfall • GAB[1]	169	12.5	3014	23092
Lake Perseverance Dam	LPD	1965	• Potable water supply	• Perseverance Creek • rainfall	117	23.1	2200	30140
Lake Cressbrook	LCB	1983	• Potable water supply	• Cressbrook Creek • rainfall	321	34.0	5170	81840
Lake Wivenhoe	WIV	1985	• Potable water supply • Flood control • Hydroelectric • Recreation	• Brisbane River • Flood • Rainfall • recycled water	7020	44.0	108000	1165000
Lake Somerset Dam	LSD	1953	• Potable water supply • Flood control • Recreation • Hydroelectric	• Stanley River • Rainfall	1330	42.1	43500	380000
Lake Weyba	LWE	Natural lake	• Recreation	• Weyba Creek	-	8.1	-	-
Lake Samsonvale	SAM	1976	• Potable water supply • Recreation	• North Pine • Rainfall	347	23.0	21800	215000
Tingalpa Reservoir	TIN	1968	• Potable water supply	• Tingalpa Creek • Rainfall	87.5	18.2	4700	24800
Advancetown Lake	ADV	1976	• Potable water supply	• Nerang River • Rainfall	207	29.4	9720	161070
Lake Leslie Dam	LLD	1965	• Irrigation • Potable water supply • Recreation	• Sandy Creek • Rainfall	603	28.9	12880	106200
Lake Moogerah	MOO	1961	• Irrigation • Potable water supply	• Reynolds Creek • Rainfall	225	31.5	8270	83700

Knowing these reservoirs composition is important to understand how the sources of the organic matter (especially allochthonous) in the reservoir affect the optical properties of CDOM and its remote sensing reflectance. The results of this understanding provide stronger evidence for the high reliability of the validity.

[1] Great Artesian Basin

2.9 Samples Collection (Field Data Sampling)

2.9.1 Sampling SEQ Selected Reservoirs

The field data were collected during the Australian autumn between April and May of 2017. The field data were collected from the water surface of 11 reservoirs with a total of 47 stations were sampled (Table 2-2 and Figure 2-6) in south-east Queensland using the described sampling methods below.

Water samples were collected from 0.5 - 0.7 m below the water surface from a small boat. Most sampling points were far of the shore in different distances (10 - 15 m) depending on the water depth where shallow places were avoided. Samples were collected into 1000 ml clean amber (brown) glass bottle. Care was taken to prevent cross-sample contamination by organic material as possible before reusing the sample bottles. The cleaning procedure was according to Roesler et al. (1989), first, the bottles were cleaned with soapy water, and then rinsed six times with tap water then deionized distilled water (DDW). After that, they were left overnight in an acid bath (10% of HCl) followed by a tripled rinsed with deionized distilled water and dried in the lab oven at 60°C. These dry bottles were baked at 104°C for 4 hours (maximum safe temperature for bottles. These sampling bottles were kept sealed and dry to prevent airborne interface contamination and microbial growth for better DOC and CDOM results. All cleaning filtration and measurement in this work were performed using Nitrile gloves.

In situ, the sampling bottle was well rinsed with station water three times before collection and it was filled with water sample without overfilling (below the bottle's neck). The sampling bottle was sealed with Parafilm M® tape and PTFE screw cap (Polytetrafluoroethylene, best known is Teflon), then it was kept in a dark and cold ESKY™ box filled with ice cubes.

2.9.2 In Situ pH Measurements

In situ pH data collecting were conducted during collection the samples for all stations in the selected SEQ water bodies. Measurements process was performed using SPER SCIENTIFIC ADVANCED pH meter model (850055) with an accuracy specification ±0.02 of the pH scale. The instrument was calibrated in the lab the day before every data collection trip by using standard pH buffer calibration solutions.

Field pH measurements of collected samples were conducted using (CSIRO land and water) standard procedures. First, the instrument probe rinsed with Milli-Q water three times away from the collecting station. Then, a 400 ml clean glass beaker was rinsed three times in Milli-Q water after that, it was rinsed again three times in the water collected from the station before filling it with water from the station. To measure station pH, the probe placed and immersed into the beaker keeping it away from the sides and bottom of the beaker until the pH meter reading was stabilized.

2.10 Filtration Process and Samples Preparation

The filtration process is the most important preparation step for CDOM and DOC analysis, it is used to separate suspended particles from the solution. Suspended particles in water samples can affect the measurements, not to mention, it contains live organisms that produce or metabolize organic matter or organic carbon and leads to change concentration and composition during sample storage (Miller et al. 2007; Wurl 2009). For water samples that contain great amount from suspended particles, it is favoured to do pre-filtration with a larger pore diameter size for better filtration results (Shen et al. 2015). However, it must be taken into consideration that it is recommended to minimise the use of the pre-filters so we can reduce the possibility of contamination (Huckins et al. 2006). Thus, it is imperative that data resulting from analysing water samples to passing through an appropriate filter and follow standard procedures to reduce sample contamination and alteration.

2.10.1 Types of Filters Membranes and Filters Pore Sizes

Filter membranes may be made of diverse organic and inorganic materials. The choice of the filter type and the pore size is generally determined according to the application or the objective. They distributed among nylon, polysulfone, mixed cellulose esters (CE) and polycarbonate filters (PC) with pore sizes between 0.2 and 0.45 μm. Moreover, there are glass fibre filters (GF/F) with a nominal pore size of ≤ 0.7 μm are also used (Table 2-3). For remote sensing application generally, glass fibre filters (GF/F 0.7 μm) and polycarbonate filters (PC 0.45-0.2 μm) are the most frequently and commonly used especially for CDOM analysis due to their lack of contamination, ease of cleaning and high flow rates in addition to their large filtration capacity (Moran et al. 1999; Yoro et al. 1999). In this thesis, to achieve better accuracy in improving CDOM retrieve away from the influence of other water components, the 0.2 μm filter is adopted.

2.10.2 Types of Filtration Methods

There are many different methods of filtration, but all have the same purpose of separating solid particles from the sample. Filtering of samples for the determination of organic constituents requires using equipment constructed from inorganic materials. All filtration equipment parts must be cleaned sequentially with acetone, methylene chloride, or ethyl alcohol then rinse them thoroughly with Milli-Q water or deionized water (DIW) before using. Three common types of filtration method are used in laboratories:

1. Syringe - Disc Filtration.
2. Vacuum - driven filtration.
3. Positive gravity filtration.

In aquatic ecology and from literature, vacuum filtration is a common filtration method involved in a variety of studies that aim to measure water quality parameters. Also, it is recommended that the filtration pressure should be at the lowest (<125 mm Hg or < 5 in Hg) to pass the analyte in a regular flow relative to

minimize cell disruption and leakage of cell contents into the DOC during filtration (Miller et al. 2007).

In Table (2-3), below a list of some reference literature shows the filter membrane and the type of filtration that used:

Table 2-3: Some Literature of Filtration Types

Reference	Filter membrane type	Pore size	Filter design
(Vantrepotte et al. 2015)	- Polycarbonate membranes (Whatman Nuclepore, 47 mm)	0.2 µm	Low vacuum filtration
(Shao et al. 2015)	- Glass fibre filters (pre-filtration) - Polycarbonate membranes (Whatman Nuclepore, 47 mm)	0.7 µm 0.2 µm	Did not mentioned
(Mannino et al. 2014)	- Whatman GF/F glass fibre filter - Whatman Nuclepore (polycarbonate) filters	- 0.2 µm	Low vacuum filtration
(Matsuoka et al. 2013)	- Whatman GF/F filter	-	-
(Linnemann et al. 2013)	- Cellulose-acetate filters	0.45 µm	-
(Goldman et al. 2013)	- GF/F glass fibre filter - Teflon filter (Gelman Acrodisc)	0.2 µm 0.45 µm	Low vacuum filtration (below 200 mmHg (27 kPa))
(Bai et al. 2013)	- Millipore™ glass filtration - Polycarbonate filter	0.2 µm	low vacuum less than around 125mmHg
(Sun et al. 2011)	- 47-mm Whatman fibreglass GF/F filter (Whatman Inc., UK) - 25-mm Millipore filter	0.7 µm 0.22 µm	-
(Para et al. 2010)	- GF/F filter - Nuclepore polycarbonate filter	0.7µm 0.2 µm	-
(Qin 2008)	- 47 mm-Whatman GF/F glass fibre filters.	0.7 µm	Low vacuum filtration

2.10.3 SEQ Collected Samples' Filtration Methodology

The two most significant reasons for samples instability are microbial growth and exposure to light (Wurl 2009). To minimize the microbial growth, all samples were filtered and prepared within 24 hours of collection before storage. Along with CDOM measurements, dissolved organic carbon was also measured from the same filtered water samples in parallel. Therefore, selecting the appropriate filter is very important to minimize and to avoid contamination (Moran et al. 1999) in addition to, an initial treatment by intensive flushing with Millipore® milli-Q water for the selected filter

was done. This treatment significantly minimizes the potential organic contamination of using membrane filters (Yoro et al. 1999).

The filtration process was done by using a clean glass filtration rig, it was rinsed with the filtrate 3 times for every filtered sample before collecting the final filtrate. First, all samples were pre-filtered with 47 mm glass fibre (GF/F) filters nominal pore size was 0.6 µm from ADVANTEC®. Then, the filtrates were transferred to another clean glass bottles. After that, a 47 mm Whatman® Nuclepore™ 0.22 µm polycarbonate (PC) membranes filters were used for the filtrate. For remote sensing application and specifically for measuring the inherent optical properties (IOPs) in the lab, the 0.22 pore size filters are most commonly used (Bukata 1995; Chavez et al. 1995b). A low-pressure vacuum pump was used, and the filtration pressure used no less than (5 in Hg) (125 mm Hg) (Del Castillo & Miller 2011). Finally, the work was done on a clean surface and free of any organic contamination.

2.11 SEQ Samples Storing

Unlike seawater samples that can remain stable if frozen immediately for a couple of months, freshwater samples should not be stored for a long time (Yoro et al. 1999). The reason is back to high organic matter content in these freshwaters and also, to the biological activities that do not stop with sample collection (Grasshoff et al. 2009). Freezing and thawing freshwater samples change some optical properties, fluorescence intensity and peak position in a wide range of the samples (Spencer et al. 2007). Therefore, all filtered samples were refrigerated at 4°C for short-term (no more than one week) in the dark and were analysed as soon as possible after collection.

2.12 Laboratory Analysis and Measurements

2.12.1 DOC Concentration Measurements

All the collected filtered samples were analysed by SHIMADZU total organic carbon analyser model (TOC-V CSH) as shown in Figure (2-7) and the Table (2-4) gives some of its specifications. High-temperature combustion analysis was used to measure the non-purgeable organic carbon concentration and CSIRO protocol as described in the following sections (Page & Dillon 2007), was followed.

Figure 2-7: Total Organic Carbon Analyser (SHIMADZU TOC-V CSH) in USQ Water Lab.

TC: 0-500 ìg/L to 0-25,000 mg/L variable
Flow rate: Approx. 0.1 to 1 L/min **Sample volume**: 5 to 7 mL per measurement **Temperature**: 0 to 90ºC
680ºC combustion catalytic oxidation/NDIR method 720ºC combustion catalytic oxidation/chemiluminescence method (when TNM-1 is connected)

Table 2-4: (SHIMADZU TOC-V CSH) Specifications

2.12.2 CDOM Optical Measurements

The optical density (absorbance) of CDOM samples were measured using Cary 300 UV-Vis double beam spectrophotometer from Agilent Technology. The instrument has photometric precision using double aperture method at 0.3 Abs is ± 0.00016 Abs (see Table 2-5 for the instrument specifications).

Table 2-5: Agilent Cary 300 UV-Vis Specification

UV-Vis limiting resolution	≤ 0.193 nm
Wavelength Range	190–900 nm
Wavelength Accuracy	± 0.02 nm at 656.1 nm / ± 0.04 nm at 486.0 nm
Wavelength Repeatability	Standard deviation of 10 measurements < 0.02 nm
Photometric range	6.0 Abs
Photometric Accuracy	± 0.00016 using double aperture method at 0.3 Abs
Photometric noise	At 0 Abs, ≤ 0.000030 Abs /At 3 Abs, ≤0.00025 Abs / At 5 Abs, ≤ 0.0022 Abs
Scan Speed	3000 nm/min at 0.1 nm data steps

The absorbance scans were done by using 10 cm path length quartz cell cuvette. The cuvette was stored in 10% HCl to minimize organic coating. It was tripled rinsed with Millipore® milli-Q water before starting and the exterior windows of the cuvette were cleaned with ethanol and lens paper to eliminate excess water.

A fresh Millipore® milli-Q water was used as a reference control solution for CDOM. Before measuring the absorbance, the samples and the reference (control solutions) were left in a water bath at room temperature for optimum results. The temperature has a great effect on the absorption results; sometimes it appears and observes as a negative absorption (Pegau et al. 1997). This negative absorption might happen after a period from start measurements and this means, there is a difference between the temperature of the sample and the temperature of the reference (control solution) or, between them and the instrument room temperature (Belzile et al. 2006). In addition, it might happen with the first sample and that means, the sample is not at room temperature and needs to bring it to room temperature before scanning it (Belzile et al. 2006). Finally, before start scanning, it has taken into consideration no bubbles have formed in the reference solution or in the samples because it leads to negative absorption in the 745 nm range and a hump in the 850 nm range too.

The control solution was used as a zero and blank scan. The blank scan was measured twice, and it was ensured that there were no significant variations from the zero scan. Then, the optical density (absorbance) of the samples was measured and taken between 200-900 nm, at 1.0 nm interval.

The absorption coefficients ($a(\lambda)$) in m^{-1} at wavelengths (λ) between (200-900 nm) for the samples were calculated from the following expression:

$$A(\lambda) = OD(\lambda) - OD_{null} \quad (2.1)$$

$$a(\lambda) = 2.303 * \frac{A(\lambda)}{l} \quad (2.2)$$

Where, $A(\lambda)$ is the absorbance, $OD(\lambda)$ is the optical density measured at a given wavelength λ across path length (l) in meters. While OD_{null} is the shift observed in the red region of the spectrum and equal to the average of the optical density $OD(\lambda)$

from 750 to 850 nm. This offset is important to correct the samples from scattering error of small particles (it will be explained in details in chapter 4) (Bricaud et al. 1981; Green, S. A. & Blough, N. V. 1994; Helms et al. 2008; Matsuoka et al. 2012).

The absorption spectral shape of CDOM and the fractions represented by spectral slope coefficients (S), was typically determined and fitted as a single-exponential non-linear curve model in multispectral ranges (Stedmon et al. 2000) as shown in the equation below:

$$a(\lambda) = a(\lambda_o)e^{(-S(\lambda-\lambda_o))} + K \quad (2.3)$$

Where, $a(\lambda)$ represents the absorption coefficient at wavelength λ, $a(\lambda_o)$ is the absorption coefficient at a reference wavelength λ_o and (S) is the spectral slope coefficient. While K is a constant for background noise (a correction parameter will be explained in detail in chapter 4).

S calculated in the broad region of the visible and UV range, Fichot and Benner (2012) used the range between (275 – 295) nm ($S_{275-295}$) and 300 – 350 nm ($S_{300-350}$) in tracing for terrigenous DOC and as potential indicators of lignin dominated sources of DOC. Also, it calculated between 350-680 nm ($S_{350-680}$), the range used by Brando et al. (2012); Schroeder et al. (2012), and for the narrow region 350-400 nm ($S_{350-400}$) the range used by Helms et al. (2008); Spencer et al. (2012). The selection of these two ranges was chosen according to their wide use in the literature and contain spectral regions most relevant to remote sensing applications. S is important to characterizing CDOM and can provide further understanding about its general properties (size, source) than the absorption value alone (Brown 1977).

The absorption coefficient values $a(\lambda)$ are proportional with the accompanying absorbance value at 440 nm of CDOM and that represents the specific inherent optical properties (SIOPs). The specific absorption spectra for CDOM were fitted to the model (Dekker et al. 1995; Van der Meer & De Jong 2011; Nguy-Robertson et al. 2013):

$$a^*_{CDOM} = a^*_{CDOM}(\lambda_o)exp^{(-S(\lambda-\lambda_o))} \quad (2.4)$$

Where, λ_o = 440 nm and $a^*_{CDOM}(\lambda_o)$ = 1 by definition.

SIOPs are optical features of water components that are independent of the light field and essential for optical modelling (Campbell et al. 2011b).

2.13 Statistical Analysis of the Measured Parameters

Statistical tests were performed to determine whether there was a certain and specific relationship between the measured parameters. The descriptive statistics were used to analyse, summarize, and present the data that were subjected to random and systematic errors from the measurements and the instruments. The univariate analysis was used to describe the percentage representation of the fractions, mean, median, standard deviation, and the standard error. Whilst, Kendall's rank correlation coefficient or commonly known as tau-test (τ), which is a non-parametric test, was used to assess the strength of the relationship between $a(\lambda_o)$ and (S). The reason for using this test is not all sites met parametric assumptions for correlation analysis "distribution-free". It takes a value between minus and plus one, the positive correlation shows that a perfect relationship while zero has no relationship. A multivariate regression analysis was used also to improve the prediction of DOC concentration based on the value of $a(\lambda_o)$ and (S). Finally, the statistical significance is reported as a significant if ($\rho \leq 0.05$) and as highly significant if ($\rho \leq 0.001$), conversely if ($\rho > 0.05$). All analyses were performed using the SPSS statistics 17.0 and Microsoft® EXCEL software.

2.14 Results and Discussions

2.14.1 pH Measurements Results of All Stations in SEQ Study Sites

The results of measuring the acidity and the alkalinity on a scale ranges from 0.0 to 14.0 for the 47 stations along 11 water bodies in SEQ are shown in Figure (2-8). The pH scale is the negative logarithm of the hydrogen ions concentration (H^+) shows how acidic or alkaline or neutral is the solution (Kotyk & Slavík 1989). The measured values that are less than 7.0 are acidic and the measured values greater than 7.0 are alkaline (basic). The lowest measured pH value was 6.89 recorded in Tingalpa Reservoir, whilst the highest measured pH value was 8.66 recorded in Cooby Creek Reservoir and the average pH value of all the sites (N = 47) was 7.69 ± 0.38 pH unit.

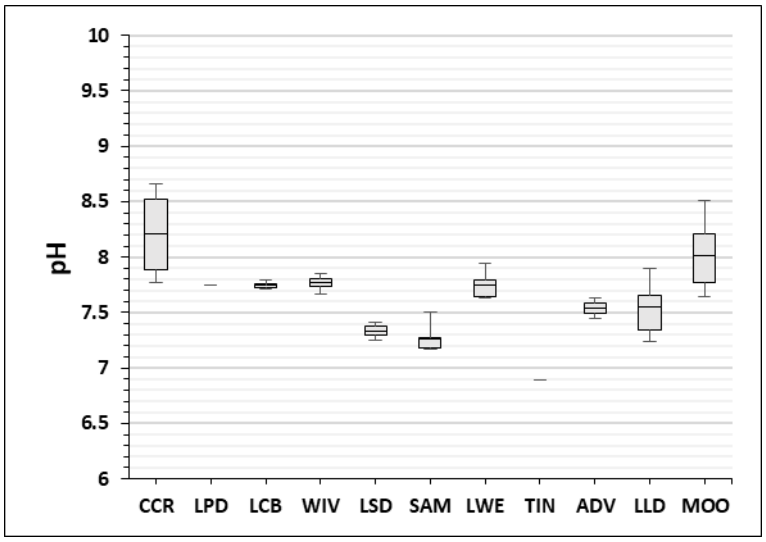

Figure 2-8: Boxplot to the Measured pH Values Per Reservoir for 47 Stations Along the Study Area Sites in SEQ.

There was no significant variation in pH values within the same waterbody excluding three reservoirs; Cooby Creek Reservoir (CCR), Lake Leslie Dam (LLD) and Lake Moogerah (MOO) where the variation value was around 1.0 pH unit between its stations. Generally, the variation in pH values between all sites was significant, ranging between ± 0.7 pH unit around their average along all sites. Most of the pH results of the study area water bodies tend to alkalinity where all measured values were above 7.0 except Tingalpa Reservoir (TIN) was under 7.0.

2.14.2 Absorption Spectra and Specific Absorption Coefficients of CDOM in SEQ Study Sites

Mean absorption curves of CDOM samples per each reservoir (N = 11) in the study area of SEQ are shown in Figure (2-9 A) and the total measured absorption curves of all stations per reservoir (N = 47) are shown in Figure (2-10). The CDOM spectral absorption is described by an exponential curve declining towards longer wavelengths. The curve approaches 0 near 700 nm and reaches the maximum at 350 nm within the selected wavelength domain. The focus of this work is to characterise the CDOM absorption over the UV-visible spectrum in the range 350 – 680 nm and 350 - 440 for remote sensing applications, therefore, the absorbance data from 200 - 350 nm was excluded even it was measured maybe could be useful in future works. Figure (2-9 B) illustrates the quasi-linearization fit of the natural log-transformed of these absorption spectra curves along all of the study sites in SEQ (N = 11).

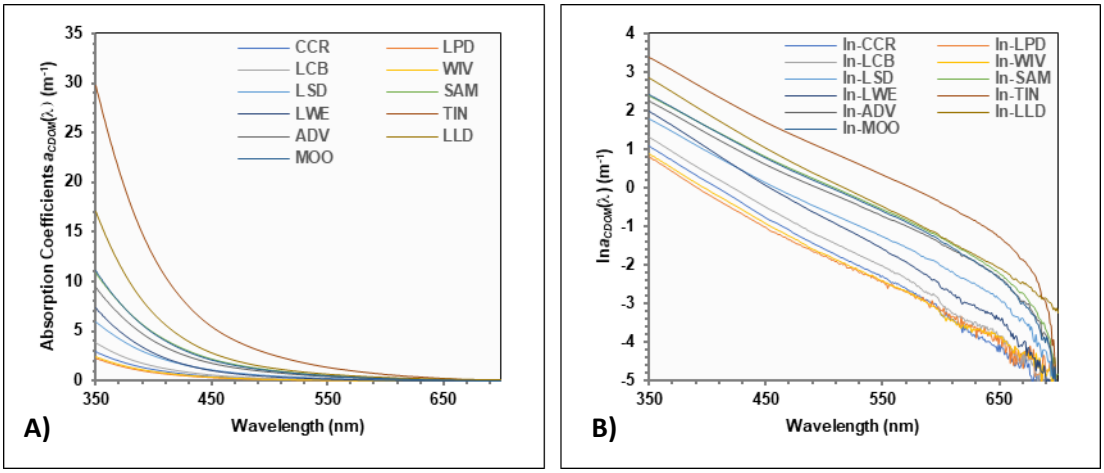

Figure 2-9: A) CDOM absorption spectra of the mean curves of each reservoir along all sites B) Natural log-transformed absorption spectra of the mean curves of each reservoir along all sites.

From Figure (2-9 A) large variations in the absorption between the reservoirs can be seen, Tingalpa Reservoir (TIN) showed the highest measured absorption values, the opposite, Lake Wivenhoe (WIV) has the lowest measured absorption values (mean). While in Figure (2-10), Lake Somerset Dam (LSD) measured spectra showed high variability CDOM concentration between its stations. Also, each of Lake Samsonvale (SAM), Cooby Creek Reservoir (CCR) and Lake Weyba (LWE) showed moderate variation.

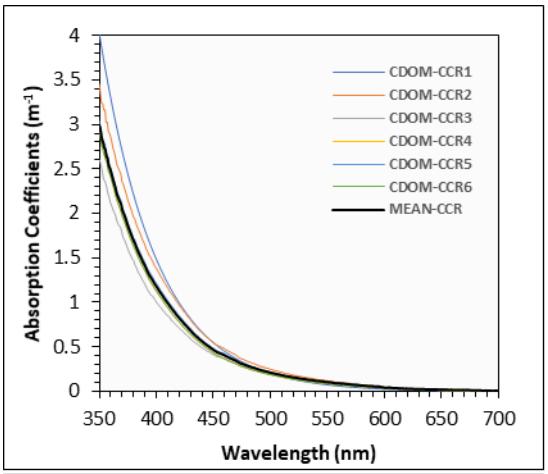
Absorption Coefficients (m-1)
Wavelength (nm)
CDOM-CCR1
CDOM-CCR2
CDOM-CCR3
CDOM-CCR4
CDOM-CCR5
CDOM-CCR6
MEAN-CCR

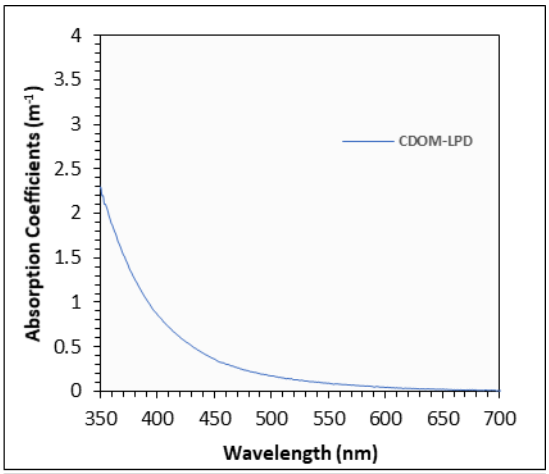
Absorption Coefficients (m-1)
Wavelength (nm)
CDOM-LPD

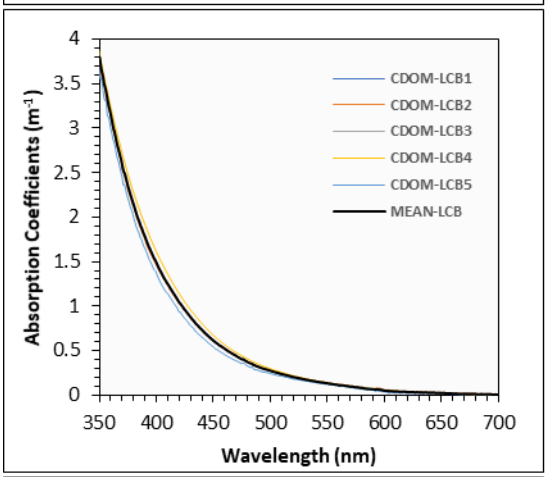
Absorption Coefficients (m-1)
Wavelength (nm)
CDOM-LCB1
CDOM-LCB2
CDOM-LCB3
CDOM-LCB4
CDOM-LCB5
MEAN-LCB

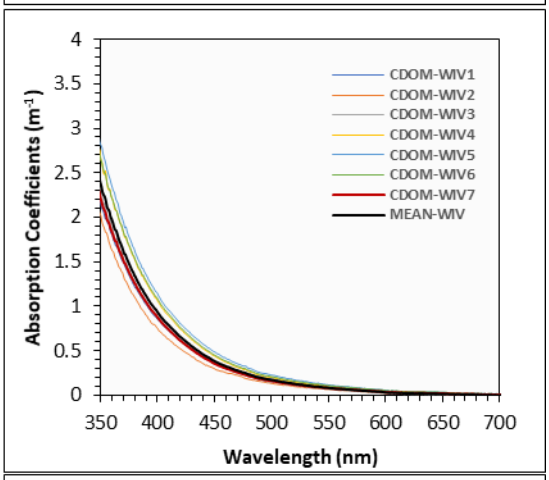
Absorption Coefficients (m-1)
Wavelength (nm)
CDOM-WIV1
CDOM-WIV2
CDOM-WIV3
CDOM-WIV4
CDOM-WIV5
CDOM-WIV6
CDOM-WIV7
MEAN-WIV

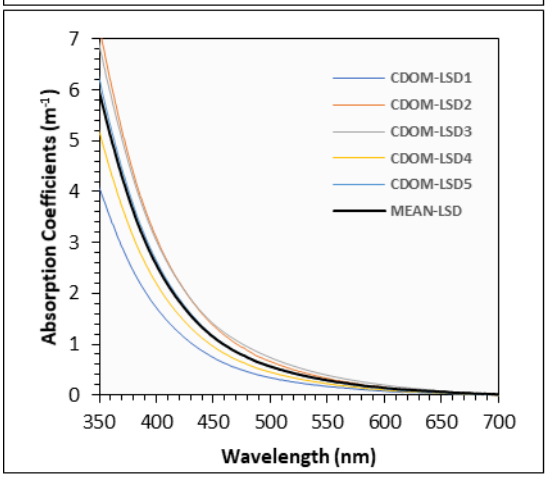
Absorption Coefficients (m-1)
Wavelength (nm)
CDOM-LSD1
CDOM-LSD2
CDOM-LSD3
CDOM-LSD4
CDOM-LSD5
MEAN-LSD

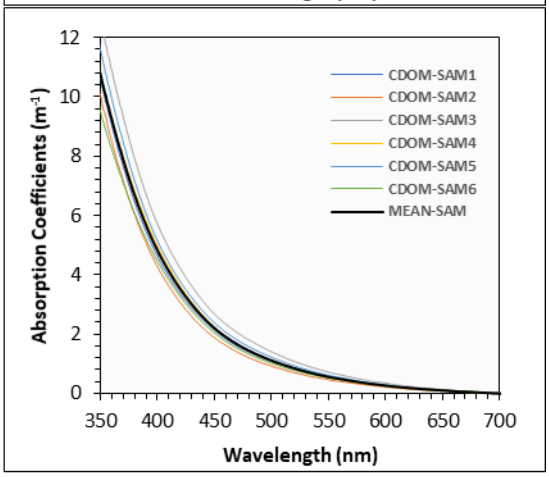
Absorption Coefficients (m-1)
Wavelength (nm)
CDOM-SAM1
CDOM-SAM2
CDOM-SAM3
CDOM-SAM4
CDOM-SAM5
CDOM-SAM6
MEAN-SAM

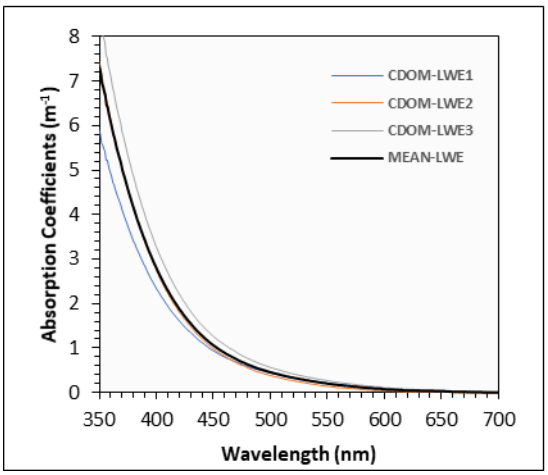
Absorption Coefficients (m-1)
Wavelength (nm)
CDOM-LWE1
CDOM-LWE2
CDOM-LWE3
MEAN-LWE

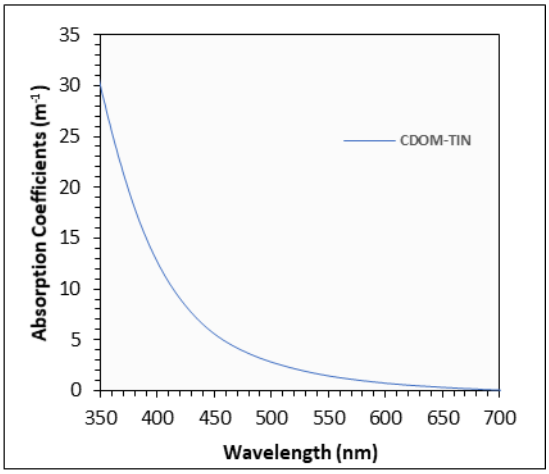
Absorption Coefficients (m-1)
Wavelength (nm)
CDOM-TIN

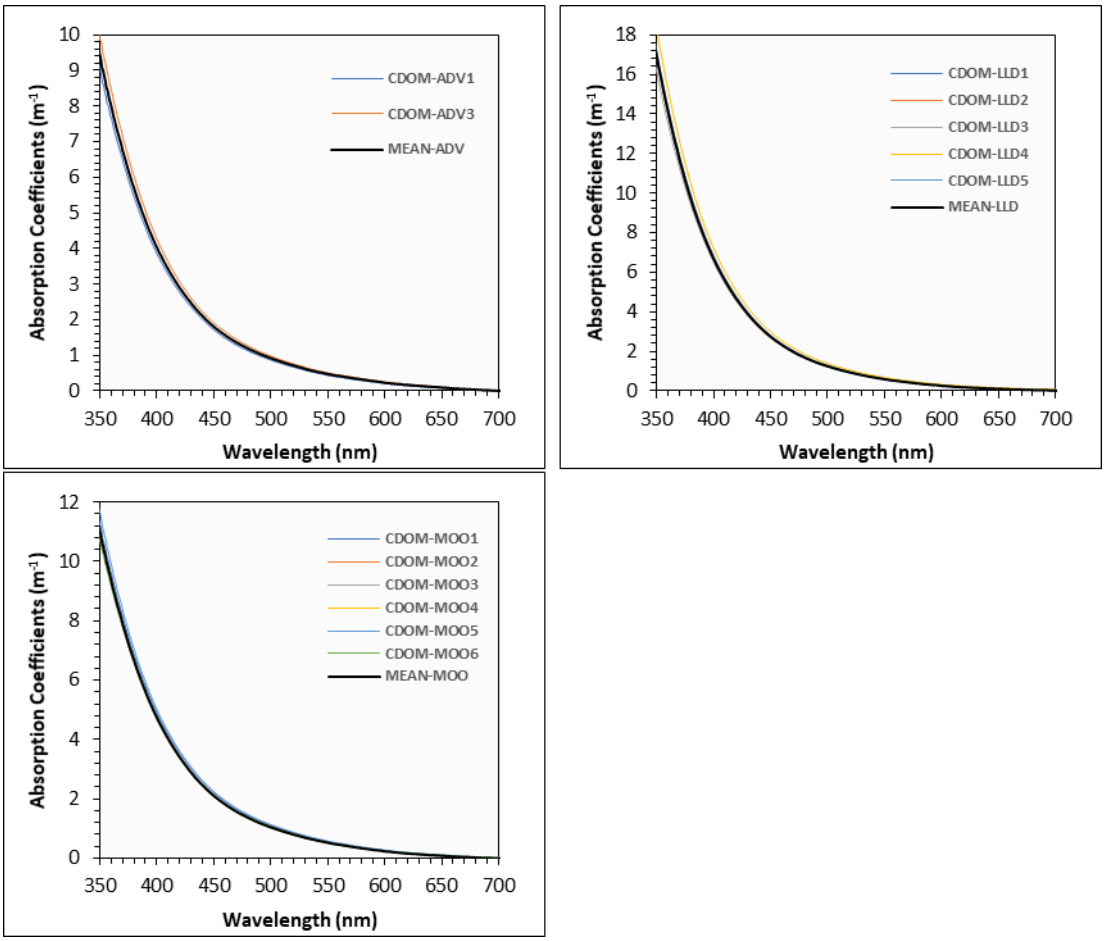

Figure 2-10: Coloured dissolved organic matter (CDOM) absorption spectra curves of all stations for each reservoir along the study area sites in SEQ

The mean specific absorption spectra per each reservoir (N = 11) in the study area are shown in Figure (2-11 A) and the linearization fit of the natural log-transformed of these spectra are shown in Figure (2-11 B). Knowing the forms of these specific absorption spectra is important to understand variations in CDOM types due to their source (Miller et al. 2007; Qin 2008).

The $a^*_{CDOM}(440)$ was calculated from equation (2.4), by normalizing CDOM absorption to the measured absorbance at 440 nm (Dekker et al. 1995; Gallie 1997; Nguy-Robertson et al. 2013). The results showed no significant spatial variation in $a^*_{CDOM}(440)$ over all sites in a water-body. Hence, the mean value of CDOM absorption of each reservoir could be used for the total reservoir area and it should be sufficient for the bio-optical model (Stedmon et al. 2000; Campbell 2010).

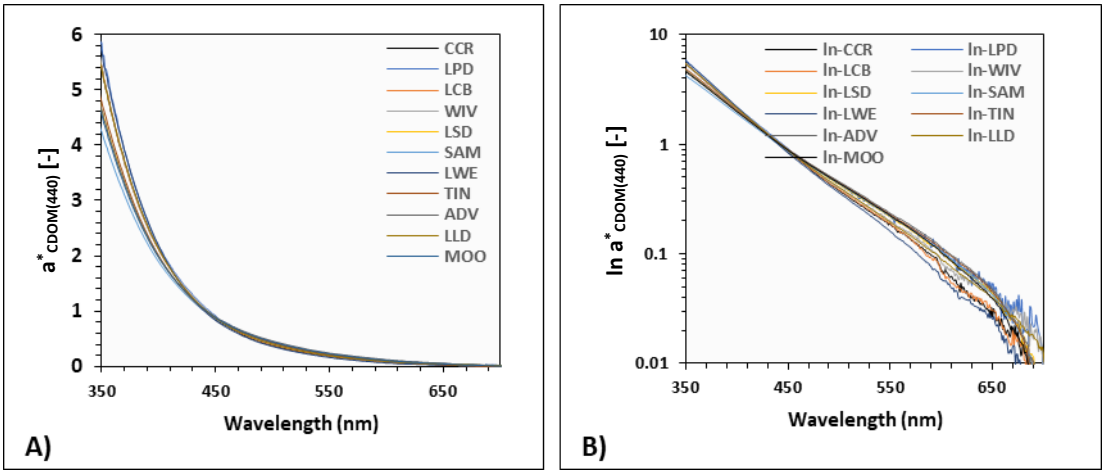

Figure 2-11: A) The mean specific absorption spectra of each reservoir along the study area sites in SEQ. B) Natural log-transformed mean specific absorption spectra of each reservoir in the study area.

The full Figures of the specific absorption spectra of each station per reservoir are given in Figure (2-12) below with no significant disparity.

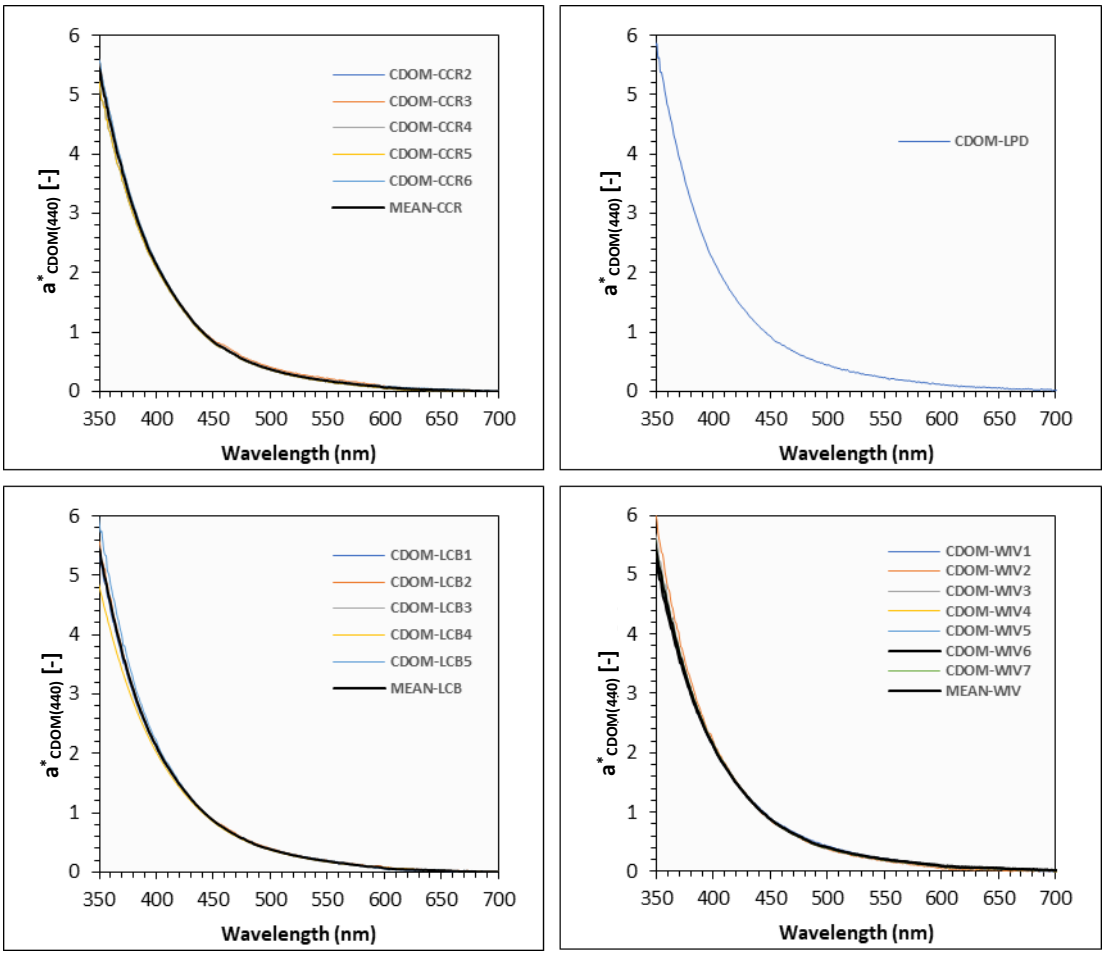

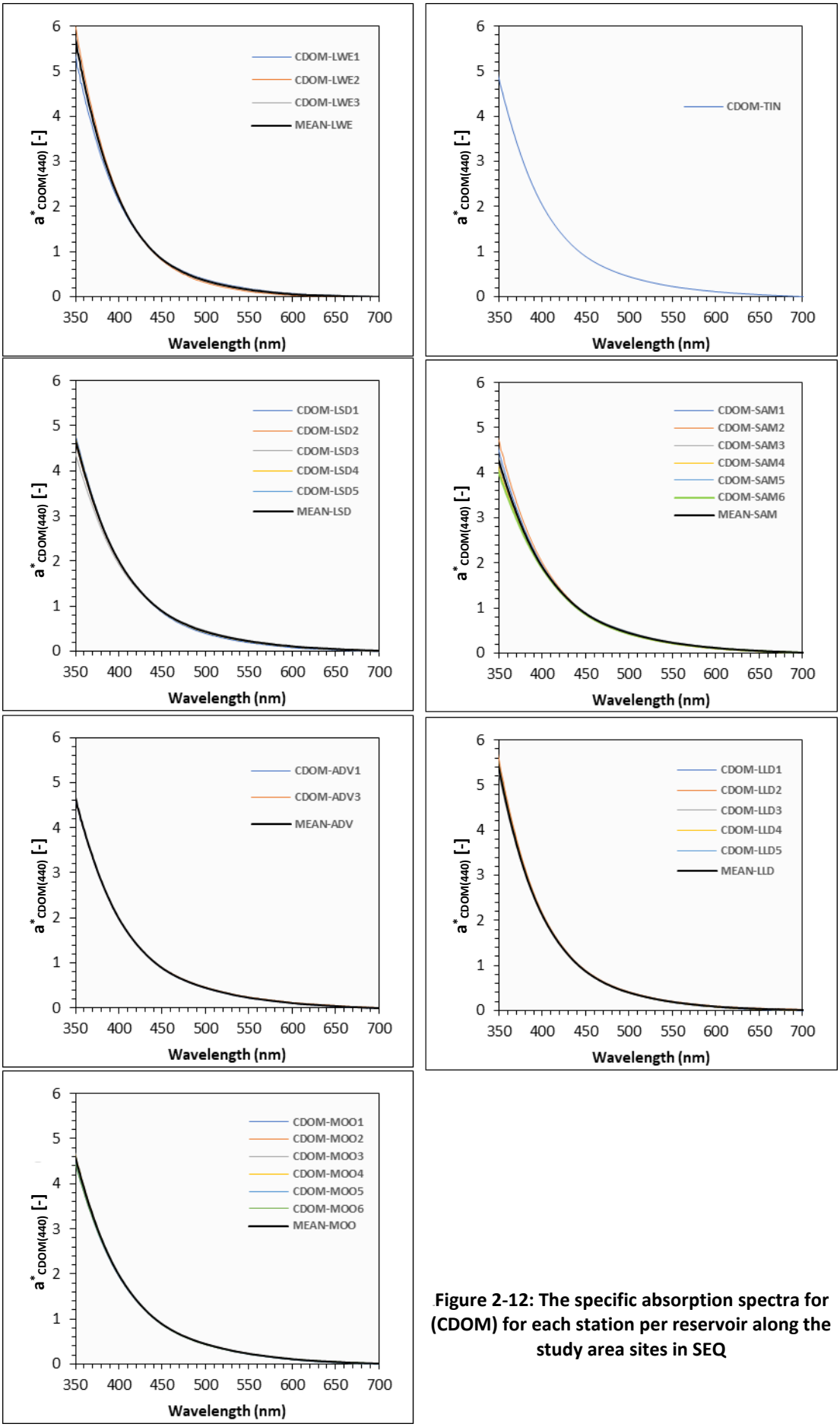

Figure 2-12: The specific absorption spectra for (CDOM) for each station per reservoir along the study area sites in SEQ

2.14.3 Spectral Slope Coefficients (*S*) of CDOM in SEQ Study Sites

CDOM spectral slope values (*S*) of the 47 stations were calculated using equation (2.3). It was done by fitting the measured absorption coefficient in two different wavelength domains i.e. (350 - 440 nm) and (350 - 680 nm) and adoption reference wavelength at (440 nm). The derived (*S*) values are denoted as $S_{350}(350-440)$ and $S_{440}(350-680)$. The resulting (*S*) values varied from 0.014 – 0.021 nm^{-1} for the two selected wavelength domains as shown in Figure (2-13 A and B). There were moderate CDOM slope differences among the reservoirs in the $S_{440}(350-680)$ domain and big disparity in CDOM slope in the $S_{350}(350-440)$ domain. A comparison of CDOM spectral slope derived for $S_{440}(350-680)$ with literature for the Australian inland waters shows similar agreement. The slope domain ($S_{350}(350-440)$) is generally adopted for assessing CDOM in the UV and near-visible bands which is not very useful for remote sensing uses. Therefore the $S_{440}(350-680)$ only will be used on the coming chapters of this work because it covers spectral regions most relevant to remote sensing applications and it is readily comparable to the literature.

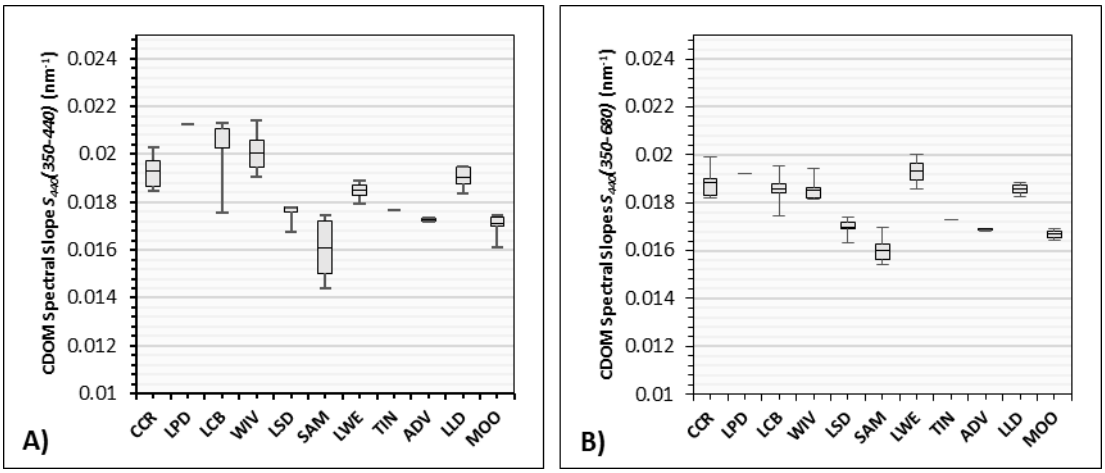

Figure 2-13: CDOM spectral slope ranges for each reservoir over all sites in SEQ. A) Boxplot of CDOM slopes values at 350 nm for the range (350-440 nm). B) Boxplot of CDOM slopes values at 440 nm for the range (350-680 nm).

The *S* values obtained from exponential fitting within the two wavelength domains, all were within the range 0.010 – 0.025 nm^{-1} reported for surface layer in shallow reservoirs by Stedmon et al. (2000) and a little bit higher than *S* values of Australian

inland waters reported by Kirk (1994), Campbell (2010), and Dekker and Hestir (2012) that ranged from 0.012 – 0.018 nm^{-1}.

2.14.4 CDOM and DOC Concentrations' Variations in SEQ Study Sites

The measured absorption coefficient values of CDOM concentrations at 440 nm ($a_{CDOM}(440)$) for all stations (N=47) along all the study area sites are shown in Figure (2-14). Low CDOM absorption coefficient values were measured at the stations in the northern part of SEQ between the area from North Toowoomba and North Brisbane to Noosa, whilst the highest values were measured in the southern part of the SEQ region. In general, there were significant variations in $a_{CDOM}(\lambda_o)$ values measured at 440 nm ranging from 0.35 m^{-1} in Lake Wivenhoe to 6.52 m^{-1} measured in Tingalpa Reservoir.

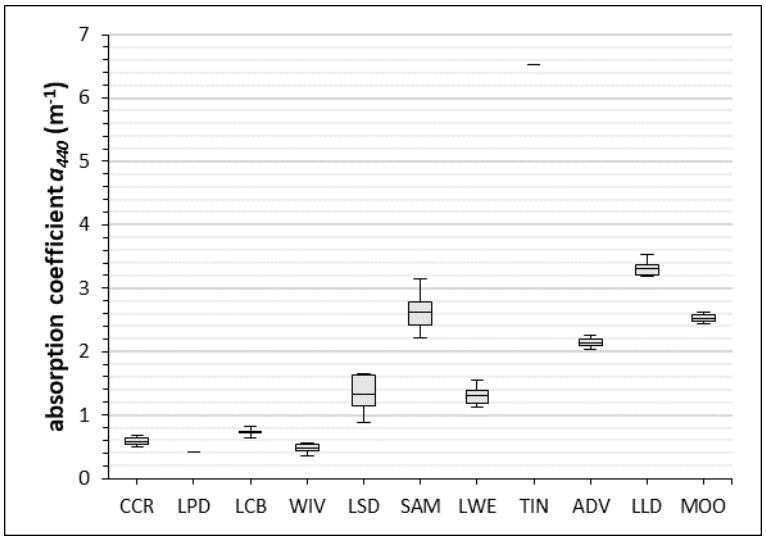

Figure 2-14: Box-and-whisker plots shows the (minimum, first quartile, mean, third quartile and maximum) values ranges of CDOM absorption coefficient at 440 nm along all stations in the study area.

The analysis of variance was used to determine whether there were any significant differences between the reservoirs in the measured $a_{CDOM}(\lambda_o)$. It showed different variations in the measured $a_{CDOM}(\lambda_o)$ values of CDOM concentrations between

some stations for the selected wavelength ($a_{CDOM}(440)$). Where Lake Somerset Dam (N = 5) showed high percentage disparity around the average (mean 1.33 ± 0.11 m^{-1}) between its stations was around (8%), then each of Lake Samsonvale (N = 6) was 4.2% (mean 2.62 ± 0.11 m^{-1}) and Lake Weyba (N = 3) was 3.5% (mean 1.31 ± 0.05 m^{-1}). As for the rest of the reservoirs, variance percentage was ≤ 1%, except (WIV = 1.25%; N = 7) and (ADV = 1.1%; N = 2) as shown in Figure (2-15).

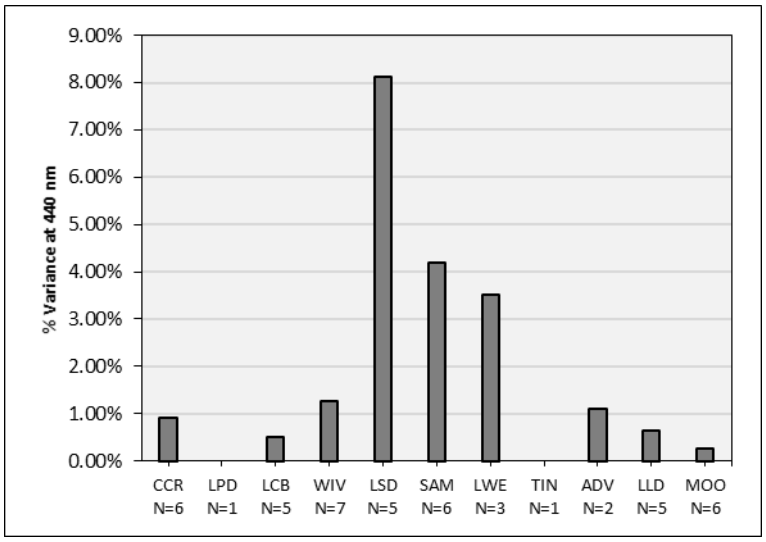

Figure 2-15: Percentages of ANOVA single factor bar charts of CDOM absorption coefficient values per each reservoir at 440 nm

Samples collected from SEQ study sites demonstrate variability in dissolved organic carbon concentrations as shown in Figure (2-16 A and B). The lowest recorded value was 3.41 $mg.L^{-1}$ in Lake Moogerah and the highest recorded value was 19.35 $mg.L^{-1}$ in Lake Leslie Dam. All measurements of DOC concentrations in the reservoirs found within the Australian normal range of lakes which ranged from 0.3 $mg.L^{-1}$ to 29.50 $mg.L^{-1}$ (CSIRO and Bureau of Meteorology 2015).

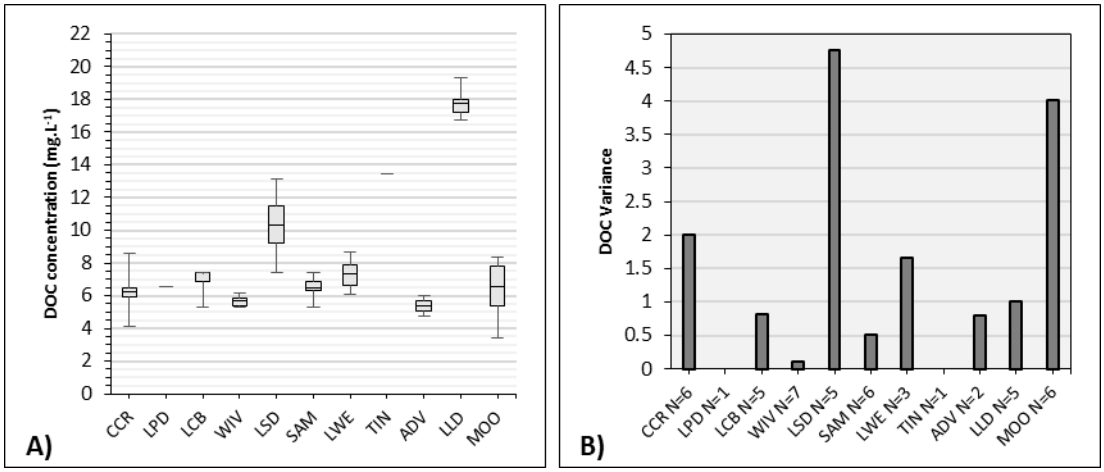

Figure 2-16: A) Box-and-whisker plot shows the (minimum, first quartile, mean, third quartile and maximum) values of DOC concentrations ranges for each reservoir. B) DOC variance between each reservoir station

Figure (2-16 B) showed that most of the reservoirs have significant variance in *DOC* values between its stations, the highest variation was in Lake Somerset Dam (Var = 4.76) then follows by Lake Moogerah (Var = 4.01). While Lake Wivenhoe has the lowest variance between its stations (Var = 0.11) then Lake Samsonvale (Var=0.51). This variability in CDOM and DOC concentrations is most likely due to the spatial differences between the sites and local inflows. It is unlikely to be due to the seasonal changes because most of the data were collected at the beginning of the Australian dry season and during very close periods of time.

The locations and spatial distribution[*] of CDOM and DOC concentrations over all sites in SEQ study area are shown in Figure (2-17). High CDOM and DOC concentrations can be noticed at the stations close to the inflow sites of each reservoir due to the discharge of the feeder's rivers and streams except Lake Moogerah because the CDOM variation is not significant between its stations and the size of the lake.

[*] ArcGIS 10.2 software was used to create the spatial analysis distribution of CDOM and DOC concentrations over all sites in SEQ study area.

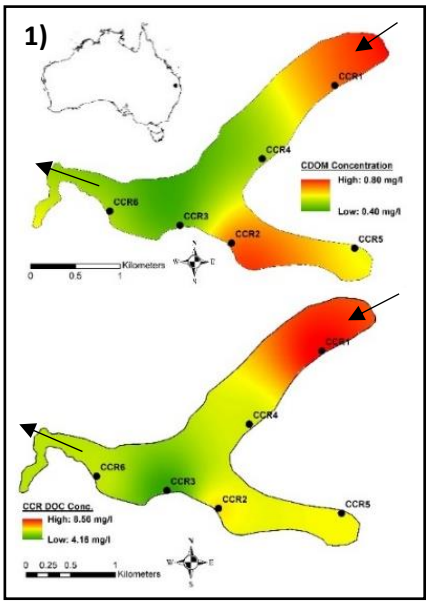
1)
CCR1
CCR4
CCR6
CCR3
CCR2
CCR5
CDOM Concentration
High: 0.80 mg/l
Low: 0.40 mg/l
Kilometers
CCR DOC Conc.
High: 8.56 mg/l
Low: 4.18 mg/l

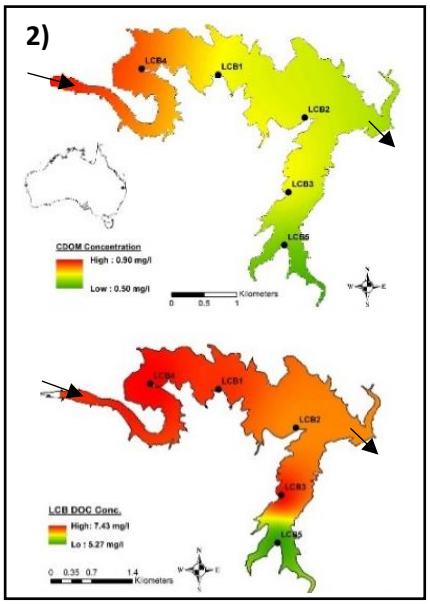
2)
LCB4
LCB1
LCB2
LCB3
LCB5
CDOM Concentration
High : 0.90 mg/l
Low : 0.50 mg/l
Kilometers
LCB DOC Conc.
High: 7.43 mg/l
Lo : 5.27 mg/l

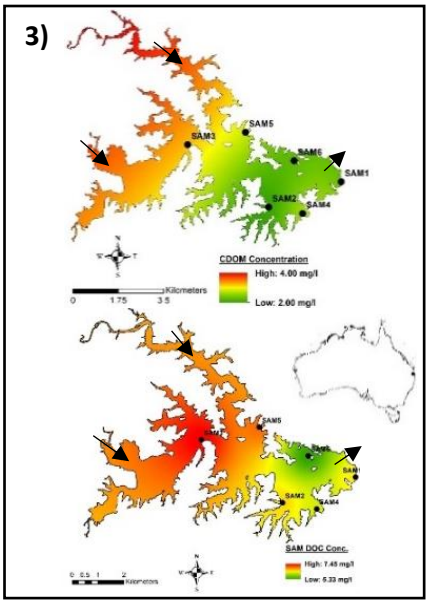
3)
SAM5
SAM3
SAM6
SAM1
SAM2
SAM4
CDOM Concentration
High: 4.00 mg/l
Low: 2.60 mg/l
Kilometers
SAM DOC Conc.
High: 7.48 mg/l
Low: 5.33 mg/l

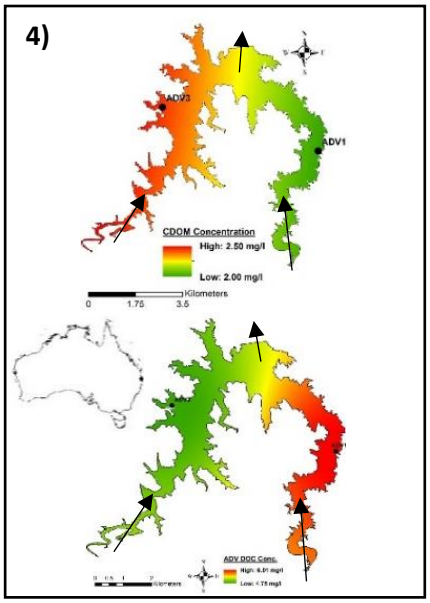
4)
ADV3
ADV1
CDOM Concentration
High: 2.50 mg/l
Low: 2.00 mg/l
Kilometers
ADV DOC Conc.

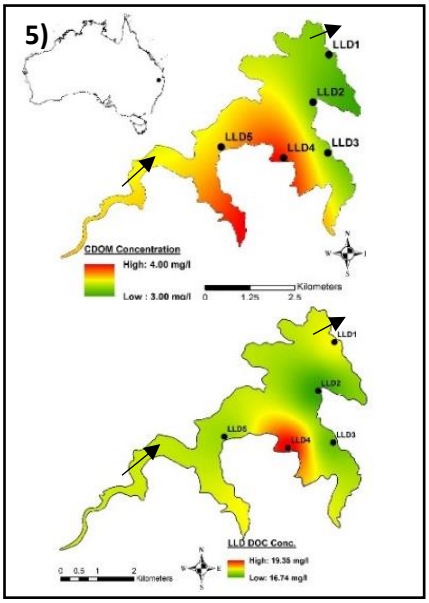
5)
LLD1
LLD2
LLD5
LLD4
LLD3
CDOM Concentration
High: 4.00 mg/l
Low : 3.00 mg/l
Kilometers
LLD DOC Conc.
High: 19.35 mg/l
Low: 16.74 mg/l

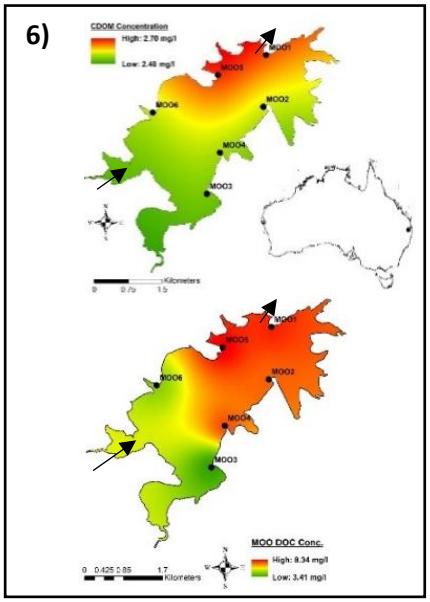
6)
CDOM Concentration
High: 2.70 mg/l
Low: 2.40 mg/l
MOO1
MOO5
MOO6
MOO2
MOO4
MOO3
Kilometers
MOO DOC Conc.
High: 8.34 mg/l
Low: 3.41 mg/l

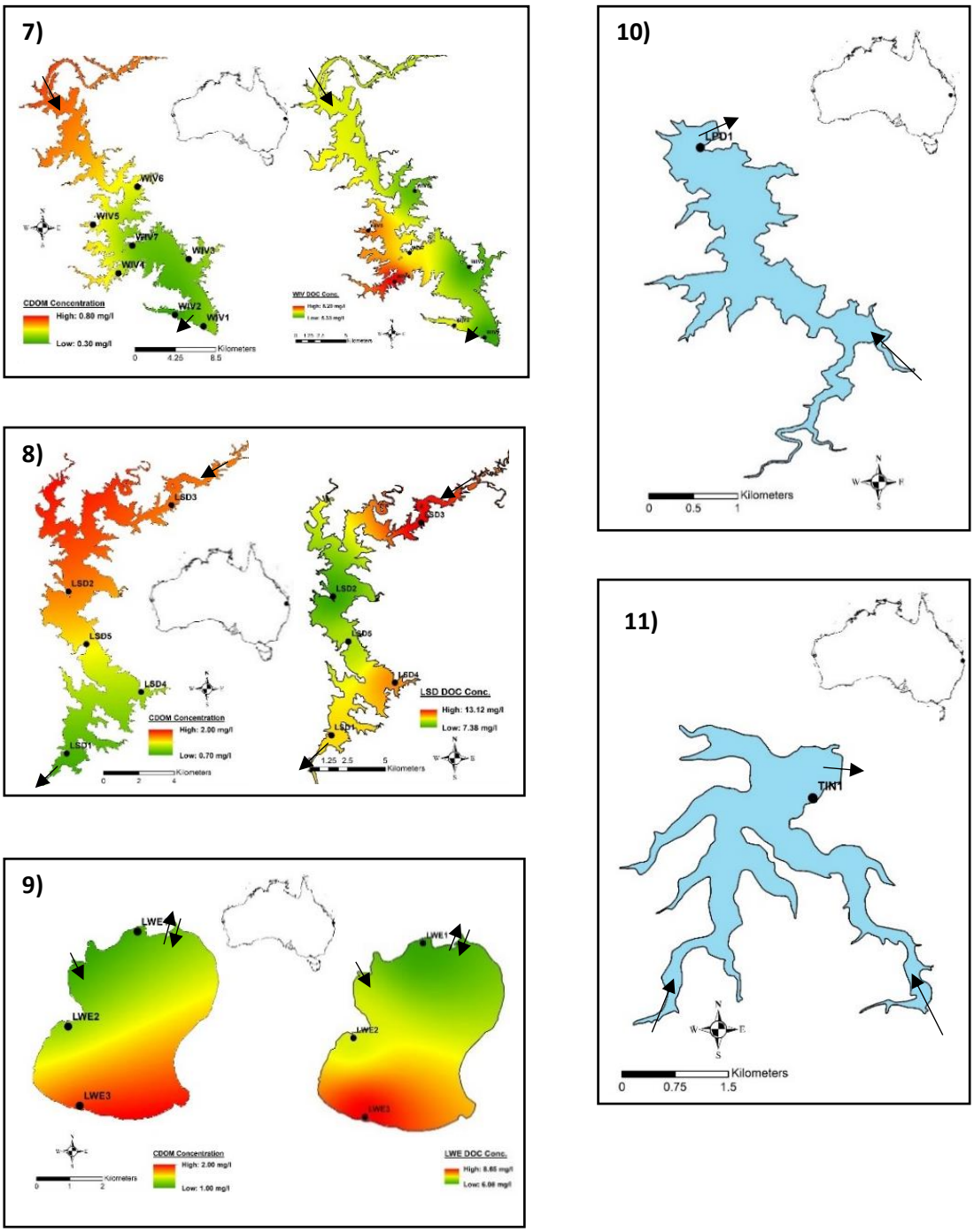

Figure 2-17: Spatial distribution of CDOM and DOC concentrations and location of sampling stations in 1) Cooby Creek Reservoir (CCR), 2) Lake Cressbrook (LCB), 3) Lake Samsonvale (SAM), 4) Advancetown Lake (ADV), 5) Lake Leslie Dam (LLD), 6) Lake Moogerah (MOO), 7) Lake Wivenhoe (WIV), 8) Lake Somerset Dam (LSD), 9) Lake Weyba (LWE), 10) Lake Perseverance Creek Dam (LPD), 11) Tingalpa Reservoir (TIN). The black arrows referring to reservoirs' inlets and outlets.

Please note: "The limited number of sample sites at most water bodies means that these concentration interpolations should be treated with caution."

2.14.5 The Relationship Between CDOM Absorption and Slope Parameters (*S*) in SEQ Study Sites

It is important to test the relationship between CDOM optical properties and its chemical composition to understand the effect of this relationship on estimation DOC in the study area. The spectral slope (*S*) of the exponential function that expresses the CDOM absorption curve has been used widely as a proxy of CDOM composition in water (Fichot & Benner 2012; Traub 2012). Therefore, it is essential to display the evidence if there was any local variation in the CDOM sources affects this relationship. Statistical calculations were performed to find the degree of correlation between (*S*) and $a_{CDOM}(\lambda_o)$ in the SEQ study area. Kendall rank correlation coefficient (τ) was used to measure the strength of dependence between (*S*) and $a_{CDOM}(\lambda_o)$ and the ρ-value was used to discover if there was a statistically significant relationship. Two different reference wavelength at 350 nm and 440 nm were selected, the basis of selection of these two wavelengths is CDOM absorbance increase with decreasing the wavelength and is much greater at 350 nm which represents the lowest wavelength within the UV-A band. The 440 nm is the most commonly used and readable reference wavelength in literature. As well two different slope domains $S_{350}(350-440)$ and $S_{440}(350-680)$ were selected. The reasons for choosing these two wavelengths domains to calculate (*S*) are mentioned in §2.12.2.

The results of using tau correlation showed moderate negative correlation between spectral slope (*S*) and $a_{CDOM}(\lambda_o)$ over all reservoirs, it was (τ = 0.466, N = 47 and ρ ≤ 0.01) at the wavelength 350 nm and was (τ = 0.406, N = 47 and ρ ≤ 0.01) at the wavelength 440 nm as shown in Figure (2-18 A and B) and Table (2-6). Also, there are clear differences between reservoirs varied from high negative correlation at LCB (τ = 0.800 and 1.0) and at WIV & LSD (τ = 0.667 and 0.939), to moderate and low at CCR (τ = 0.414 and 0.072), LLD (τ = 0.200 and 0.200) and SAM (τ = 0.067 and 0.200).

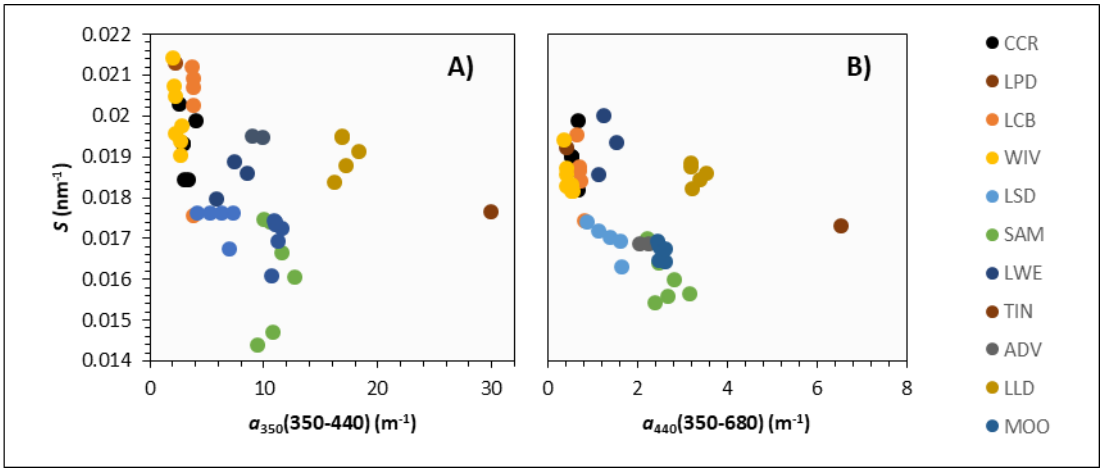

Figure 2-18: $a_{CDOM}(\lambda_o)$ versus CDOM Spectral Slope (*S*) Plotted for All Reservoirs A) Between a_{350} (m^{-1}) and *S(350-440)* (nm^{-1}) B) Between a_{440} (m^{-1}) and *S(350-680)* (nm^{-1})

Table 2-6: Kendall's Tau (τ) Correlation Coefficient and Probability Values (ρ) Between CDOM Spectral Slope (*S*) and $a_{CDOM}(\lambda_o)$ for All Reservoirs[1] A) Between a_{350}(350-440) (m^{-1}) and S_{350}(350-440) (nm^{-1}) B) Between a_{440}(350-680) (m^{-1}) and S_{440}(350-680) (nm^{-1})

		a_{CDOM}(350) and S_{350}(350-440)		a_{CDOM}(440) and S_{440}(350-680)	
	N	τ	ρ*	τ	ρ*
All	47	-0.466	<0.01	-0.406	<0.01
CCR	6	-0.414	0.251	0.072	0.845
LCB	5	-0.800	0.050	-1	<0.01
WIV& LSD	12	-0.667	<0.01	-0.939	<0.01
SAM	6	0.067	0.851	-0.200	0.573
LLD	5	-0.200	0.624	-0.200	0.624
MOO	6	-0.200	0.573	-0.600	0.091

* Correlation is significant if ρ ≤ 0.01

A possible explanation for this diversity is due to the presence of different discharge sources between the reservoirs. Also, these results are differed than what was recorded in coastal zone studies by Stedmon et al. (2000); Fichot and Benner (2011); Das et al. (2017) as an inverse high correlation relationship between $a(\lambda_o)$ and (*S*).

[1] Only samples with n>5 are shown in line with the recommendations of de Gruijter (1999) and Dekker and Hestir (2012).

To extend the analysis further, CDOM is considered the optically measurable of DOC fraction, therefore, CDOM optical characteristics could be an outcome of the amount, magnitude, nature and origin of DOC (Fichot & Benner 2011; Osburn & Bianchi 2017). According to this hypothesis, normalizing CDOM absorption by the carbon mass per volume concentration may provide a more direct link with (*S*). Measurements of DOC and $a_{CDOM}(\lambda)$ were used to find *DOC-normalized absorption coefficients*, it will be denoted as ($a^*_{DOC}(\lambda_o)$) in this work and expressed in (L.mg^{-1}.m^{-1}). A simple exponential model similar to the model derived by Fichot and Benner (2012) as shown by equation (2.5) was applied to the relationship between the absorption slopes (*S*) and the DOC-normalized absorption coefficients.

$$a^*_{DOC}(\lambda_o) = \alpha . e^{\beta . S} \qquad (2.5)$$

The results of this normalization that carried out over all stations in SEQ are shown in Figure (2-19 A and B) and illustrated in the Table (2-7).

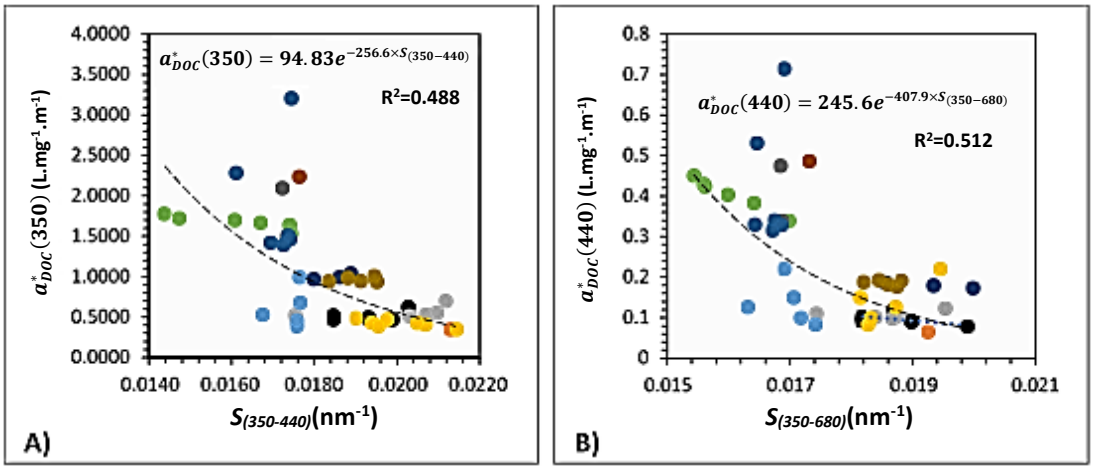

Figure 2-19: Relationship between *DOC-normalized absorption coefficients* ($a^*_{DOC}(\lambda_o)$) with CDOM Spectral Slope (*S*) Plotted for All Reservoirs; A) Between $a^*_{DOC}(350)$ and $S_{(350-440)}$ (nm^{-1}); B) Between $a^*_{DOC}(440)$ and $S_{(350-680)}$ (nm^{-1})

Table 2-7: R^2, Adjusted-R^2, Probability Values (ρ), Coefficients Associated with ($a^*_{DOC}(\lambda_o)$) Estimation Model and Model Standard Errors Between ($a^*_{DOC}(\lambda_o)$) and CDOM Spectral Slopes (*S*) Over All Reservoirs In SEQ; Upper) Between ($a^*_{DOC}(350)$) and $S_{(350-440)}$ (nm^{-1}); Lower) Between ($a^*_{DOC}(440)$) and $S_{(350-680)}$ (nm^{-1})

$a^*_{DOC}(350)$ and $S_{(350-440)}$							
					Model Coefficients		
	N	R^2	Adj.-R^2	ρ**	α	β	Std. Error of the Estimate
All	47	0.488	0.477	<0.05	94.834	-256.621	0.441
CCR	6	0.241	0.051	0.323	0.128	71.202	0.105
LCB	5	0.246	0.006	0.396	0.239	42.091	0.126
WIV& LSD	12	0.337	0.271	<0.05	3.394	-111.071	0.245
SAM	6	0.761	0.702	<0.05	2.886	-33.940	0.028
LLD	5	0.067	0.243	0.673	0.692	17.250	0.036
MOO	6	0.027	0.216	0.755	11.729	-110.381	0.378

$a^*_{DOC}(440)$ and $S_{(350-680)}$							
					Model Coefficients		
	N	R^2	Adj.-R^2	ρ**	α	β	Std. Error of the Estimate
All	47	0.512	0.502	<0.05	245.654	-407.875	0.482
CCR	6	0.391	0.239	0.184	1.278	-138.356	0.123
LCB	5	0.134	0.155	0.545	0.048	42.988	0.482
WIV& LSD	12	0.610	0.571	<0.05	20.987	-300.265	0.227
SAM	6	0.988	0.985	<0.05	6.236	-170.801	0.012
LLD	5	0.087	0.218	0.630	0.315	-42.014	0.039
MOO	6	0.450	0.194	0.688	0.001	359.428	0.371

** Correlation is significant if ρ ≤ 0.05

Results provided from using the *DOC-normalized absorption coefficient* exhibited moderated relationship with (*S*) for both ranges; (R^2 = 0.488, N = 47 and ρ ≤ 0.05) for the (350 nm) and (R^2 = 0.512, N = 47 and ρ ≤ 0.05) for the (440 nm) in the spectral slope ranges that had used (350 - 440) and (350 - 680) respectively. Also, low values of (*S*) indicative of high $a^*_{DOC}(\lambda_o)$ in the reservoirs of the study area, whereas high (*S*) values correspond to low $a^*_{DOC}(\lambda_o)$ as appeared in the plot in Figure (2-19).

Some studies (Stedmon & Markager 2001; Anderson & Stedmon 2007; Fichot & Benner 2011; Harvey et al. 2015) reported a strong relationship between CDOM absorption and slope, which it is possible through this relationship to examine the 'freshness' of the DOM. Long residence times and marked DOM degradation (the

DOM is bleached and the absorption decreases) indicates a lack of recent inputs from catchments. In contrast, Hestir et al. (2015) found a weak relationship between $a(\lambda_o)$ and (*S*) in their study to some reservoirs along the eastern part of Australia. Finally, the correlation between $a(\lambda_o)$ and (*S*) is a negative inverse relationship ranging from moderate to weak in most cases in SEQ study area. The different relations that obtained suggested that many of the reservoirs in the study area have different optical properties depends on the local discharge, chemical composition and physical properties. In addition, these relationships could be a reflection of different types of DOM sources, whether was autochthonous or allochthonous depending on the relationship between slope values and molecular weight. So, in this study the observed relationship between $a(\lambda_o)$ and (*S*) was moderate to low, while a slight improvement occurred when ($a_{CDOM(\lambda_o):DOC}$) was used and that could provide further insight information about reservoirs' DOM formation and its colour.

2.14.6 Identifying the Strength of the Regional CDOM-DOC Relationship in the SEQ Selected Reservoirs

The relationship between *DOC* concentrations with $a_{CDOM}(\lambda_o)$ as a predictor variable for DOC values was tested using univariate linear regression. This relationship was tested first for each reservoir separately provided that each reservoir achieves the minimum traditional in-situ water sampling requirements. According to de Gruijter (1999); Dekker and Hestir (2012), the minimum sampling points required for inland water (case II) observations to find the coefficient of determination (R^2) between the dependent and the independent variable(s) are five points. Thus, only 7 of 11 reservoirs in the study area met the required minimum sampling point and the rest did not, due to some reasons such as the difficulty of reaching pre-planned sample points or damage in some samples. Also, Lake Wivenhoe and Lake Somerset Dam have the same water source and are connected together, therefore both were considered as one waterbody. Then, the linear regression models were done along all the stations in the study area for the two selected a_{CDOM} at (350 nm) and (440 nm).

The results of the linear regression models between a_{CDOM} (350) and a_{CDOM} (440) with DOC are shown in Figure (2-20 A and B).

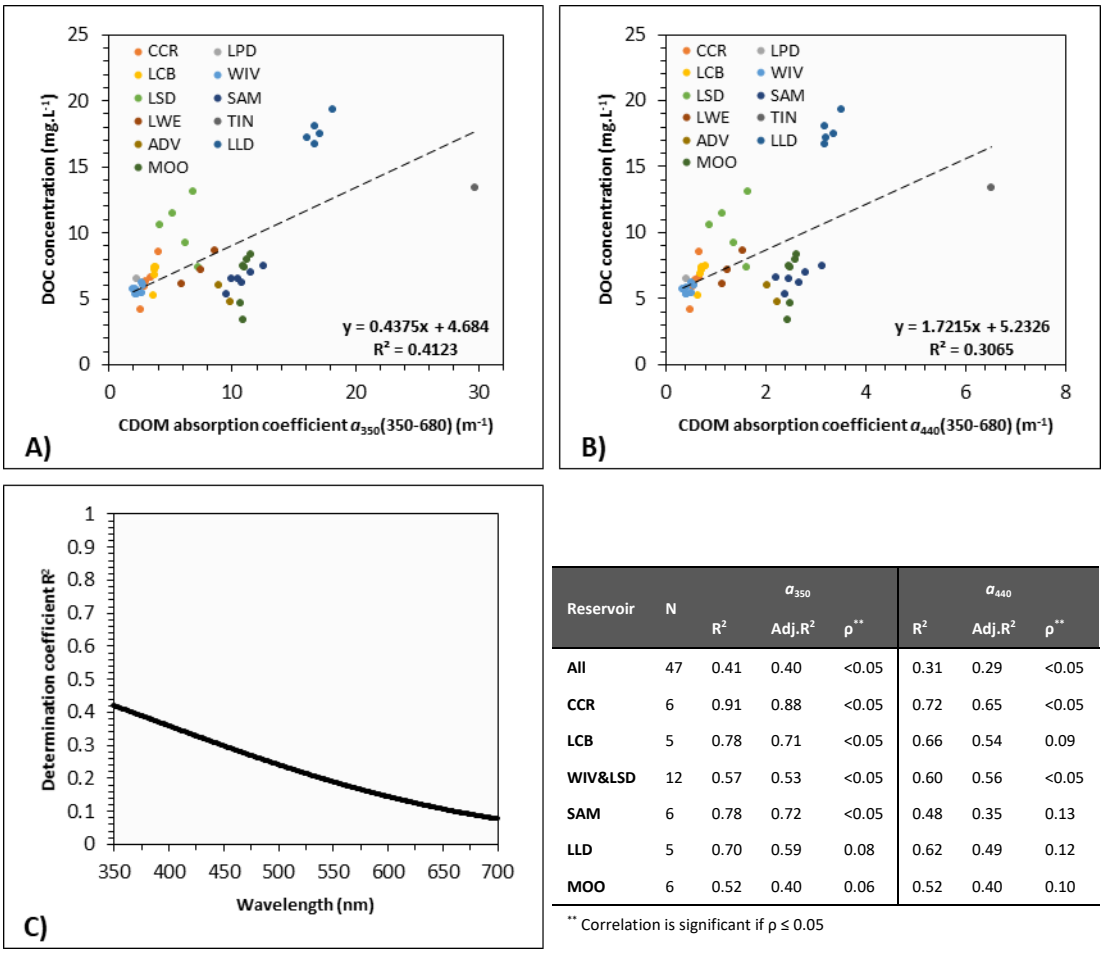

Reservoir	N	a_{350}			a_{440}		
		R^2	Adj.R^2	ρ**	R^2	Adj.R^2	ρ**
All	47	0.41	0.40	<0.05	0.31	0.29	<0.05
CCR	6	0.91	0.88	<0.05	0.72	0.65	<0.05
LCB	5	0.78	0.71	<0.05	0.66	0.54	0.09
WIV&LSD	12	0.57	0.53	<0.05	0.60	0.56	<0.05
SAM	6	0.78	0.72	<0.05	0.48	0.35	0.13
LLD	5	0.70	0.59	0.08	0.62	0.49	0.12
MOO	6	0.52	0.40	0.06	0.52	0.40	0.10

** Correlation is significant if ρ ≤ 0.05

Figure 2-20 and Table 2-8: The coefficients of determination (R^2) and probability values (ρ) for the relationship A) between a_{350} (m^{-1}) (independent variable) and DOC ($mg.L^{-1}$) (dependent variable) B) between a_{440} (m^{-1}) (independent variable) and DOC ($mg.L^{-1}$) (dependent variable) C) wavelength versus R^2 between $a(I_o)$ and DOC.

The overall results showed a poor positive correlation in the relationship between DOC concentration and CDOM absorption coefficient. The highest coefficient of determination value was (R^2 = 0.41, N = 47 and ρ ≤ 0.05) at 350 nm. While each of the reservoirs that have the minimal stations number mentioned before was significantly correlated. Relationships between DOC and CDOM absorption along all stations in SEQ and for each reservoir are presented in Table (2-8).

Different values of R^2 were recorded for each reservoir in the study area ranged from maximum (R^2 = 0.91, N = 6, ρ ≤ 0.05) to the minimum (R^2 = 0.52, N = 6, ρ = 0.06) which

are higher than overall values for all stations. Values of R^2 between CDOM absorption and DOC decrease by increasing the wavelength as shown in Figure (2-20 C).

However, differences suggest a limited decoupling between DOC and CDOM linked to regional and within reservoirs variations as confirmed by different relationships recorded among all stations in SEQ. The concentrations of CDOM controlled by local independent activities, such as photodegradation that reduce CDOM absorption without a concomitant reduction in DOC concentration (Vodacek et al. 1997). Or contrariwise, biological activity can increase concentrations of DOC without affecting CDOM concentrations.

2.15 Chapter 2 Conclusions

In SEQ a total of 47 stations in 11 water bodies (Cooby Creek Reservoir (CCR), Lake Perseverance Creek Dam (LPD), Lake Cressbrook (LCB), Lake Wivenhoe (WIV), Lake Somerset Dam (LSD), Lake Weyba (LWE), Lake Samsonvale (SAM), Tingalpa Reservoir (TIN), Advancetown Lake (ADV), Lake Moogerah (MOO) and Lake Leslie Dam (LLD)), were sampled and analysed. The results are important to understand how CDOM sources in SEQ affect CDOM absorption spectra (optical properties) varies before moving to the next objective in this work. In general, this chapter can be summarised as follows:

2.15.1 pH Data

Although pH values can naturally vary and some site-specific factors (such as regional discharges) influence pH values, the results of pH measurements categorised as good according to the Australian and New Zealand guidelines for fresh and marine water quality (2000). The majority of the measured pH values of the study sites were within the natural freshwater systems range, which is between 6.5 to 8.0 in mean except Cooby Creek Reservoir was over 8.0. However, the study sites showed a variance in the measured pH values between all the water bodies.

2.15.2 CDOM Measurements and DOC Concentrations

Analysing the spatial distribution of DOC concentrations showed high values were observed close to the inflow stations and a gradual decrease in DOC concentrations were observed in the direction of the outflow stations. While, the measured CDOM values were within the ranges of measured and documented values in Australian waters (Blondeau-Patissier et al. 2009; Campbell 2010; Kirk 2011; De Deckker & Williams 2012) and the difference is most likely due to the relative inputs from the surrounding area.

2.15.3 CDOM Specific Absorption Coefficient ($a^*_{CDOM}(\lambda_o)$)

CDOM specific absorption spectrum of the selected SEQ water bodies were described in this chapter to allow for CDOM fractions comparison in the next and if it is possible to distinguish the sources and types of CDOM. There were only a small variation in the $a^*_{CDOM}(\lambda_o)$ within each reservoir and this shows the consistency of CDOM origins.

2.15.4 CDOM Spectral Slope Coefficient (*S*)

Differences in CDOM slope values between reservoirs in SEQ study sites in the same wavelength domain attributed to the chemical composition of CDOM, where low *S* values could link to reservoirs that are rich in allochthonous CDOM while, high *S* values could link to reservoirs that are rich in autochthonous CDOM as proved by Carder et al. (1989). Thus, the composition of CDOM showed moderate variation between some reservoirs as it was coming from different sources and different soluble organic substances. The mean *S* was comparable to reported values and published data in the literature (Kirk 1976; Campbell et al. 2011a; Kirk 2011; Aryal et al. 2014; Hestir et al. 2015). No strong relationships between CDOM spectral slope and other parameters tested were verified during this study, while it improved slightly when $a^*_{DOC}(\lambda_o)$ was used and that could provide further insights information about reservoirs' DOM composition.

2.15.5 SEQ Regional CDOM-DOC Relationship

Assessing the coefficient of determination between $a_{CDOM}(\lambda_o)$ and DOC shows significant correlation within the same reservoir and the relationship is acceptable. But, the overall results were showed a poorly positive correlated relationship among all reservoirs similar to that obtained by Hestir et al. (2015) and contrast with other inland freshwater studies (Ferrari et al. 1996; Vodacek et al. 1997; Del Castillo et al. 1999; Fichot & Benner 2011). The linear relationship between $a_{CDOM}(\lambda_o)$ and DOC is complicated by environmental factors and human related contaminants mainly affected their correlation. Including both $a_{CDOM}(\lambda_o)$ and S in multiple linear regressions improved in the estimation of DOC concentration and assist in obtaining a better understanding of this relationship. We do not address CDOM-DOC seasonal changes in this study for the purpose of the next chapter to check in case that CDOM fractionations will improve the estimation of DOC for the same collected samples. The results may be positively significant and can be used in the future in remote sensing in estimating DOC accurately.

Chapter 3

The Absorption Behaviour of CDOM Fractions and Its relationship with DOC Concentration in SEQ Water bodies

3.1 Introduction

The ability to estimate DOC concentration from optical remote sensing by using satellite sensors relies on the strength of the relationship between CDOM and DOC and it is necessary to understand this relationship well (Fichot & Benner 2011). Over larger geographical areas a consistent single relationship does not exist for all inland water bodies as the CDOM properties depend on the discharge of the surrounding catchments that have their own varying properties (Vodacek et al. 1997). This inflow varies quantitatively, qualitatively and spatially which changes the dissolved organic matter composition and complicates the relationship between CDOM and DOC (Hestir et al. 2015).

The previous chapter demonstrated the relationship between CDOM and DOC was weakly positively correlated among all reservoirs. For large scale DOC estimation where there is a weak correlation with CDOM absorption, it is important first to determine how the local discharge influences the relationship before searching for an alternative way to obtain an accurate DOC concentration estimation. This can be done by investigating the major components of the natural organic matter in water.

In this chapter, the structure of the major components of the aquatic natural dissolved organic matter will be described first, with emphasis on their influence on the estimation of DOC. The DOM isolation techniques have been used in this work to fractionate and analyse the collected samples will be evaluated and compared to the standard samples of the International Humic Substances Society (IHSS). As well its focuses on the general types of the selected isolation technique that used in samples preparation. Thus, this chapter evaluates and test the hypothesis that includes CDOM major fractions in the relationship with the DOC.

3.2 Structure Characterization of NOM and its Molecular Size Distribution

The main components of natural organic matter (NOM) in the aquatic environment are divided into two categories: dissolved organic matter (DOM) and particulate organic matter (POM) or non-dissolved matter (phytoplankton* and tripton**). However, POM only represents a small amount of NOM leaving DOM as the main fraction (Ibrahim & Aziz 2014). The size limit that is used to differentiate between dissolved organic matter from particulate organic matter are shown in Figure (3-1).

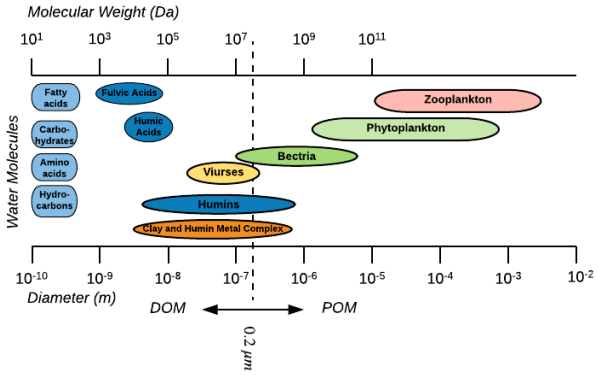

Figure 3-1: The Continuum of Sizes for Organic Matter in Seawater (Azam & Malfatti 2007)

* Photosynthetic biota.
** Inanimate particulate matter.

DOM present in natural waters mainly composed of humic substances (HS) which are hydrophobic components normally consist about 80% - 90% of DOM and sometimes up to 95% (Hansell & Carlson 2014). Unfortunately, in Australia, there is no fixed percentage data for these values that have been recorded and adopted (Campbell et al. 1992a, 1992b). The yellowish colour in natural waters is due to the appearance of the humic substances and some of the autochthonous acids from algal or phytoplankton origins, which absorb light in the blue and ultraviolet wavelength (Coble 1996; Zhang et al. 2007). Humic substances can be broken down into three major fractions according to their formative groups which are (MacCarthy et al. 1990):

a. **Humic acid:** it is the greatest allochthonous portion of the organic matter, soluble in alkaline and insoluble in acid and alcohol (Steelink 1963) and it is dark brown to black in colour. It contains free and bound phenolic hydroxyl groups (-OH), carboxyl groups (-COOH), quinone structures (aromatic rings), nitrogen (N), carbon (C) and oxygen (O) as bridge units. The hypothetical structure of humic acid is shown in Figure (3-2) (Mirza et al. 2011).

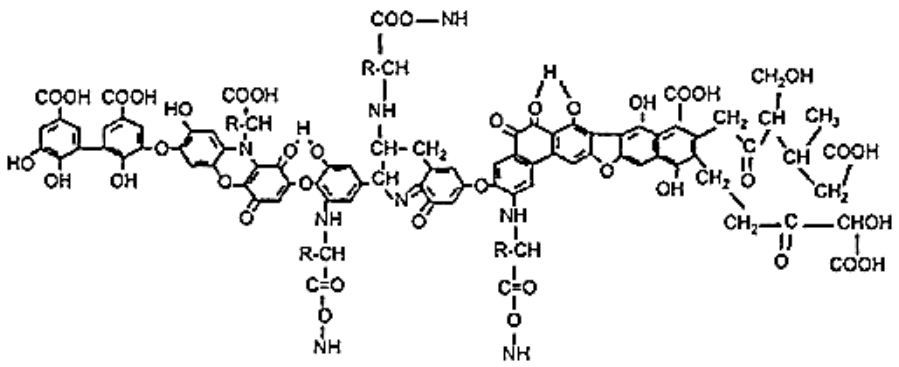

Figure 3-2: The Hypothetical Model Structure of Humic Acid (Mirza et al. 2011)

b. **Fulvic acid:** it is yellow components of humic substances soluble in strong acid pH=1 and originate from both allochthonous and autochthonous sources (Oliver et al. 1983). Its lower molecular weight contains both aromatic and aliphatic structures, both extensively substituted with oxygen-containing functional groups (Aiken et al. 1992). Fulvic acid is very active biologically and its average elemental composition consists of: Oxygen (44 – 49%), Carbon (44

– 49%), Hydrogen (3 – 5%), Nitrogen (2 – 4%). The hypothetical model structure of fulvic acid is shown in Figure (3-3) (Alvarez-Puebla et al. 2006).

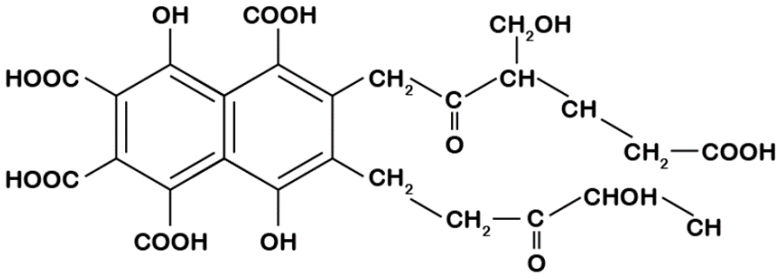

Figure 3-3: The Hypothetical Model Structure of Fulvic Acid (Alvarez-Puebla et al. 2006)

c. **Humins:** they are a black humic substance that is not soluble in water under all pH values (Rice 2001). They are inhomogeneous solids and the major components are predominantly aliphatic hydrocarbon functional groups from lipids and waxes (Hayes et al. 2017).

Table (3-1) illustrates the typical range of DOC and HS concentrations in different water systems.

Table 3-1: Typical Ranges For Dissolved Organic Carbon (DOC) Concentrations and Humic Substances Contribution (HS) in Some Aquatic Systems (Thurman 1985)

ID	Source	Humic Substances (HS) (mg/L)	Dissolved Organic Carbon (DOC) (mg/L)
1	Sea water	0.06 - 0.6	0.2 - 2.0
2	Groundwater	0.03 - 0.6	0.1 - 2.0
3	River	0.5 - 4.0	1 - 10
4	Lake	0.5 - 40	1- 50

The molecular size classification of DOM varies significantly in natural waters (Tan 2003) as an example, allochthonous fulvic acid is mostly composed of low molecular size fractions whilst allochthonous humic acid is mostly composed of high molecular size fractions (Chin et al. 1994). Therefore, molecular size fractions could be a useful indicator to distinguish between the origins of the dissolved organic matter DOM in a variety of natural waters.

Figures (3-2) and (3-3) shows the molecular structure of humic substances that they form largely from carbon, oxygen, hydrogen and nitrogen in complex carbon chains. Also, carbon atoms are distributed in the rings form as C-C-C-C and 4, 5, to 6 members connected with C, N, H and O atoms. Table (3-2) shows HS elemental composition percentages.

Table 3-2: Elemental Composition of Humic Substances (Thurman 1985)

Substances	C%	H%	O%	N%
Fulvic acids	44-49	3.5-5.0	44-49	2.0-4.0
Humic acids	52-62	3.0-5.5	30-33	3.5-5.0
Proteins	50-55	6.5-7.3	19-24	15.0-19.0
Lignin	62-69	5.0-6.5	26-33	-

On the other hand, due to the complex heterogeneity of the NOM, it can be fractionated and categorized mainly to hydrophobic and hydrophilic fractions (Aiken et al. 1992). This chemical classification depends on the relationship between the fractions' chemical groups. For example, polar groups with hetero-elements such as oxygen and nitrogen contribute to the hydrophilic character of DOM and subject to acid-base equilibria. So, their contribution to the hydrophilic character of HS is basically pH-dependent (De Wit et al. 1993). According to that, DOM hydrophobic and hydrophilic components can be further divided into three classes of acids, bases and neutrals which have different chemical groups that are shown in Figure (3-4).

Humic and fulvic acids are examples of hydrophobic acids associated with soil organic matter and residues from woody plants tissues. While sugars and carbohydrates are examples of hydrophilic groups associated with the algal activity or aquagenic compound resulting from primary productivity. Knowledge of the chemical composition of humic substances comes from degradation studies in which more complex humic substances are broken down into simpler and distinguishable substances (York & Bell 2020).

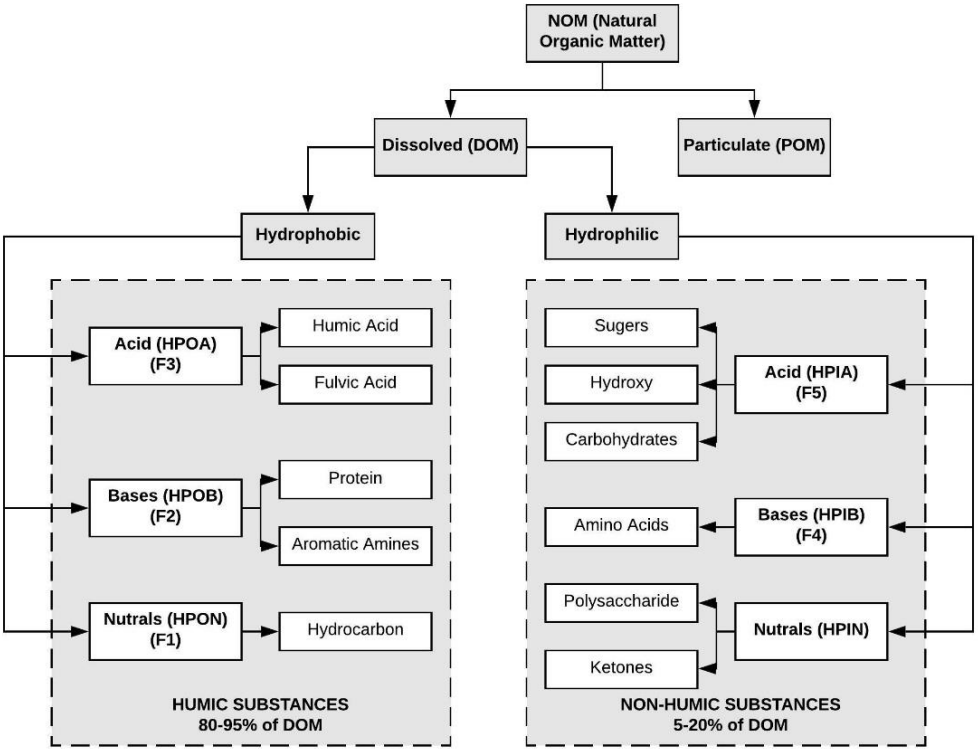

Figure 3-4: The Relationship Between NOM Fractions (Aiken et al. 1992; Averett et al. 1994; Marhaba et al. 2003)

According to Figure (3-4), the subgroups of NOM can be classified as:

1. **Fraction 1 (Hydrophobic Neutral (HPON)):** contains hydrocarbon and ether.
2. **Fraction 2 (Hydrophobic Base (HPOB)):** contains protein and aromatic amines.
3. **Fraction 3 (Hydrophobic Acid (HPOA)):** contains mainly HA and *FA*.
4. **Fraction 4 (Hydrophilic Base (HPIB)):** contains amino acids.
5. **Fraction 5 (Hydrophilic Acid (HPIA)):** contains hydroxy, carbohydrates and sugars.
6. **Fraction 6 (Hydrophilic Neutral (HPIN)):** contains ketones and polysaccharide.

Table (3-3) shows a greatly simplified list of some organic carbon compounds that have been reported in natural waters (Steinberg 2003). Numerous of these compounds in Australian natural waters are complex polymers which comprise of

large molecules made up of many repeating subunits (monomers) (Australian State of the Environment Committee 2001).

Table 3-3: Naturally Occurring Substances (Steinberg 2003)

Life Substances	Intermediates and Products Typically Found in Non-polluted Natural Waters
Proteins	NH_4^+, CO_2. HS^-, CH_4, HPO_4^{2-}, peptides, amino acids, urea, phenols, indole, fatty acids, mercaptans
Lipids	CO_2. CH_4. aliphatic acids, acetic, lactic, citric, glycolic, malic, palmitic, stearic, oleic acids, carbohydrates, hydrocarbons
Carbohydrates	HPO_4^{2-}, CO_2, CH_4, glucose, fructose, Galactose, arabinose. ribose, xylose
Porphyrins and Plant Pigments	Phytane Pristane, carotenoids Isoprenoid, alcohols, ketones, acids Porphyrins

In conclusion, in aquatic ecosystems, DOM is classified using size limit structure to HA, FA and Humins or by using chemical classification that depending on DOM chemical fractions of hydrophobic and hydrophilic groups. More than 80% of the dissolved organic material is HS contains the major and more effective components which are HA and FA. However, the general characteristics of both HA and FA from different sources are remaining remarkably similar.

3.3 Approaches of Humic Substances Isolation (Particulate and Dissolved)

Numerous studies have been performed in studying humic substances for more than 200 years; Berzelius in the early 1830 investigated humic substances isolated from natural water (Tan 2003; Mingos 2016). Researchers' attention remained slight until early 1970 where Rook (1974) reported about the potentially hazardous of humic substances interaction and association with hydrocarbons and metals in natural waters. Since then improving and developing new technologies for the measuring and isolation of proper quantities of humic substances of natural waters samples has helped researchers to achieve great outcomes.

Methods of humic substances isolation vary depending upon whether they are being extracted from soil or water. In this work, the interest is in humic substances from

natural waters to determine its composition. According to the fractionation scheme of Averett et al. (1994) Figure (3-4), humic substances in natural waters are fractionated into separate groups depending on their structural group's properties and their subject to acid-base equilibria. Therefore, isolation is an effective way to characterize HS portions and their contribution to the hydrophilic character of humic substances, and it is strongly pH-dependent (De Wit et al. 1993).

There are several different fractionation methods commonly available (Leenheer 1985; Aiken et al. 1992; Leenheer & Croué 2003; Chow et al. 2005):

1. Chemical fractionation methods (using resins (XAD-8) and (XAD-4)).
2. Physical fractionation methods (electrophoresis, ultrafiltration, size exclusion chromatography, and ultracentrifugation).

Thus, the fraction of humic substances often is required to determine its composition. As a result, a variety of humic substances isolation methods are available, but not all of these methods are reliable to aquatic humic substances studies for remote sensing purposes.

3.4 Methods of Extracting Dissolved Organic Matter Fractions of Inland Waters Samples

The proportion of DOC in surface inland waters is up to 50 mg/L (Winn 2008), but in Australian inland waters, the value is lower with the highest recorded value of 25 mg/L in West Australia (State of the Environment Committee 2011). In this work, the maximum DOC value was 19.35 mg/L has been recorded in the lake Leslie Dam (LLD). Because of the low concentration of DOC in most of the Australian inland waters, not all the fractionation methods mentioned in the previous part (§ 3.3) will give accurate results and can be applied. Therefore, the most common way of distinguishing between aquatic humic substances is to determine whether or not it is adsorbed onto a specific resin (resin adsorption method) (Thurman & Malcolm 1981; Aiken et al. 1992; Peuravuori et al. 2001; Peuravuori et al. 2002).

Resin fractionation technique is used to isolate HS in water for various subgroups of constituent that have comparable properties (Leenheer & Croué 2003; Ratpukdi et

al. 2009). This technique has been used for different reasons such as; investigate the HS composition in natural waters (surface and groundwater), investigate which HS fractions have the potential to form the disinfection by-products in water (Leenheer 1985). The accepted protocol for HS fractionation was developed by Aiken et al. (1992) and it has adopted and used by the International Humic Substances Society (IHSS) to isolate standard and reference humic and fulvic acids ((IHSS)), it is also called (Separation Column Technique (SCT)) (Peuravuori et al. 2001).

The most recent method is by fractionation HS initially into hydrophobic and hydrophilic fractions through preferential adsorption of the hydrophobic fraction (Uyguner et al. 2007). The manufacturer of the most popular adsorbent resin is Amberlite® XAD-8 and XAD-4 resin. The XAD-8 resin is used for the isolation of the hydrophobic base (HPOB), hydrophobic acid (HPOA), and hydrophobic neutral (HPON) while the hydrophilic fraction does not adsorb onto the resins, Figure (3-5) is a schematic diagram of the major resin of this isolation.

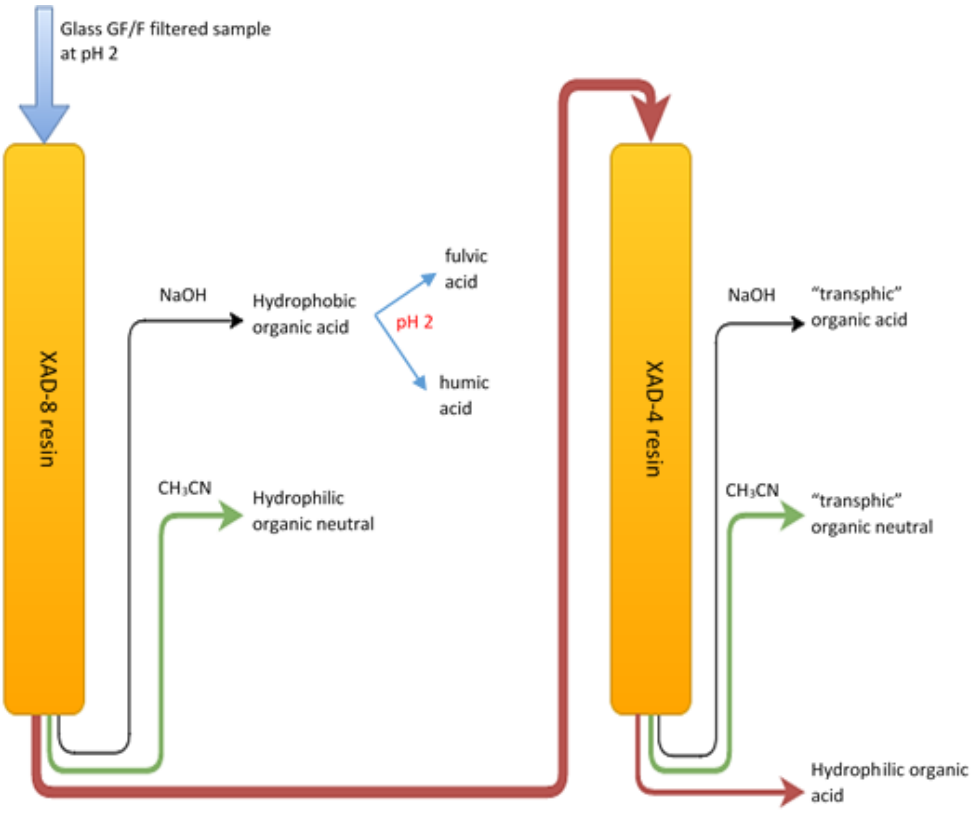

Figure 3-5: Schematic Diagram of The XAD-8 / XAD-4 Isolation Scheme. (Leenheer 1981)

Recently, a new fractionation procedure using pre-packed sorbent that can separate NOM into their fractions called solid-phase extraction (SPE) was developed. It can be defined as a sample preparation and isolation process to target components that are dissolved or suspended in a solution according to their physical and chemical properties from other compounds in the mixture. Natural organic matter fractionations are based on the polarity, acidity, alkalinity and neutrality of its components. The main steps of the SPE procedure are (Anumol & Snyder 2015):

1. **Condition Step:** it removes trapped air and activates the surface of the SPE particle. This enables the sorbent to interact more effectively with the target analyte.

2. **Equilibrate Step:** it removes the residual solvent from the conditioning step and equilibrates the sorbent in order to maximize the sorbent interacts with the target analyte.

3. **Load Step:** In this step, the sample is slowly loaded onto the sorbent. Target analyte will interact with the sorbent while contaminants will not.

4. **Wash Step:** it removes contaminants that are not bound to the sorbent. Target analytes are undisturbed and remain in the sorbent.

5. **Elute Step:** it releases the target analyte from the sorbent and the sample in this step ready for further analysis.

The SPE technique can restrict the problems associated with SCT isolation and it was chosen in this work for some advantages. It is simple and cost-effective where it uses pre-packed sorbents in cartridges that can extract NOM into six fractions of hydrophobic and hydrophilic subgroups. As well, it is less time consumption, has fewer sample setups, smaller volumes of samples and it reduces the fractionation time where it requires 6 hours only for 1L of the sample which is 4 times much faster than SCT (24 hours) (Ratpukdi et al. 2009).

3.5 Laboratory Measurements

3.5.1 SEQ Collected Samples Preparation and Isolation Using SPE Technique

Sampling, filtering and storing SEQ study area was explained in chapter 2. The collected samples were processed using the SPE method to isolate and extract DOM effective fractions to measure their optical properties and DOC concentration content. The fractionation procedure using pre-packed SPE Sorbents to separate NOM from water samples into its fractions was done in CSIRO, Ocean and Atmosphere water lab according to the developed method by Ratpukdi et al. (2009). The fractionation system consisted of five pre-packed cartridges were determined based on the nature of the work that requires extracting organic residues without any impact from cartridge's Sorbent as defined below and shown in Figure (3-6) and Table (3-4) describe their properties.

1. Three Bond Elut-ENV cartridges from Agilent Technologies: designed for the extraction of polar organic matter for high volume applications.

2. One Strata^{TM} X-C cartridge from Phenomenex®: is a strong cation-exchanger functionalized polymeric sorbent making 100% organic wash.

3. One Strata^{TM} X-AW cartridge from Phenomenex®: is a weak anion-exchanger functionalized polymeric sorbent.

Figure 3-6: SPE pre-packed cartridges.

Sorbent	Category	Sorbent mass	Unit
Bond Elut-ENV	Non-Polar	1g	20 mL
Strata^{TM} X-C	polymeric strong cation-exchanger	1g	12mL
Strata^{TM} X-AW	polymeric weak anion-exchanger	1g	12 mL

Table 3-4: Sorbent properties.

The isolation procedure has been conducted according to the method developed by Ratpukdi et al. (2009) and it requires 7-8 hours for every 1L of the sample and was done as follows (Figure (3-7)):

1. All cartridges were cleaned with 10 mL of methanol (MeOH). Then, Strata™ X-C and Strata™ X-AW cartridges were conditioned with 10 mL of 1N HCl. After that, all cartridges were rinsed with 1250-1500 mL of Millipore® milli-Q water (this volume of milli-Q water were specified after some lab tests until DOC of the rinsate was less than 0.1 mg/L).

2. One litre of water sample was adjusted to pH≈7 by using either 98% concentrated sulfuric acid (H_2SO_4) if the sample pH is higher than 7, or by using sodium hydroxide (1N NaOH) if the sample pH is less than 7, and then drawn through the first Bond Elut-ENV cartridge. The organic fraction retained in this cartridge column was defined as HPON.

3. The water sample was adjusted to pH≈10 using (1N NaOH) and loaded to the second Bond Elut-ENV cartridge. HPOB was captured in this cartridge.

4. The sample after the second Bond Elut-ENV cartridge was adjusted to pH≈2 using 98% concentrate H_2SO_4 and drawn through the third cartridge, in which HPOA was retained.

5. The water sample was drawn through the Strata™ X-C cartridge without pH adjustment. The fourth *NOM* fraction retained by it was defined as HPIB.

6. The water sample after passing in the fourth cartridge was adjusted to pH≈7 and then drawn through the Strata™ X-AW cartridge. The HPIA fraction remained in this cartridge.

7. The organic fraction that was not retained by all the five cartridges (residual) was considered as HPIN fraction.

All the water samples were drawn through all the cartridges using low vacuum pressure (was less than 5 in Hg) because the flow rate can affect the retention of certain compounds (Anumol & Snyder 2015). A 50 mL of the samples were collected in 100 mL acid-washed DURAN® glass bottles after passing through each cartridge for DOC analysis and stored in cold and dark place.

The added volumes of both 1N NaOH and H_2SO_4 that was used to change and adjust the pH for every water sample through all the fractionation procedure was recorded. Later, these recorded values were used to make a control solution (reference) with the milli-Q water dedicated for each HPIN fraction to measure its optical density.

3.5.2 Recovering CDOM Fractions

The final step of the SPE fractionation was to eluted and release the target analyte (HPON, HPOB, HPOA, HPIB and HPIA) from the cartridges. It was as follow according to Ratpukdi et al. (2009):

1. The first fraction (HPON) was eluted from the first cartridge by using 10 mL of MeOH. The isolate was evaporated to dryness over 60°C (evaporating point of Methanol (Pure et al. 1993)) using a water bath.

2. The second fraction (HPOB) in the second cartridge was extracted by adding 10 mL of 0.1 N HCl.

3. The HPOA, HPIB and HPIA fractions were eluted respectively, by passing 10 mL of 0.1 N NaOH through the third, fourth and fifth cartridges.

Each eluted fraction was redissolved in fresh Millipore® milli-Q water in the same volume amount of the original water sample. Finally, they were stored in a dark and cold place for further analysis.

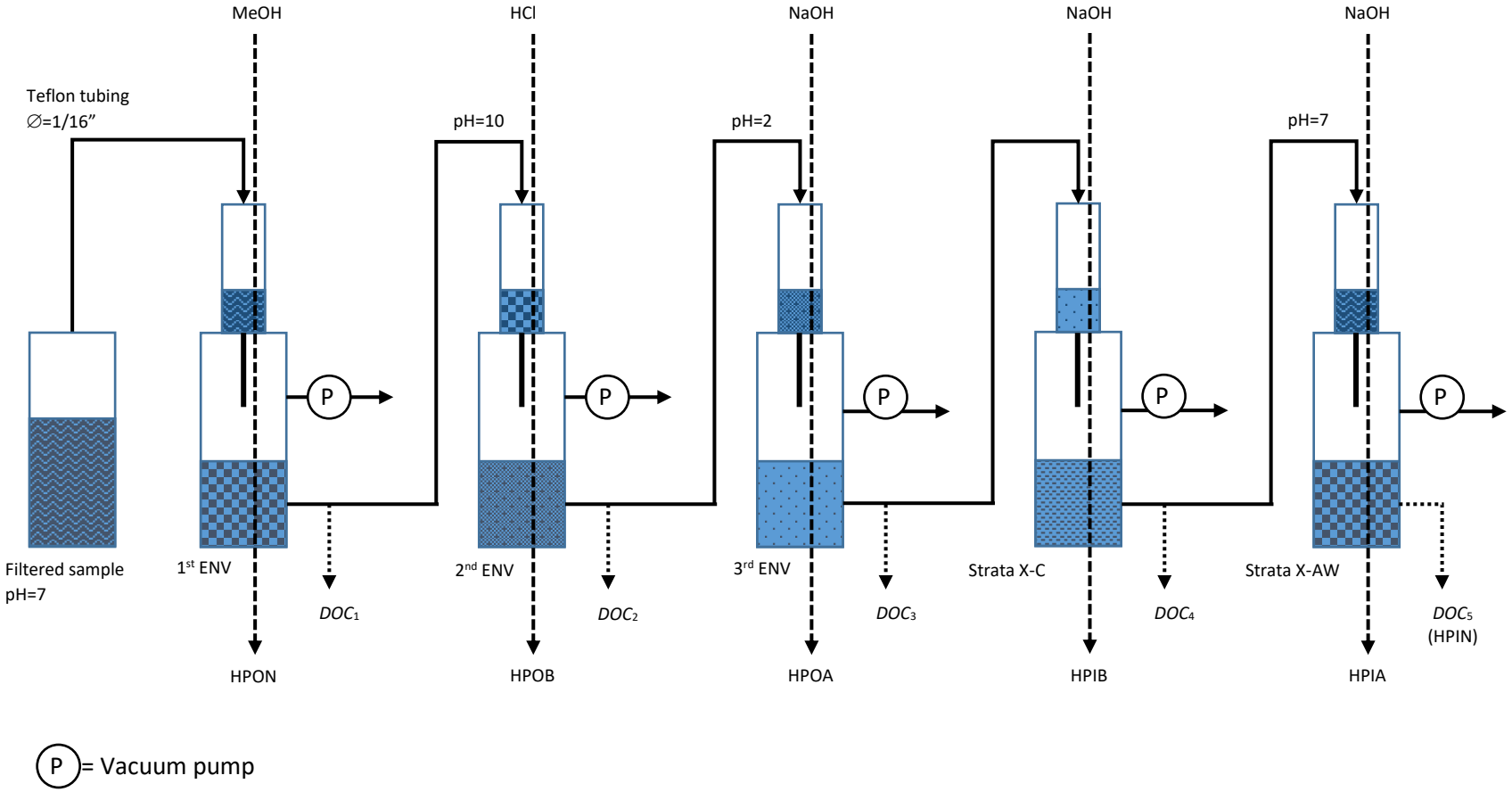

Figure 3-7: SPE Fractionation Setup and Procedure

3.5.3 DOC Concentration Measurements

All the collected samples and the isolated fractions were analysed with SHIMADZU (TOC-V CSH) TOC analyser (Figure 2-7 and Table 2-4). Thirty millilitres of samples were collected after passing through each one of the five cartridges. Then, the DOC concentration of each fraction was measured and nominated as DOC_1, DOC_2, DOC_3, DOC_4, and DOC_5 respectively. DOC values of each fraction and the sample were calculated as shown:

$$DOC_{HPON}=DOC_{sample}-DOC_1 \quad (3.1)$$

$$DOC_{HPOB}=DOC_1-DOC_2 \quad (3.2)$$

$$DOC_{HPOA}=DOC_2-DOC_3 \quad (3.3)$$

$$DOC_{HPIB}=DOC_3-DOC_4 \quad (3.4)$$

$$DOC_{HPIA}=DOC_4-DOC_5 \quad (3.5)$$

$$DOC_{HPIN}=DOC_5 \quad (3.6)$$

3.5.4 Absorption Coefficient Measurement of CDOM Fractions

The optical density (absorbance) of all the collected samples and the extracted CDOM fractions were measured with a (Cary 300 UV-Vis) (Table 2-5) double beam spectrophotometer. The measurements were done sequentially for each CDOM sample and its extracted fractions. A fresh Millipore® milli-Q water was used as a reference control solution for CDOM and fraction 1 (HPON) only, while another control solution was prepared for fraction 2 (HPOB) of diluting 10 mL of 0.1 N HCl in 1000 mL of fresh Millipore® milli-Q water. Also, a third reference control solution was prepared for fraction 3 (HPOA), fraction 4 (HPIB) and fraction 5 (HPIA) by diluting 10 mL of 0.1 N NaOH in 1000 mL of fresh Millipore® milli-Q water (Table 3-5).

Table 3-5: Types of Control Solutions Prepared for Samples Zero and Blank Scan

Control Solution (Reference)	Sample
Millipore® Milli-Q water only	CDOM and HPON fractions samples
10 mL (0.1 N HCl) + 1000 mL Millipore® milli-Q water	HPOB fractions samples
10 mL (0.1 N NaOH) + 1000 mL Millipore® milli-Q water	HPOA, HPIB and HPIA fractions samples

Preparing the reference control solution for the last fraction (HPIN), was more complicated because it required preparing a solution for each fraction of every station according to the amount of H_2SO_4 and 1N NaOH that was added to adjust fraction pH. These control solutions were used as a zero and blank scan. The blank scan measured twice and ensured no significant variations from the zero scan ther were. Then, the optical density (absorbance) of the samples measured and was taken between 200-900 nm, at 1.0 nm interval using 10 cm path length quartz cell cuvette. The absorption coefficients $a(\lambda)$ and the spectral slope coefficients (S) calculations were explained earlier in §2.12.2 and from recalling equations (2.1), (2.2) and (2.3).

3.6 Fractions Recovery Efficiency

A case study was conducted to test the applied method, its efficiency and its volume capacity of the cartridges before start with data collection from the study area, by using two sources of data. The first one was Suwannee River (SWR) natural organic matter (will be denoted as SWR-NOM); a 100 mg was purchased from International Humic Substances Society (IHSS) (Saint Paul, MIN 55108 USA) came in powder as shown in Figure (3-8 A). The reason to choose Suwannee river NOM was due to the extensive studies on it and easily comparability of results. The second source was 3 water samples (1 L per sample) were collected from a local creek in Toowoomba, QLD 4350 (Kearneys Spring Creek (KSC)) (Figure 3-8 B, C and D), samples were used from this source to test the fractionation technique and examine the recovery efficiency and volume capacity for the selected SPE cartridges.

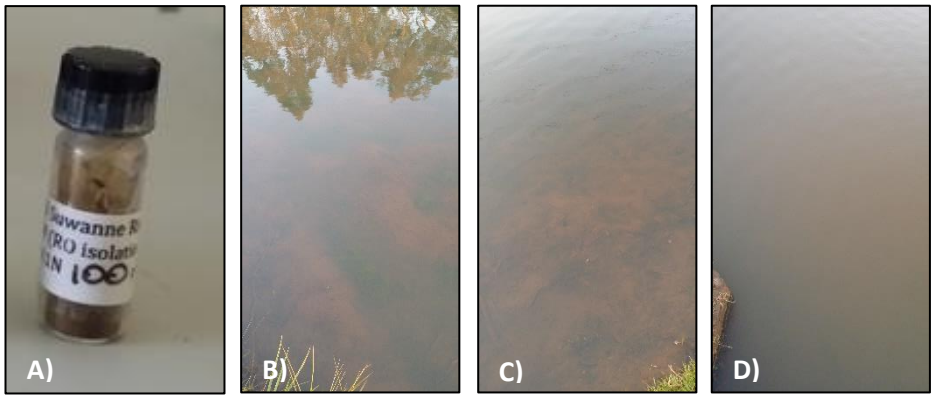

Figure 3-8: A) Suwannee River NOM (100 mg) B, C and D) Sampling Locations KSC1, KSC2 and KSC3 Respectively from Kearneys Spring Creek Location.

A 30 ± 0.25 mg of SWR -NOM powder* was redissolved in 1 L of Milli-Q water to obtain a solution. The isolation and fractionation procedures that were described earlier in this chapter were performed for all KSC samples and the SWR-NOM sample.

The elution procedure is to release target analyte from the sorbent as described earlier in §3.4, it was able to recover about 95% of SWR-NOM isolated fractions in total and this result was compared with the results obtained by Croue et al. (2000) and Ratpukdi et al. (2009). Also, the total fractions recovery result was above 98% for KSC samples when compared with the total measured DOC concentrations and absorption coefficients. No large substantial changes in the per cent distribution in SWR-NOM and KSC samples have been observed between the measured and observed values.

As for SEQ study area samples, the coefficient of determination between directly measured CDOM concentrations of the collected samples (N=27), with the calculated CDOM concentrations that obtained from the aggregate fractions' concentrations can be expressed as follows:

$$C_{CDOM} = C_{TOTAL} \tag{3.7}$$

* It was selected because it is moderated value of NOM within an acceptable range in the Australian Inland Fresh Waters.

Where,

$$C_{TOTAL} = C_{HPON} + C_{HPOB} + C_{HPOA} + C_{HPIB} + C_{HPIA} + C_{HPIN} \quad (3.8)$$

The coefficient of determination between C_{CDOM} values and C_{TOTAL} was (R^2 = 0.998, ρ ≤ 0.001 and N = 27). The results are shown in Figure (3-9 A) to give how well the SPE method has performed the minimum per cent recovery for all CDOM fractions in this study.

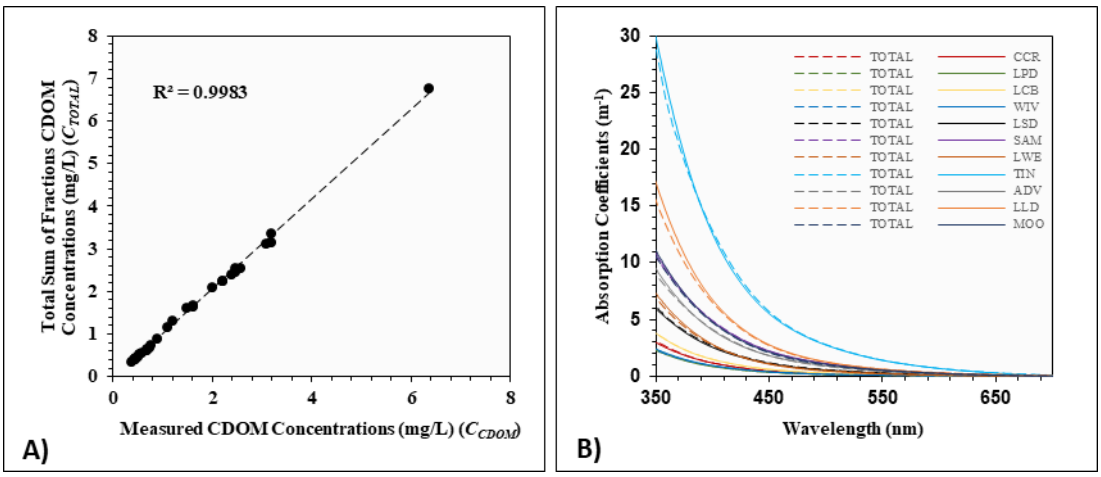

Figure 3-9: A) Coefficient of Determination between C_{CDOM} and C_{TOTAL} concentrations for (N=27), B) Curve Matching between $a_{CDOM}(\lambda)$ and $a_{TOTAL}(\lambda)$ for samples and fractions

As well, curve matching was checked between direct measured $a_{CDOM}(\lambda)$ spectrum to the samples with the calculated $a_{TOTAL}(\lambda)$ spectrum that measured for each isolated fraction, where;

$$a_{CDOM}(\lambda) = a_{TOTAL}(\lambda) \quad (3.9)$$

And,

$$a_{TOTAL}(\lambda) = a_{HPON}(\lambda) + a_{HPOB}(\lambda) + a_{HPOA}(\lambda) + a_{HPIB}(\lambda) + a_{HPIA}(\lambda) + a_{HPIN}(\lambda) \quad (3.10)$$

Where; λ = 350 to 700 nm, the matching results are shown in Figure (3-9 B), where the solid curves represent the mean spectra of $a_{CDOM}(\lambda)$ for all reservoirs, while the long dash curves represent the mean spectra of $a_{TOTAL}(\lambda)$ of the fractions.

Thus, the applied technique to extract and recover CDOM fractions in this study has proved its efficiency based on the results gained. The ratio between direct measured and the calculated values of CDOM sample and the fractions was significantly acceptable and reliable for this study.

3.7 Results and Discussions

3.7.1 Characteristics of Absorption Spectra of CDOM Fractions and Their Specific Absorption Coefficients

Figure (3-10) shown the laboratory analysis results of measuring the absorption spectrum curves of the six isolated fractions and their total absorption curves within the selected wavelengths from 350 nm to 700 nm for some stations in the study sites. While the full laboratory analysis results figures of all isolated stations (N = 28) are shown in appendix (B). Fractionation was not implemented for all the collected 47 samples because of the limited amount of SPE cartridges, therefore 28 stations were selected from the total (Table (3-6)). Reservoirs that have 3 stations and less were all fractionated, while which have more than 3, half of them have been fractionated.

Table 3-6: Numbers of CDOM Samples and the Fractionated Selected Samples from SEQ Water Bodies.

	Reservoir	Abbreviation	No. of CDOM Samples	No. of Fractionated Samples
1	Cooby Creek Reservoir	CCR	6	3
2	Lake Perseverance Dam	LPD	1	1
3	Lake Cressbrok	LCB	5	2
4	Lake Wivenhoe	WIV	7	5
5	Lake Somerset Dam	LSD	5	3
6	Lake Samsonvale	SAM	6	3
7	Lake Weyba	LWE	3	3
8	Tingalpa Reservoir	TIN	1	1
9	Advancetown Lake	ADV	2	2
10	Lake Leslie Dam	LLD	5	2
11	Lake Moogera	MOO	6	3
			total 47	total 28

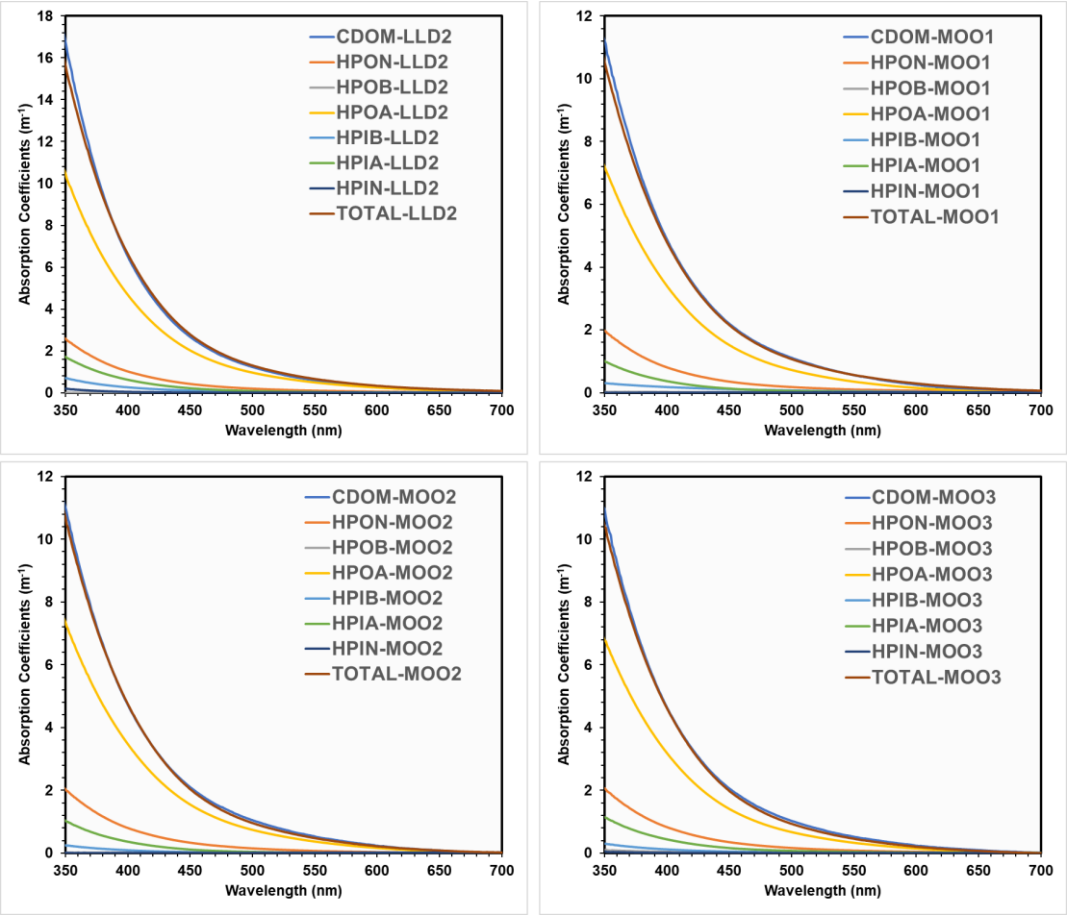

Figure 3-10: CDOM and its fractions' absorption spectra curves of some SEQ selected samples (LLD2, MOO1, MOO2 and MOO3) (the rest figures for the other samples are in Appendix (B)).

It is noticeable from the Figure (3-10) there were significant variations between the absorption curves of the isolated fractions. The HPOA fraction has the highest absorption ability in all samples with a very large percentage. Its absorption values ranged from 0.93 m^{-1} in Lake Wivenhoe to reach 19.15 m^{-1} in Lake Tingalpa at 350 nm. Then, the second-largest absorption values were for the HPON fraction in varying proportions for all samples ranged between 0.53 m^{-1} in Lake Wivenhoe to 5.94 m^{-1} in Lake Tingalpa at 350 nm. While the absorption amounts of the other fractions were low ranging between 0.0006, 0.007 and 0.005 m^{-1} to 0.08, 1.08 and 0.18 m^{-1} for the isolated fractions HPOB, HPIB and HPIN sequentially which decays and approaches zero in the short wavelengths. Figure (3-11 A) shown the specific absorption coefficients $a^*(440)$ obtained from equation (2.3) for the most influential and major isolated fractions (HPON, HPOA and HPIA) which only have the highest spectral absorptivity. Also, Figure (3-11 B) shown their linearization fit of the natural log-transformed.

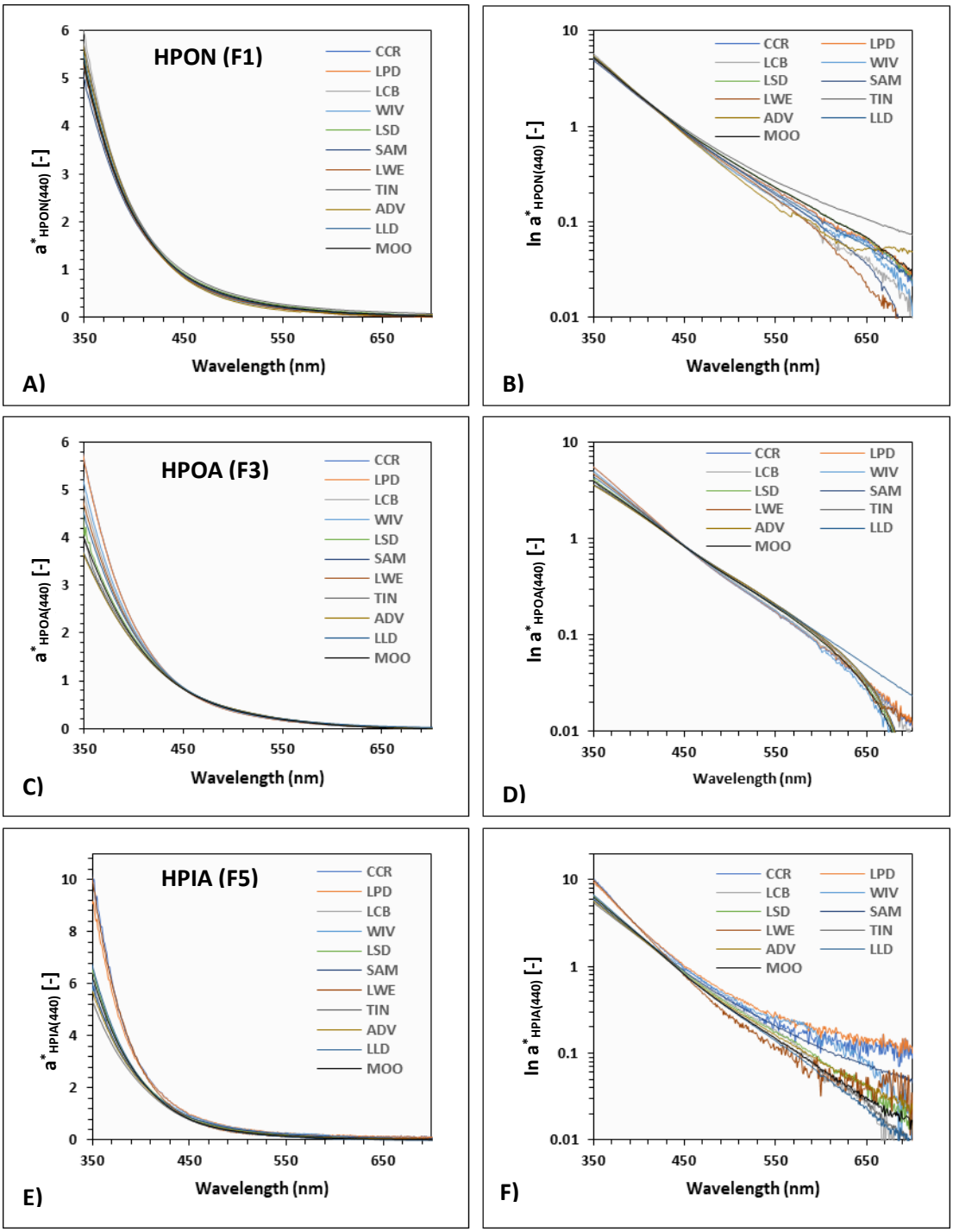

Figure 3-11: A, C & E) The Mean Specific Absorption Spectra of HPON, HPOA and HPIA Fractions Respectively for Each Reservoir Along the Study Area Sites in SEQ. B, D & F) Natural Log-Transformed Mean Specific Absorption Spectra of HPON, HPOA and HPIA Fractions Respectively for Each Reservoir in the Study Area.

The isolated HPOB, HPIB and HPIN fractions, their specific absorption coefficients were unreliable due to their low contribution to the total CDOM absorption and the type of their components. In Figure (3-11 A), the variation is almost non-existent in the HPON absorption and hence one mean spectrum is sufficient to cover the entire fraction. The variation in the absorption increased in the HPOA fractions (Figure (3-11 C)), but it is possible to use one single mean spectrum to cover all the fractions as well. In Figure (3-11 E) there are some anomalous spectrums for CCR, LPD and LWE reservoirs that could represent valid measurements of minor secondary sources.

A large number of fractions could be complex to deal with in the optical model so in order to achieve a satisfactory degree of DOC estimation and not neglect any CDOM fraction that has weak absorption (e.g. HPOB, HPIB and HPIN) but may contain DOC, the results have been pooled to what are called hydrophobic (HPO) and hydrophilic (HPI) portions as a function of humic and non-humic substances rather than the previous explanation using polarity and acid-base characterization. Figure (3-12) shows the absorption spectra curves between 350-700 nm of hydrophobic fractions that obtained from the aggregated measured absorption curves of HPON, HPOB and HPOA and for hydrophilic fraction which were obtained in the same way but from HPIB, HPIA and HPIN absorption curves for SEQ study area samples. Noticeably, the hydrophobic portion was the major absorption fraction dominated with 79% to 85% ± 1% from the total absorption of CDOM samples, whereas, hydrophilic portion contributed only in 22% to 14% ± 1% from CDOM total absorption.

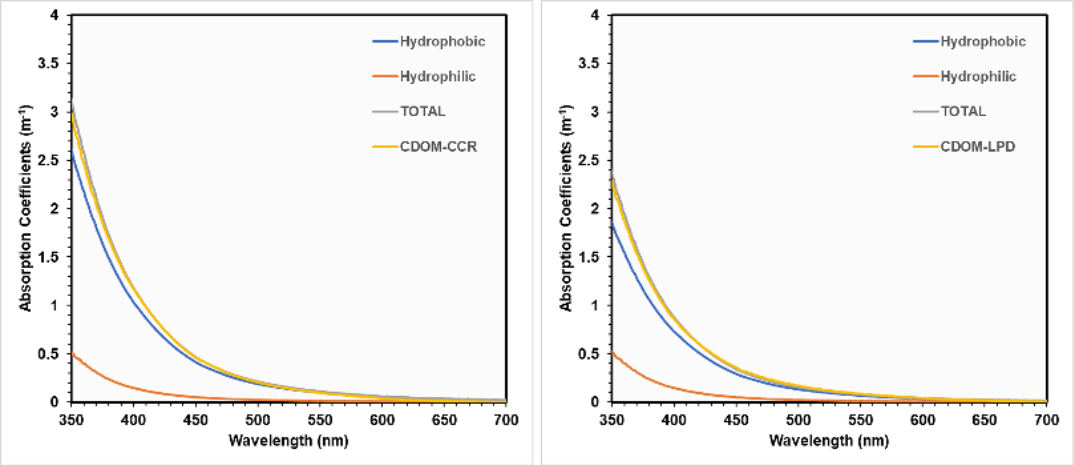

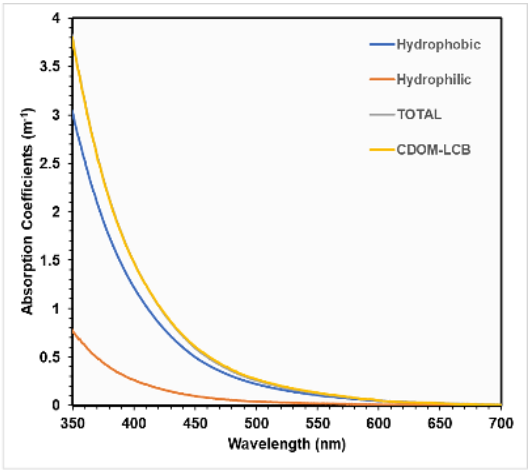
Hydrophobic
Hydrophilic
TOTAL
CDOM-LCB
Absorption Coefficients (m-1)
Wavelength (nm)

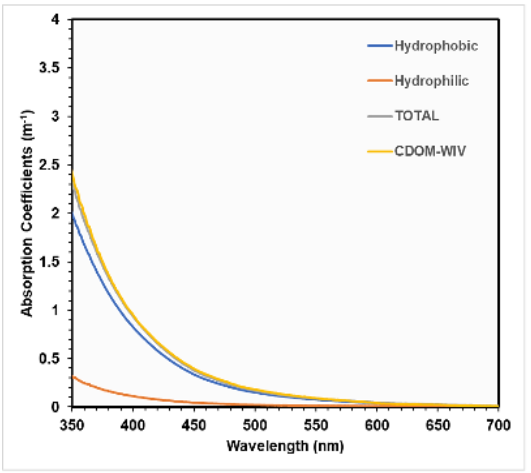
Hydrophobic
Hydrophilic
TOTAL
CDOM-WIV
Absorption Coefficients (m-1)
Wavelength (nm)

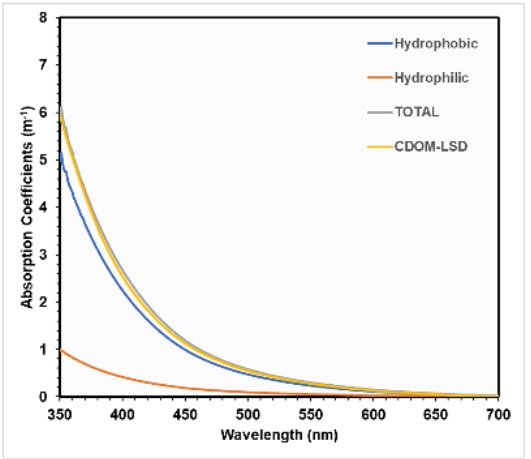
Hydrophobic
Hydrophilic
TOTAL
CDOM-LSD
Absorption Coefficients (m-1)
Wavelength (nm)

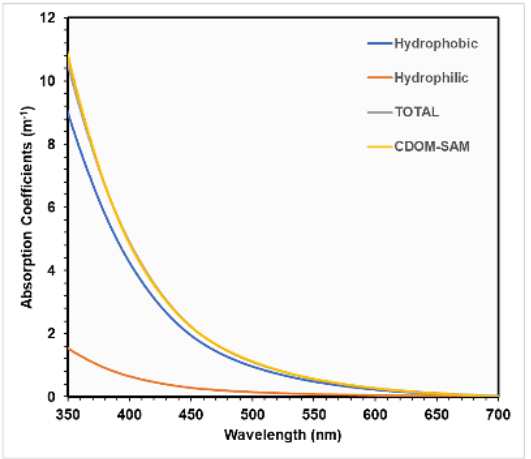
Hydrophobic
Hydrophilic
TOTAL
CDOM-SAM
Absorption Coefficients (m-1)
Wavelength (nm)

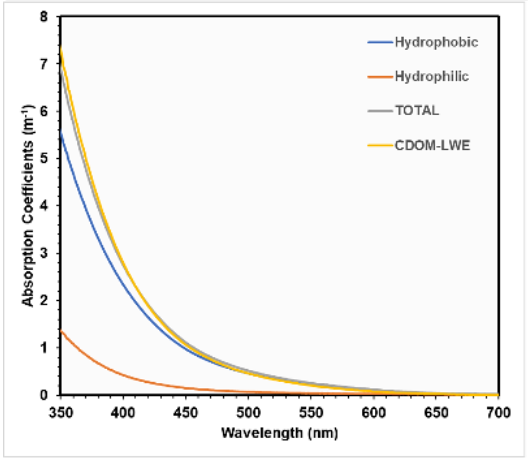
Hydrophobic
Hydrophilic
TOTAL
CDOM-LWE
Absorption Coefficients (m-1)
Wavelength (nm)

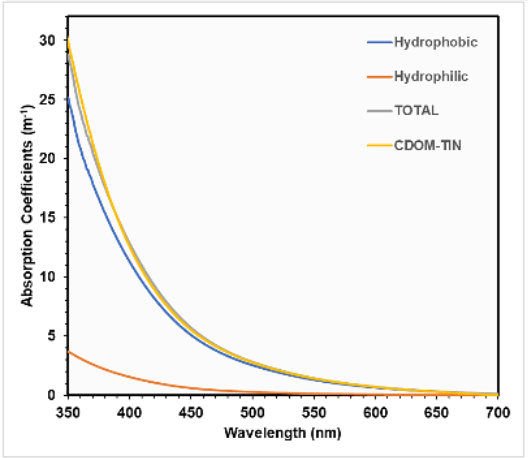
Hydrophobic
Hydrophilic
TOTAL
CDOM-TIN
Absorption Coefficients (m-1)
Wavelength (nm)

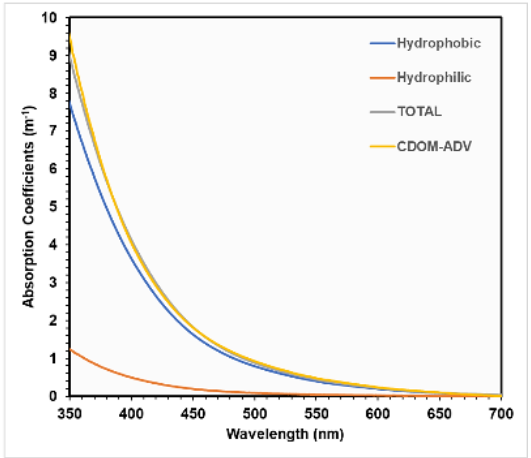
Hydrophobic
Hydrophilic
TOTAL
CDOM-ADV
Absorption Coefficients (m-1)
Wavelength (nm)

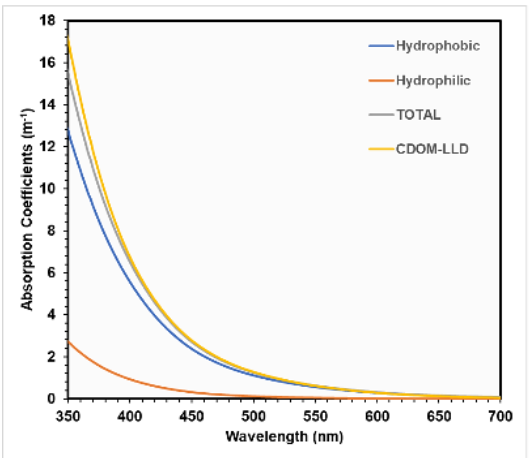
Hydrophobic
Hydrophilic
TOTAL
CDOM-LLD
Absorption Coefficients (m-1)
Wavelength (nm)

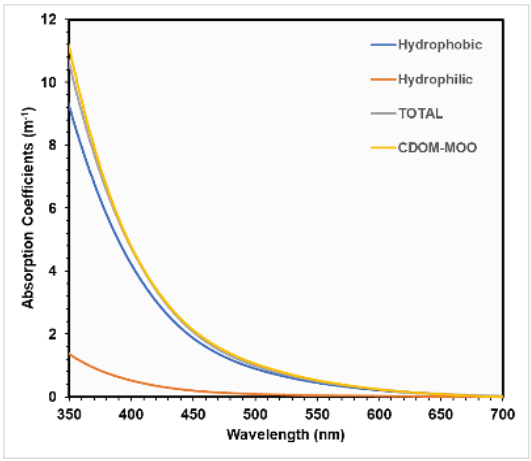

Figure 3-12: Absorption Spectra of Hydrophobic and Hydrophilic from HPON, HPOB, HPOA, HPIB, HPIA, and HPIN Measured CDOM Fractions for each SEQ Selected Samples.

3.7.2 Spectral Slope Values (*S*) of the Isolated CDOM Fractions

To analyse the absorption spectra of the fractionated CDOM samples; spectral slope values (S) and the coefficients $a_{HPON}(\lambda_O)$, $a_{HPOB}(\lambda_O)$, $a_{HPOA}(\lambda_O)$, $a_{HPIB}(\lambda_O)$, $a_{HPIA}(\lambda_O)$ and $a_{HPIN}(\lambda_O)$ were determined at (440 nm) using equation (2.3) as before. As a comparison between the fractions, the results of the $a(\lambda_o)$ of CDOM and the fractions are shown in Figure (3-13).

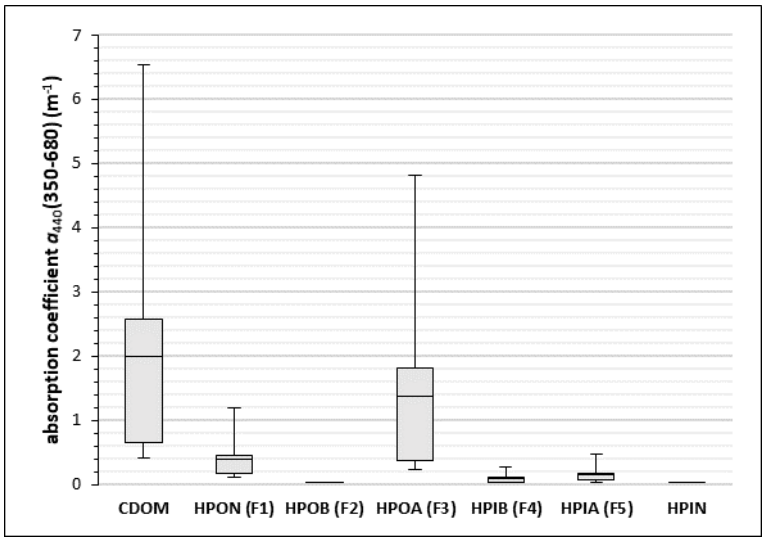

Figure 3-13: Box-and-whisker plot shows the (minimum, first quartile, mean, third quartile and maximum) values of $a(\lambda_o)$ for CDOM fractions compared to CDOM at 440 nm.

It is clear that the absorption values of the fractions HPOB, HPIB and HPIN are limited and close to zero, especially the second fraction HPOB and the last fraction HPIN. In contrary, the dominant fraction was HPOA in both reference wavelengths in varying absorption similar to the same variance of the collected CDOM samples, it was ranged from 1.252 – 18.645 (m^{-1}) measured at 350 nm and ranged from 0.231 – 4.822 (m^{-1}) measured at 440 nm.

Calculation the spectral slope values of the isolated major CDOM fractions in two different ranges (350-440 nm) and (350-680 nm) revealed different trends, as shown in Table (3-7). In the (350-440 nm) range, the minimum (*S*) value was (0.0123 nm^{-1}) recorded for the HPOA fraction in Advancetown Lake, and the maximum (*S*) value recorded for Lake Perseverance Creek Dam for the fraction HPIA and was (0.0262 nm^{-1}). While in the range (350-680 nm), the minimum (*S*) value calculated for Advancetown Lake as well (0.0144 nm^{-1}) but the maximum value was (0.0295 nm^{-1}) in the HPIA fraction for Lake Samsonvale.

Table 3-7: The Mean Spectral Slope Values (*S*) of the Major CDOM Fractions of the Selected SEQ Water Bodies.

	S_{350}(350-440)					S_{440}(350-680)				
Reservoir	HPON Slope (*S*) (nm^{-1})	HPOA Slope (*S*) (nm^{-1})	HPIA Slope (*S*) (nm^{-1})	HPO Slope (*S*) (nm^{-1})	HPI Slope (S) (nm-1)	HPON Slope (*S*) (nm^{-1})	HPOA Slope (*S*) (nm^{-1})	HPIA Slope (*S*) (nm^{-1})	HPO Slope (S) (nm-1)	HPI Slope (S) (nm-1)
CCR	0.0196	0.0188	0.0243	0.0180	0.0252	0.0192	0.0191	0.0235	0.0187	0.0256
LPD	0.0186	0.0186	0.0262	0.0179	0.0252	0.0182	0.0191	0.0245	0.0188	0.0256
LCB	0.0213	0.0175	0.0225	0.0189	0.0238	0.0200	0.0175	0.0206	0.0181	0.0215
WIV	0.0180	0.0178	0.0225	0.0174	0.0271	0.0182	0.0180	0.0195	0.0180	0.0213
LSD	0.0193	0.0153	0.0210	0.0175	0.0181	0.0183	0.0158	0.0207	0.0164	0.0173
SAM	0.0180	0.0126	0.0199	0.0124	0.0163	0.0265	0.0218	0.0295	0.0152	0.0176
LWE	0.0182	0.0161	0.0252	0.0160	0.0236	0.0182	0.0171	0.0256	0.0175	0.0238
TIN	0.0198	0.0147	0.0174	0.0201	0.0176	0.0189	0.0150	0.0188	0.0158	0.0180
ADV	0.0175	0.0123	0.0185	0.0127	0.0180	0.0189	0.0144	0.0194	0.0155	0.0188
LLD	0.0192	0.0153	0.0210	0.0156	0.0219	0.0186	0.0166	0.0211	0.0170	0.0215
MOO	0.0190	0.0136	0.0195	0.0140	0.0195	0.0182	0.0154	0.0205	0.0160	0.0197

The slope (*S*) of the hydrophobic and hydrophilic components for SEQ area as shown in the previous Table (3-7), showed that HPI fraction has high slope values, in general, ranged between (0.0163 – 0.0271 nm^{-1}) with an average value (0.0215 nm^{-1}). In contrast, the HPO fraction slope values for SEQ area have distributed between a minimum low value (0.0124 nm^{-1}) to a maximum high value (0.0201 nm^{-1}) in the spectral range (350-440 nm) with an average value (0.0164 nm^{-1}). This distribution attributed to the compounds of these components and their molecular weight, besides their aromatic content (carbon rings) (Yee et al. 2009). Because of the very low absorption values for HPOB, HPIB and HPIN and their DOC content, their $a^*(\lambda)$ spectra appeared distorted and (*S*) does not express on their expected spectral shape, therefore they were neglected. This oscillating will be explained in the section of the relationship between DOC and fractions absorption.

3.7.3 Chemical Composition Effect in the Relationship Between Fractions Absorption Coefficients and their Slope Values

The spectral slope parameter describes the spectral dependence of the absorption coefficient; therefore, it is important to explore if $a(\lambda_o)$ of the isolated fractions at a specific wavelength (350 nm and 440 nm) and (S) are coupled or not. Also, it is important to know if a fractions chemical composition has a negative effect on this relationship to determine its extent in the sample. The same statistical tests that used in the previous chapter to examine the correlation between $a(\lambda_o)$ and (S) in the samples have been used for the fractions as well. Test results from using the non-parametric Kendall's tau correlation coefficient are shown in Figure (3-14) and Table (3-8).

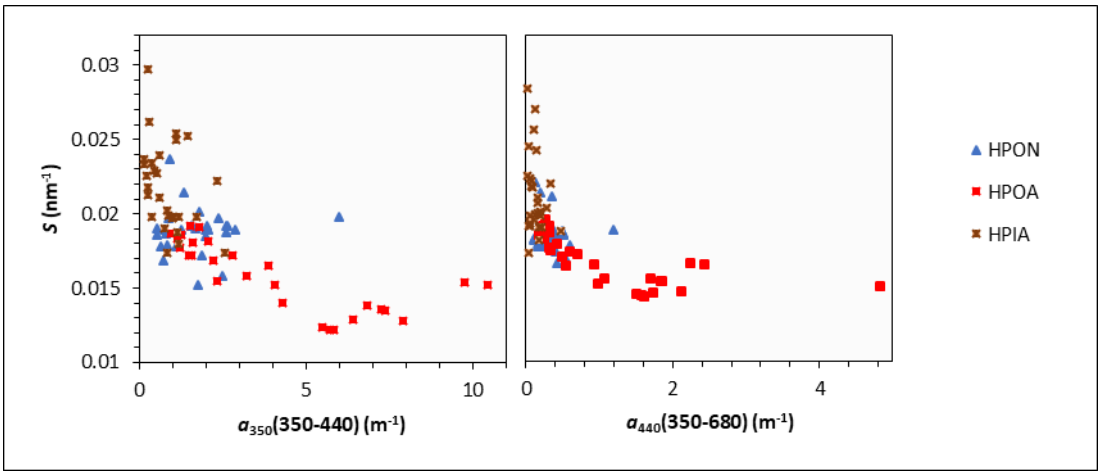

Figure 3-14: Scatter plot to the major absorption fractions (HPON, HPOA and HPIA) with (*S*) left) at a_{350} (m^{-1}) and *S(350-440)* (nm^{-1}), right) at a_{440} (m^{-1}) and *S(350-680)* (nm^{-1})

Table 3-8 for Kendall's tau (τ) correlation coefficients and probability values (ρ) between (S) and $a(\lambda_o)$ for all fraction.

		a_{350} and S_{350}(350-440)		a_{440} and S_{440}(350-680)	
	N	τ	ρ*	τ	ρ*
HPON (F1)	28	0.338	<0.01	0.377	<0.01
HPOB (F2)	27	0.028	0.011	0.036	0.084
HPOA (F3)	28	-0.608	<0.01	-0.601	<0.01
HPIB (F4)	28	-0.333	0.013	0.176	<0.01
HPIA (F5)	28	-0.339	<0.01	0.117	0.393
HPIN (F6)	27	0.311	0.023	0.071	0.612

* Correlation is significant if ρ ≤ 0.01

The outcomes of testing the relationship between $a(\lambda_o)$ and (*S*) for CDOM samples explained in the previous chapter, briefly there is moderate negative correlation along all CDOM samples (τ = 0.446, N = 46 and ρ ≤ 0.01) at 350 nm and (τ = 0.406, N = 46 and ρ ≤ 0.01) at 440 nm. But the examined CDOM fractions shoed different relationships that can easily be noticed in Figure (3-14) in the two selected ranges. Only HPOA fraction showed a high correlation between the absorption coefficient with the spectral slope is (τ = 0.608, N = 27 and ρ ≤ 0.01) at 350 nm and is (τ = 0.601, N = 27 and ρ ≤ 0.01), whereas the other fractions did not show any correlation significantly relationship except HPON fraction.

It is known that both the amount and composition of DOM affect the spectral properties of CDOM, therefore normalizing the major DOC content and the most CDOM stable fractions (Leenheer et al. 2000) by the carbon mass per volume may provide a good direct link with (*S*) and it will be denoted as ($a^*_{DOC}(\lambda_o)$). Table (3-9)

and Figure (3-15) illustrates the non-linear relationship results between $a^*_{DOC}(\lambda_o)$ measured at 350 nm and 440 nm that normalized to the DOC concentration with (*S*).

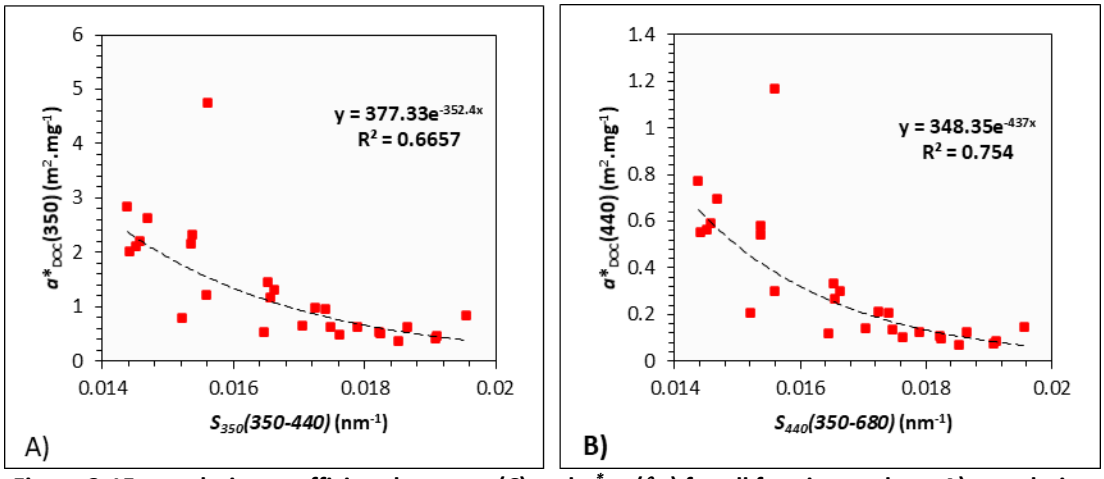

Figure 3-15 correlation coefficient between (*S*) and $a^*_{DOC}(\lambda_o)$ for all fractions, where A) correlation between $a^*_{DOC}(350)$ (m^{-1}) and S(350-440) (nm^{-1}) for fraction HPOA only. B) correlation between $a^*_{DOC}(440)$ (m^{-1}) and S(350-680) (nm^{-1}) for fraction HPOA only.

The striking relationship obtained between $a^*_{DOC}(\lambda_o)$ and *S* for HPOA fraction is an excellent indicator of the DOC-normalised absorption coefficient in this environment. Also, figures (3-15 A and B) are highly similar to Fichot and Benner (2012) figure (3B).

Table 3-9 Kendall's tau (τ) correlation coefficient and probability values (ρ) between (*S*) and $a^*_{DOC}(\lambda_o)$ for all fractions.

		$a^*_{DOC}(350)$ and $S_{350}(350\text{-}440)$		$a^*_{DOC}(440)$ and $S_{440}(350\text{-}680)$	
	N	τ	ρ*	τ	ρ*
All	46	0.405	<0.01	0.494	<0.01
HPON (F1)	27	0.014	0.917	0.168	0.219
HPOB (F2)	27	0.425	<0.01	0.248	0.070
HPOA (F3)	27	0.613	<0.01	0.658	<0.01
HPIB (F4)	27	0.151	0.269	0.419	<0.01
HPIA (F5)	27	0.145	0.288	0.048	0.723
HPIN (F6)	27	0.413	<0.01	0.009	0.950

* correlation is significant if ρ ≤ 0.01

It is noted from the Table (3-9) that the same results that explained in the previous chapter in the §2.14.5 for CDOM samples have not been obtained for the isolated CDOM fractions. Where no change or improvement observed in the relationship between $a^*_{DOC}(\lambda_o)$ and (*S*) for the fractions. A possible explanation could be back to the carbon content in each fraction and its stability where it is proportional with it which will be interpreted later in this chapter because it is related to with DOC content.

3.7.4 Spectral Slope (*S*) and Molecular Weight (MW) of the Isolated Fractions

In Figure (3-11), there are different specific absorption spectra obtained for collected SEQ samples. There are visible differences between them because of their different composition and different sources. Helms et al. (2008), De Haan et al. (1982) and Green, S. A. and Blough, N. V. (1994) argues that the slope value (*S*) of the exponential spectra curve of CDOM can be an indicator for the molecular weight of the optically measurable substances that present in water. Two relationships have been identified:

1. There is an inverse relationship between (*S*) and molecular weight.
2. Fulvic acid has a higher (*S*) value than humic acid in the sample.

From Table (3-7) both HPON and HPIA have high spectral slope values, where the lowest values calculated was 0.0182 (nm^{-1}) and 0.0188 (nm^{-1}) respectively. These high values may back to the composition structure of these fractions which consist mostly of hydrocarbon and carbohydrate molecules that have low molecular weight as shown in Figure (3-1). Back again to Table (3-7), results exhibited of (*S*) for the HPOA fraction ranged from 0.144 (nm^{-1}) to 0.218 (nm^{-1}). The general trend to explain this gradual rise from low to high values in (*S*) is probably linked to being this fraction a mixture of HA and FA. Humic acid molecules are relatively larger than fulvic acids, and also contain relatively more aromatic carbon rings according to the previous explanation. So, low (*S*) values could indicate that HA is dominated in this fraction and high (*S*) values could be related of being FA dominated in this fraction. Therefore, for the isolated CDOM fraction the spectral slope value could be an indicator for the molecular weight of its constituent components and this finding will use in the next chapter.

3.7.5 Absorption Percentages in CDOM Water Samples of the Isolated Fractions Obtained from Using SPE Technique

The results of CDOM samples fractionation that obtained by SPE technique in this work and measured optically showed a good approximation to the various sub-groups of aquatic dissolved organic matter that illustrated in Figure (3-4). The isolated CDOM fractions are distributed in different proportions according to their absorption coefficients at 440 nm compared to the total measured as illustrated in Figure (3-16 A and B). As CDOM concentration can be expressed using the absorption coefficient at some reference wavelength, typically 350 nm or 440 nm (Stedmon et al. 2000; Kirk 2011), therefore, these results possible to represents the concentrations too.

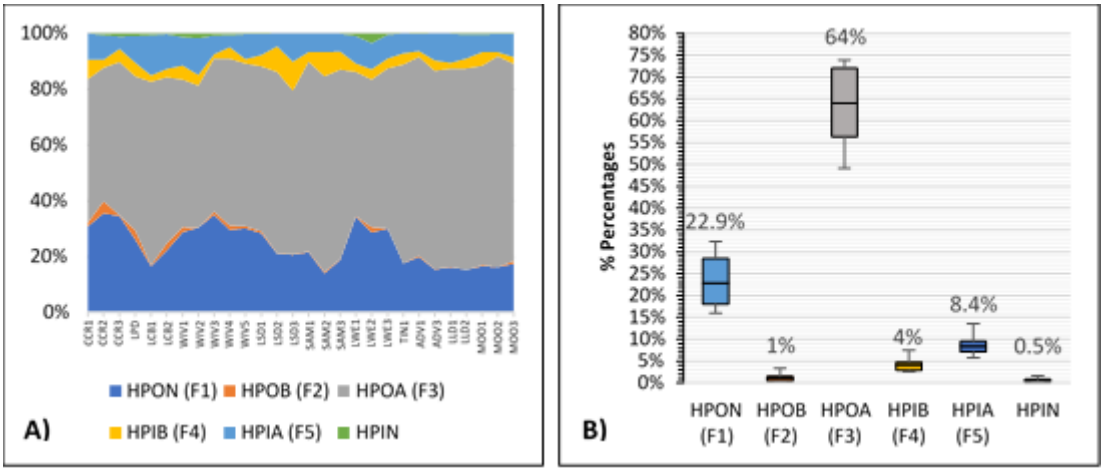

Figure 3-16: A) Chart Shows the Percentage Distribution of The Concentration of Each Fraction Per Station (N=28) and Highlight the Magnitude of Change to The Percentage at Every Station. B) MIN, MAX and Average Percentage of Each Fraction.

CDOM composition of the hydrophobic part has an average percentage of approximately 88% distributed as follows: 23%, 1% and 64% for HPON, HPOB and HPOA fractions, respectively. While, the hydrophilic part percentage on average was approximately 13% dispersed between HPIB, HPIA and HPIN fractions as 4%, 8.4% and 0.5%, respectively. Table (3-10) summarizes the absorption percentage of each fraction per station and the maximum and minimum percentage.

Table 3-10: The SPE Fractionation Percentages of HPON, HPOB, HPOA, HPIB, HPIA and HPIN in the Collected SEQ CDOM Samples (N=28).

	% OF ABSORPTIONS OF THE FRACTIONS at 440					
Sample	**HPON (F1)**	**HPOB (F2)**	**HPOA (F3)**	**HPIB (F4)**	**HPIA (F5)**	**HPIN**
CCR	32.3%	2.1%	49.2%	4.6%	7.6%	0.7%
LPD	26.0%	3.4%	54.9%	4.9%	9.4%	1.0%
LCB	19.2%	1.5%	62.8%	2.5%	13.5%	0.4%
WIV	30.8%	1.4%	56.0%	3.1%	8.4%	0.8%
LSD	24.0%	0.5%	64.1%	7.4%	5.7%	0.1%
SAM	18.5%	0.4%	69.2%	6.2%	6.6%	0.1%
LWE	32.2%	0.8%	56.7%	3.6%	9.6%	1.7%
TIN	18.2%	0.1%	73.9%	4.2%	7.4%	0.0%
ADV	17.9%	0.3%	72.5%	3.0%	8.1%	0.1%
LLD	16.0%	0.1%	73.1%	2.9%	9.6%	0.3%
MOO	16.4%	0.6%	71.4%	2.9%	6.9%	0.3%
Mean	22.9%	1.0%	64.0%	4.1%	8.4%	0.5%
Standard Error	1.9%	0.3%	2.6%	0.5%	0.6%	0.2%
Min	16.0%	0.1%	49.2%	2.5%	5.7%	0.0%
Max	32.3%	3.4%	73.9%	7.4%	13.5%	1.7%

The HPOA fraction present in all the isolated samples has the highest absorption percentage ranged from 49% in the fractions isolated from CCR stations (N = 3) to 74% in the fractions isolated from TIN station (N = 1). While HPOB and HPIN fractions have the minimum concentration percentages ranged between 1% to 0.5% on average for both respectively. Comparison of obtained values to literature fractions compositions ranges showed it was similar to Ratpukdi et al. (2009), Ibrahim and Aziz (2014), (Marhaba et al. 2003) and others. In general, HPOA fraction is the dominant fraction in all collected samples from SEQ waterbodies and the HPOB and HPIN were the weakest absorptions and the least concentrations.

3.7.6 DOC Concentration for Each Fraction of the Isolated Water Samples

The variation in DOC concentrations between all stations (N = 47) was demonstrated and explained in the previous chapter in §(2.14.4) and was shown in Figure (2-17 A and B). This part of this chapter will deal with the DOC content in and among CDOM fractions of a sample size of 1L. Fractions DOC concentration values were calculated by carrying out the equations (3.1) to (3.6) and by adopting the method described in §3.5.3; Figure (3-17) present these results.

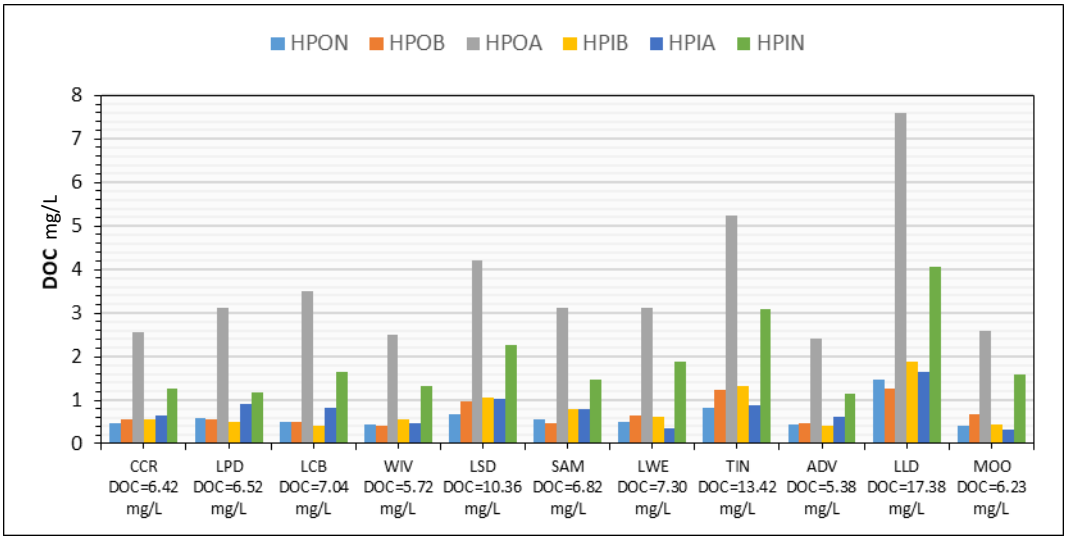

Figure 3-17: Column Chart to The Mean *DOC* Values for Each Fraction in Every Reservoir in SEQ Study Area (N=11).

The presented results reflect fractions proportion, where it indicates that the major fraction is HPOA consisting of about 41% to 47% of the whole DOC content. While the other five fractions contributed only 43% to 49% of the total DOC and the HPIN fraction has the greatest share in this percentages started from 37% to hit 42% in the total from these five fractions. The average ratio for HPON, HPOB, HPIB and HPIA is 7%, 8%, 9% and 9% respectively from the total DOC content that can be noticed in Figure (3-18 A). Moreover, the percentage analysis of DOC measurements for the isolated CDOM fractions shown small varying of DOC concentration proportions for each fraction along all stations ranged from 2% in HPON to 9% in HPIN as in Figure (3-18 B).

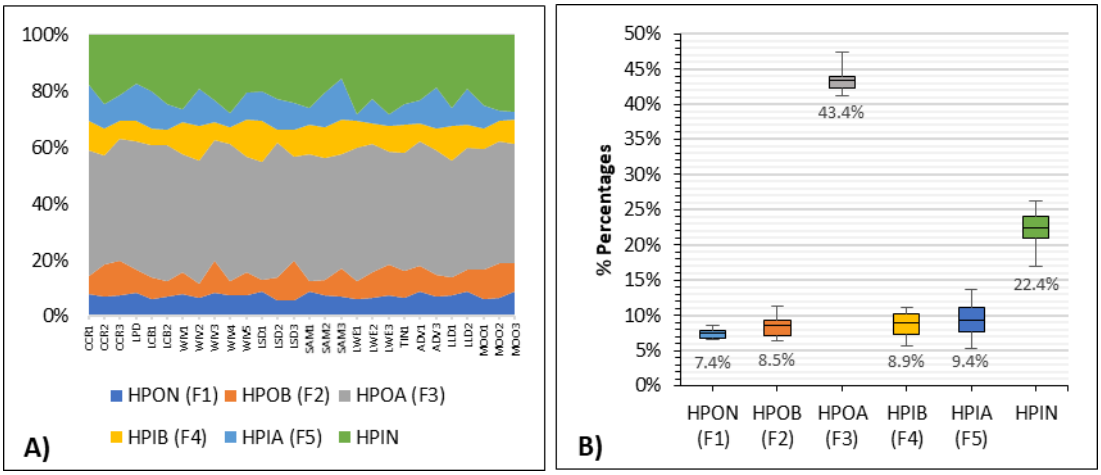

Figure 3-18: A) Chart Shows the Percentage Contribution of the Measured DOC Concentration of Each CDOM Fraction Per Station and Highlight the Magnitude of Change to The Percentage Along All Stations (N=28). B) MIN, MAX and Average Percentage of Each Fraction.

Beside acid-base classification, DOC values were also characterized in according to its hydrophobicity. Data from the literature indicated that most inland water bodies (especially lakes and reservoirs) have a preponderance of hydrophobic dissolved organic carbon, where the direct comparison among the results of this study and the results of other studies as in Table (3-11) shows great convergence.

Table 3-11: Comparison of the SEQ HPO and HPI Fractions percentage values to literature percentage values.

Study	Hydrophobic (DOC)	Hydrophilic (DOC)	No. of fractionated samples
(Croué et al. 1993)	41% - 56%	21% - 34%	14
(Hwang et al. 2001)	50% - 62%	14% - 32%	-
(Croue et al. 1999)	51% - 60%	19% - 30%	5
(Goslan et al. 2002)	61% - 79%	13% - 34%	-
(Ratpukdi et al. 2009)	53% - 72%	26% - 44%	7
In this Study	54% - 67%	28% - 51%	27

3.8 Reliability of the Relationship Between CDOM Fractions and DOC Concentration to the Collected Water Samples of SEQ Study Area

Early work in examining the relationship between DOC and CDOM like Ferrari et al. (1996) concentrated on coastal waters but further work to investigate riverine and lakes environments was done to improve the DOC flux estimation through a robust CDOM-DOC relationship (Mannino et al. 2014). This robust relationship not always been found in these environments due to many local factors. These obtained results demonstrated and discussed in the previous chapter when this relationship evaluated from the collected samples from the study area in SEQ that ended with a limited relationship. To determine and assess how these local factors implicate this relationship in these environments, CDOM fractions that derived in this work have been compared with DOC to study the potential results of the valuation of these new relationships.

Statistically, the results of using univariate and multivariate linear regressions that were conducted to estimate DOC concentration from CDOM fractions showed different trends for SEQ reservoirs. The univariate linear regression test for $a(350)$ and $a(440)$ to each fraction against its DOC value were highly variable among the fractions. When using $a(440)$, four fractions exhibited as having statistically poor and insignificant relationships with their DOC concentrations such as HPOB ($R = 0.279$, $R^2 = 0.078$; $\rho = 0.159$), HPIB ($R = 0.356$, $R^2 = 0.126$; $\rho = 0.063$), HPIA ($R = 0.391$, $R^2 = 0.153$; $\rho = 0.039$) and HPIN ($R = 0.077$, $R^2 = 0.006$; $\rho = 0.699$). While, the HPON ($R = 0.413$, $R^2 = 0.171$; $\rho < 0.01$) and HPOA ($R = 0.517$, $R^2 = 0.267$; $\rho < 0.01$) are the only two fractions that showed a statistically slight significant relationship at the ($\rho < 0.01$) significance level for $a(\lambda_o)$ versus DOC and modest coefficient of determination. The same results were obtained for $a(350)$ indicating that $a(\lambda_o)$ alone is a poor predictor to estimate DOC in SEQ regions as shown in Table (3-12).

Then, the multiple linear regression analysis was used with each fraction thus embedding both $a(\lambda_o)$ and (S) as independent variables to predict DOC as a dependent variable in the relationship. The adjusted coefficient of determination (adj. R^2) is adopted to compare the results because it is sensitive to any improvement that may occur in the model due to adding a new term which is (S), and this did not

happen. Overall, there is no statistically significant improvement can be noticed when conducting the multiple linear regression analysis, the reason could be linked with the differences in the absorption ratio, DOC content, and source of each fraction, once more the results are in Table (3-12).

Another possible way was by using the absorption coefficient of the hydrophobic and hydrophilic parts separately as a predictor variable in a univariate linear regression model to predict DOC concentration. A modest and insignificant relationship was obtained too; (Table 3-12) (R^2 = 0.313, ρ = 0.074) for HPO fraction and (R^2 = 0.367 - 0.419, ρ = 0.028 - 0.031) for HPI fraction. These results even after test using $a(\lambda_o)$ and (S) together of the HPO and HPI in the multiple regression analysis, were not able to provide additional information that led to a better prediction of the DOC concentration and remained poor predictor in SEQ region. The main reason is that the predictor variables uncorrelated.

Model (DOC = β $a(\lambda_o)$ + α)												
	a_{350} VS DOC						a_{440} VS DOC					
	R	R^2	adj. R^2	β	α	ANOVA ρ	R	R^2	adj. R^2	β	α	ANOVA ρ
HPON	0.419	0.175	0.144	0.109	0.390	0.004*	0.413	0.171	0.139	0.532	0.396	0.010*
HPOB	0.270	0.073	0.036	-3.139	0.766	0.173	0.279	0.078	0.041	-14.187	0.801	0.159
HPOA	0.570	0.325	0.299	0.207	2.425	0.002	0.517	0.267	0.239	0.714	2.574	0.005*
HPIB	0.504	0.254	0.225	0.958	0.446	0.006*	0.356	0.126	0.093	2.348	0.562	0.063
HPIA	0.347	0.120	0.087	0.237	0.507	0.070	0.391	0.153	0.121	1.599	0.494	0.039
HPIN	0.327	0.107	0.072	7.409	1.580	0.090	0.077	0.006	0.032	7.626	1.743	0.699
HPO	0.559	0.313	0.236	0.730	3.683	0.074	0.559	0.313	0.236	0.725	3.673	0.74
HPI	0.656	0.430	0.367	5.507	2.125	0.028	0.647	0.419	0.354	5.290	2.170	0.031

Model (DOC = (β_o $a(\lambda_o)$ + β_1 (S)) + α)														
	a_{350}-$S_{(350-440)}$ Vs DOC							a_{440}-$S_{(350-680)}$ Vs DOC						
	R	R^2	adj. R^2	β_o $a(\lambda_{350})$	B_1 ($S_{(350-440)}$)	α	ANOVA ρ	R	R^2	adj. R^2	β_o $a(\lambda_{440})$	B_1 ($S_{(350-680)}$)	α	ANOVA ρ
HPON	0.431	0.185	0.120	0.108	18.347	0.047	0.077	0.421	0.177	0.112	0.546	19.373	0.034	0.087
HPOB	0.297	0.088	0.012	-2.749	-5.928	0.844	0.331	0.296	0.088	0.012	-11.682	-6.357	0.844	0.332
HPOA	0.654	0.428	0.382	0.294	247.005	-1.874	0.001*	0.578	0.334	0.281	1.048	310.873	-2.987	0.006*
HPIB	0.509	0.259	0.200	1.017	6.091	0.312	0.023	0.366	0.134	0.065	2.587	6.393	0.430	0.165
HPIA	0.402	0.162	0.094	0.180	-31.854	1.250	0.111	0.408	0.167	0.100	1.474	-19.097	0.915	0.102
HPIN	0.347	0.120	0.050	7.109	5.837	1.417	0.201	0.447	0.199	0.135	6.926	36.826	1.348	0.062
HPO	0.623	0.388	0.235	0.186	153.455	1.032	0.141	0.629	0.395	0.244	1.049	628.570	-7.589	0.134
HPI	0.778	0.606	0.507	1.471	114.221	-1.001	0.024	0.673	0.453	0.316	127.448	6.406	-0.775	0.089

* correlation is significant if ρ ≤ 0.01

Table 3-12: Univariate and Multivariate linear regression model parameters (R, R^2, adj. R^2, model constants and ρ value); upper table) between $a(\lambda_o)$ and DOC, while lower table) between $a(\lambda_o)$ + (S) and DOC for CDOM fractions.

Also, this variability is expected between the fractions because of their carbon composition is different (Hansell & Carlson 2014) and its relationship with their absorption ability. Comparison the obtained results from measuring DOC of the fractions and their absorption coefficient showed that not all DOC is chromophoric; as an example, the HPIN fraction has 0.5% of the total CDOM absorption at the time it dominates on about 22.4% from the total DOC in the sample; Table (3-13).

Table 3-13: Percentage fractions distribution to the total absorption coefficient and DOC

Fraction	N	% $a_{(350)}$	% $a_{(440)}$	% DOC
HPON	28	23.7%	22.9%	7.4%
HPOB	28	0.7%	1%	8.9%
HPOA	28	59.5%	64%	43.4%
HPIB	28	4.2%	4%	8.9%
HPIA	28	11.3%	8.4%	9.4%
HPIN	28	0.3%	0.5%	22.4%

3.9 Chapter 3 Conclusions

NOM in the aquatic system as mentioned in chapter two §2.4 is the portion of the DOC pool that absorbs light in both the ultraviolet and visible ranges and it is controlled by local independent processes. The obtained results in this chapter showed several consistent trends, NOM can be characterized by grouping it into a limited set of categories (fractions) depending on their structure and size limit (e.g. humic and non-humic substances) or their molecules (e.g. HPO and HPI). For SEQ fractionated samples, more than 80% of DOM are humic substances they determine only the most stable end products of formations of organic matter in the water, these include the so-called fulvic acids (FA) and humic acids (HA). Humic substances dominated on 54% - 67% of the total DOC in water.

Different approaches are available to isolate humic substances, they differ in reliability and purpose. SPE method is a chemical separation method that uses pre-packed sorbent to extract DOM into six fractions based on acid-base and neutral groups. It is simple, cost-effective and more accurate, also it takes less time than other isolation methods. The fractionation efficiency was checked by examining if the

grand total of the average fractions' concentrations were approaching and matching the total average of CDOM concentration. The standard deviations of this process were ± 5% and ± 2% at 350 nm and 440 nm respectively.

The composition information of DOM fractions provided a better understanding of NOM behaviour for water quality in the study area. CDOM fractions have demonstrated a variety of light absorption behaviour by measuring their absorption spectra. The light absorption spectra of CDOM fractions extracted from collected water samples are one of the analytical methods for identifying some information about the chemical structure (e.g. carbon content, protein and carbohydrates). Analysis of the spectral slope can be used as evidence to deduce the chemical properties of CDOM in natural waters. The humic acid dominated water bodies (humic lakes) evidence CDOM spectrum a low spectral slope (*S*) and high absorption like some of the water bodies in the area (*e.g. Tingalpa reservoir (S = 0.0147), Lake Leslie Dam (S = 0.0153) and Advancetown Lake (S = 0.0123)).* In comparison those water bodies that showed HPON and HPIA fraction spectra with high spectral slope indicate that they are most likely dominated by hydrocarbon and carbohydrate molecules that have low molecular weight as explained in Figure (3-1). The investigation in the relationship between CDOM fractions and DOC showed different relationships such as not all DOC in CDOM can be chromophore.

The major goal of NOM isolation is to understand and predict CDOM fractions reactivity and their DOC content. Typically, increasing HPOA fraction in water indicates to increase the contribution from allochthonous organic matter sources (i.e., terrestrial), whereas a lower fraction HPOA is indicative of organic matter from autochthonous sources (i.e., algal or microbial) or photodegraded DOM. These results are consistent with previous studies that found that microbial processes in reservoirs and the spatial surrounding discharge could shift the spectral slope from high to low. A clear non-linear relationship observed between fractions slope coefficient (*S*) and $a(\lambda_o)$ and discovered whether they could be interrelated so that both parameters could be included in the bio-optical model later, thus reducing uncertainty in the slope.

Chapter 4

The Spectral Decomposition of CDOM Absorption Spectrum by Using Multi-Components Modelling to Characterize the Relationship with Dissolved Organic Carbon in SEQ.

4.1 Introduction

CDOM absorption spectrum shape may be used for tracing DOC sources as well as it is a proxy of CDOM composition in water. Therefore, it is important that CDOM absorption spectrum be clear, clean and free from any errors if possible (systematic or random). Within the context of water quality remote sensing the current approach to model CDOM absorption spectrum is by fitting a single exponential decay shape to a measured absorption spectrum (Woźniak 2007; Kirk 2011). This fitting technique is performed to smooth measurement noise and to obtain a clear shape of CDOM spectral curve then to calculate the spectral slope accurately (Mobley 1995). CDOM spectral curve shape is described by the slope coefficient that can be used to study the patterns change of the chemical properties between different water bodies

(Helms et al. 2008). Also, it provides insights into CDOM processes (e.g. photobleaching), nutrient availability and carbon cycling.

Examining the relationship between CDOM parameters ($a(\lambda_o)$, $a^*_{DOC}(\lambda_o)$ and (S)) with DOC in Chapter Two did not show a robust relationship between them. However, further study of the CDOM fractions in Chapter Three that showed some positive signs in this relationship and provided extra information. Thus, the range of contribution of these CDOM fractions and their implication on CDOM absorption spectrum discussed in the context of this chapter. Also, it investigates to identify sources of errors that result from using a simple exponential model and to determine if another model using CDOM fractions may be more applicable to represent the correct shape of CDOM spectrum that can be used as inputs into the optical model in the next chapter. Lastly, the obtained outcomes of this chapter are important to achieve objective three of this work.

4.2 Concept of CDOM Absorption Modelling

Deep understanding of CDOM spectrum characteristics is essential, especially in remote sensing. Fitting an accurate CDOM model is a significant matter confirmed by different researchers (Mobley 1996; Gordon 2002; Ma et al. 2006; Laanen 2007) because of its importance later as an input for the bio-optical modelling to retrieve accurate concentrations of CDOM and then DOC. The CDOM absorption spectrum is described by the spectral slope parameter that is often a proxy of CDOM composition and molecular weight. While the amplitude of the absorption coefficient is a proxy of CDOM content that is inversely proportional to the increased wavelength as a function of it (Jerlov 1968).

Some studies widely used a fixed value of (S) in their models. Jerlov (1968); Morel and Prieur (1977) used 0.015 nm^{-1} for coastal and open ocean waters (case I waters), while the value 0.014 nm^{-1} used by Zepp et al. (1981) for the freshwater measurements (case II waters). Nowadays, the evolution in the measurement instruments made it possible to measure CDOM absorption and calculate (S) over a

broad range of wavelengths, but the need for a good fitting model remains essential for several reasons will be reviewed in this chapter.

Sources of large random errors affect the absorption measurement of the filtered CDOM sample. One of these errors is result by small particles that may pass through the filter due to their irregular shape. These particles prevent the light beam to reach the instrument detector by scattering it. It will appear as a noise in the measured CDOM absorption spectrum; Figure (4-1). In case of R^2 between the measured and the fitted values less than 0.9, that means there is a contamination in the sample or an instrument issue and the result cannot be relied upon (Massicotte & Markager 2016).

Another reason illustrates the need to use a good-fitting model associated with the absorption spectrum of low CDOM content. Usually, the used reference wavelength for inland water to determine CDOM content is at 440 nm. Therefore, the measurement noise will affect the accuracy of the fitted $a_{CDOM}(440)$ when using a simple fitting model in case R^2 between measured and fitted values greater than 0.9 (Hansell & Carlson 2014).

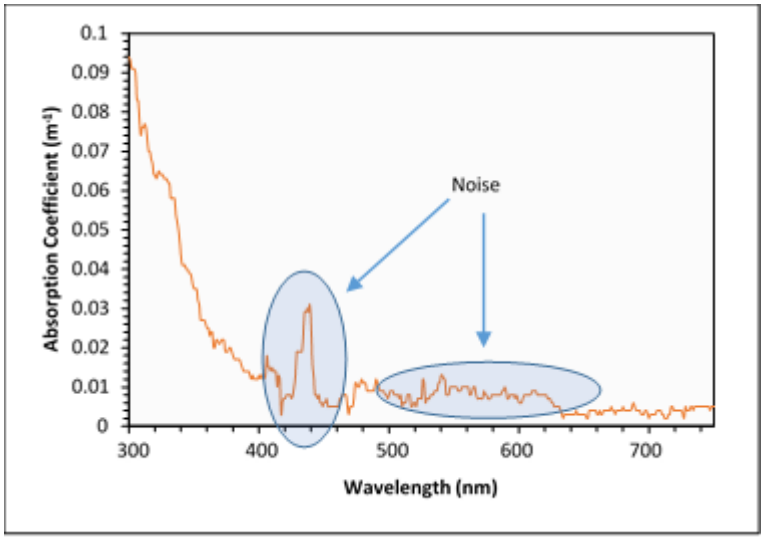

Figure 4-1: The Influence of The Small Particles and Scattering on Low CDOM Absorption Spectrum Due to A Contamination in The Sample from KSC (R^2 < 0.9), It Was Measured by Using JENWAY 6705UV/VIS Spectrophotometer (Split Beam Device).

It is necessary to use a good-fitting model to retrieve CDOM accurately, and CDOM must be isolated away from any influence of other water components such as phytoplankton (Roesler et al. 1989; Roesler & Perry 1995) because of the absorption area of CDOM is overlap with the absorption area of chlorophyll in the blue wavelength (Gitelson et al. 2000).

Currently, there are different fitting models to characterise the CDOM absorption spectrum, such as; simple exponential model (SEM), hyperbolic and two-components CDOM absorption model and more; Table (4-1) (Twardowski et al. 2004; Hansell & Carlson 2014).

Therefore, the process of modelling CDOM absorption spectrum may be subject to limitations as a consequence of CDOM composition and the measurement method. These limitations affect data interpretation and retrieving in case inappropriate fitting model used by not express about CDOM composition correctly.

Table 4-1: Some Available Fitting Models of CDOM Absorption Spectrum

Model	Function	Parameters	Fitting Method	Reference
Natural logarithm of the single exponential model	$\ln y = A - S * \lambda$	A, S_{ln}	Linear	(Fichot & Benner 2011)
Single exponential (SEM)	$y = Ae^{-S_e * \lambda}$	A, S_e	Nonlinear	(Bricaud et al. 1981)
Single exponential with offset (SEM-O)	$y = Ae^{-S_o * \lambda} + O$	A, O, S_o	Nonlinear	(Laanen 2007)
Double exponential with two fixed slope values (DEM)	$y = A_1 e^{-0.0111 * \lambda} + A_2 e^{-0.0189 * \lambda}$	A_1, A_2	Nonlinear	(Carder et al. 1989)
Double exponential with one fixed slope (DEM-F)	$y = A_1 e^{-S_1 * \lambda} + A_2 e^{-0.010 * \lambda}$	A_1, A_2, S_1	Nonlinear	(Twardowski et al. 2004)
Double exponential (DEM)	$y = A_1 e^{-S_1 * \lambda} + A_2 e^{-S_2 * \lambda}$	A_1, A_2, S_1, S_2	Nonlinear	(Krijgsman 1994)
Hyperbolic	$y = A(\frac{\lambda}{440})^{-S_h}$	A, S_h	Nonlinear	(Zhang et al. 2011)

Where, *y* is the absorption, *A* is the absorbance, *O* is the offset and *S* is the slope.

4.3 Simple Exponential CDOM Absorption Model (SEM)

Before examining the effect of CDOM fractions on the absorption spectrum and develop the fitting model to suit the needs of this research, it is necessary to understand the standard model that will rely upon them. The first derivation of the simple fitting model based on using CDOM absorption in a single exponential function with a fixed slope value as defined below in equation (4.1) (Jerlov 1968):

$$\boldsymbol{a_{CDOM}(\lambda) = a_{CDOM}(\lambda_o) * exp^{(-0.015*\lambda)}} \quad (4.1)$$

Nevertheless, this equation was modified by Bricaud et al. (1981) to the commonly used and well-known formula that mentioned in chapter two (equation 2.3), but this equation can be expressed in the general form as below:

$$y = Ae^{-S_e*\lambda} \quad (4.2)$$

Where; A is the amplitude and S_e is the slope parameter.

SEM is suitable to use within the visible wavelength range between 340-540 nm for CDOM absorption measurements (Gege 2000) because there are few deviations in this range for CDOM due to its high absorbability within this range (Jerlov 1968; Bricaud et al. 1981; Stedmon et al. 2000; Stedmon & Nelson 2014). A least-squares regression was used to solve the SEM model using equation (2.3) to describe the appropriate curve of CDOM absorption spectrum for SEQ water samples and the fractions in chapters two and three. A programming code generated in IDL (Interactive Data Language) software to simplify the fitting procedure.

4.4 The Optimal Correction of CDOM Absorption Spectrum and the Offset Value (K) of the Baseline

Necessary corrective action must be taken to obtain a clear and clean CDOM absorption spectrum curve and to remove any errors resulting from the reasons mentioned in §4.2. CDOM absorption coefficient for λ ≥ 650 nm is assumed to be null (Green, S. A. & Blough, N. V. 1994; Helms et al. 2008; Matsuoka et al. 2012). However,

at these long wavelengths, most of inland water samples show an attenuation not caused by CDOM (e.g. from small particles), and it is not negligible as proven by Laanen (2007).

Two types of scattering correction of the measured raw data for CDOM absorption spectrum can be done on the water source and type.

The first type of correction will be mentioned for clarification only, Bricaud et al. (1981) advised to correct the oceanic CDOM samples from the scattering resulted from small particles through the following equation:

$$A_{CDOM}(\lambda) = OD(\lambda) - OD(700) * (\frac{\lambda}{700}) \quad (4.3)$$

The explanation of selecting 700 nm in equation (4.3) based on the effect of the small particles appears at longer wavelengths in CDOM sample measurements.

On the other hand, the second type of the scattering correction preferred for inland waters by subtracting the mean of the optical density value between 750 - 850 nm (Green, Sarah A & Blough, Neil V 1994), as described in §2.11.2; equations (2.1) and (2.2). This scattering correction was adopted in this work because it is better for inland water bodies.

Some studies (Green, S. A. & Blough, N. V. 1994; Markager & Vincent 2000; Stedmon et al. 2000) have determined a small constant offset in the absorption measurements of water samples when using benchtop dual-beam spectrophotometer. It is not due to CDOM, but it is due to the refractive index (e.g. temperature or cuvette). This offset value could be positive or negative and sometimes approaches zero depending on CDOM levels. The offset parameter (K) should be added to the measurements to correct the fitted baseline as shown in equation (2.3). Also, it is crucial and essential as a correction parameter cannot be neglected.

In other words, two scattering corrections used in this work for all CDOM samples (N = 47) and all CDOM fractions (N = 28 x 6 fractions). The first correction is from the effect of small particles on the absorption spectrum curves (scattering correction).

While the second correction is for the fitted curve due to the effect of the refractive in the light beam and by the systematic errors (offset correction).

4.5 Double Exponential CDOM Absorption Model (DEM)

Some researchers Zepp and Schlotzhauer (1981); Carder et al. (1989); Boyle et al. (2009) and others argued that the CDOM absorption spectrum model of inland waters with high CDOM content can be accurately described by using two-components exponential fitting model. It is a combination of two simple exponential models of the major CDOM components (humic and fulvic acids) and can give a better description of the CDOM absorption spectrum.

Carder et al. (1989) were the first to perform it by using the measured values of humic and fulvic acids from the chemical separation. The below equation (4.4) describes the two-components model of humic and fulvic acid as suggested by the above researchers as follows:

$$a_{CDOM}(\lambda) = a_{HA}(\lambda_o)e^{0.0111(\lambda_o-\lambda)} + a_{FA}(\lambda_o)e^{0.0189(\lambda_o-\lambda)} \quad (4.4)$$

The above equation developed to be more comprehensive as stated by Laanen (2007) and Stedmon et al. (2000) also adding an offset parameter and it rewritten in the following form:

$$a_{CDOM}(\lambda) = a_{HA}(\lambda_o)e^{(-S_{HA}(\lambda-\lambda_o))} + a_{FA}(\lambda_o)e^{(-S_{FA}(\lambda-\lambda_o))} + K \quad (4.5)$$

The five parameters used in equation (4.5) refers to the absorption of HA and FA and their slopes, in addition to the offset parameter (K). This equation will be developed in the coming sections of this chapter to describe the CDOM absorption spectrum optimally according to its components. Table (4-2) gives the most common different exponential CDOM absorption fitting models.

Reference	Exponential Model
Jerlov (1968)	$a_{CDOM}(\lambda) = C_{CDOM} * exp^{(-0.015*\lambda)}$
Bricaud et al. (1981)	$a_{CDOM}(\lambda) = a_{CDOM}(\lambda_o)e^{S(\lambda_o-\lambda)}$
Carder et al. (1989)	$a_{CDOM}(\lambda) = a_{HA}(\lambda_o)e^{S_{HA}(\lambda_o-\lambda)} + a_{FA}(\lambda_o)e^{S_{FA}(\lambda_o-\lambda)}$
Stedmon et al. (2000)	$a_{CDOM}(\lambda) = a_{CDOM}(\lambda_o)e^{S(\lambda_o-\lambda)} + K$
Laanen (2007)	$a_{CDOM}(\lambda) = a_{HA}(\lambda_o)e^{(-S_{HA}(\lambda-\lambda_o))} + a_{FA}(\lambda_o)e^{(-S_{FA}(\lambda-\lambda_o))} + K$

Table 4-2: Some Common Exponential CDOM Absorption Models from Literature

4.6 CDOM Spectral Decomposition Approaches

Using the currently accepted method of fitting (SEM) can lead to loss and not fully capture most of the information provided in the CDOM absorption spectrum curve (Twardowski et al. 2004). This shortcoming in the current SEM influences on the usefulness of (*S*) parameter also, which is characterized by its sensitivity towards the selected wavelength range (e.g. 350-400 nm) as shown in Figure (4-2 A).

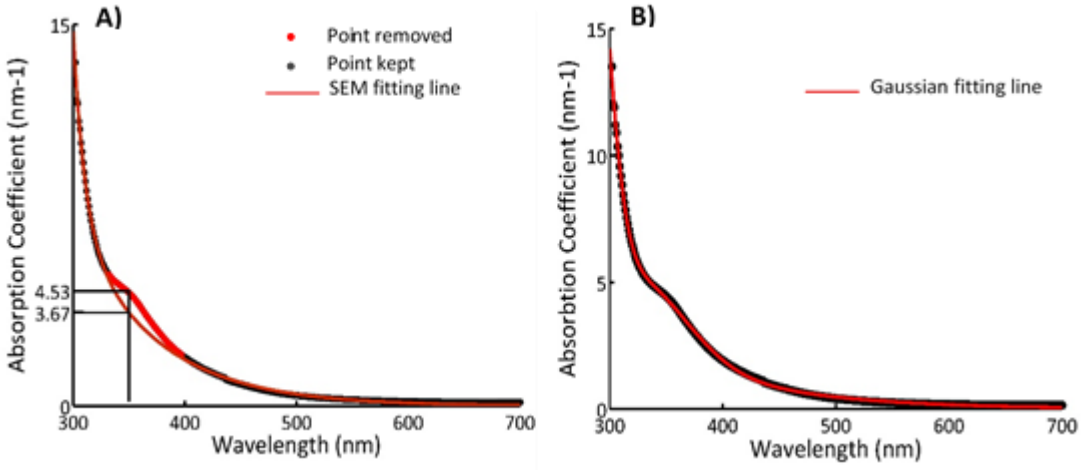

Figure 4-2: Example of Different Fitting Models of CDOM Absorption Spectra from KSC Sample. A) Results of Using SEM; Orange Points Have Been Discarded to Calculate the Baseline Curve. B) Results of Using Gaussian Decomposition Fitting.

The SEM has been challenged by many researchers and they have resorted to using different fitting models. Gege (2000) reported that the Gaussian model has a better fit than using SEM in high CDOM concentration samples; Figure (4-2 B). While others have turned to use different approaches to obtain a more reliable and robust

estimation of (*S*) by using CDOM spectral decomposition technique (Aiken et al. 1992; Leenheer et al. 2000; Hansell & Carlson 2014).

CDOM spectral decomposition technique developed to provide better and additional information about CDOM pool and dynamics from the absorption spectrum curve (Grunert et al. 2018). Different solutions have been found to perform this technique; it can be done by direct measurements of CDOM components that obtained from the chemical separation for CDOM sample as carried out by Carder et al. (1989). Then including these measurements into an appropriate fitting model. Another way, it can be done by using the algebraic method of the linear, nonlinear or Gaussian decomposition approaches (Gege 2000; Laanen 2007; Zhang, Y. et al. 2014; Massicotte & Markager 2016). In this work a combination between the chemical and the algebraic methods selected due to different reasons illustrated in section §4.7.3.1 of this chapter.

4.6.1 Gaussian Decomposition Method

This technique addresses peaks of deviations in the CDOM absorption spectrum curve that results from individual chromophore (e.g. Lignin) (Figure (4-2 B). This decomposition method is based on a model construction of two sections, the first section is the SEM. While, the second section is a function of three parameters which are (height, position and width of the deviation peak) (Gege 2000). Gaussian decomposition will not be performed in this work because it deals with an individual absorption contribution of some unclassified and uncontrolled components could not appear in all CDOM samples. Therefore, it has been resort to use CDOM fractions decomposition because it is more comprehensive in dealing with CDOM classified components (e.g. HA, FA or HPI).

4.6.2 The Linear and Nonlinear Decomposition Methods

The use of these decomposition methods is associated with the equations that will be used to retrieve the measured CDOM components. In this point of view, selecting an appropriate equation model from various types that were introduced in Table (4-

1) to fit CDOM absorption spectra accurately is important for valid and accurate results as possible. It has been taken into consideration a number of possible advantages and disadvantages in selecting between the linear and the nonlinear methods to solve these models. Modelling performance can be done by using least-squares regression approach or by using a nonlinear least-squares optimization technique depending on the selected method.

4.7 Decomposing the Measured Absorption Spectra of SEQ Inland Water-Bodies

4.7.1 Introduction

The concept of CDOM decomposition modelling could offer a broad understanding of chemical interactions affecting CDOM molecular structure. In this section, the appropriate decomposition model will be applied to the measured and collected data from SEQ study area to examine the participation of the different CDOM fractions in the absorption spectrum curve.

The linear and nonlinear decomposition approaches will be used in parallel with using the chemical isolation data of CDOM samples in this study. The underlying hypothesis and the goodness of fit to the normalized values of the results will be checked. Also, all the selected and the developed models will be tested using F statistic parameter to determine their efficiency and their reliability to use them as a proxy for CDOM retrieval and DOC estimation in the SEQ regions.

4.7.2 Data and Materials

Only the fractionated 28 CDOM stations that collected from the 11 water bodies in the SEQ study area used. The chemical separation and isolation of these samples (represented by using the SPE technique) were described in the previous chapter in §3.5.1 and §3.5.2. Also, the optical measurements and DOC concentration measurements of these CDOM samples and their fractions that previously reported have been used CDOM and DOC measurements in chapter two also CDOM fractions and their DOC from chapter three).

In addition, different slope values of CDOM fractions, so-called end-members candidate slope values were chosen carefully from literature which corresponds with the study area characteristics. These end-members values used in the Linear Least Squares regression modelling method, further details will be in the context of the coming sections in this chapter.

4.7.3 Methods and Approaches

4.7.3.1 The Decomposition Modelling Framework

Carder et al. (1989) found that extracting CDOM components are considered as an alternative way to direct measurements of CDOM absorption coefficient and that can be done by using the major CDOM components of the HA and FA. Carder's et al. original exponential model combined of two exponential functions but with different fixed slope values for the HA and FA to give a better description to the CDOM absorption modelling. Later, their model developed by Laanen (2007); Stedmon (2014) to be more broadly by including an offset parameter (K) to correct the absorption measurements from the systematic errors that occurring due to the cuvette wall, baseline shift between the reference and the sample, temperature differences and used instrument itself; and they redrafting the equation (4.4) to configure the equation (4.5).

4.7.3.2 Developing the Proposed Model of the Measured CDOM Absorption Spectra for SEQ Study Area Locations

Dissolved organic matter sampled from the study area was separated according to their different chemical properties into hydrophobic and hydrophilic parts. Each one of these parts has different chemical groups and components (e.g. proteins, carbohydrates, humic acid, fulvic acid and various other components as illustrated in Figure (3-4)). For complex and high DOM concentration water-samples such as SEQ study area, HA and FA are not the only absorbing dissolved organic constituents as explained in the previous chapter, but they can be considered as the major components of the DOM hydrophobic part. Additionally, there are other diverse

organic compounds generated from different processes within the water column or from the surrounding areas represented by the hydrophilic DOM part (Figure 3-4) and they contribute by (8.2% - 22.6%) of the total CDOM absorption. This hydrophilic DOM part cannot be neglected because it is responsible for nearly (28% - 51%) of the entire DOC content in the collected water samples (Table 3-11). Therefore, the modelling equation of CDOM absorption spectrum can be developed and reformulated according to the results obtained in this work as follows:

$$a_{CDOM}(\lambda) = a_{HPO}(\lambda) + a_{HPI}(\lambda) \tag{4.6}$$

Since the hydrophobic part contains two important fractions (HA and FA) which both have a direct relationship with DOC, a two-component decomposition model was used. The decomposition process can be done on the absorption spectrum of the HPO part only to the major HA and FA fractions as in the equation below:

$$a_{HPO}(\lambda) = a_{HA}(\lambda) + a_{FA}(\lambda) \tag{4.7}$$

On the other hand, the multi-decomposition technique can be done directly on the whole CDOM absorption spectrum to HA, FA and HPI.

$$a_{CDOM}(\lambda) = a_{HA}(\lambda) + a_{FA}(\lambda) + a_{HPI}(\lambda) \tag{4.8}$$

And in terms of the concentrations, the final developed model will be as follows:

$$a^*_{CDOM}(\lambda) = \frac{a_{HA}(\lambda)}{C_{HA}} . e^{(-S_{HA}(\lambda-\lambda_o))} + \frac{a_{FA}(\lambda)}{C_{FA}} . e^{(-S_{FA}(\lambda-\lambda_o))} + \frac{a_{HPI}(\lambda)}{C_{HPI}} . e^{(-S_{HPI}(\lambda-\lambda_o))} + K \tag{4.9}$$

The multi-exponential CDOM absorption model given by equation (4.9) will be used as the CDOM absorption spectral decomposition model and for optical modelling of remote sensing in this work to get better results to describe the CDOM absorption spectrum curve accurately. It is expected by using this model for the normalised CDOM absorption spectrum (SIOP) an improving on CDOM and DOC concentrations retrieval.

There are two suggested techniques to test and then solve this model by performing both linear and nonlinear approaches. The results of the best end-members that produced from using the linear methods will be compared with the single exponential model depending on the goodness of fit, offset parameter and the concentration of CDOM and DOC values. Figure (4-3) summarise the framework of the decomposition approaches.

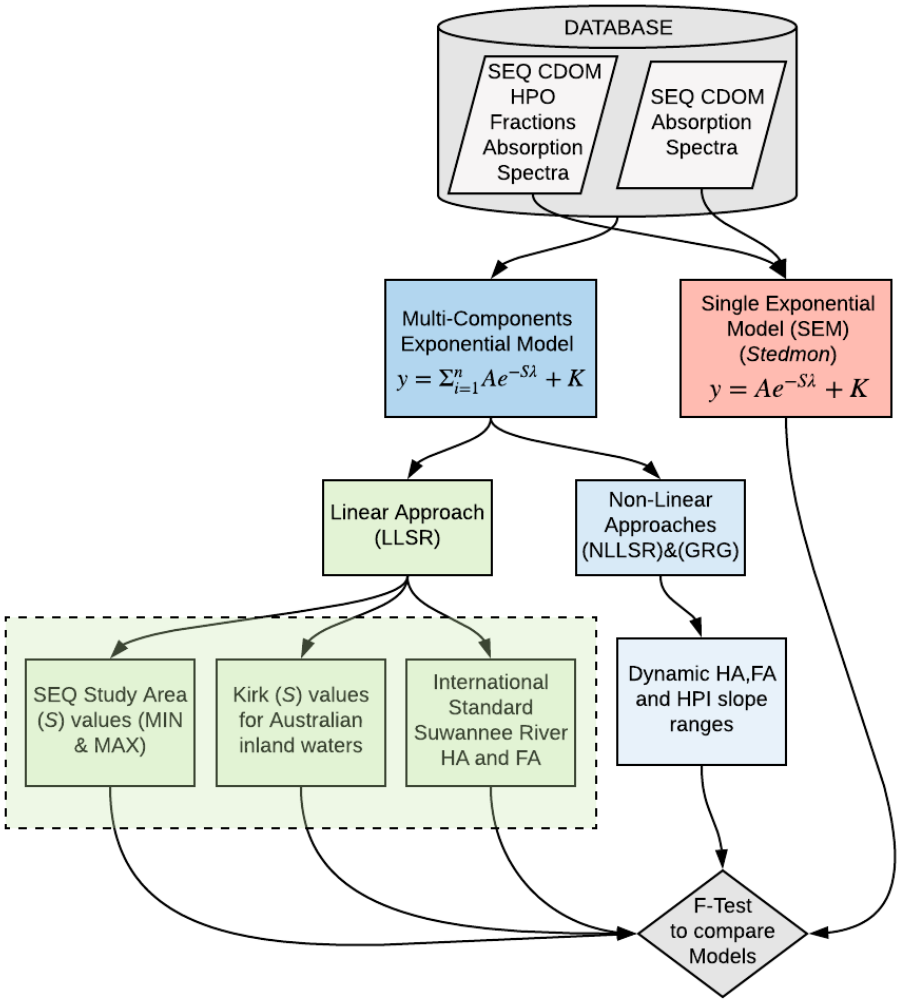

Figure 4-3: The Outline Framework of SEQ CDOM Absorption Spectrum Decomposition Adopting Linear and Nonlinear Approaches.

4.7.3.3 Linear Least Squares Regression (LLSR)

Mathematically, in order to find ideal values that provided from solving the equation (4.9) by using LLSR, the best approximation is defined by minimizing the sum of squared differences between the measured values and their corresponding estimated values. The linear least-squares regression solution implemented using fixed end-members values that chosen accurately and taking into account the characteristics of the study area. Below are several possible end-members values that examined in this research and can be applied for Australian inland waters:

1. **SEQ study area end-members**

It is unlikely under natural conditions that only one fraction of HA or FA will be present in the water sample, but it is more probable that one fraction could dominate so heavily that it can be treated as thus for practical purposes. Based on this assumption, the minimum slope value of the measured HPO fractions that found in the SEQ study area samples is assumed to be set as (S_{HA}) corresponds to a sample containing only HA, and the maximum measured slope value is assumed to be set as (S_{FA}) corresponds to a sample containing only FA. While the HPI fraction slope value was set as the average of the measured slope values for the reservoirs in the SEQ study area and was (0.0215 nm^{-1}).

2. **Kirk end-members**

These end-members values are compatible with Kirk slope values that were measured for different Australian inland waters (Kirk 2011). The reason for using these end-members is to compare the results of using SEQ data set with the Australian nationwide dataset. The same mechanism that was adopted in choosing SEQ end-members for HA, FA and HPI applied here.

3. **International standard and reference end-members**

There are several different types available of international humic substances standards and references to select from. The commonly used types are Suwannee river HA and FA standard samples from IHSS, Aldrich HA standard from Sigma-Aldrich, and Nordic HA and FA reference samples from IHSS. The slope values of these standard and reference samples are available from literature to allow for comparison.

The general properties of the selected end-members for this work should be valid to be applied in SEQ or at least in Australian inland waters. Therefore, the selection was made for Suwannee river HA and FA standards from IHSS for some basic reasons:

- It has a high concentration of functional groups of dissolved humic substances forming sufficient quantities of different constituents beside HA and FA (Hessen & Tranvik 2013). While Sigma-Aldrich HA is extracted and derived from terrestrial sources (Bob & Walker 2001) and has high ash content (Valentine 1998).
- Its source is located in a subtropical/tropical climate zone (rises in the Okefenokee Swamp in South Georgia, USA and flows southwest to the Gulf of Mexico passing Florida, USA) unlike Nordic HA and FA reference samples which their source located in the polar climate zone.
- The HA and FA slope values of Suwannee River are close to the existing values that recorded of the study area and Australia, while Aldrich HA slope value is (0.0089 nm^{-1}) where no such value recorded for Australian inland freshwater.
- Suwannee River is well characterized and believe to be a good model for actual aquatic humic substances due to the intensive researches that are available on the site more than the other HA and FA standards and references.

The fixed end-members values that will be included and tested by using the LLSR method on equation (4.8) are given in Table (4-3).

Table 4-3: The End-Member Sets and Their HA and FA Slope Ranges That Used in LLSR In This Work.

	End-members Set	S_{HA} and S_{FA} (nm^{-1})	S_{HPI} (nm^{-1})
1	SEQ **HPO** fraction dataset (MIN & MAX (*S*))	0.0124 and 0.0201	Average of the reservoirs in SEQ (0.0215)
2	Kirk slope values for Australian Inland waters	0.0120 and 0.0180	Average of the reservoirs in SEQ (0.0215)
3	Suwannee river standard HA and *FA* Slope values	0.0137 and 0.0172	Average of the reservoirs in SEQ (0.0215)

4.7.3.4 Nonlinear Optimisation Technique

Various nonlinear optimization techniques are available and can be used for calculating the decomposition equations (4.5) and (4.9). Unlike the LLSR method that uses fixed slope values, in the nonlinear decomposition technique the slope values of HA, FA and HPI are allowed to be changed within a certain range between (350-680 nm) and can be called (dynamic slope values). Two different nonlinear techniques were selected and tested, the nonlinear least-squares regression (NLLSR) and the generalized reduced gradient techniques (GRG)*. The NLLSR were solved by using the optimization solver (lsqnonlin) in MATLAB R2013a software from MathWorks®, while the GRG solving technique is embedded in Microsoft® Excel Solver.

4.7.4 The Results and Discussion of Using the Linear and Nonlinear Approaches

4.7.4.1 Testing the Reliability of Using GRG and NLLSR in the Nonlinear technique

Three possible types of solution sets can be obtained from using the nonlinear equation or model. These solution sets possible to be; no solution, a unique solution or an infinite number of solutions (Rheinboldt 1998). One of the disadvantages of using a nonlinear optimization technique is the resulting solution may not be unique (Ruszczyński & Ruszczynski 2006) and the valid solutions may be considerable, due to the parameter space range that gives the same degree of accuracy.

Therefore, a test was conducted first to check the efficiency of the two selected nonlinear techniques (GRG and NLLSR) if they lead to a possible unique solution or not. The test was implemented using the standard Suwannee River fulvic acid (*SRFA*) available in CSIRO, Ocean and Atmosphere water lab and was purchased from the International Humic Substances Society (Saint Paul, MIN 55108 USA) (Figure (4-4 B)). The measured SRFA absorption spectrum curve (Figure (4-4 A)) contains only FA and decomposed by using the two suggested nonlinear decomposition techniques

* GRG is one of the robust methods for solving nonlinear equations of general structure to find an optimal solution.

adopted for this work. The unique solution should be similar to the fitted parameters ($a_{FA}(\lambda_o), S_{FA}$ and K) that found from using SEM (equation 2.3).

In this test the following different exponential fitting models used:

1. SEM of Stedmon et al. (2000) (equation 2.3) was included as a reference to check the results.
2. The two-components exponential model (DEM) (equation 4.5).
3. The suggested exponential model for this study (equation 4.9) (multi-components exponential model of HA, FA and HPI).

An important note, the retrieved parameters $a_{HA}(\lambda_o)$ and $a_{HPI}(\lambda_o)$ for the second and the third fitting models should be equal to zero to have a correct unique solution. Also, the goodness of fit as a measure of the performance (Chi-square divided by the degrees of freedom *(df=n-1)*) and the model validity were calculated for each used model.

The Chi-square (X^2) was computed from the given following equation:

$$X^2 = \sum_{i=1}^{n} \frac{(O_i - E_i)^2}{E_i} \tag{4.10}$$

Where, O_i is the observed value and E_i is the expected value for $i = 1$ to n.

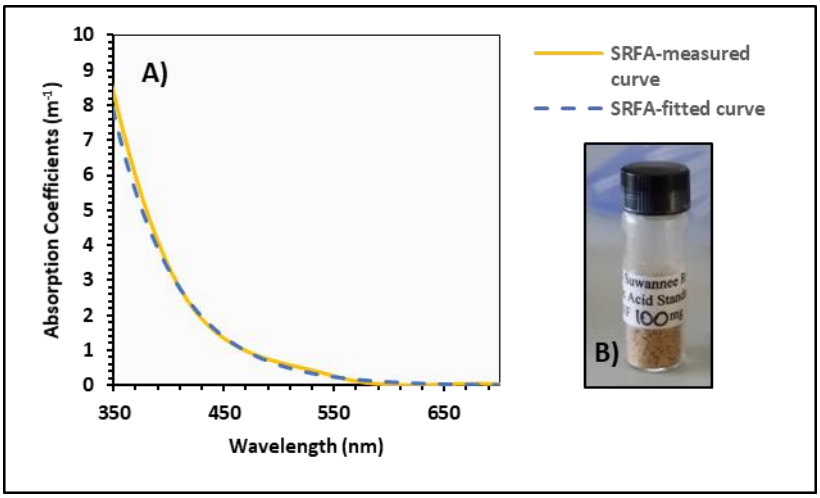

Figure 4-4: A) The Measured Absorption Spectrum Curve of SRFA (Solid Line) And the Fitted Curve (Dotted Line) (Fitting Was Done Using Equation (2.3)), B) SRFA Standard Sample (100 Mg) From IHSS.

The results of the implementation of the nonlinear approaches using the different fitting models that were illustrated above in (1,2 and 3) on the measured spectral values of SRFA are given in Table (4-4).

Table 4-4: SRFA Slope Values, Absorption Coefficients, Offset Values and The Goodness of Fit for The Selected CDOM absorption Decomposition Models and for The Two Nonlinear Optimization Techniques.

	GRG			NLLSR		
	Single Model (eq. 2.3)	Two-Components Model (eq. 4.5)	This study Model (eq. 4.9)	Single Model (eq. 2.3)	Two-Components Model (eq. 4.5)	This study Model (eq. 4.9)
a_{HA} (m^{-1})	-	0.00	0.00	-	0.00	0.01
S_{HA} (nm^{-1})	-	0.0137	0.0124	-	0.0137	0.0124
a_{FA} (m^{-1})	1.66	1.69	1.67	1.67	1.65	1.64
S_{FA} (nm^{-1})	0.0172	0.0172	0.0172	0.0172	0.0172	0.0172
a_{HPI} (m^{-1})	-	-	0.00	-	-	0.00
S_{HPI} (nm^{-1})	-	-	0.215*	-	-	0.215*
K	0.04	0.04	0.04	0.03	0.03	0.03
X^2/df	0.065	0.077	1.741	0.067	0.081	1.749

* The average HPI slope values of all stations in the SEQ study area

From Table (4-4), the values found for a_{FA}, S_{FA} and K from using GRG and NLLSR for the SEM model are nearly the same fitted values. The developed model for this study has a normalized X^2 a value greater than (1) for both the used nonlinear approaches, indicating a poor model fit. The reason back to the source of SRFA that came from NOM fractionated to HA and FA only, while there is another part apparently has different characteristics which are HPI in the model. But the case is different for the study area because the HA and FA will be spectrally decomposed from the HPO part that does not contain any of HPI part's components.

There are no significant differences between GRG and NLLSR techniques and the values of X^2/df are equal or slightly different for each model. Also, the applied GRG technique did not indicate any value of a_{HA} and a_{HPI} in the sample, while the NLLSR technique yields a humic acid absorption of 0.01 m^{-1} which records against it.

When applying the nonlinear optimization onto the 11 waterbodies (N = 28) of SEQ datasets in the selected study area, some of the results in the solution space were out of the lower and upper boundaries of the slope values. In another meaning, not all the slope values of HA were within their customary range between 0.008 – 0.014 nm^{-1}. Also, the value of the X^2/df for most models > 1 and that indicates it is not valid to use for this sample. Thus, this solution of using GRG and NLLSR leads to unreliable and invalid results with negative absorption coefficients for some values.

4.7.4.2 The Results of Using Linear Decomposition Approach

The results of using the three selected end-member values which had already been clarified in §4.7.3.3 for the 11 SEQ waterbodies (N=28) were compared with the results from using SEM and with the measured DOC values. The SEM (equation 2.3) was solved in this work to find the three unknown parameters $a(\lambda_o)$, S and K; by using the partial derivatives in terms of each parameter arranged in an array $A[x]$ containing the measured absorbance values as a function to the wavelength from (350-700 nm) as explained in the following equations:

$$A\begin{bmatrix} f(x_i) = a * exp(b * x_i) + c \\ \vdots \\ n \end{bmatrix} \quad (4.11)$$

$$\frac{\partial f}{\partial a} = exp(b * x_i) \quad (4.12)$$

$$\frac{\partial f}{\partial b} = a * x_i * exp(b * x_i) \quad (4.13)$$

$$\frac{\partial f}{\partial c} = 1 \quad (4.14)$$

Where; $\boldsymbol{x_i}$ is the independent variable of the wavelength, $\boldsymbol{a}$ is the absorption coefficient at λ from 350 to 700 nm, *n* = 700 - 350, b the slope value and c is the offset.

The same parameters and procedures that were used in assessing the reliability of the nonlinear approaches have been applied. The multi-component model is

combining these seven parameters $a_{HA}(\lambda_o)$, $a_{FA}(\lambda_o)$, $a_{HPI}(\lambda_o)$, C_{HA}, C_{FA}, C_{HPI} and K that should lead to the best agreement between the measured and the modelled concentration values.

While the slope value was selected and fixed according to the three previously nominated end-members for the HPO fraction and it was fixed on (0.0215 nm^{-1}) computed from the average of the measured SEQ values for the HPI fraction.

The results of performing the linear spectral decomposition technique on the HPO fraction according to the first suggested hypothesis by using LLSR for the three fitting models are shown in Table (4-6) below.

Table 4-6: Showing the results of using different fitting models for HPO fractions to estimate the ratio of HA and FA in SEQ samples by using LLSR.

RESERVOIR	SEM_{HPO}				$a_{HPO}(440)^*$ (m^{-1})	$DOC_{HPO}{}^{**}$ mg/l
	C_{HPO} (440) mg/l	S_{HPO} (nm^{-1})	K_{HPO}	SSE		
CCR	0.50	0.53	0.03	0.02	0.53	3.59
LPD	0.35	0.37	0.02	0.06	0.37	4.26
LCB	0.61	0.67	0.06	0.10	0.67	4.50
WIV	0.40	0.40	0.00	0.02	0.40	3.35
LSD	1.18	1.22	0.04	0.38	1.22	5.85
SAM	2.25	1.83	-0.42	0.26	1.83	4.14
LWE	1.14	1.05	-0.09	0.07	1.05	4.26
TIN	6.00	6.26	0.26	0.04	6.26	7.29
ADV	1.89	1.43	-0.46	0.07	1.43	3.33
LLD	2.79	2.53	-0.26	0.15	2.53	10.35
MOO	2.16	1.81	-0.35	0.17	1.81	3.68

* Computed from SEM ($\boldsymbol{f(x) = a_{HPO} exp^{(-S*x)} + K}$)
** Measured from using SPE technique
R^2 (C_{HPO} with DOC_{HPO}) = 0.313; ρ > 0.05

RESERVOIR	Fitting model using MAX and MIN HPO Slope values $\boldsymbol{f(x) = a_{HA} exp^{(-0.0124*x)} + a_{FA} exp^{(-0.0201*x)} + K}$							DOC_{HA} mg/l	DOC_{FA} mg/l	$a_{HPO}(440)$* (m^{-1})
	C_{HA} mg/l	C_{FA} mg/l	K	SSE	%HA	%FA	RMSE			
CCR	0.030	0.470	0.03	0.04	6%	94%	0.0083	0.22	3.38	0.53
LPD	0.169	0.183	0.02	0.06	48%	52%	0.0142	2.05	2.22	0.37
LCB	0.297	0.309	0.06	0.13	49%	51%	0.0164	2.21	2.30	0.67
WIV	0.206	0.198	0.01	0.01	51%	49%	0.0865	1.71	1.64	0.41
LSD	0.930	0.247	0.03	0.42	79%	21%	0.0221	4.62	1.23	1.21
SAM	2.203	0.045	-0.41	0.22	98%	2%	0.0237	4.05	0.08	1.84
LWE	0.640	0.503	-0.07	0.08	56%	44%	0.0296	2.38	1.87	1.07
TIN	5.700	0.300	0.26	0.09	95%	5%	0.0332	6.93	0.37	6.26
ADV	1.775	0.113	-0.45	0.02	94%	6%	0.0261	3.13	0.20	1.44
LLD	1.760	1.034	-0.27	0.16	63%	37%	0.0285	6.52	3.83	2.52
MOO	1.818	0.346	-0.35	0.13	84%	16%	0.0260	3.09	0.59	1.81

* Computed from (C_{HA}+C_{FA}+K)
R^2 (C_{HA} with DOC_{HA}) = 0.624; ρ < 0.05 and R^2 (C_{FA} with DOC_{FA}) = 0.560; ρ > 0.05

RESERVOIR	Fitting model for HPO fractions using Kirk Slope values for Australian inland waters $f(x) = a_{HA}exp^{(-0.0120*x)} + a_{FA}exp^{(-0.0180*x)} + K$							DOC_{HA} mg/l	DOC_{FA} mg/l	$a_{HPO}(440)$* (m^{-1})
	C_{HA} mg/l	C_{FA} mg/l	K	SSE	%HA	%FA	RMSE			
CCR	0.062	0.415	0.03	0.10	13%	87%	0.0940	0.47	3.13	0.50
LPD	0.175	0.162	0.02	0.05	52%	48%	0.0260	2.22	2.05	0.36
LCB	0.242	0.349	0.01	0.16	41%	59%	0.0850	1.85	2.66	0.60
WIV	0.138	0.257	0.01	0.03	35%	65%	0.0570	1.17	2.17	0.41
LSD	0.956	0.224	0.01	0.36	81%	19%	0.0380	4.74	1.11	1.19
SAM	2.278	0.070	-0.04	0.22	97%	3%	0.0810	4.01	0.12	2.31
LWE	0.638	0.522	0.02	0.05	55%	45%	0.1220	2.34	1.91	1.18
TIN	5.467	0.541	0.02	0.03	91%	9%	0.1410	6.63	0.66	6.03
ADV	1.770	0.197	-0.02	0.09	90%	10%	0.0710	3.00	0.33	1.94
LLD	2.018	0.785	0.05	0.20	72%	28%	0.0810	7.45	2.90	2.86
MOO	1.972	0.269	-0.01	0.14	88%	12%	0.1490	3.24	0.44	2.23

* Computed from (C_{HA}+C_{FA}+K)
R^2 (C_{HA} with DOC_{HA}) = 0.570; ρ < 0.05 and R^2 (C_{FA} with DOC_{FA}) = 0.263; ρ > 0.05

RESERVOIR	Suwannee River Standard HA and FA end-members Slope values $f(x) = a_{HA}exp^{(-0.0137*x)} + a_{FA}exp^{(-0.0172*x)} + K$							DOC_{HA} mg/l	DOC_{FA} mg/l	$a_{HPO}(440)$* (m^{-1})
	C_{HA} mg/l	C_{FA} mg/l	K	SSE	%HA	%FA	RMSE			
CCR	0.037	0.427	0.04	0.22	8%	92%	0.0214	0.29	3.30	0.49
LPD	0.252	0.320	0.27	0.11	44%	56%	0.0154	1.88	2.39	0.59
LCB	0.273	0.296	0.03	0.28	48%	52%	0.0259	2.16	2.34	0.58
WIV	0.084	0.299	0.02	0.35	22%	78%	0.0145	0.74	2.61	0.39
LSD	1.077	0.133	0.00	0.03	89%	11%	0.1766	5.21	0.64	1.22
SAM	2.237	0.195	-0.08	0.14	92%	8%	0.0727	3.80	0.33	2.39
LWE	0.475	0.684	0.03	0.17	41%	59%	0.0198	1.74	2.51	1.17
TIN	5.823	0.506	-0.11	0.35	92%	8%	2.8810	6.71	0.58	6.35
ADV	1.835	0.227	-0.07	0.02	89%	11%	0.0805	2.96	0.37	2.04
LLD	1.721	0.669	0.40	0.04	72%	28%	1.2714	7.45	2.90	2.44
MOO	2.001	0.326	-0.06	0.14	86%	14%	0.0792	3.16	0.52	2.31

* Computed from (C_{HA}+C_{FA}+K)
R^2 (C_{HA} with DOC_{HA}) = 0.509; ρ < 0.05 and R^2 (C_{FA} with DOC_{FA}) = 0.283; ρ > 0.05

In Table (4-6) the Root Mean Square Error (RMSE), offset parameters (*K*) and the Sum of Squared Error (SSE) are shown. The maximum and minimum end-members for HPO fraction slope values of the SEQ study area gives the best goodness of fit than Kirk and Suwannee River end-members. Where, the SSE and RMSE are (0.12 and 0.028) closely followed by the Kirk end-members (0.13 and 0.086) then Suwannee River end-members (0.16 and 0.423).

In addition, using the maximum and minimum end-members lead to improvements in the relationship between absorption coefficients and DOC when using simple linear regression as presented in Table (4-7). The highest correlation of regression coefficient between the modelled HA with DOC is for the maximum and minimum end-members ($R^2 = 0.635;\ \rho < 0.05; N = 28$) then Kirk end-members ($R^2 = 0.564;\ \rho < 0.05; N = 28$) and Suwannee River end-members ($R^2 = 0.512;\ \rho > 0.05; N = 28$). Furthermore, linear regression using the modelled FA with DOC is less than 0.3 for Kirk and Suwannee River end-members while, it is ($R^2 = 0.552;\ \rho < 0.003; N = 28$) for the maximum and minimum end-members.

Table 4-7: Linear Correlation of Regression Between; Upper Table) Absorption coefficients of HPO fractions calculated by using SEM with DOC concentrations; Lower Table) Absorption Coefficients of the decomposed HA and FA fractions calculated by using three types of End-embers with DOC concentrations, in addition to, the significance of the regression, *F* parameter and significance *F*.

Model	HPO - DOC			
	R^2	ρ	*F*	Significance *F*
SEM	0.329	0.0001	7.735	0.009

End-Members	HA - DOC				FA - DOC			
	R^2	ρ	*F*	Significance *F*	R^2	ρ	*F*	Significance *F*
MAX-MIN	0.635	0.002	12.654	0.002	0.552	0.003	10.591	0.008
Kirk	0.564	0.004	8.945	0.007	0.221	0.028	4.250	0.171
Suwannee River	0.512	0.065	9.412	0.017	0.284	0.172	2.948	0.094

The F-parameter in Table (4-7) was computed to describe observed absorption coefficients of HPO, HA and FA from using different models. It was computed by using equation (4.14):

$$F = \frac{{R^2}/{D_m}}{{(1-R^2)}/{D_e}} \tag{4.15}$$

Where D_m is the degrees of freedom of the model ($D_m = No.of\ model\ parameters - 1$), and D_e is the degrees of freedom of the error ($D_e = No.of\ data\ stations - No.of\ model\ parameters$).

The higher the F value, the more useful the model is. So, the maximum and minimum end-members provided a high F value (F_{HA} = 12.654; $\rho < 0.05$ and F_{FA} = 10.591; $\rho < 0.05$) besides its high R^2 for both fractions HA and FA.

As for, the test results obtained from using Kirk end-members directly in equation (2.9) were close to the results achieved from using Suwannee River end-members with approximately close values of F-parameters (table 4-7). The comparison between the measured and the modelled values was in order to assess the influence of using the different nominated end-members. The average measured and modelled $a_{CDOM}(440)$ values of each reservoir are shown in Table (4-8).

The results showed that the maximum and minimum end-members too are consistently close to the measured CDOM (R^2 = 1; ρ < 0.05). It gives the best goodness of fit between the measured and the modelled CDOM values and the average offset values are also the lowest.

Table 4-8: The Modelled a_{CDOM} Values at 440 nm from Using the Multi-Components Decomposition Model

RESERVOIR	Measured $a_{CDOM}(440)$	Modelled $a_{CDOM}(440)$ using MAX-MIN end-members	Modelled $a_{CDOM}(440)$ computed from using Kirk end-members	Modelled $a_{CDOM}(440)$ using Suwannee River end-members
CCR	0.57	0.56	0.54	0.53
LPD	0.39	0.38	0.38	0.61
LCB	0.76	0.72	0.69	0.67
WIV	0.42	0.45	0.43	0.41
LSD	1.37	1.38	1.34	1.37
SAM	2.06	2.11	2.14	2.62
LWE	1.18	1.22	1.31	1.3
TIN	6.67	6.84	6.44	6.76
ADV	1.56	1.46	2.07	2.17
LLD	2.78	2.63	2.44	2.69
MOO	1.95	1.86	1.77	2.45

4.7.5 Discussion and Conclusions

The CDOM spectra of 28 sampling stations were decomposed into their major influential components that affect absorption and DOC content. The spectral decomposition was carried out using the linear and nonlinear approaches where the linear approach requires fixed slope values for the model parameters (HA, FA and HPI) referred to as end-members. A number of end-members were selected that can be applied for the Australian inland waters: the SEQ study area end-members from adopting the maximum and minimum slope values of the major CDOM-HPO fraction, Kirk slope values that were measured for Australian freshwaters and the international standard Suwannee River fulvic acid end-members.

The results of both nonlinear approaches (GRG and NLLSR) not capable to provide reliable results and some of the results in the solution domain out of the minimum and maximum boundaries of the slope values. In contrast, the results of using linear decomposition showed that the SEQ maximum and minimum end-members yielded the best outcomes. The correlation of regression was improved, and that could be useful for the next step in this work to do the remote sensing measurements between CDOM and DOC. Finally, there was no significant difference between the two suggested model in case the decomposition model was done on the HPO absorption spectrum or into the CDOM absorption spectrum.

4.8 Chapter 4 Conclusions

CDOM absorption spectrum models essentially based on using an exponential function despite their multiplicity of types. With high CDOM absorption values in the blue wavelength region, it is possible to interfere with the chlorophyll produced by the phytoplankton in the water causing scattering error (§4.2). Another source of error results from the presence of some small particles causing attenuation in CDOM absorption measurements and it is not negligible. Also, CDOM absorption measurements affected by systematic errors originated from the cuvette wall, baseline shift between the reference and the sample, temperature and the instrument. The correction of these errors can be done by including an offset parameter to the fitting model. Different fitting models are available to characterize

the CDOM absorption spectrum, but the selection may be subject to restrictions due to CDOM components.

Some fitting models can lead to a loss in and not fully capture all the information provided by CDOM absorption curve as explained in §4.6 and (figure 4-2). Also, to describe the CDOM absorption spectrum accurately apart from the effect of other components, the adoption of decomposition methods is commonly recommended. When to choose between complex alternatives and decide the correct model should be used to reduce measurements noise from CDOM components.

Linear and nonlinear regression approaches used to decompose the CDOM absorption curve. Using the linear and nonlinear decomposition of CDOM absorption spectrum that described in the previous sections and was implemented by fitting the sum of multi-exponential functions to the measured absorption spectrum to obtain an acceptable solution.

The linear decomposition approach was easier to apply than the nonlinear decomposition approach and less complicated because of the slope parameters that are not allowed to be changed within a specific range. Non-linear problems were intrinsically more difficult to solve than linear problems and the goal of NLLSR is to minimize the sum of squared errors, so it seems as though the model with the smaller sum-of-squares is the best.

The final results of using CDOM spectral decomposition were useful and helpful to give a good explanation to the relationship between CDOM absorption and DOC concentration on the one hand and between CDOM absorption and its chemical composition on the other.

The results of the decomposition showed that SEQ water bodies tend to be dominated by humic acid due to the high ratio of HA compared to FA. Another finding, the calculated slope values of the study area were superior to the calculated slope values of Kirk for the Australian inland waters when they used in CDOM decomposition model to characterize the relationship with DOC. While Suwannee River slope values were not applicable within Australian inland waters when it used in CDOM decomposition model.

Sometimes even with high R^2 for the model, the model cannot be useful as a descriptor of CDOM absorption spectra and R^2 alone was insufficient as a determinant of how well the model fits the data. Therefore, the F parameter was used to provide a better test of the usefulness of the nominated models that used different end-members. Same for the offset parameter, the method with the lowest average offset is considered the best. Finally, the advantage of using the multi-exponential model is convenient for optical modelling and remote sensing applications.

Chapter 5

Subsurface Reflectance Spectra Extraction of SEQ Water-bodies Using Radiative Transfer Simulation and Bio-Optical Modelling

5.1 Introduction

As it is clear from the title of this work and to achieve its objectives, the main focus is to improve DOC estimation from CDOM measurements remotely. In the previous chapters, CDOM-DOC relationship in SEQ was examined in different ways, starting with the simple relationship then investigated the effect of CDOM fractions on this relationship and their association with their sources. Also, the previous chapters have demonstrated that when performing CDOM absorption spectrum decomposition into multi-components the results were acceptable for high CDOM concentrations and reasonable for enhancing this relationship for almost all the selected locations in the study area. This chapter comes to complete the aims of this work in two ways. First, by assessing the remote sensing reflectance spectra for the study area using

different water components and CDOM fractions data. Second, by validating the improvement of the inverse retrieval of CDOM and then DOC and how will reflect on their relationship.

Chapter Five will begin by briefly reviewing the physical aspects of the energy transfer and the radiative transfer equation (RTE) after giving a presentation about the inherent and apparent optical properties of the natural water-bodies. As well, the theory and reasons for using the analytical and semi-analytical optical models of water reflectance and their types (e.g. Gordon-Walker model) will be discussed. This brief background is essential because it allows the reader to conceptualise the necessary knowledge used to support the purpose of the research.

The primary contribution of this piece of the work is to demonstrate whether CDOM fractions can be used as SIOPs inputs in the optical model to get better retrieval to estimate DOC. It will assess the variability in remote sensing reflectance spectra for the study area samples to achieve objective (4) of this work which is to parameterize and assess the contribution of the various water components beside CDOM major fractions on the simulated and modelled water reflectance spectra. Examining this variability and the classification will be through obtaining simulated spectral reflectance curves ($R(0-)_{simulated}$) from running the RTE using different concentrations for water components (CDOM, Chl and TR). Then to achieve objective (5) of this work, the effect of the humic (HS) and non-humic (NHS) substances (or Hydrophilic (HPI) and Hydrophobic (HPO) the same) will test using the multi-components absorption model to estimate $R(0-)_{optical-model}$ (reflectance obtained from the optical model) in order to make a relevant contribution to improve DOC estimation in the study area. Figure (5-1) address the objectives listed above for chapter five.

So, the effect of CDOM variation and also the other water components on the spectral reflectance curves in SEQ reservoirs will be simulated first by using ECOLIGHT® solver development to describe the optical properties of the selected water-bodies in the study area through which light propagates (the reflectance spectrum of water). Then, parameterising and modelling the measured specific absorption coefficients ($a^*(\lambda)$) of CDOM's main active fractions to drive the modelled

irradiance reflectance. Finally, to achieve a successful expressing to the output models, some issues need to resolve such as the correct inputs to the optical models and the right used model which are related to finding the correct formulation of the optical model in SEQ that could improve DOC estimation.

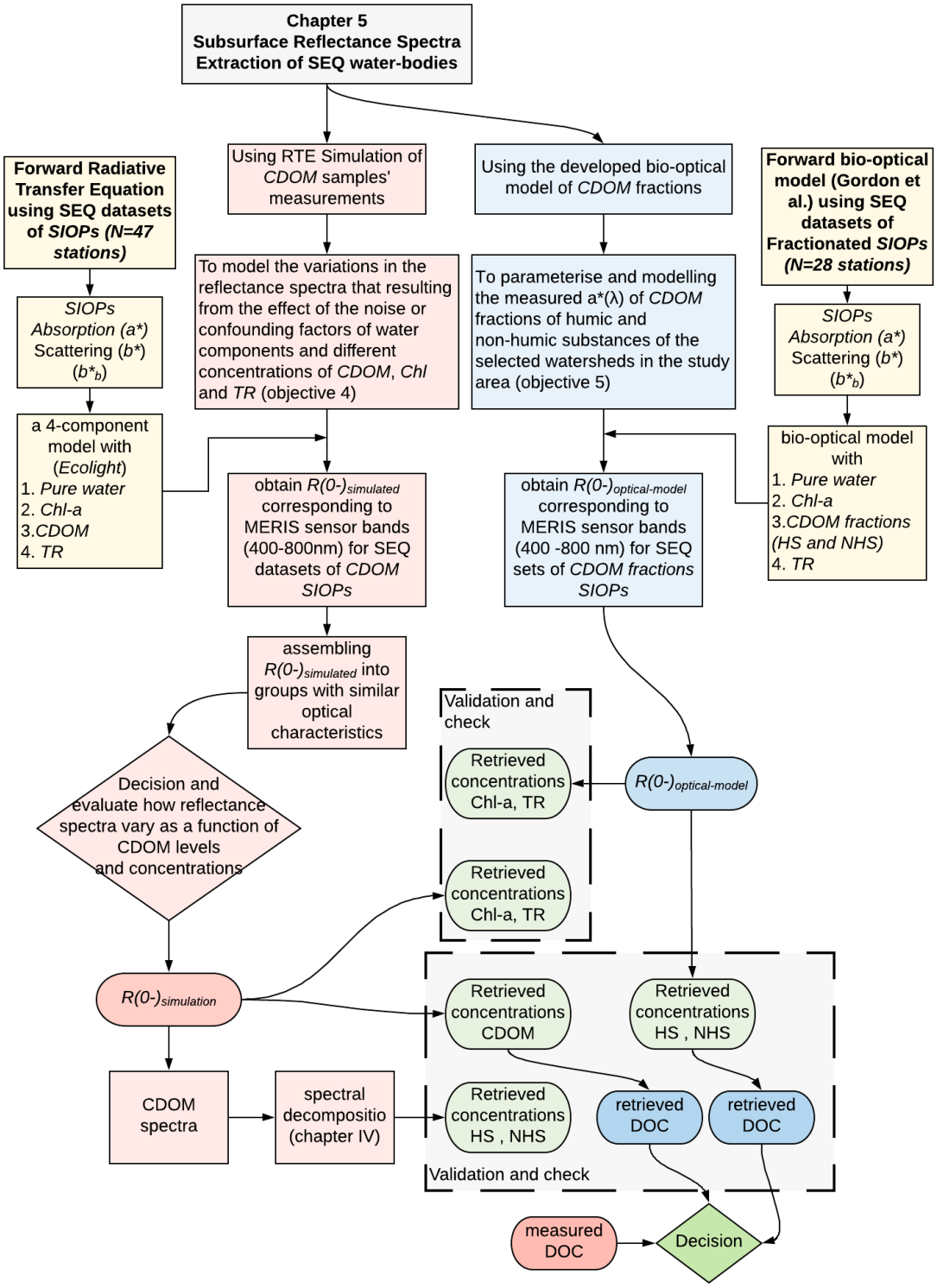

Figure 5-1: A Representation Scheme of Chapter Five Objectives.

5.2 Hydrologic Optics Properties of Water Substances that Required for SEQ Modelling (Inherent and Apparent Optical Properties)

Natural waters have four optical components: the water itself, some photosynthetic pigments and chlorophyll-a (Chl-a), solid particulate residues, and coloured dissolved organic matter (CDOM) (Liang 2017; Mishra et al. 2017). The different types of water are classified based on the levels of its various optical components. Therefore, extracting measurements of remote targets requires knowledge with the optical properties of these different water components.

The theoretical description and conceptual foundations of light flux in any aqueous solution are related to the electromagnetic radiation (Green, Sarah A & Blough, Neil V 1994). In electromagnetic quantum theory, electromagnetic radiation consists of photons, the primary particles responsible for all electromagnetic reactions. The quantitative effect provides additional sources of electromagnetic radiation, such as the transmission of electrons to lower or higher energy levels in the atom.

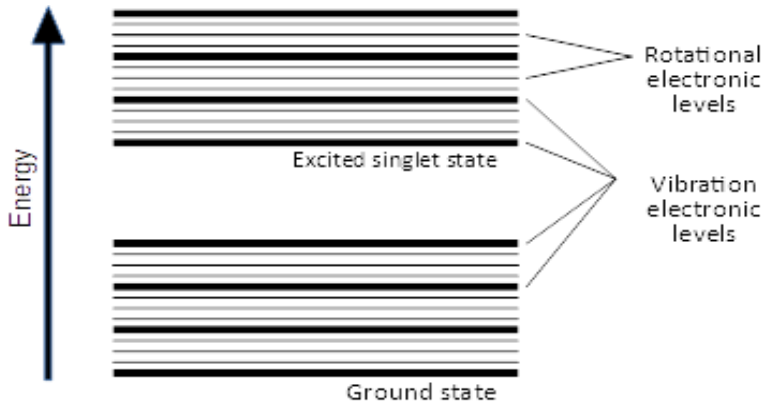

Figure 5-2: A Schematic Energy Level Diagram for An Organic Molecule (Mostofa et al. 2013)

The chromophore of CDOM absorbs photons in the UV and visible bands in the wavelength range between (200-700 nm) which affect its optical properties and could be an indicator for its constituent. The theory of photon absorption for a chromophoric organic molecule in water or solution can be summarised by catalysing

the electron to transition from its ground level to the excited level (Mostofa et al. 2013); as shown in Figure (5-2). So, the electron transition could provide information on the structure of the organic molecule properties such as colour due to the energy change associated with this transition.

5.2.1 Inherent Optical Properties

When a photon interacts and encounters with the matter, it may be absorbed, scattered or transmitted depend on the properties of the matter (e.g. water) (Sabins 2007). These absorption and scattering properties of the matter to the photon are defined as the *Inherent Optical Properties* (IOPs) (Mobley et al. 2010). The inherent optical properties of each optically active constituent are required to parameterise the used model in this study.

IOPs do not depend on the volume of the matter or on the ambient light field but, they depend only on the water itself and its suspended or dissolved substances in it (e.g. concentration of the substances) (Hoge et al. 1995). Therefore, they can be measured in the laboratory from collecting water samples as well as in situ. IOPs could mainly describe in terms of the total attenuation coefficient $c(\lambda)$, absorption coefficient $a(\lambda)$, scattering coefficient $b(\lambda)$, and volume scattering function (*VSF*) or (β). The two important fundamental coefficients of IOPs are; the absorption coefficient and the scattering coefficient (Bukata et al. 1995) and will be discussed in more detail below.

5.2.1.1 Absorption of Water Components

Natural waters have four main optical components which they: the water itself, chlorophyll-a (Chl-a) and other pigments, Non-Algal particles, and CDOM. These water components affect the light field within the water column when photons enter this medium, they are absorbed, and it is expressed as a linear sum of the absorption of each of the components as shown in the equation by (Gordon 1973):

$$a_T(\lambda) = a_w(\lambda) + a_{CDOM}(\lambda) + a_{TR}(\lambda) + a_\phi(\lambda) \quad (5.1)$$

Where, $a_T(\lambda)$ is the total absorption coefficient, $a_w(\lambda)$ is pure water absorption coefficient, $a_{CDOM}(\lambda)$ is CDOM absorption coefficient, $a_{TR}(\lambda)$ is tripton absorption coefficient and $a_\phi(\lambda)$ is phytoplankton absorption coefficient.

1. Absorption of Pure Water

Pure water can be defined as the chemically pure substance that consists of hydrogen (H) and oxygen (O) atoms only without any other components or impurities in it. Broad references to the literature on the spectral absorption of pure water are available (Heavens 1992; Pope & Fry 1997; Mueller et al. 2003). Pope and Fry (1997) determined the absorption coefficient of pure water $a_w(\lambda)$ between 350-727 nm. The $a_w(\lambda)$ in the blue region of the visible spectrum at ($\lambda = 440\ nm$) is significantly low (less than 0.01 m^{-1}) and rises towards the yellow and red bands (Pope & Fry 1997) (Figure 5-3). Pure water absorption coefficient varies with temperature and salinity where it increases when the temperature increases (Smith & Baker 1981), the typical absorption curve illustrated in Figure (5-3) is measured at temperature = 20°C.

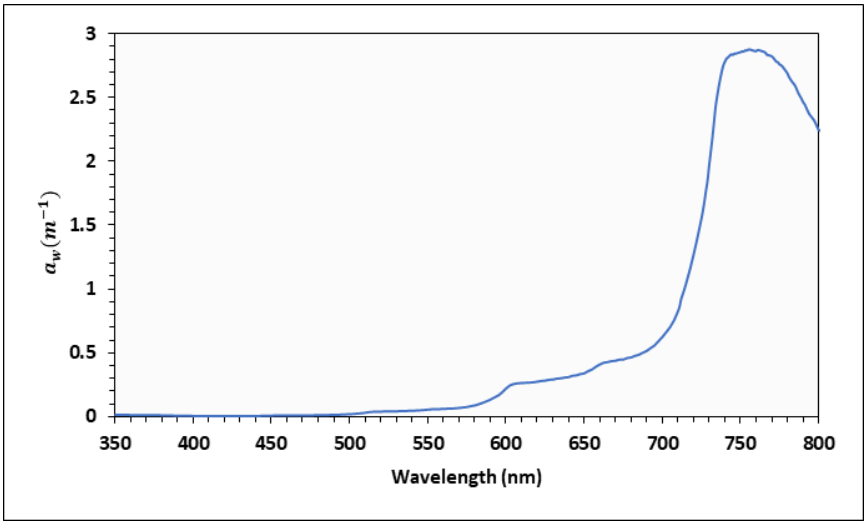

Figure 5-3: Absorption Coefficients of Pure Water as A Function of Wavelength (Data From (Pope & Fry 1997))

2. Absorption of Phytoplankton

Phytoplankton plays a principal role in determining the absorption of natural water because it is a strong absorber of visible light. Its absorption determined by the composition and concentration of a mixture of various species (cryptophyte type (L) and (H), diatoms, dinoflagellates and green algae) (Roesler & Perry 1995; Roesler & Barnard 2013) as shown in Figure (5-4).

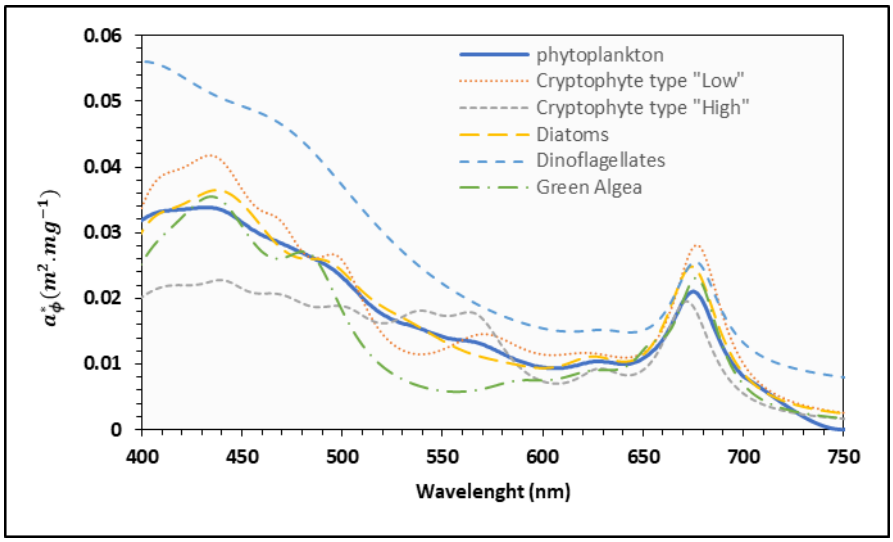

Figure 5-4: Normalised Phytoplankton Absorption Spectrum and Some of Its Pigment Classes (Data From (Gege 2004))

Figure (5-4) showing that each individual pigment of phytoplankton species has a unique spectrum. In addition, phytoplankton absorption can be reconstructed from the sum of the individual pigment absorption spectrum. Generally, the phytoplankton absorption spectrum exhibit peaks in the blue and red regions due to the chlorophyll-a (Chl-a).

3. Absorption of Tripton (TR)

The non-algae particles (NAP) or (Tripton) are defined as the particulate materials suspended in water and comprise of nonliving debris, some organic particles such as bacteria and zooplankton, non-pigment parts of phytoplankton and suspended inorganic particles (Morel 1991; Phlips 1995). The absorption spectra of these particles were well described by an exponential function (Babin et al. 2003):

$$a_{TR}(\lambda) = a_{TR}(\lambda_o)e^{-S(\lambda-\lambda_o)} \quad (5.2)$$

Tripton absorption is characterized by a monotonic increase in the short wavelengths and the absorption spectrum in the blue region decreasing exponentially towards the red region as shown in Figure (5-5) (Roesler et al. 1989; Bricaud et al. 1998).

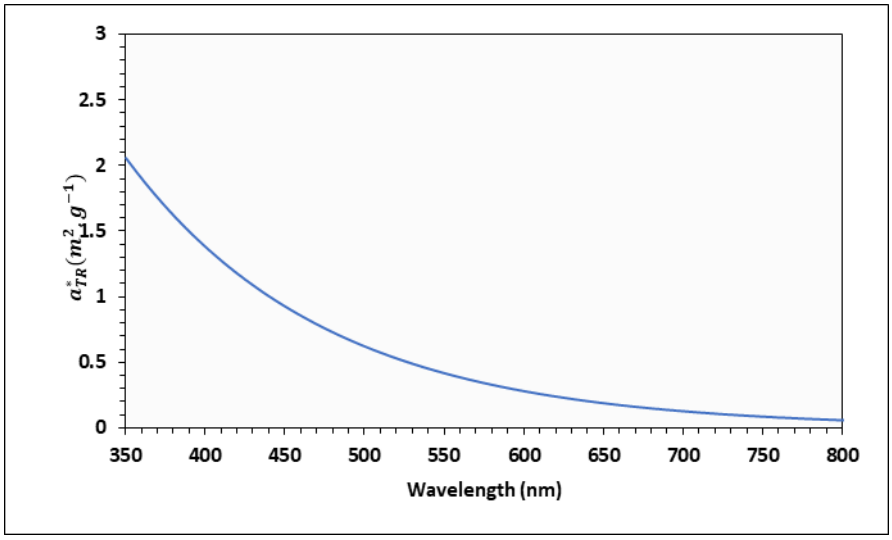

Figure 5-5: Normalised Tripton Absorption Spectrum (Data From (Gege 2004))

4. Absorption of CDOM

CDOM absorption is very similar to that of tripton due to in part of similarity in content (organic material) but generally demonstrate a steeper exponential slope. As explained in the previous chapters, CDOM can operationally separate from water constituent by filtration using a 0.2 nm or 0.7 nm nominal pore sized filters. CDOM absorbs most actively in the ultraviolet to blue region, and the value of absorption depends on its concentration in water.

5.2.1.2 Light Scattering by Water Components

The scattering properties of the aqueous medium can determine the angular distribution of the scattered flux created from different kinds of particles in water and resulting from the primary scattering process (Twardowski et al. 2001).

The *total scattering coefficient* (b) is the sum of the water constant molecular scattering in all directions, whether in the forward or backward directions and a variable contribution that results from differing particles in the water. So, the scattering geometry of the incident light beam distinguished between two important scattering terms, *forward scattering coefficient* (b_f) and *backward scattering coefficient* (b_b), where:

$$b = b_f + b_b \tag{5.3}$$

The *volume scattering function* (*VSF*) is essential to calculate the backward scattering coefficient that derived by integrating the VSF over the angles $\pi/2$ (90°) and π (180°) (Laanen et al. 2011), where;

$$b_b = 2\pi \int_{\frac{\pi}{2}}^{\pi} \beta(\theta) \sin\theta \, d\theta \tag{5.4}$$

More additive expression where the total backscattering can be further modified and defined as the sum of the identified backscattering of water components and it compute according to Morel (1974):

$$b_b(\lambda) = b_{bw}(\lambda) + b_{bTR}(\lambda) + b_{b\phi}(\lambda) \tag{5.5}$$

Equation (5.5) is only valid for water, tripton and phytoplankton except of CDOM, where its scattering contribution in watershed somewhat is neglected (Mobley 1996). Also, the scattering properties of the watershed can vary by orders of magnitude of the various constituents causing a fundamental problem of optical oceanography.

5.2.2 Apparent Optical Properties

The *apparent optical properties* (AOPs) are the above water measurements that depend on both the *IOPs* of the water body and the geometric structure of the ambient light field (Mishra et al. 2017). AOPs will give useful information if handled accurately about the significant constituents within the water body and their concentrations (e.g. CDOM). The proper definitions in the field of light geometry are essential in hydrologic optics. Radiometric measurements of electromagnetic energy depend on photons travelling in different directions within the light field (Mishra et al. 2017). Thus, it is crucial to describe the geometric relations of photon fluxes that are affecting the AOPs such as the *zenith angle* (θ) (the angle between the vertical and the incident light beam). Furthermore, besides the zenith angle, another expression in relation to the direction of the light beam is the *azimuth angle* (ϕ) which is the horizontal angle between the vertical plane of the incident light beam and with some other specified plane such as the sun. These angular relations are illustrated in Figures (5-6 A and B).

It is important to understand some terms and definitions of AOPs parameters to study and monitor the water body, which are:

1. Radiance (L)

The total photon's energy (radiant energy) falling on an area unit of a plane that arriving at a direction (θ) can be expressed by the term *radiance* (L) and is measured in ($W/m^2.steradian$) (Van der Meer & De Jong 2011). Figures (5-6 A and B) illustrate the definition of radiance and its field geometry. The mathematical expression to compute (L) can be done using the following equation:

$$L(\theta, \phi) = \frac{d^2\Phi}{ds\, cos\, \theta\, d\omega} \tag{5.6}$$

Where, $\boldsymbol{d\Phi}$ is the radiant flux at a determined direction in an infinitesimal cone, and $\boldsymbol{d\omega}$ is the solid angle of the cone.

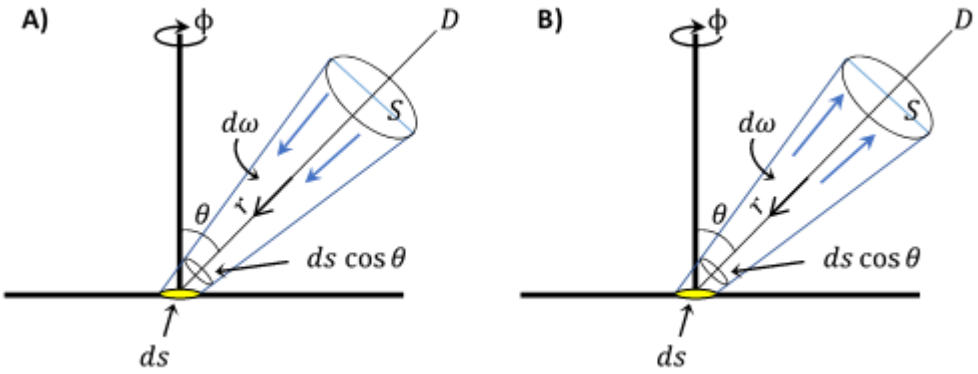

Figure 5-6: Illustration of Light's Radiant Flux A) Field Radiance Flux Passes $ds \cos\theta$ Area To ds Project Area at A Point in Plane Surface B) Surface Emits Radiation Upward in The Same Direction of Radiant Fluxes (Kirk 2011).

The *radiant flux* (Φ) term is the radiant energy of N photons emitted, transmitted, reflected or received per time unit:

$$\Phi(\lambda) = \frac{N\varepsilon(\lambda)}{t} \tag{5.7}$$

Where $\varepsilon = h.c/\lambda$ (**J.s**) with *h* = Plank's constant (6.6 $\times 10^{-34}$) (**J**) and *c* = speed of light in vacuum (3 $\times 10^{8}$) (**m/s**). While *radiant intensity* (I) is a measure of the radiant flux per unit solid angle in a certain direction measured in ($W/steradian$);

$$I = \frac{d\Phi}{d\omega} \tag{5.8}$$

2. Upward and Downward Irradiance (E)

Irradiance (E) is a directional parameter linked with the exchange in energy for the radiant flux received by a given area of a flat surface (Walker 1994). Irradiance SI base unit is the watt per square meter (W/m^2). The radiation received by a target in a horizontal plane surface from a specific direction represents the *downward irradiance* (E_d); Figure (5-7). It can be obtained at a particular point in the surface by integrating with respect to the zenith and azimuth angles. In contrast, the *upward irradiance* (E_u) is related to the radiance leaving the flat surface or the target in a specific direction (Albert & Gege 2006).

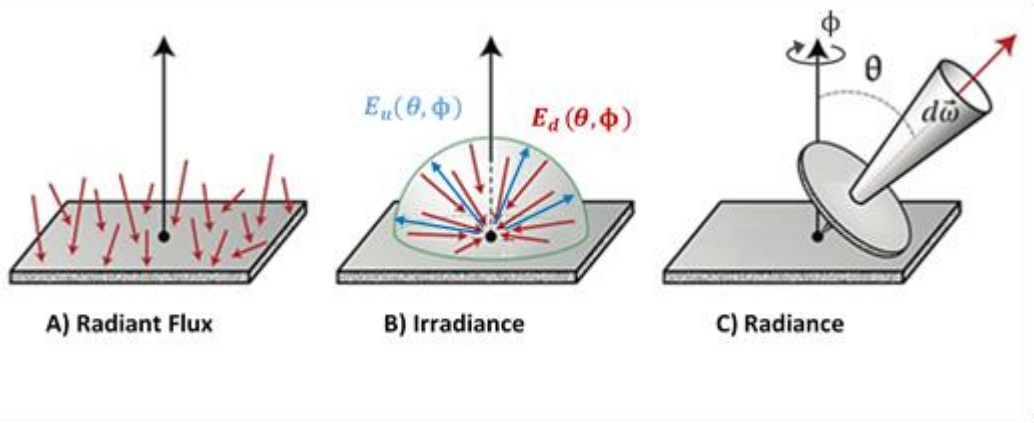

Figure 5-7: Graphical Illustration of; A) Radiant Flux B) Irradiance and C) Radiance (Abdellah 2017)

The angular structure of the light field can be beneficial as a relative contribution to the AOPs of the medium (Mobley 1994). In more details Table (5-1) showing the quantities of irradiance types and its equations:

Table 5-1: The Quantities of Irradiance

Formula	Quantities	Unit
$E = \int_0^{2\pi} \int_0^{\pi/2} L(\theta,\phi) cos\ \theta\ sin\ \phi\ d\theta\ d\phi$	Irradiance	$[W.m^{-2}]$
$E_d = \int_0^{2\pi} \int_0^{\pi/2} L(\theta,\phi) cos\ \theta\ sin\ \phi\ d\theta\ d\phi$	Downward irradiance	$[W.m^{-2}]$
$E_u = -\int_0^{2\pi} \int_{\pi/2}^{\pi} L(\theta,\phi) cos\ \theta\ sin\ \phi\ d\theta\ d\phi$	Upward irradiance	$[W.m^{-2}]$
$E_0 = \int_0^{2\pi} \int_0^{\pi} L(\theta,\phi) sin\ \theta\ d\theta\ d\phi$	Scalar irradiance*	$[W.m^{-2}]$
$E_{0d} = \int_0^{2\pi} \int_0^{\pi/2} L(\theta,\phi) sin\ \theta\ d\theta\ d\phi$	Downward scalar irradiance	$[W.m^{-2}]$
$E_{0u} = \int_0^{2\pi} \int_{\pi/2}^{\pi} L(\theta,\phi) sin\ \theta\ d\theta\ d\phi$	Upward scalar irradiance	$[W.m^{-2}]$

* The integral of radiance distribution at point overall directions about the point.

A useful and straightforward parameter calculated from the sun zenith angle and of the diffuse downward light's direction above the water is the average cosine of light. It could define as in the following equation (Mobley 1994):

$$\bar{\mu}_d = \frac{E_d}{E_{0d}} \tag{5.9}$$

And another one is for the upward average cosine given by:

$$\bar{\mu}_u = \frac{E_u}{E_{0u}} \tag{5.10}$$

These are measures of the directional structures of the downward and upward light fields. The average cosine can also be defined for the net downward irradiance:

$$\bar{\mu} = \frac{E_d - E_u}{E_0} \tag{5.11}$$

The quantities E_d, E_{0d}, E_u, E_{0u} and E_0 were shown in Table (5-1).

3. Water Reflectance

The ratio of the energy reflected relative to the total energy incident on the water body called the *irradiance reflectance* $R(0-)$ or in another expression, it is the ratio between the upward irradiance facing up on a horizontal surface to the downward irradiance facing down on a horizontal surface as given in the equation:

$$R(z,\lambda) = \frac{E_u(z,\lambda)}{E_d(z,\lambda)} \tag{5.12}$$

In hydrologic optics, there are some important quantitative measurements of the water column beside irradiance reflectance such as *remote sensing reflectance for above* and *below the water* R_{rs} and r_{rs} respectively (Mishra et al. 2017). In inland water remote sensing applications, the most commonly used *AOPs* is the R_{rs} that can be expressed as defined and measured in (sr^{-1}) (Yang et al. 2013):

$$R_{rs}(\theta, \phi, \lambda) = \frac{L_w(in\ air, \theta, \phi, \lambda)}{E_d(in\ air, \lambda)} \tag{5.13}$$

The above water remote sensing reflectance is the ratio of water-leaving radiance to the downward irradiance. Mobley et al. (2010) defined another important reflectance parameter is the *remote sensing ratio* (r_{rs}) or the below water remote sensing reflectance as indicated by the depth of the water column (z) measured in (sr^{-1}), where:

$$r_{rs}(z) = \frac{L_u(z)}{E_d(z)} \tag{5.14}$$

Thus, as presented the above water remote sensing reflectance is a function of wavelength only, while all other AOPs are functions of both wavelength and depth.

In order to clarify the concept of water remote sensing data and optical modelling, a number of spectra examples are given using Bio-Opti Toolkit (Version 2.0)*. Firstly, Figure (5.8 A) shows that the increase in CDOM from (0.25 to 5 m^{-1}) at fixed Chl (0.969 $mg.m^{-3}$) and tripton (22.265 $g.m^{-3}$) for different depths (0.5 m to 25 m) has directly proportional in $R(0-)$ spectrum especially in the blue and green region of the spectrum.

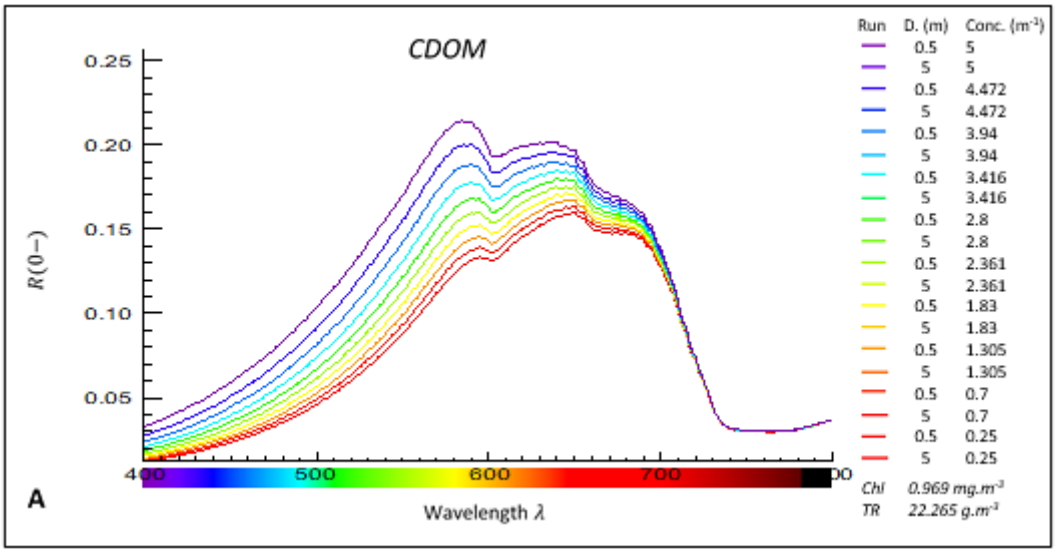

* It is a software program providing interactive visualization of the relationship of water components concentrations and the optical properties of water

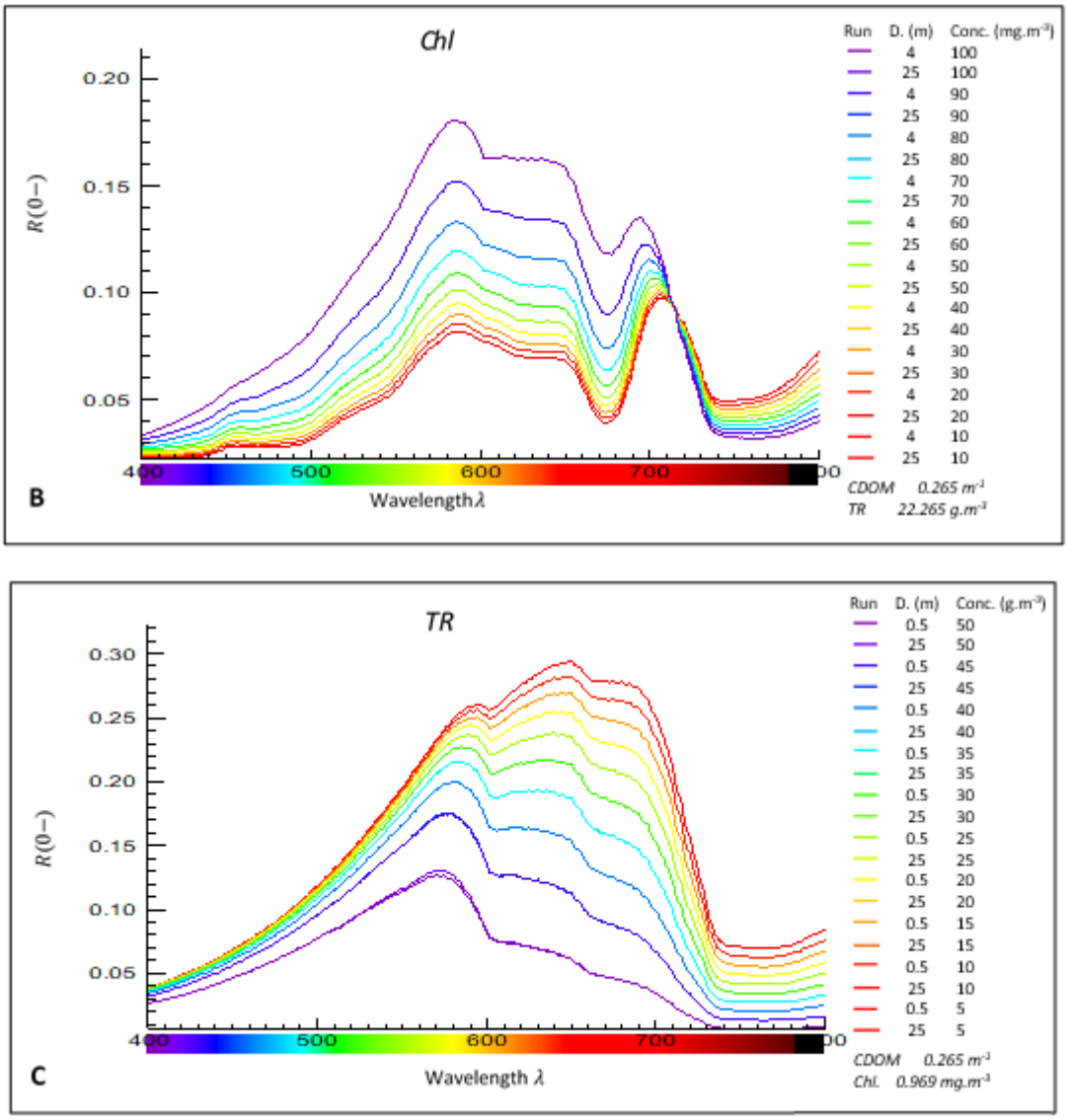

Figure 5-8 : The Simulated Reflectance Spectra Using Bio-Opti Toolkit V2.0 Where: A) *CDOM* Reflectance, B) *Chl* Reflectance, and C) Tripton Reflectance. The legend represents program runs (20 runs each case) with fixed one component concentration.

Secondly, Figure (5.8 B) illustrate the effect of the concentration of the Chl on $R(0-)$ spectrum with the depth of the water column (z). When the concentration changed between 10 and 100 mg.m^{-3} at fixed CDOM value (0.265 m^{-1}) and tripton 22.265 g.m^{-3}) for two different depth (4 m and 25 m) it shows that there are a decrease in $R(0-)$ spectra because of the absorbing of Chl. Another point, depth changing did not significantly affect the reflectance spectrum $R(0-)$ at these two values (0.5 m and 25 m) because it considered deep waters as no light reflected from the bottom exits the water surface.

Finally, Figure (5.8 C) shows that when the concentration of tripton (*TR*) increased from (5 to 50 g.m^{-3}) and fixing the concentrations of Chl at (0.969 mg.m^{-3}) and CDOM value at (0.265 m^{-1}) for water column depth (0.5 m and 25 m). An increase in the reflectance spectra caused by particles that scattering rather than an absorbing light.

Thus, the simulated reflectance shows the individual effects of Chl, CDOM and TR, also it found that at high concentrations, Chl has a high impact on retrieving CDOM concentration and this case will cause a problem when CDOM concentrations will retrieve accurately for aquatic remote sensing applications .

5.2.3 Radiative Transfer Equations (RTE)

The propagation of light within the water-atmosphere system is governed by radiative transfer equations (RTE) which is a mathematical expression (integral-differential equation) describes the changes of light paths from the source to the sensor with the depth, and it is related to the inherent optical properties of water (Thomas & Stamnes 2002). The main IOPs that RTE depending on are the absorption and scattering parameters of the water body. The analytical approaches of RTE can utilise in the water-atmosphere system to obtain more information and test approximate solutions in optical oceanography.

The widely used description to determine this relationship is based on suitable simulations to arrive at an accurate description for the unpolarised radiance in a particular medium. It summarised by the following expression (Gordon 1973; Bukata et al. 1995; Kirk 2011):

$$\frac{dL(z,\theta,\phi)}{dr} = -cL(z,\theta,\phi) + L^{*}(z,\theta,\phi) \qquad (5.15)$$

Where $L^{*}(z,\theta,\phi)$ is the radiance at depth (z) of a photon beam diffusing in the direction (zenith and azimuthal angles (θ,ϕ)) as shown in Figure (5-9), (dL/dr) represents the change in radiance along the direction (r) experienced by this photon beam due to the combined processes of absorption and scattering, and (c) is the total beam attenuation coefficient appropriate to the medium.

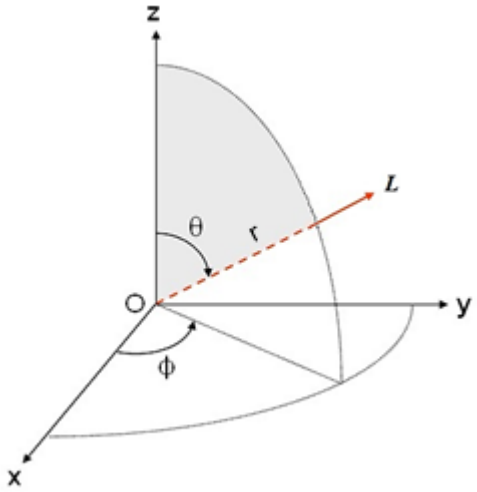

Figure 5-9: The Geometry and Definition of RTE

The first term in the right-hand side $(-cL(z,\theta,\phi))$ of the equation (5.15) represents a loss by attenuation in light intensity due to both absorption and scattering. While the second term $(L^*(z,\theta,\phi))$ at the same side of the equation; represents the gain by scattering. It involves all volume elements in the medium as a source of scattering and called the path function or final radiance (Gordon & Morel 1983; Kirk 2011) and is given as:

$$L^*(z,\theta,\phi) = \int_{2\pi} \beta(z,\theta,\phi,\theta',\phi')L(z,\theta',\phi')d\omega(\theta',\phi') \tag{5.16}$$

The volume scattering function $\beta(z,\theta,\phi,\theta',\phi')$ represents the probability that the radiance will be scattered between the initial light direction (θ',ϕ') of scattering and the direction (θ,ϕ). In addition, the term $L(z,\theta',\phi')d\omega(\theta',\phi')$ is the element of irradiance of a solid angle $d\omega(\theta',\phi')$ forming an infinitesimal cone.

In oceanography remote sensing, it usually more convenient to use depth (z) from the mean sea surface rather than using direction (r) along the beam path. Then, since (r) is a function related to (θ,ϕ) same as (z) (Figure (5-9)) therefore:

$$dr = \frac{dz}{cos\,\theta} \tag{5.17}$$

And by recalling equation (5.15) we will get the relation:

$$cos\,\theta \frac{dL(z,\theta,\phi)}{dz} = -cL(z,\theta,\phi) + L^{*}(z,\theta,\phi) \tag{5.18}$$

By integrating each term of the equation (5.18) to all angles:

$$\int_{4\pi} cos\,\theta \frac{dL(z,\theta,\phi)}{dz} d\omega = -\int_{4\pi} c(z)L(z,\theta,\phi)d\omega + \int_{4\pi} L^{*}(z,\theta,\phi)d\omega \tag{5.19}$$

The developed and the exact analytical solution of RTE of the equation (5.19) will be as finalized (Mobley 1999):

$$\begin{aligned} &cos\,\theta \frac{dL(z,\theta,\phi,\lambda)}{dz} \\ &= -[a(z,\lambda) + b(z,\lambda)]L(z,\theta,\phi,\lambda) \\ &+\ b(z,\lambda)\int_{0}^{2\pi}\int_{0}^{\pi} L(z,\theta',\phi',\lambda)\,\tilde{\beta}(z,\theta',\phi' \rightarrow \theta,\phi,\lambda)\,sin\,\theta'\,d\theta' d\phi' \\ &+ S(z,\theta,\phi,\lambda) \end{aligned} \tag{5.20}$$

Given the *IOPs* $a(z,\lambda)$, $b(z,\lambda)$ and the scattering phase function $\tilde{\beta}(z,\theta',\phi' \rightarrow \theta,\phi,\lambda)$ that gives an angular distribution of scattered energy in a specific direction (θ,ϕ) versus radiance being scattered in other direction (θ',ϕ'); the internal sources $S(z,\theta,\phi,\lambda)$; and boundary conditions at the air-water surface and the bottom.

A number of approximate analytical and semi-analytical solutions to the RTE can be derived after simplifying it in various ways as will be clarified in the following paragraph. Thus, these approximate solutions are useful for isolating the main factors influencing underwater radiances.

5.2.4 Bio-Optical Modelling and Algorithms Solution

In many aquatic systems, the optical properties of the water bodies are affected by the biological activities (Widder et al. 2001). Therefore, the bio-optical modelling designate to analyse and predict the optical properties of the water and its related constituent substances. Based on this assumption, water studies started to remotely

monitor the optical properties of water constituents such as chlorophyll-a (Chl-a) as a proxy of *phytoplankton* and algal bloom, and CDOM as a measurable part of DOC, while the total suspended solids (TSS) as an indicator for minerals and other solid substances in water (Jerlov 1968). Bio-optical modelling and its solutions have been concerned with the forward modelling theory or the inverse problem of water components. The basic concept of the forward bio-optical modelling is by converting the measured IOPs of water components to find the radiance distribution throughout and leaving the water (Gordon et al. 1975), as shown by the scheme in Figure (5-10).

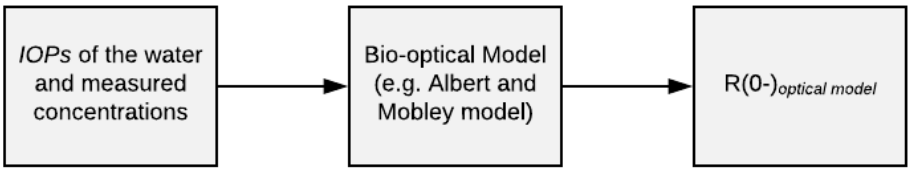

Figure 5-10: Schematic Diagram of Forward Bio-Optical Elements

In contrast, the inverse solution is to obtain water components from water colour measurements as in the scheme in Figure (5-11). Given radiometric measurements of underwater or water-leaving light fields target is to determine the IOPs of the water.

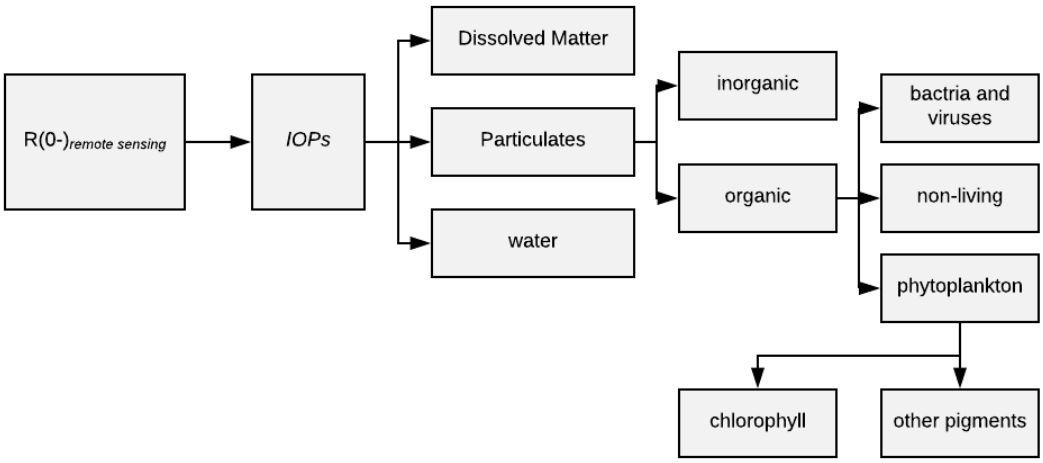

Figure 5-11: Schematic Diagram of Inverse Bio Optical Elements

Currently, bio-optical models were developed by the oceanographer to monitor and measure the optically active water constitutes. Various studies in aquatic remote sensing (Keith et al. 2016; Li et al. 2013; Miller et al. 2009) have demonstrated the need for regional model based on a developed algorithm in order to obtain better estimation for water constitutes. So, bio-optical models that might be developed and could be locally useful in some areas are not in general applicable in other areas.

Water quality retrieval algorithms can be classified in different types according to their formulation and goals (Odermatt et al. 2012). Five broad categories are found in literature, and they classify into empirical, semi-empirical, analytical, semi-analytical and quasi-analytical models, Figure (5-12). Empirical and semi-empirical models are based on statistical relationships between in-situ measurements and radiometric data. They generally use statistical relationships such as least square regressions, neural network and stepwise regressions. While, semi-analytical and quasi-analytical are depended on using RTE to establish a relationship between AOPs and IOPs (Lee et al. 2002).

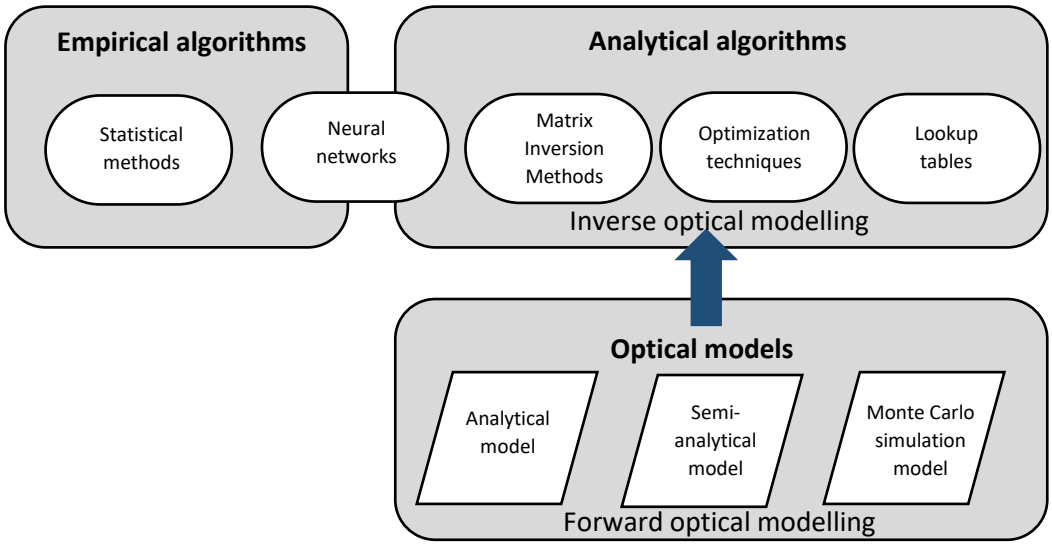

Figure 5-12: Schematic overview of Bio-optical algorithms types

The process used to estimate the absorption and backscattering is differed between semi-analytical and quasi-analytical models. Where the estimation of $a(\lambda)$ and $b_b(\lambda)$ in the semi-analytical model is compute by the sum of main the water components (*tripton*, *phytoplankton* and CDOM). On the other hand, absorption coefficients of water components is compute using spectral decomposition in quasi-analytical models directly from remote sensing reflectance.

The semi-analytical approach was chosen for this work for a number of reasons. It has the advantage to be easily adapted with the sensitivity of the different concentrations of water components and requires fewer field data. Also, it has better performance in retrieval accuracy.

5.3 Materials and Methods

Some studies conducted by Gordon (1973); Jerlov (1976) and Mobley (1995) on the spectral shapes of marine waters leads to a classification scheme of water components that have a relation with the water-colour. These spectra such as absorption, attenuation and remote sensing reflectance connect to water components, can be used with different types of numerical or analytical models to describe the distribution in light field and solve a wide range of problems in optical remote sensing (Mobley & Sundman 2001; Gege 2005). They can be either simulated or analysed using effective concentrations of the water components (e.g. CDOM, phytoplankton and tripton).

Accordingly, the materials and methods section below describes the dataset and the measured SIOPs of each SEQ station used to simulate and model the reflectance spectra as a computer-simulated dataset or modelled in the inversion to achieve the objectives of this chapter as presented in §5.1 and in Figure (5-1). Also, it introduces the different simulation and modelling scenarios used to investigate the influence of varying CDOM fractions and the other water components depending on the surrounding environment for the inversion methods and how they could affect the estimation of DOC remotely in the study area.

5.3.1 Inputs Parameters and Synthetic Ancillary Data for the Forward Modelling

The required dataset to implement the simulation and the forward optical modelling of the developed algorithm were obtained from different sources, and it is divided into:

a. Specific Inherent Optical Properties and Concentrations Dataset

The specific inherent optical properties and concentrations data of CDOM were taken from water samples of the study area measured and determined as described in (§2.9). While, the specific inherent optical properties of CDOM fractions (humic and non-humic substances) extracted, determined and measured for some water samples of the study area as described in detail in (§3.5). Data from Pope and Fry (1997) used for *pure water* IOPs (absorption and scattering values). The other water quality parameters, Chl-a and tripton concentrations were taken from published standard values of the study area that were taken by O'Bree (2007); Campbell (2010); Kirk (2011); Aryal et al. (2014); CSIRO and Bureau of Meteorology (2015).

b. Computer-Simulation Inputs Dataset to the Reflectance Spectra

Water reflectance spectrum can be simulated either with HYDROLIGHT® or ECOLIGHT® software from "Sequoia Scientific Inc.". Both study the connection between the various inputs and outputs of a marine light field in a controlled environment. They are radiative transfer numerical models that compute the AOPs of water such as (irradiances, reflectances, diffuse attenuation functions, etc.) but, they solve different versions of the radiative transfer equation with the same inputs and much of the same outputs. The main difference between HYDROLIGHT® and ECOLIGHT® is that ECOLIGHT® computes the azimuthally averaged radiance within each solid angle band, while HYDROLIGHT® computes the directionally averaged radiance within each quad as shown in Figure (5-13) (Mobley & Sundman 2001).

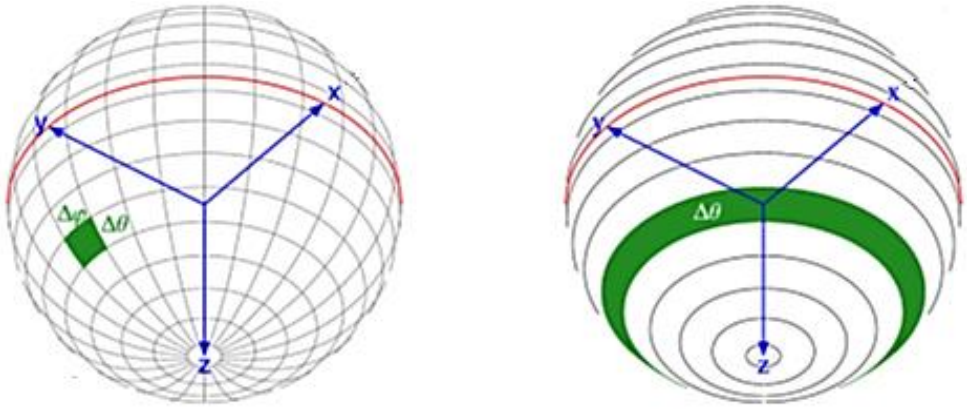

Figure 5-13: Interpretation of computation theory of; left) HYDROLIGHT® right) ECOLIGHT®

The selection of using ECOLIGHT® was made in this work to avoid the need to use the directional structure of the radiance distribution. Also, it is 100 times faster (Mobley & Sundman 2001) and reduces the calculation requirement of HYDROLIGHT®, and the upwelling light field contains all the optical information of IOPs relative to the depth (Babin et al. 2008). Finally, it gives more accurate and faster simulation by band averaging over azimuthal angles, as was explained in the previous paragraph of this section. Simulation by ECOLIGHT® 5 that will be carried out in this work will not only cover the natural concentrations of water constituents found in reservoirs of SEQ; it covers the concentrations below and above the range for more general variety. This extends the validity of the developed parameterisations to a wide number of case-II waters. Therefore, water reflectance of CDOM samples in SEQ was simulated numerically using ECOLIGHT® 5 software product (Sequoia Scientific, Inc.) for high-resolution dataset to achieve objective four of this work.

The input parameters of the selected 11 SEQ reservoirs were the measured spectral slopes and absorptions of CDOM, Chl-a concentrations in addition to tripton concentrations. The simulations did over contiguous wavelength bands corresponding to MERIS sensor for SEQ sets of SIOPs values.

The water column has been assumed to be infinitely deep with disabling bottom effects, and the radiometric quantities calculated for the subsurface only with typical

weather parameters. The wind speed set at 1 m/s with assumes no cloud cover (clear sky). The sun position was selected by default too so that the sun zenith angle was (45˚) while the Petzold phase function was selected and disabling the inelastic scattering and a fixed value of f equal (0.38) was used.

A total number of (18424) simulation scenario were performed in ECOLIGHT® for all reservoirs. For each reservoir, there were a number of simulations parameterized with different SIOPs and different concentration values of CDOM, Chl-a and tripton. We used different concentrations to closely represent the optical variability observed in the study area, which affects the DOC concentrations and therefore on the CDOM-DOC relationship as explained in Chapters Two and Three. Chl-a concentration values recorded for SEQ reservoirs varied between 5 to 60 $\mathrm{mg.\,m^{-3}}$ and recorded between 0.9 to 11.2 $\mathrm{g.\,m^{-3}}$ for tripton concentration values the ranges measured by SEQWater and CSIRO and from the literature that was mentioned in (a.) in (§5.3.1).

Three levels between the minimum and the maximum concentration values of Chl-a and tripton were used in addition to the values above and below the natural range (7 discrete concentration values in total for each one) so as to provide sufficient coverage without producing large numbers of very similar spectra. While six discrete concentration values of CDOM were selected and ranged between the minimum to the maximum measured values for each station in addition to the values above and below the natural range too (8 values in total) as shown in Table (5-2).

Thus, depending on the number of parameter values identified, resulting in 18424 concentration combinations.

Table 5-2: The Measured and Natural Concentrations Range of SEQ Watersheds' Constituents With the MIN and MAX Values and No. of Simulations Used to Simulate the Reflectance Spectra for Each Reservoir in SEQ (sun zenith angle =45°) (Wind Speed 1 m/s) (Clear Sky Condition) ($f = 0.38$)

ECOLIGHT ® run	Water constituent concentrations' inputs (the min and max values below and over the measured and natural range)				No. of Simulation per each reservoir (interval)	No. of Stations and SIOPs	No. of Spectra
	Chlorophyll-a ($mg.m^{-3}$)	Tripton ($g.m^{-3}$)	CDOM ($a_{CDOM}@440$) (m^{-1})				
			measured range (min-max)	Input range (min – max)			
1	5 – 60 (natural range) 3.75 - 75.0 (input range)	0.9 – 11.2 (natural range) 0.67 – 14.00 (input range)	0.49 – 0.66	0.37 – 0.82	392 ($7C_\phi \times 7C_{TR} \times 8C_{CDOM}$)	6	2352
2			0.42 - 1.00	0.31 – 0.75		1	392
3			0.65 - 0.81	0.49 – 1.01		5	1960
4			0.35 - 0.56	0.26 – 0.70		7	2744
5			0.87 - 6.00	0.65 – 7.50		5	1960
6			2.19 - 3.10	1.64 – 3.87		6	2352
7			1.11 - 1.51	0.83 – 1.89		3	1176
8			6.43 - 8.00	4.82 – 10.00		1	392
9			2.01 - 2.22	1.51 – 2.77		2	784
10			3.18 - 3.51	2.38 – 4.39		5	1960
11			2.40 - 2.59	1.80 – 3.24		6	2352
Total No. of simulations							18424

To capture most of the spectral variations of the simulated spectra, the simulated reflectance spectra then convolved and resampled with MERIS (MEdium Resolution Imaging Spectrometer) bands because there is a good agreement when using MERIS data for CDOM estimation (Candiani et al. 2007; Doerffer & Schiller 2007; Hu et al. 2007). Table (5-3) show the multispectral bands of MERIS sensors and their application that is suitable enough to use for monitoring case-II waters in general. The resampling done over the first 12 of 15 bands ranged between (400 – 800 nm).

Table 5-3: Table of the MERIS spectral bands and their applications (Lee & Carder 2002).

MERIS Channel Number	Centre Wavelength ± Bandwidth (nm)	Application
1	412.5 ± 10	Yellow substance and detrital pigments
2	442.5 ± 10	Chlorophyll absorption maximum
3	490 ± 10	Chlorophyll and other pigments
4	510 ± 10	Suspended sediment, red tides
5	560 ± 10	Chlorophyll absorption minimum
6	620± 10	Suspended sediment
7	665± 10	Chlorophyll absorption and fluorescence reference
8	681.25 ± 7.5	Chlorophyll fluorescence peak
9	708.75 ± 10	Fluorescence reference, atmospheric corrections
10	753.75 ± 7.5	Vegetation, cloud
11	760.625 ± 3.75	Oxygen absorption R-branch
12	778.75 ± 15	Atmosphere corrections
13	865 ± 20	Vegetation, water vapour reference
14	885 ± 10	Atmosphere corrections
15	900 ± 10	Water vapour, land

Finally, no need to set the atmospheric parameters based on longitude and latitude due to use ECOLIGHT® in contrast to HYDROLIGHT® that requires it. Only the wind speed, cloud cover and solar zenith angle introduced to the model as mentioned earlier. Using these simulations instead of measured spectra collected via air- or space-borne remote sensing to be able to test the effects of different confounding factors individually.

c. The Forward Bio-Optical Model to Derive Water Reflectance Based on the Chemically Isolated CDOM Fractions

To derive $\mathrm{R}(0-,\lambda)$ of the study area using forward bio-optical model, the use of semi-analytical approaches and the need for IOPs dataset is required. The primary inputs for the parameterisations this time were the measured SIOPs of CDOM fractions and their concentrations, in addition to the dataset that was explained in (§5.3.1.a and b) for pure water, phytoplankton and tripton. Linking the measured SIOPs of CDOM

fractions with the reflectance spectra is essential for this study to achieve objective five of this work and to progress to the next step of estimating DOC.

The parameters required for the model are the total absorption and the total backscattering. For optical modelling purposes, the measured IOPs values are proportional to the accompanying concentration values and represent the specific inherent optical properties. That means the total absorption can be modelled as:

$$a_T(\lambda) = a_w(\lambda) + a^*_\phi(\lambda).C_\phi + a^*_{TR}(\lambda).C_{TR} + a^*_{CDOM}(\lambda).a_{CDOM}(440) \quad (5.21)$$

The chlorophyll a specific absorption coefficient a^*_ϕ was obtained by normalising the absorption due to phytoplankton by the chlorophyll a concentration. Similarly, the tripton mass specific absorption coefficient a^*_{TR} was obtained by normalising the absorption due to nonalgal particles by the weight of the total suspended material less the weight of the phytoplankton.

The specific absorption spectra for tripton were fitted to the model:

$$a^*_{TR} = a^*_{TR}(\lambda_o)exp^{(-S(\lambda-\lambda_o))} \quad (5.21a)$$

With λ_o = 550

To give a better description of the CDOM estimation and to achieve the objectives, using two components of the CDOM absorption model was adopted in the bio-optical model that used in this study. Assuming this hypothesis has been based on some research conducted by Carder et al. (1989) and Laanen (2007). From the obtained results in chapter three and four of this work that which showed that the estimation of DOC had slightly improved when using these CDOM fractions. But, the most important finding in this work, not all DOC in CDOM can be chromophoric. Therefore, equation (5.21) was reformulated to suit the requirements and hypothesis of this work to become:

$$a_T(\lambda) = a_w(\lambda) + a^*_\phi(\lambda).C_\phi + a^*_{TR}(\lambda).C_{TR} + [a^*_{HS}(\lambda).a_{HS}(440) + a^*_{NHS}(\lambda).a_{NHS}(440)] \quad (5.22)$$

While a three-part backscattering model used in this work:

$$b_b(\lambda) = 0.5b_w + b^*_{bTR}(\lambda)C_{TR} + b^*_{b\phi}(\lambda)C_{\phi} \quad (5.23)$$

Where, $a^*_i(\lambda)$ the specific absorption coefficients, $b^*_{bi}(\lambda)$ the specific backscattering coefficient both at wavelength λ for a unit constituent of water component i, $b_b(\lambda)$ the backscattering coefficient at wavelength λ, and C_i the concentrations of the ith component of the water column.

For this study, the most common semi-analytical optical model developed by Gordon et al. (1975) for waters was utilised and designed to find $R(0-,\lambda)$. Therefore, the selection was made, and the following equation is to link *IOPs* with $R(0-,\lambda)$:

$$R(0-,\lambda)_{optical-model} = f(\omega_b,\mu_o)\frac{b_b(\lambda)}{a(\lambda)+b_b(\lambda)} \quad (5.24)$$

For convenience ω_b will be defined as:

$$\omega_b = \frac{b_b(\lambda)}{a(\lambda)+b_b(\lambda)} \quad (5.25)$$

Where $f(\omega_b,\mu_o)$ (proportionality factor) is an empirical factor depends mainly on the illumination conditions such as zenith angle (set to be 45°) and water scattering (solar and viewing geometry). Formulas proposed for estimating $R(0-,\lambda)$ in the literature (Dev & Shanmugam 2014; Pravin et al. 2015; Neukermans & Fournier 2018) showed acceptable results when the $f-factor$ was expressed as $f = 0.975 - 0.629$ or even as a constant equal to 0.33 or 0.38. Hence, in this study, the $f-factor$ will be constant equal (0.38) because there is no need to study its effect due to sun position on $R(0-,\lambda)$. Thus, the $R(0-,\lambda)_{optical-model}$ calculated from the forward bio-optical model and $R(0-,\lambda)_{simulated}$ simulated on ECOLIGHT® should be optically matched. Furthermore, the utilised bio-optical model has included the effect of CDOM fractions mainly because it based on the combined of HS and NHS SIOPs.

5.3.2 Inversion the Forwarded $R(0-,\lambda)$ using Matrix Inversion Method (MIM)

Inverting the reflectance spectrum of both $R(0-,\lambda)_{optical-model}$ and $R(0-,\lambda)_{simulated}$ to estimate the DOC concentration was done with respect to changes in IOPs and AOPs. A correct inversion approach is required for better DOC estimation from the reflectance spectrum. There are several inversion methods available to use including the Matrix Inversion Method (MIM), Lookup Tables (LUTs) and Neural Networks techniques. This work concentrated on MIM approach because it leads to a fast and easily unique solution to the problem and yield the best results. MIM theoretically is the best but in practice, it does not necessarily achieve the best outcomes because of its sensitivity to small errors in the spectrum. MIM was done by linearizing and subsequently solving the Gordon et al. model (Gordon et al. 1975) that shown in equation (5.24).

Two inversion methods were used, the direct simple MIM method and the developed MIM method. The direct simple MIM method was applied by inclusion equations (5.21 and 5.23) into equation (5.24) to the $R(0-,\lambda)_{simulated}$ to derive (Chl, TR and CDOM) and the results were validated against the inputs values. While the developed MIM method was applied to the $R(0-,\lambda)_{optical-model}$ to derive (Chl, TR, HS and NHS) and the results were validated against the inputs values. The developed MIM method was implemented by substituting equations (5.22) and (5.23) into equation (5.24). Constructed a linear algorithm system relating to the input data to MIM was as follows:

$$\frac{R(0-,\lambda)}{f(\omega_b,\mu_o)} = \frac{(0.5b_w + b^*_{bTR}(\lambda)C_{TR} + b^*_{b\phi}(\lambda)C_\phi)}{(a_w + a^*_\phi(\lambda).C_\phi + a^*_{TR}(\lambda).C_{TR} + [a^*_{HS}(\lambda).a_{HS}(440) + a^*_{NHS}(\lambda).a_{NHS}(440)]) + (0.5b_w + b^*_{bTR}(\lambda)C_{TR} + b^*_{b\phi}(\lambda)C_\phi)} \quad (5.26)$$

Where μ_o is the cosine of the sun zenith angle and ω_b is the backscattering albedo.

Since the IOPs and AOPs depends on the wavelength, unlike the water component concentrations. Therefore, if there are n bands, the equation (5.26) will be a set of n equations as shown:

$$\begin{aligned} &a_{HS}(440).a^*_{HS}(\lambda).\frac{R(0-,\lambda)}{f(\omega_b,\mu_o)} + a_{NHS}(440).a^*_{NHS}(\lambda).\frac{R(0-,\lambda)}{f(\omega_b,\mu_o)} + C_{TR}.\left(a^*_{TR}(\lambda).\frac{R(0-,\lambda)}{f(\omega_b,\mu_o)} - b^*_{bTR}(\lambda).\left(1 - \frac{R(0-,\lambda)}{f(\omega_b,\mu_o)}\right)\right) \\ &\quad + C_\phi.\left(a^*_\phi(\lambda).\frac{R(0-,\lambda)}{f(\omega_b,\mu_o)} - b^*_{b\phi}(\lambda).\left(1 - \frac{R(0-,\lambda)}{f(\omega_b,\mu_o)}\right)\right) \\ &\quad = 0.5.b_{bw}.\left(1 - \frac{R(0-,\lambda)}{f(\omega_b,\mu_o)}\right) - a_w.\frac{R(0-,\lambda)}{f(\omega_b,\mu_o)} \end{aligned} \quad (5.27)$$

Equation (5.27) can represent in a matrix form as:

$$\begin{bmatrix} a^*_{HS}(\lambda_1).\frac{R(0-,\lambda_1)}{f(\omega_b,\mu_o)} & a^*_{NHS}(\lambda_1).\frac{R(0-,\lambda_1)}{f(\omega_b,\mu_o)} & a^*_{TR}(\lambda_1).\frac{R(0-,\lambda_1)}{f(\omega_b,\mu_o)} - b^*_{bTR}(\lambda_1).\left(1-\frac{R(0-,\lambda_1)}{f(\omega_b,\mu_o)}\right) & a^*_{\phi}(\lambda_1).\frac{R(0-,\lambda_1)}{f(\omega_b,\mu_o)} - b^*_{b\phi}(\lambda_1).\left(1-\frac{R(0-,\lambda_1)}{f(\omega_b,\mu_o)}\right) \\ \vdots & \vdots & \vdots & \vdots \\ a^*_{HS}(\lambda_n).\frac{R(0-,\lambda_n)}{f(\omega_b,\mu_o)} & a^*_{NHS}(\lambda_n).\frac{R(0-\lambda_n)}{f(\omega_b,\mu_o)} & a^*_{TR}(\lambda_n).\frac{R(0-,\lambda_n)}{f(\omega_b,\mu_o)} - b^*_{bTR}(\lambda_n).\left(1-\frac{R(0-,\lambda_n)}{f(\omega_b,\mu_o)}\right) & a^*_{\phi}(\lambda_n).\frac{R(0-,\lambda_n)}{f(\omega_b,\mu_o)} - b^*_{b\phi}(\lambda_n).\left(1-\frac{R(0-,\lambda_n)}{f(\omega_b,\mu_o)}\right) \end{bmatrix}_{n\times 4}$$

$$\times \begin{bmatrix} a_{HS} \\ a_{NHS} \\ TR \\ \phi \end{bmatrix}_{4\times 1} = \begin{bmatrix} b_{bw}(\lambda_1).\left(1-\frac{R(0-,\lambda_1)}{f(\omega_b,\mu_o)}\right) - a_w(\lambda_1).\frac{R(0-,\lambda_1)}{f(\omega_b,\mu_o)} \\ \vdots \\ b_{bw}(\lambda_n).\left(1-\frac{R(0-,\lambda_n)}{f(\omega_b,\mu_o)}\right) - a_w(\lambda_n).\frac{R(0-,\lambda_n)}{f(\omega_b,\mu_o)} \end{bmatrix}_{n\times 1} \quad (5.28)$$

Or,

$$A.X = B \tag{5.29}$$

Where A and B are the dimension matrices with the n number of bands, and X is the matrix variables (a_{HS}, a_{NHS}, TR and ϕ). The solution of the above matrices typically will be:

$$A^{-1}.A.X = A^{-1}.B \tag{5.30}$$

And by simplified the solution then becomes,

$$X = A^{-1}.B \tag{5.31}$$

Because the MIM are more than three bands, it should be using the least square method to obtain water component concentrations.

5.3.3 Data Analysis

The forwarded modelled spectra and the computer-simulated reflectance spectra optically they should be close. First, the mean absolute percentage error (MAPE) calculated as:

$$MAPE = \frac{\left|R(0-,\lambda)_{simulated_i} - R(0-,\lambda)_{optical-model_i}\right|}{R(0-,\lambda)_{simulated_i}} \times 100 \tag{5.32}$$

The coefficient of determination (R^2) calculated between both curves of the $R(0-,\lambda)$ for each reservoir. Then measuring how much error there is between the two spectra of the $R(0-,\lambda)$ was done by using Root Mean Square Error (RMSE). The theoretical formula used to compute RMSE is through the following:

$$RMSE = \sqrt{\frac{\sum_{i=1}^{n}(R(0-,\lambda)_{simulated_i} - R(0-,\lambda)_{optical-model_i})^2}{n}} \tag{5.33}$$

While the inversion model performance was evaluated using the Normalized Root Mean Square Error (NRMSE). Normalising the RMSE is to facilitate the comparison between the models, and it is calculated by dividing RMSE by the concentration range using the following expression:

$$NRMSE = \frac{RMSE}{C_{max} - C_{min}} \tag{5.34}$$

In SPSS® software version 7 differences accuracy between both spectrums values were determined in addition for the rest statistical operations.

5.4 Results and Discussion

As was explained earlier, the proposed scenario for this chapter is consists of several parts; the first part is to simulate the subsurface reflectance using ECOLIGHT® parameterised with the measured total CDOM per-sample SIOPs only that we called $R(0-,\lambda)_{simulated}$. The second part is to model the subsurface reflectance using the developed bio-optical model in this work (equation (5.29)). This model is based on Gordon's et al. model, CDOM fractions of humic and non-humic substances were used. The resulted $R(0-)$ we called $R(0-,\lambda)_{optical-model}$. Also, the results of the inversion and retrieving validity were then compared between them and with the original concentrations and examine the confounding effect of other water constituents on the estimation of DOC.

5.4.1 Simulated SEQ Subsurface Reflectance using ECOLIGHT® (Radiative Transfer Model)

A four components case-II model in ECOLIGHT® was used to extract $R(0-,\lambda)_{simulated}$ using per-sample CDOM-SIOPs and various concentrations of the water constituents (CDOM, Chl and TR) that simulated SEQ reservoirs and then convolved with the most relevant MERIS bands. The simulation was performed not only over the natural concentration range of water constituents that were mentioned in this work for the study area but also below and above it for two reasons. First, to

cover a broader range of concentrations, secondly, to examine their variations and their effects on the standard inversion of the estimation of DOC in the study area. Figure (5-14) shows the outputs of the average reflectance spectra of ECOLIGHT® simulation of the 11 SEQ watersheds for this study (18424 simulations).

A closer examination of each simulated spectrum reveals that the reflectance ratio is low in the range between 400–500 nm due to the high absorption of CDOM. As well as, the high absorption of tripton and part of the phytoplankton which interferes with the absorption of CDOM in this wavelength range that affected on the reflectance spectrum. The simulated $R(0-,\lambda)$ that contains the normalised CDOM absorption dataset implicitly with the other water constituents showed high variation beside a variety in their spectral shape that can identify. The absorption feature in the red band between 650 – 700 nm is caused predominantly by algal pigments followed by low absorption caused dome-shape in the spectrum, which results from CDOM, suspended sediments and chlorophyll absorption at short wavelengths.

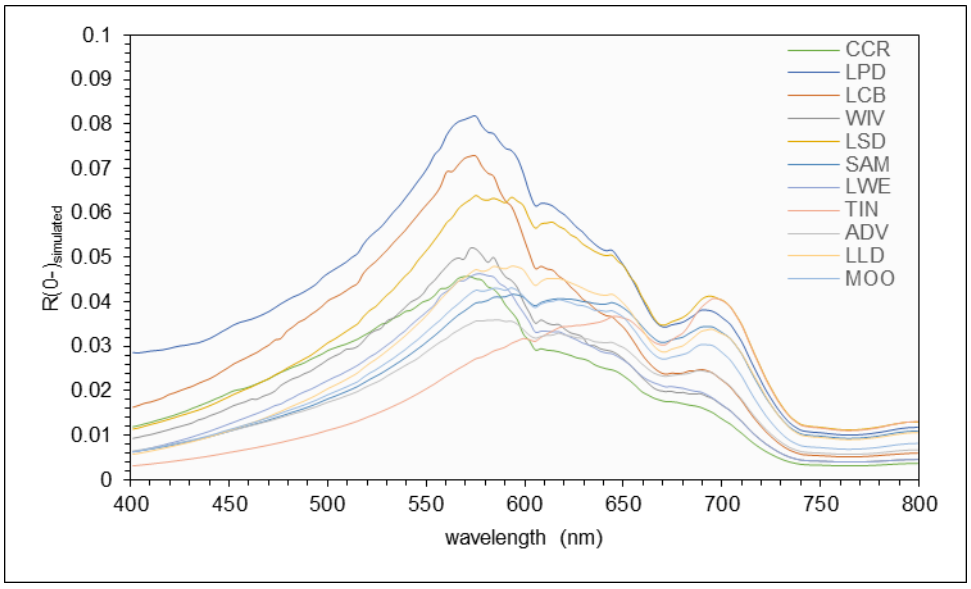

Figure 5-14: The Average Simulated $R(0-,\lambda)$ of SEQ Study Sites Using ECOLIGHT® ($f = 0.38$)

While the maximum, minimum and mean $R(0-,\lambda)_{simulated}$ values of the study area in total are shown in Figure (5-15). It increases with increasing the wavelength to reach its peak at 580 nm approximately and then begins to decrease gradually towards 700 nm. Strong hump-shape can notice at the 700 nm, which is caused by

TR. The mean $R(0-,\lambda)_{simulated}$ spectrum for the study area and the 95% confidence intervals results are shown in Figure (5-15).

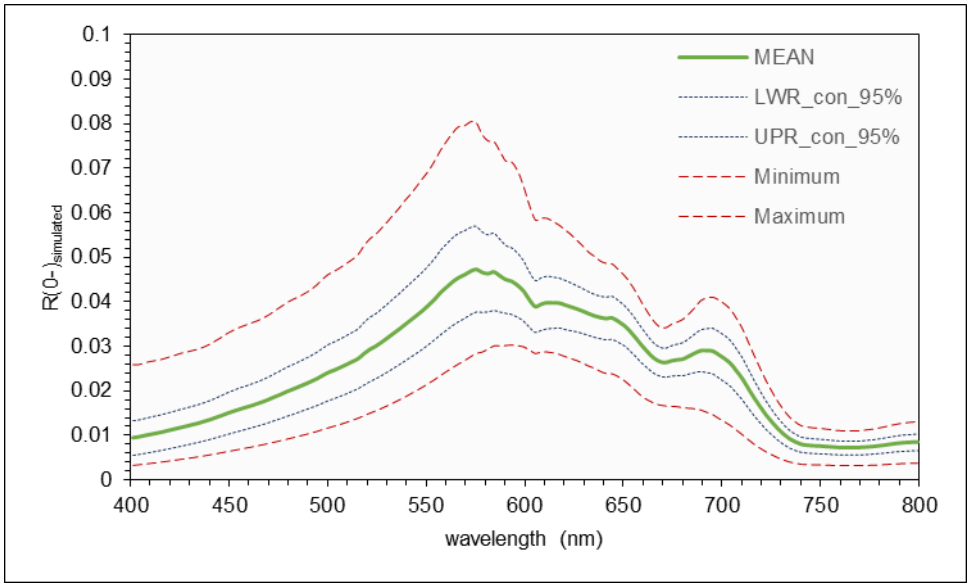

Figure 5-15: Minimum, Maximum and Mean values with the 95% Confidence Intervals of the Simulated $R(0-,\lambda)$ of SEQ Reservoirs Extracted in ECOLIGHT®

5.4.2 SEQ Subsurface Reflectance Spectra Extracted using the Bio-Optical Model

Another forward model was built to find the $R(0-,\lambda)_{optical-model}$ using the measured per-sample SIOPs of CDOM fractions this time according to the scenario and objectives of this work. The developed Gordon model in this work was used (equation 5.29), each sampling location parameterised with its own measured and fractionated concentrations and SIOPs, fixed value of f equal (0.38) was used. The execution was done using an IDL subroutine program, and the results were (10976) spectra.

Figure (5-16) shows the average $R(0-,\lambda)_{optical-model}$ of each reservoir. As expected the same spectral variations that were in the simulated spectra (Figure 5-14) have been noticed because they caused by scattering and absorption characteristics of the water body components. The reflectance values scaled between 0.03 for Advancetown Lake to 0.08 for Lake Perseverance Dam. The maximum in Chl absorption occurs between 660 nm and 680 nm bands, which reflected as a trough in the reflectance spectrum. While Figure (5-17) shows the minimum, maximum and

average $R(0-,\lambda)_{optical-model}$ spectrum of all stations and reservoirs in the study area and the calculated 95% confidence interval that contains the mean of the ranged values.

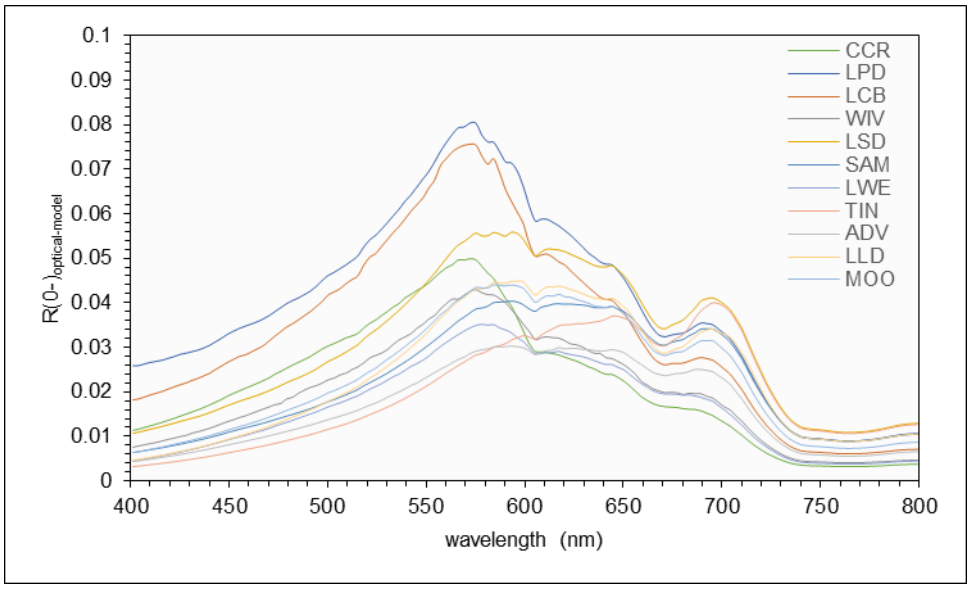

Figure 5-16: The Forwarded $R(0-,\lambda)$ Spectrum of SEQ Study Sites Derived from Using the Developed Bio-Optical Model of Gordon in This Work ($f = 0.38$) (10976 spectrum)

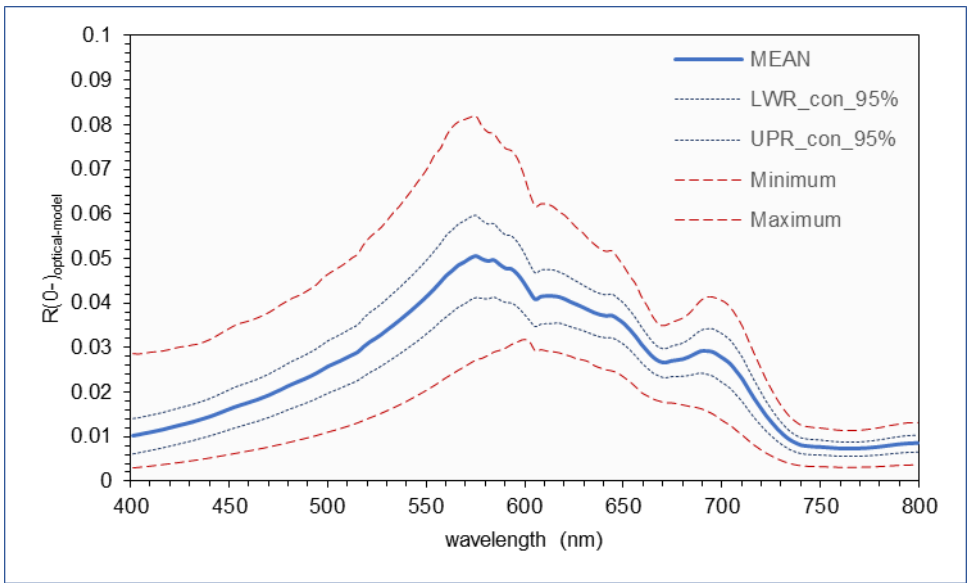

Figure 5-17: Min, Max and Mean Values with the 95% Confidence Intervals of the Modelled $R(0-,\lambda)$ of SEQ Reservoirs Extracted Using the Developed Model of Gordon in This Work.

The average modelled and simulated SIOPs of absorption and backscattering spectra of each of the 11 reservoirs are given in **Appendix (A)**.

5.4.3 Optical difference and Assessing the Similarity in Deriving Both ($R(0-)_{simulated}$ and $R(0-)_{optical-model}$)

In Figure (5-18) a comparison between the model-derived and the simulated-derived reflectance curves of all selected water bodies in the study area; the dashed blue line represents the modelled $R(0-,\lambda)$ and the solid green line represents the simulated $R(0-,\lambda)$. Both displayed the similar distribution regarding magnitude and relationship with CDOM variability and the confounding effect of both components (Chl and TR). MAPE was predominantly < 8% in overall and gradually decreases with increasing wavelength followed by a steep decline at 580 nm (Figure 5-19).

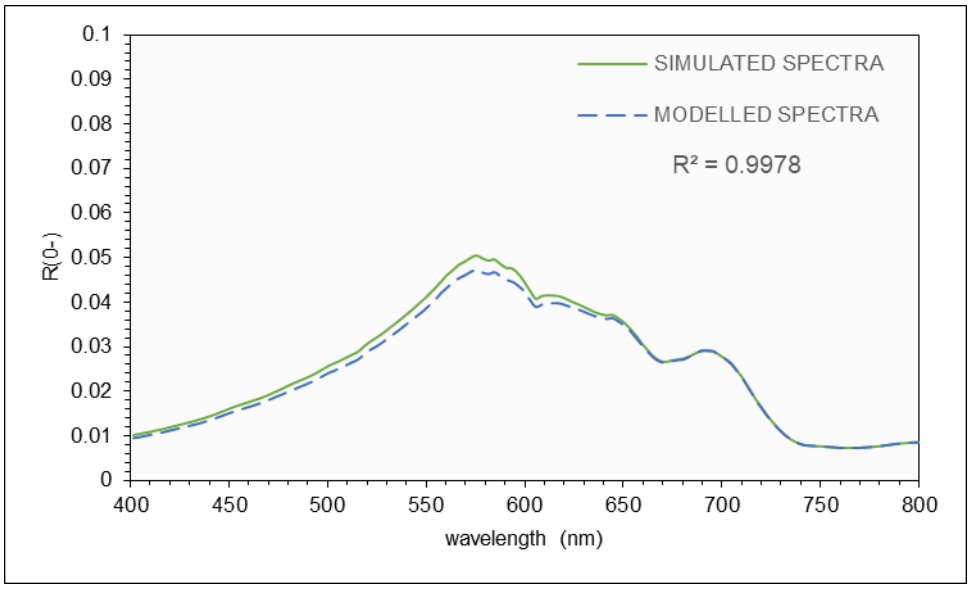

Figure 5-18: The Similarity between Both mean Simulated and mean Modelled $R(0-,\lambda)$ Spectrum of SEQ Reservoirs

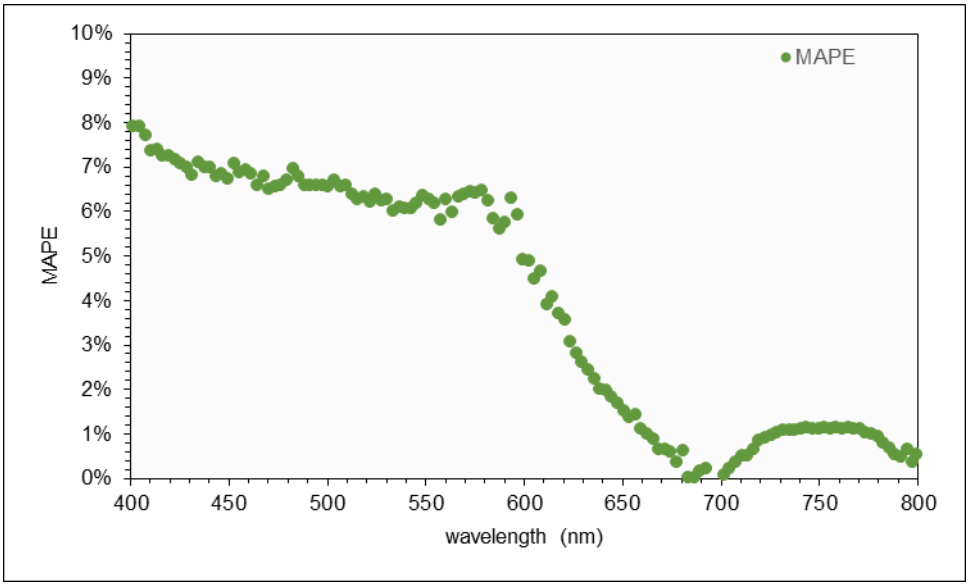

Figure 5-19: The Mean Absolute Percentage Error (MAPE) between the Simulated and Modelled $R(0-,\lambda)$ Values of SEQ Reservoirs

The average RMSE of the optical difference between the two spectra is 0.003 with a standard deviation of 0.001. The absolute mean of the modelled spectra falls very close to within the mean of the simulated values, suggesting that modelled values are reasonable and vice versa. The RMSE was used to express the differences between both spectra derived from MERIS bands data and is displayed in Figure (5-20). The simulated and modelled $R(0-)$ spectra were relatively similar at all wavelength and RMSE decrease towards longer wavelength.

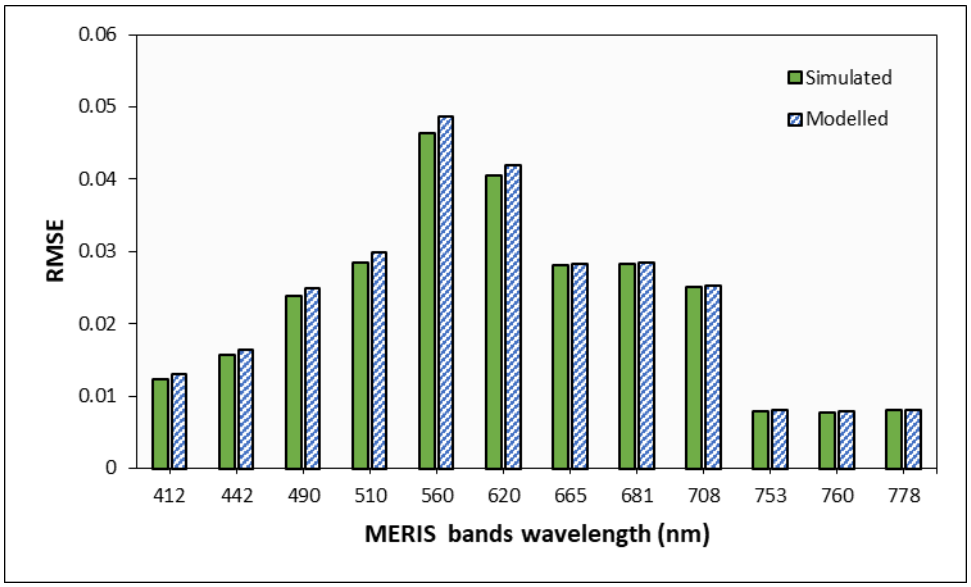

Figure 5-20: The RMSE between the Simulated and Modelled $R(0-,\lambda)$ Values of SEQ Reservoirs derived from MERIS data

Figure (5-21) shows the full visualisation of how the average simulated and modelled $R(0-,\lambda)$ spectra of each reservoir in the study area are matches.

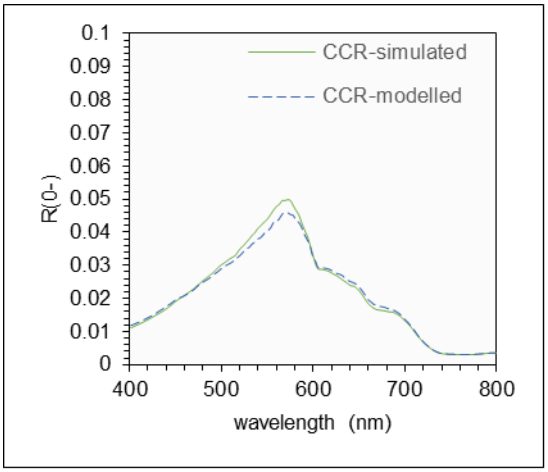
CCR-simulated
CCR-modelled
R(0-)
wavelength (nm)

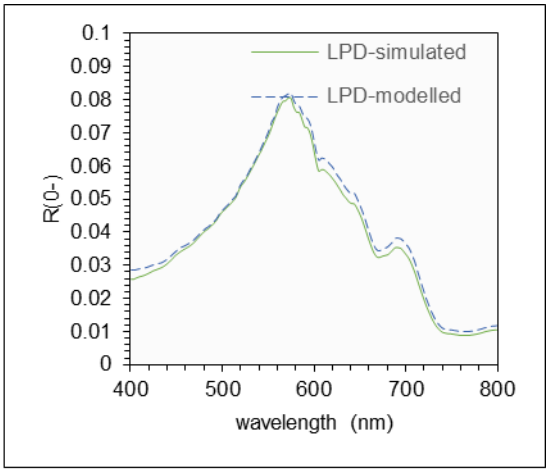
LPD-simulated
LPD-modelled
R(0-)
wavelength (nm)

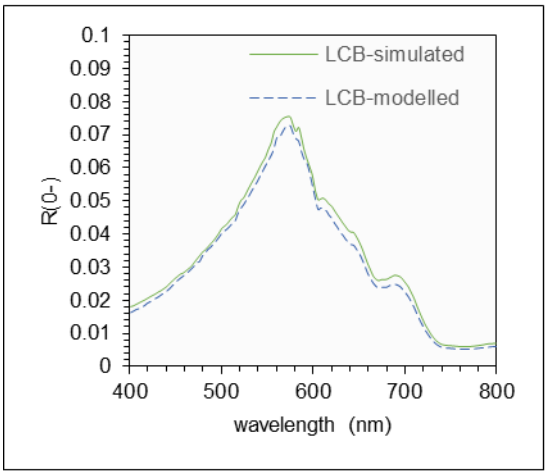
LCB-simulated
LCB-modelled
R(0-)
wavelength (nm)

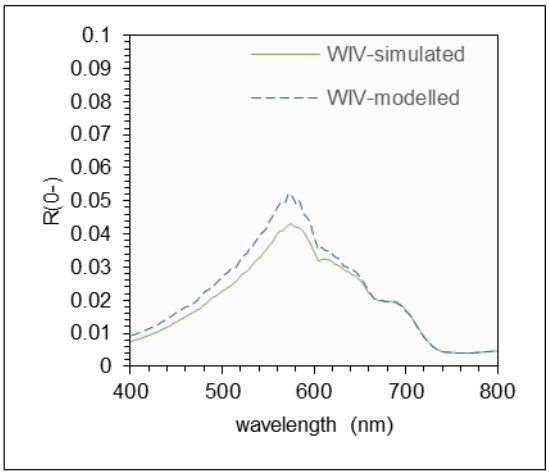
WIV-simulated
WIV-modelled
R(0-)
wavelength (nm)

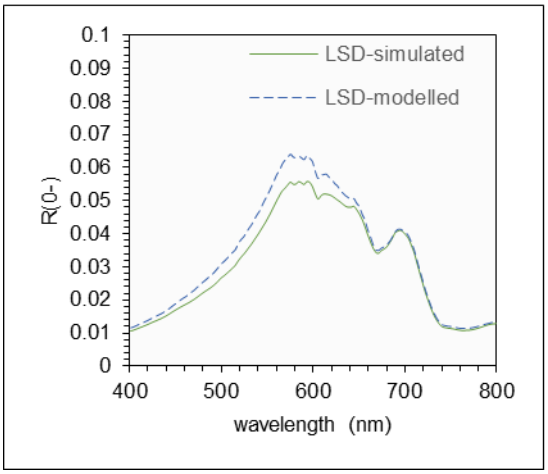
LSD-simulated
LSD-modelled
R(0-)
wavelength (nm)

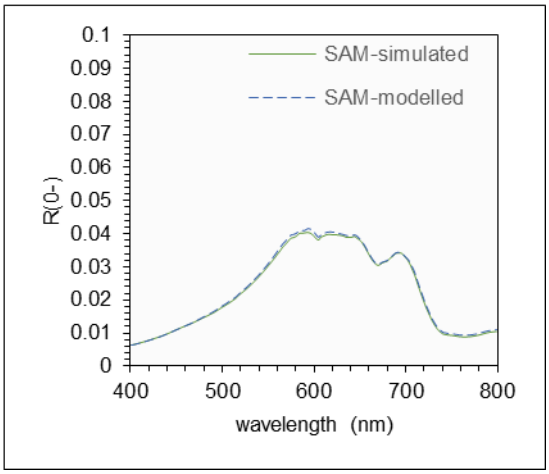
SAM-simulated
SAM-modelled
R(0-)
wavelength (nm)

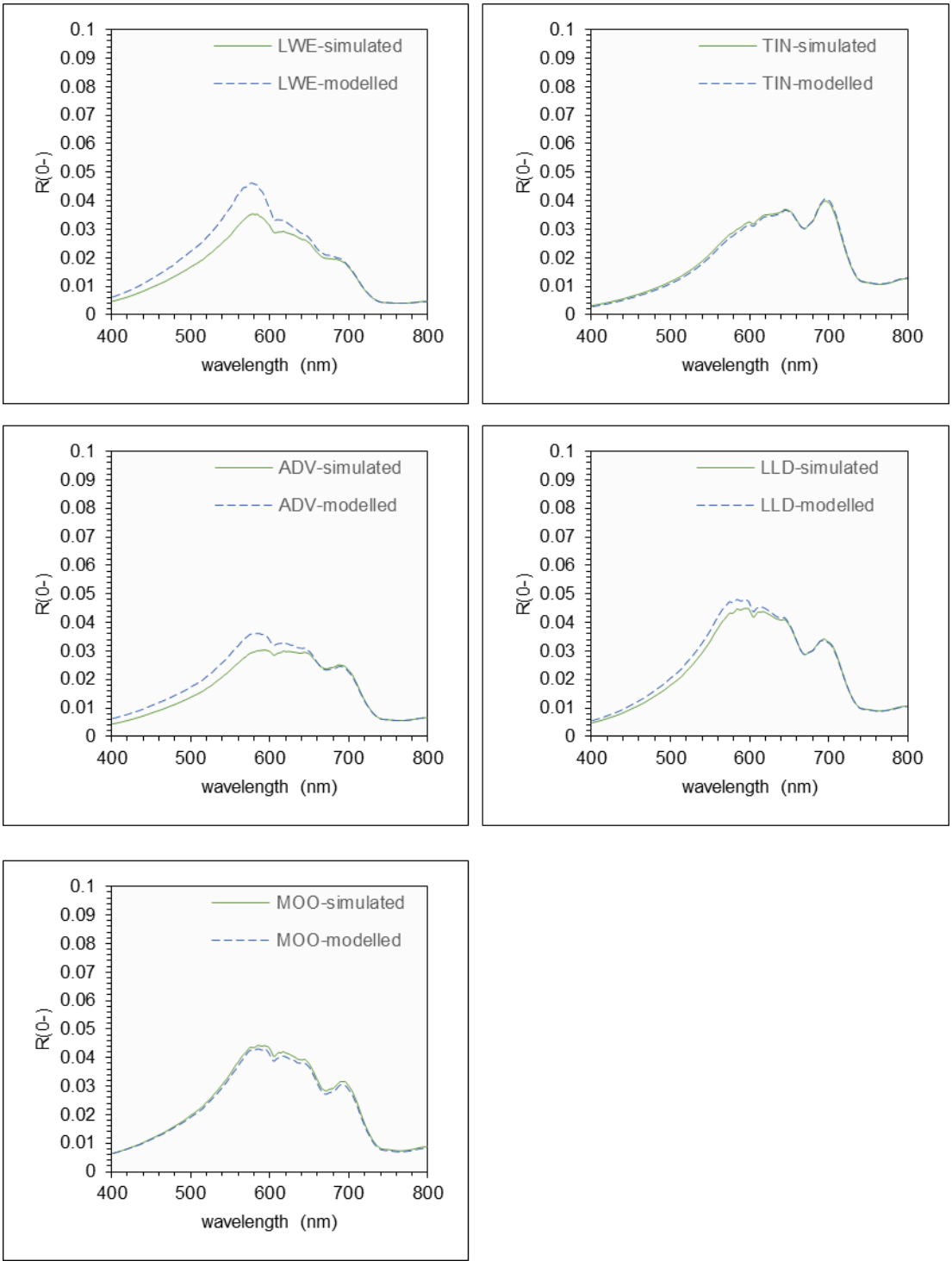

Figure 5-21: Visualisation of matching between the Simulated and Modelled $R(0-, \lambda)$ Values of Each SEQ Reservoirs

Statistical analysis between $R(0-,\lambda)$ modelled and $R(0-,\lambda)$ simulated of each reservoir were implemented. The R^2 for all reservoirs are high and the RMSE is low, it can conclude the best matches between all spectra achieved. A more detailed inspection of the statistical values listed in Table (5-4).

Table 5-4: Statistical Comparison Between Modelled and Simulated Spectra for Each Reservoir in the Study Area

Reservoir	Number of Spectra		RMSE	R^2
	modelling	simulation		
CCR	1176	2352	0.015	0.99
LPD	392	392	0.018	0.99
LCB	784	1960	0.022	0.99
WIV	1960	2744	0.037	0.98
LSD	1176	1960	0.039	0.98
SAM	1176	2352	0.005	0.99
LWE	1176	1176	0.050	0.96
TIN	392	392	0.006	0.99
ADV	784	784	0.031	0.96
LLD	784	1960	0.020	0.99
MOO	1176	2352	0.009	0.99

On average, the modelled $R(0-,\lambda)$ spectra are similar in shape and height to the simulated $R(0-,\lambda)$. Another noteworthy feature in both modelled and simulated spectra are the fact that their reflectance peak around 550 nm – 575 nm and 696 nm – 705 nm. This phenomenon is due to the relatively high specific tripton absorption observed in case-II waters.

5.4.4 The Dependency of $R(0-)$ Spectral Shapes on the Absorption and Scattering Properties

Since $R(0-)$ is related to the backscattering and absorption of all the optically significant water constituents, therefore, a non-linear dependency relationship between the simulated and modelled $R(0-)$ with *backscattering albedo* ω_b (was established, as presented in equation (5.27)). This dependency allows the influence of the variables (wind speed, solar zenith angle, the proportionality factor f) on the reflectance spectra to be analysed and adopt the results. Figures (5-22 A and B) illustrates this non-linear relationship.

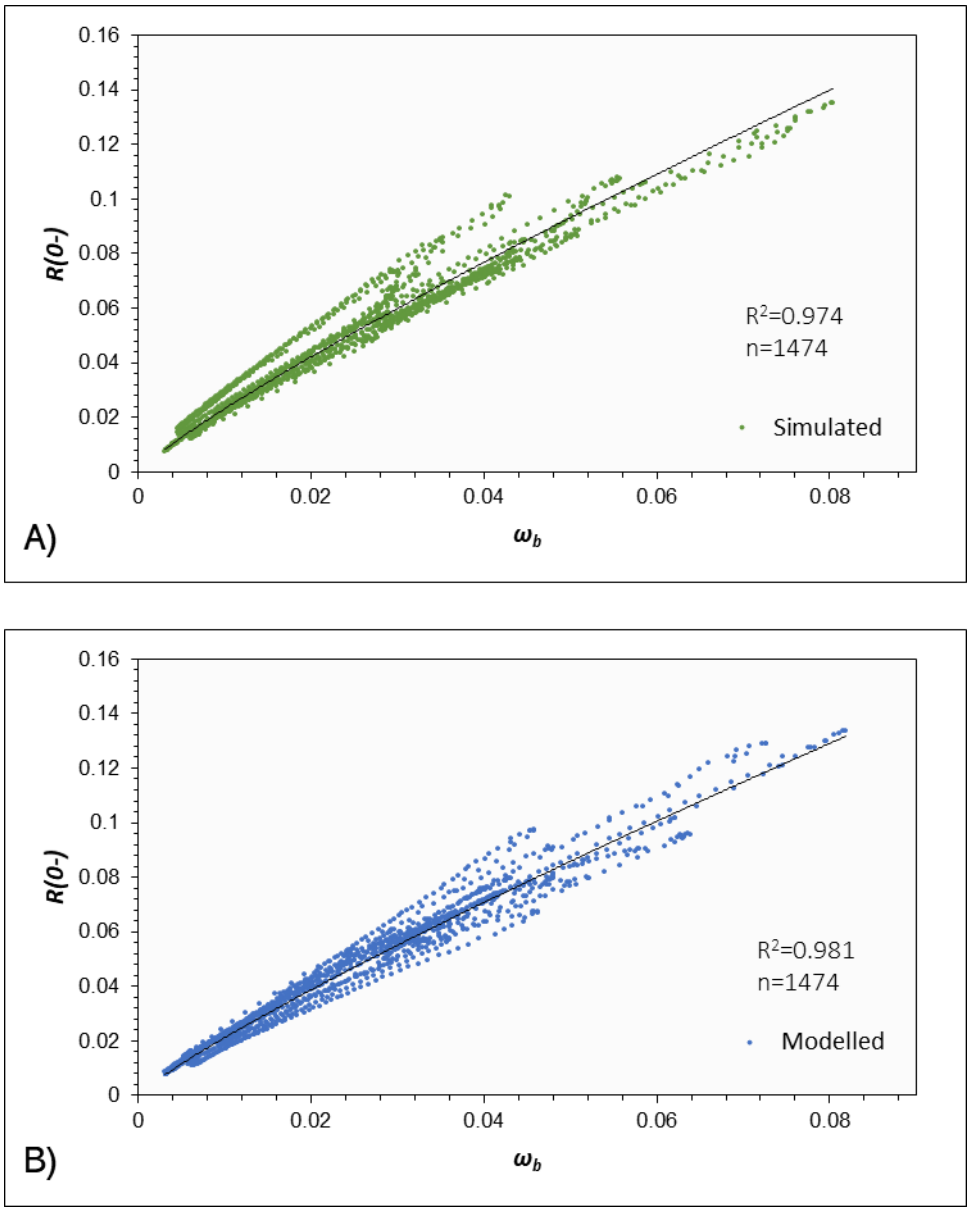

Figure 5-22: A) Simulated $R(0-)$ with ECOLIGHT® (N=1474) Depending on $\omega_b = \frac{b_b}{a+b_b}$ while B) Modelled $R(0-)$ From Using the Developed Bio-optical Model (N=1474) Depending on $\omega_b = \frac{b_b}{a+b_b}$

The advantage of this non-linear parameterisation is the separation of the dependences on the IOPs and ambient illumination conditions to ensure they have a small effect on the results. As presented in Figures (5-22 A and B), no significant observed variability related to the viewing geometry can be noticed because of the same values of the constants have been adopted for the simulation and modelling.

5.4.5 Retrieving Water Quality Parameters Using MIM Inversion

It is now possible to retrieve water component concentrations from water subsurface reflectance spectra for all the study locations using the selected inversion technique. This inversion performed under fully controlled conditions by using the simulated and the modelled data over the inputs. A flowchart represents the necessary steps to obtain a suitable final outputs data is shown in Figure (5-23).

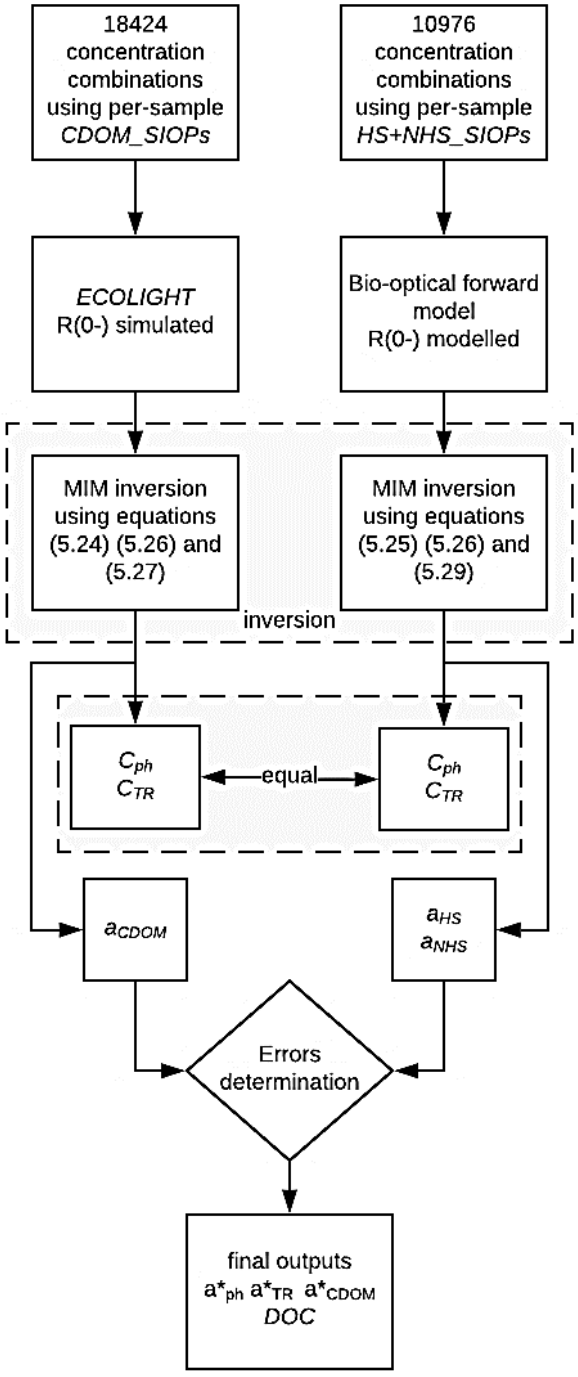

Figure 5-23: The Inversion Steps of the Simulated and Modelled $R(\mathbf{0}-,\boldsymbol{\lambda})$

First, the direct simple MIM method was applied to the $R(0-,\lambda)_{simulated}$ as was explained in §(5.3.2) to retrieve water components concentrations from 47 simulated spectra of the sampling locations. The inversion results were Chl, TR and CDOM from this inversion method to the simulated $R(0-,\lambda)$ and are shown in Figures (5-24 A, B and C) and listed in the Table (5-5).

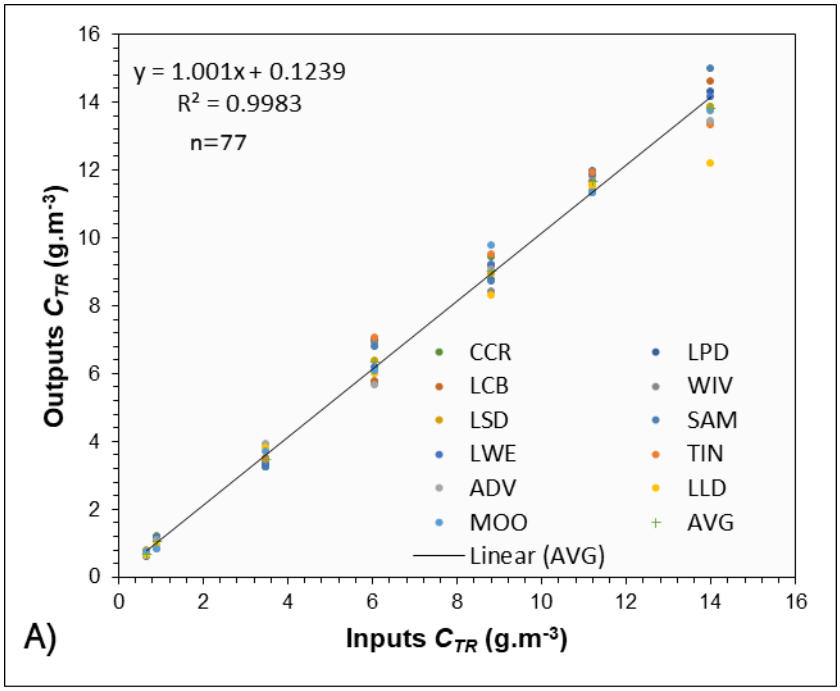

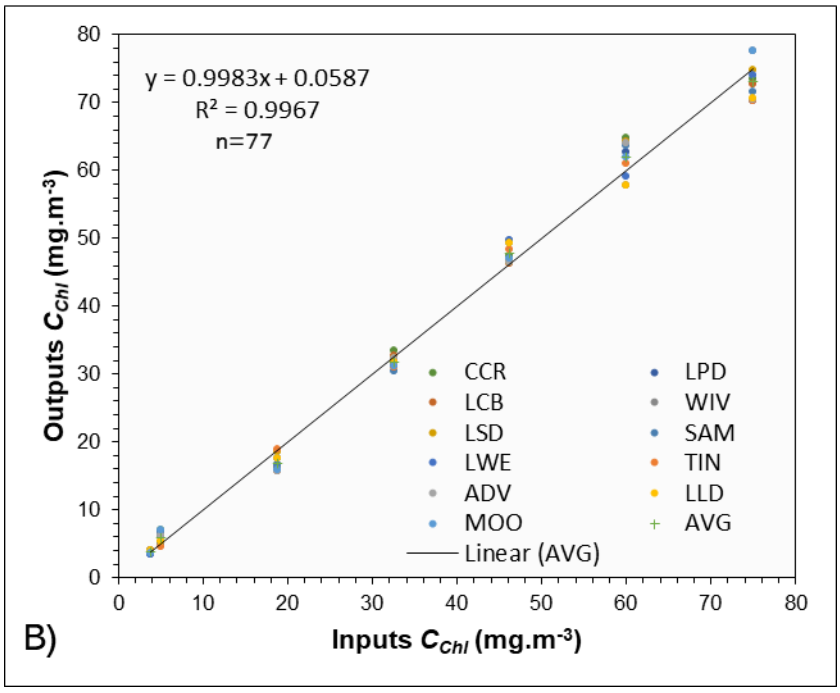

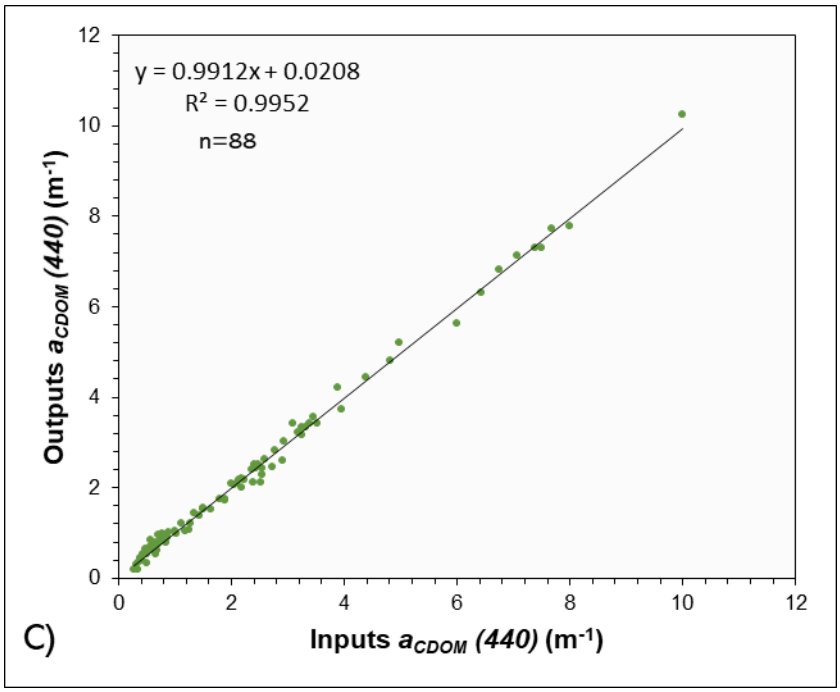

Figure 5-24: Inversion Results for A) TR, B) Chl and C) $a_{CDOM}(440)$ for the Standard Inversion by Embedding Equations (5-24) and (5-26) Into Equation (5-27)

Table 5-5: RMSE and NRMSE for the Study Location Using the Standard Inversion

Reservoir	*TR*		*Chl*		*CDOM*	
	RMSE	NRMSE (%)	RMSE	NRMSE (%)	RMSE	NRMSE (%)
CCR	0.087	6.29	0.018	2.57	0.003	0.50
LPD	0.029	2.18	0.026	3.58	0.005	0.83
LCB	0.021	1.54	0.018	2.33	0.023	3.83
WIV	0.049	3.62	0.034	4.86	0.028	4.67
LSD	0.041	3.03	0.029	3.85	0.097	6.17
SAM	0.083	6.10	0.029	4.33	0.028	4.67
LWE	0.063	4.62	0.032	4.16	0.009	1.50
TIN	0.044	3.25	0.030	4.29	0.019	3.17
ADV	0.027	2.11	0.013	1.94	0.002	0.33
LLD	0.025	1.87	0.020	2.79	0.012	2.00
MOO	0.040	2.96	0.022	3.15	0.051	8.50

The correlation coefficients for all retrieved components ranged between (0.95 – 0.99). The retrieval is very accurate when using the per-sample CDOM-SIOPs dataset not only the correlation is over 95%, but also the low NRMSE values indicate less residual variance between both inputs and outputs values for the simulated reflectance spectra. clearly the inputs and outputs values are in good agreement. This stage is essential to describe and visualises the uncertainty variation in $R(0-)$ due to the effect of a^*_ϕ and b^*_{TR}.

Moving forward to discuss the finding results of inversion the bio-optical model results performed using the linear technique of MIM and its scenario by the used equations explained previously in §5.3.2. to the spectra were inverted using an unweighted version of MIM as detailed by Campbell and Phinn (2010) and the equations detailed in §5.3.2.. The inversion was done on the forwarded modelled $R(0-)$ using the normalised absorption data of humic and non-humic substances modelled with the multi-component equation (equation 5.29). A 27 location reflectance spectra inversed represents each selected station in the study area. The outputs water quality parameters this time composed of (Chl, TR, HS and NHS). The retrieval of HS and NHS data from CDOM absorption might provide valuable additional water quality information for water quality management. The results of the inversion approach are present in Figures (5-25 A, B and C).

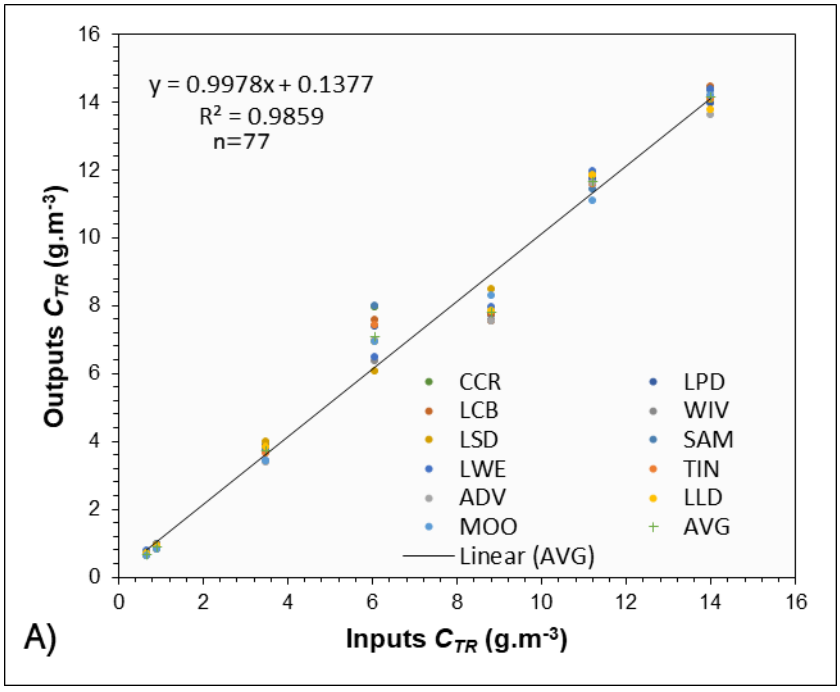

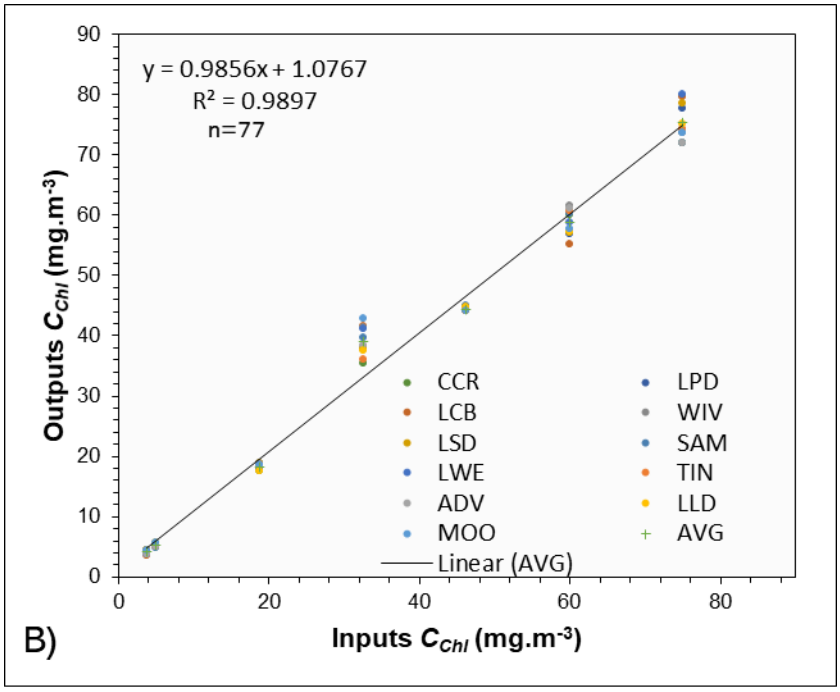

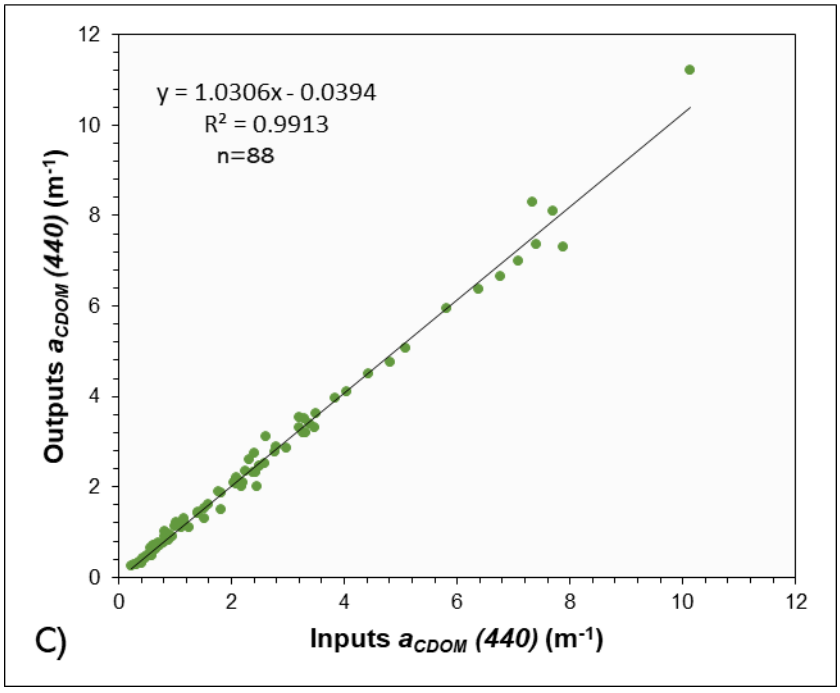

Figure 5-25: Inversion Results for A) *TR*, B) *Chl-a* and C) $a_{CDOM}(440)=(a_{HS}(440)+a_{NHS}(440))$ for the Forward Model of the Model that were Developed as Shown in Equation (5-26)

Assessing the relationship between the inputs and outputs values of this inversion for all the water components was done statistically, and the results listed in Table (5-6).

Table 5-6: RMSE and NRMSE for the Study Location Using the MIM Inversion for Bio-optical Model of Multi-component (HS and NHS)

Reservoir	*TR*		*Chl*		*CDOM (HS+NHS)*	
	RMSE	NRMSE (%)	RMSE	NRMSE (%)	RMSE	NRMSE (%)
CCR	0.040	3.01	0.224	3.23	0.009	19.59
LPD	0.057	4.21	0.173	2.59	0.012	15.37
LCB	0.051	3.69	0.174	2.53	0.012	17.86
WIV	0.070	5.53	0.309	4.19	0.015	19.61
LSD	0.037	2.84	0.277	3.89	0.021	3.06
SAM	0.047	3.27	0.198	2.93	0.022	8.27
LWE	0.048	3.55	0.205	2.91	0.008	8.64
TIN	0.049	3.90	0.179	2.70	0.010	1.90
ADV	0.061	4.81	0.202	3.02	0.004	3.47
LLD	0.058	5.01	0.275	4.12	0.012	5.23
MOO	0.081	6.26	0.331	4.47	0.019	11.71

The inputs and outputs values for the three water components linked by a highly significant linear relationship ($R^2(0.98 - 0.99)$) with a slope close to (±1).

5.5 The Implication of DOC retrieval from both ($a_{CDOM-model}$) and ($a_{CDOM-simulate}$)

Measurements of DOC concentration and CDOM absorption were used to calculate DOC-normalised specific absorption coefficients expressed here as $\boldsymbol{a^*_{DOC}(\lambda)}$. Fichot and Benner (2012) have confirmed this possibility. In this work, developing equation (2.4) (in chapter two) to calculate the specific absorption coefficients from CDOM absorption coefficient and DOC concentration to be:

$$\boldsymbol{a^*_{DOC}(\lambda) = a_{CDOM}(\lambda)/DOC} \qquad 5.38$$

A key issue for deriving DOC estimates from the $R(0-)$ observation first relies on an accurate estimation of CDOM absorption properties. A direct relationship between CDOM absorption at (440 nm) and DOC cannot be generalised because it does not represent real concentration values, as was demonstrated in Chapter Three. However, information held by $a^*_{DOC}(\lambda)$ can exploitable representing a possible alternative for deriving large scale DOC estimates.

The connection between CDOM sources and its spectral slope coefficient (S), that clarified and tested in the previous chapters has a great impact in estimating DOC by including it. Thus equation (2.3) (chapter two) is the key to include the variation of the spectral slope range of CDOM to be appropriate for investigating CDOM/DOC relationship in the study region. From the previous results of chapter two, the median value of ($S_{350-680}$) was 0.0181 for SEQ study locations which will be used in estimation *DOC* from $a_{CDOM-simulate}$.

The results of estimates DOC from CDOM absorption using the simulation data is represented in Figure (5-27). On average, DOC retrieved with a relative match-ups accuracy of 40 – 42 % between measured and estimated values ($R^2 = 0.58$, N = 47 and RMSE = 2.70). The results showed weak agreement between the measured and estimated values because of the more optically complex waters.

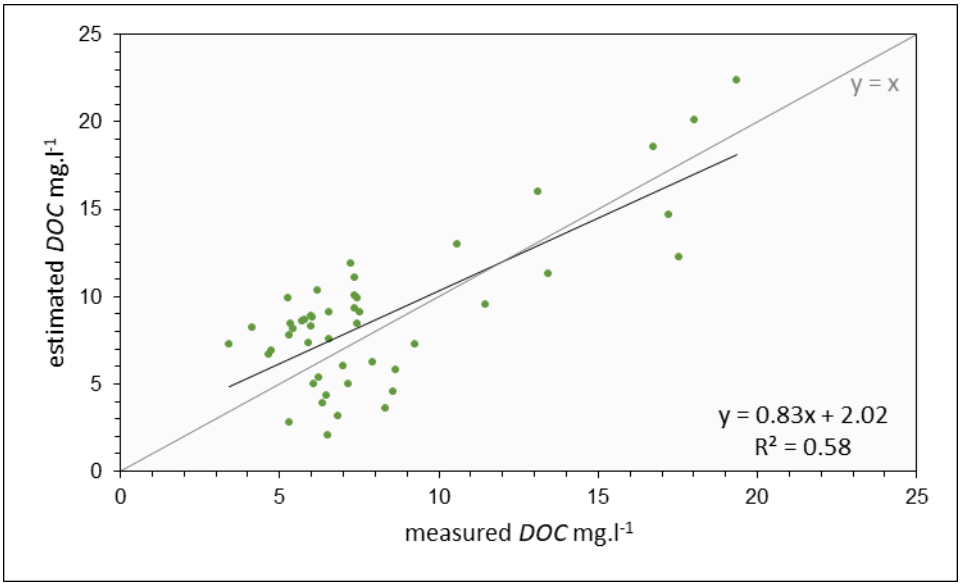

Figure 5-27: validation match-ups comparing measured and estimated DOC concentration values retrieved from ($a_{CDOM-simulate}$) spectra

The second proposed DOC concentration estimation was performed using the retrieved $a_{HS}(440)$ and $a_{NHS}(440)$ values from the $R(0-,\lambda)_{optical-model}$. Two-term models of HS and NHS have been used to predict DOC (§5.3.2) including both absorption at (440 nm) and inclusion of spectral slope ($S_{350-680}$) for average HS and NHS. The use of CDOM fractions (HS and NHS) is necessary to assess the regional variability in the relationship between CDOM and DOC across the region and examine factors that control such variability. The predicted values of $\mathrm{DOC_{HS}}$, $\mathrm{DOC_{NHS}}$ and $\mathrm{DOC_{CDOM}}$ are represented in Figure (5-28). Table (5-7) summarise all regression equations of those 11 SEQ lakes sampled in this study to predict DOC from absorption at (440 nm).

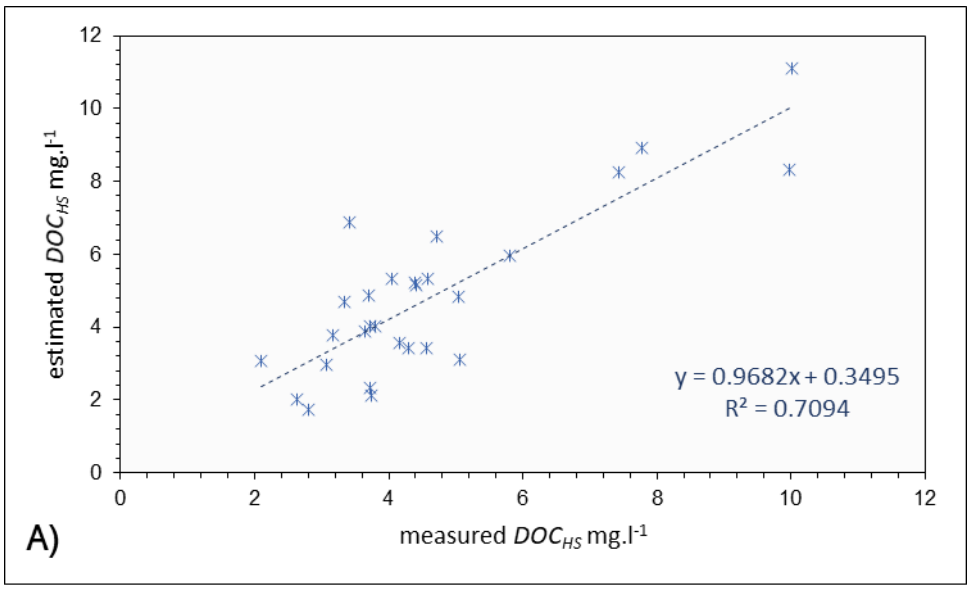

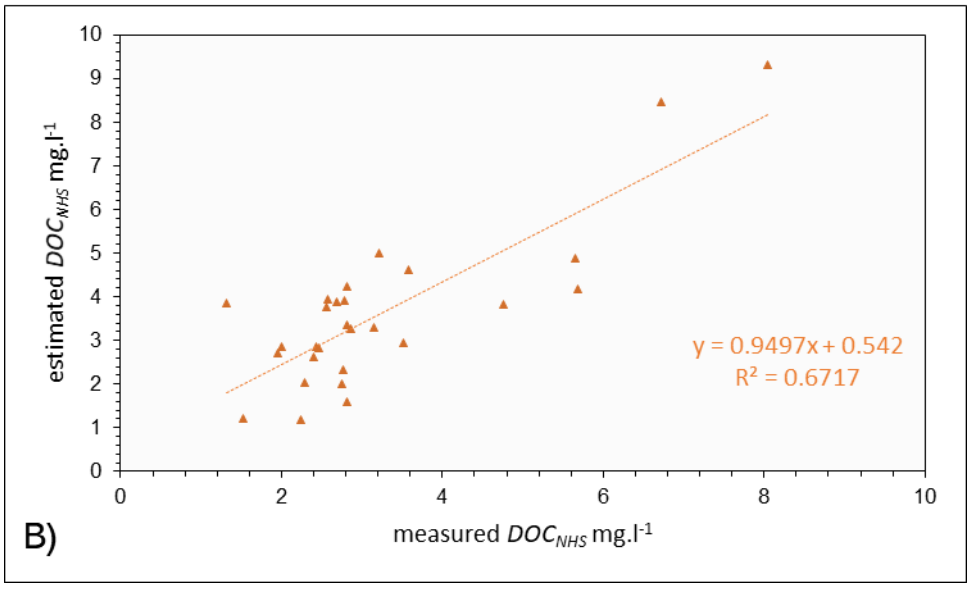

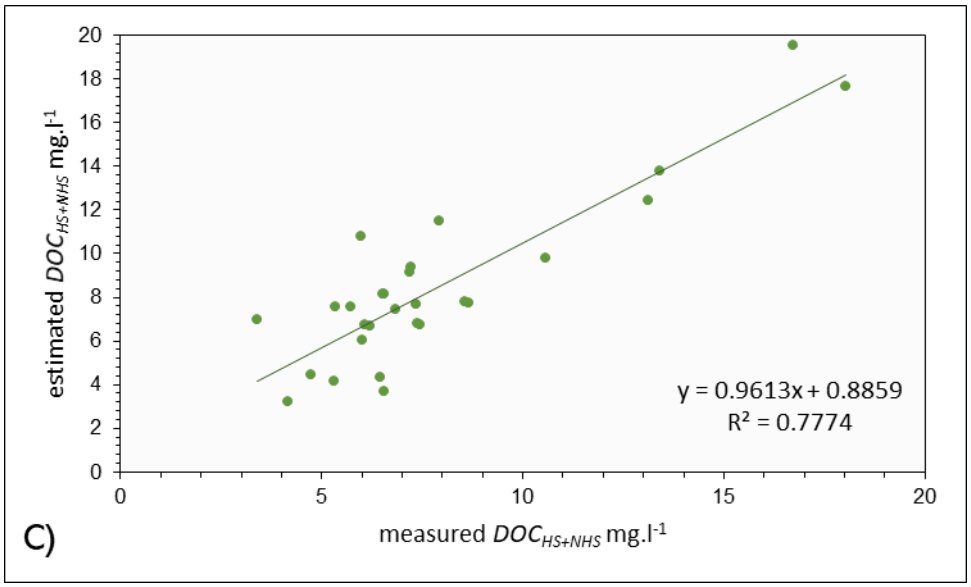

Figure 5-28: validation match-ups comparing measured and estimated DOC concentration values retrieved from; A) ($a_{HS)}$) spectra B) ($a_{NHS)}$) spectra C) Cumulative total DOC from HS and NHS

Table 5-7: Regression equations to predict DOC from CDOM absorption at (440 nm) for SEQ reservoirs. All Regression were highly significant (ρ < 0.0001)

	n	*Slope*	intercept	R^2	RMSE ($mg.L^{-1}$)
$DOC_{CDOM-simulate)}$	47	0.83	2.02	0.58	2.52
DOC_{HS+NHS}	28	0.96	0.89	0.78	3.22
DOC_{HS}	28	0.97	0.35	0.71	1.82
DOC_{NHS}	28	0.95	0.54	0.67	2.54

The DOC estimation results correlated strongly with CDOM absorption of HS and NHS ($R^2 = 0.78$) than with CDOM absorption of single exponential value ($R^2 = 0.58$) as explored in the previous chapters. The reason for the strength of this relationship is attributed to the distribution ratio of DOC among CDOM fractions according to their sources. Thus, the multi-components model leads to 20 -25 % higher estimates, comparable to the inversion using the per-sample CDOM-SIOPs sets.

5.6 Spectral Decomposition of the Simulated CDOM Absorption Spectrum

A successful inversion performed using CDOM fractions to retrieve and predict DOC concentrations were proved. In order to test if the same improvement is possible to get when implementing the same approach of separating CDOM spectrum into its fractions to provide insights into CDOM origins without resorting to chemical analysis as was applied in Chapter Three. Also, the results obtained in Chapter Three showed that not all CDOM fractions are chromophoric and these non-chromophoric fractions contain about (8.9% - 22.4%) of the total DOC in CDOM (Table 3-13). Therefore, for a better estimation of DOC concentration, describing *CDOM* absorption spectra as a multi-component curve constituent of HS and NHS instead of using CDOM as a single component is the essence of this work. As was described in Chapter Four of this work that gave a good description of the relationship between CDOM absorption and DOC concentration and between CDOM absorption and its sources, in this chapter the spectral decomposition technique will be carried out too on the simulated CDOM absorption spectra resulted from the ECOLIGHT® simulation.

A 28 $a_{CDOM-simulate}$ spectra were decomposed into their major influential components of (HS and NHS) using the linear least squared regression approach (LLSR) based on the SEQ maximum and minimum end-members (slope values) that were described and tested in §(4.7). This method adopted after test it and provided the best results compared with the other ways that tested in the previous chapter. The outputs parameters of using LLSR approach are a combining of five components $a_{HS}(\lambda_o)$, $a_{NHS}(\lambda_o)$, DOC_{HS}, DOC_{NHS} and K; they should lead to the best agreement between the measured and the estimated values for both absorption and then DOC concentration. The spectral decomposition results of $a_{HS}(\lambda_o)$ and $a_{NHS}(\lambda_o)$ were compared with the measured absorption values of the humic and the non-humic substances, as shown in Figure (5-29).

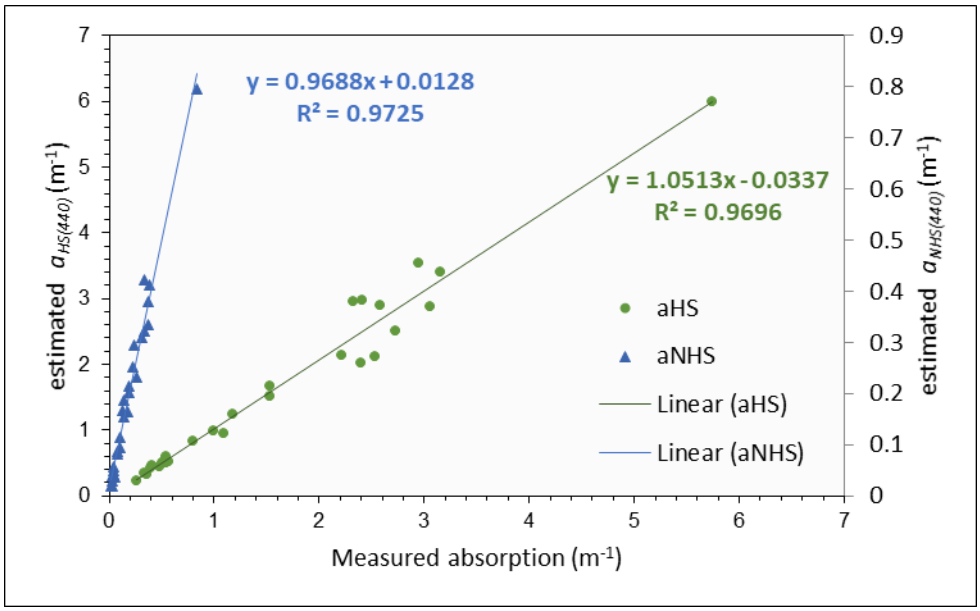

Figure 5-29: The Retrieved Values of HS and NHS Using Spectral Decomposition on the Retrieved CDOM Absorption Spectra from ECOLIGHT® ($a_{CDOM-simulate}$)

Overall the measured and the estimated absorption at (440 nm) of the two fractions were highly correlated (a_{NHS}: N = 48, R^2 = 0.9725, ρ < 0.001) and (a_{HS}: N = 48, R^2 = 0.9696, ρ < 0.001) and most values are close to the 1:1 line.

DOC concentrations were predicted from using the same expression for the combination of $a^*_{DOC}(440)$ as the ratio of a_{440} to the total DOC in §(5.5). While the other results of performing LLSR of the spectral decomposition technique showed approximately the same coefficients of determination between the predicted and measured DOC values.

5.7 Chapter 5 Conclusions

In this chapter, it was necessary to be reviewed and discussed the theoretical background of hydrologic optics of water quality parameters first to give a clear perception for the reader to consider this work as a scientific assistant reference. The analytical aspects of IOPs, AOPs and RTE, were first introduced because they serve as the basis of the characteristics of the optically active water constituents. Water reflectance is important in remote sensing of water-colour and used to estimate the concentrations of Chl, TR as a reference and CDOM (then DOC).

In general, the aim was to examine how well the estimation of DOC concentration will improve by using CDOM multi-components absorption model compared with using CDOM single exponential model in the inversion algorithm. Two forward models of water reflectance were established and then investigated how well they can be inverted using MIM inversion approach to retrieve CDOM accurately and then DOC concentration.

ECOLIGHT® simulation was used first to simulate $R(0-)$ curves under the conditions found in SEQ waterbodies. The aim was to show the contribution of various water components of different concentrations beside CDOM-SIOPs on the water reflectance. ECOLIGHT® has a unique ability to isolate changes in the reflectance ($R(0-)$) due to *SIOP's* or spectral variability.

The simulation showed how the contribution of the other colour producing agents in the water (e.g. Chl and TR) affected the retrieval accuracy of CDOM. In some SEQ locations where CDOM moderated, but other concentrations are low, water reflectance is lower in the blue band suggests a strong CDOM absorption, and the reflectance trough at about 680 nm is due to the fact that Chl effect was included in the simulations. Increasing Chl and TR generally resulted in higher reflectance across the visible and near-infrared spectrum. While increasing CDOM led to low reflectance, especially below 500 nm. Thus, an inverse relationship between the absorption and reflectance recorded. This simulation also could be essential to provide a database of $R(0-)$ curves for SEQ that can be used in future studies as a reference.

On the other hand, $R(0-)$ was modelled using Gordon-Walker semi-analytical optical model that was developed in this work by using multi-components of CDOM absorption spectrum (HS and NHS) to improve DOC estimation. Modelling the study area data revolves around two issues: (1) developing a theoretical model to present the study area data; and (2) categorising IOPs of water constituents in SEQ watersheds as a function to the consistency of CDOM origins. As a result, a bio-optical modelling approach was generated for determining and studying the variations of optically active CDOM fractions at a regional scale as presented in equation (5.29). There was no need the effect of the sun position and the atmospheric effects on $R(0-)$; were outside the scope of the work therefore, the anisotropy factor (f) was assumed as a constant equal to 0.38 in both simulation and modelling process.

For the investigation of the dependence, accuracy check was necessary to check how the forwarded models match its ECOLIGHT® simulations. The percentage error between the $R(0-,\lambda)_{simulated}$ and $R(0-,\lambda)_{modelled}$ was calculated (<8%).

The validity of MIM results from comparing both retrieved ($a_{CDOM-model}$) and ($a_{CDOM-simulate}$) showed an advantage of using the multi-component model which has the ability to provide extra water quality information given by water humic and non-humic substances. Where SEQ watersheds tend to be inhomogeneous due to their high allochthonous CDOM that reflected in a variety of spectral shapes of $R(0-)$ suggesting a diverse set of bio-optical properties for SEQ locations and at most it tends to turbidity. The presented method to estimate DOC from ($a_{CDOM-model}$) which based on the multi-component absorption model showed significant improvement (R^2 = 0.78) than using a single exponential model (R^2 = 0.58). Thus, the same good results obtained in chapters three and four in line with the goals of this research.

Finally, variation in the spectral slope among SEQ reservoirs whether for CDOM samples or for the fractions causes conspicuous inconsistency in the remote sensing reflectance spectra. The composition of CDOM in natural waters contribute to the large variability in their absorption and then in its reflectance properties.

Chapter 6

Conclusions and Outlook for Future Work

6.1 Summary of the Thesis

As reviewed at the beginning of this thesis, carbon dioxide is absorbed from the atmosphere at the water surface and converted into DOC which constitutes about 90% of the dissolved carbon in the aquatic system (Sobek et al. 2007). DOC is an important component in the carbon cycle and climate change. It enters the aquatic system from terrestrial sources such as soil or it generates within the water body itself through the primary production of phytoplankton or from organic matter. Organic matter comprises live organisms such as plants and animals, remnants of organisms, dead organisms yet to decompose, and organic compounds resulting from the decomposition processes in water. Increasing organic matter in water cause

lowering oxygen and increasing DOC in water and make it unusable for human and animal consumption and it could be identified as a source of organic pollution.

The most important fraction and the major form of the organic matter is the dissolved organic matter that plays a significant role in the aquatic system. DOM has been defined as the materials that consist of carbon atoms and could pass through a given filter below 0.22 µm (Bukata et al. 1995). It is brown in colour and in sufficient concentrations tint the water to yellowish brown. For remote sensing applications, CDOM is the optically measurable component of DOM in watersheds which is used as an indicator of the DOC in the aquatic system.

Some varieties of DOC have no colour and remote sensing cannot determine it directly, therefore, CDOM absorption could be a good indicator and can be used as a proxy to estimate the amount of DOC concentration in the aquatic environment. But, remote sensing measurements of DOC can only be done if there is a good relationship between CDOM absorption at a reference wavelength (440 nm or 350 nm) and DOC concentration. So, estimating DOC from optical remote sensing requires a durable relationship with CDOM.

This good relationship does not exist over most of the waterbodies because CDOM concentrations vary both spatially and temporally. The chemical composition and the complex heterogeneity of CDOM vary due to its sources affect the strength of the relationship with DOC too. Some studies in many Australian and some international waters showed it is not simple and not easy to estimate DOC concentration in the near-surface layer using satellite data, because it sometimes correlated with CDOM, and sometimes not. Therefore, knowing the local relationship is important to improve water constituent retrieval accuracy from remote sensing.

Based on what previously mentioned and specified in chapter one, the aim of this study was to demonstrate the use of CDOM fractions if they could help in improving the estimation of DOC in reservoirs for large scale areas that subject to heavy impact from the surrounding as in the selected study area. We investigated 11 diverse water bodies in SEQ, first, we examined if a correlation between CDOM absorption coefficient and DOC could be established to understand the variation in the CDOM

optical properties due to its composition and sources. The investigation approach was by decomposing CDOM into its major groups as addressed in chapter three and measuring their absorption spectra separately.

Also, testing the hypothesis that including the spectral slope of CDOM spectra would improve the regression between CDOM absorption coefficient and DOC. We focused on the effect of CDOM fractions in parallel with the change in concentrations of Chl-a and TR on the reflectance spectrum using the data collected from SEQ for estimating DOC and determine errors sources in retrieving CDOM.

This thesis is designed to answer the main research question that was stated in §1.5, that is:

"Can the estimation of dissolved organic carbon DOC within inland water reservoirs be improved by using different approaches to the remote sensing of CDOM concentrations?"

Besides the major question, some minor questions have emerged to answer them through this research which are:

1. *"How do the sources of organic matter (allochthonous and autochthonous) affect the optical properties of CDOM and know the remote sensing reflectance?"*

2. *"Does separating CDOM into its major groups of humic and non-humic and modelling them separately prior to input them to the optical model improve CDOM and hence DOC estimation?"*

There was a range of approaches and assumptions to support the ability to achieve out the aims and answering the research questions through a list of required objectives. In the section below each objective is restated and the key findings of each objective will list.

6.2 Objectives' Findings

In order to achieve research's aim and answering research questions the findings of each objective are summarized as below:

6.2.1 Objective 1 (CDOM Measurements)

"To sample SEQ reservoirs and determine the variation in the CDOM composition, spectral absorption and CDOM spatial changes."

The outcomes of this objective obtained from chapter two of this thesis are significant to understand the nature of SEQ watersheds. In addition collect information about some set of important parameters which considered as the key for the upcoming objectives (e.g. CDOM slope variations due to its sources). Generally, to characterize the study area, knowing pH values within the selected water bodies is significantly important. Increasing in pH of water would increase in light absorption by CDOM causing a change in its optical properties and therefore on DOC estimation. The results of measuring the acidity and alkalinity on the pH scale were within the normal values according to the Australian and New Zealand guidelines for fresh and marine water quality (2000) with some variations between the watersheds. The measured values of CDOM concentrations did not exceed the normal limit ranges of measured and documented values for Australian waters too. CDOM concentrations differed between the stations due to different inputs from the surrounding areas. There was limited variation in CDOM specific absorption within and between the sampled water bodies. The limited measurement range of CDOM specific absorption coefficient cannot be adopted in differentiate between the sources and types of CDOM because of the slight variation in this coefficient that indicates the consistency in CDOM sources.

6.2.2 Objective 2 (CDOM Fractionations and DOC Measurements)

"To examine the regional relationship between the total DOC with CDOM absorption spectra and with CDOM fractions."

This objective is based on measurements of DOC concentrations and CDOM optical measurements that were illustrated in chapter two and chapter three of this thesis. All of DOC concentrations were sitting within the Australian normal range of lakes and reservoirs. From the spatial distribution analysis to each reservoir, we observed high DOC and CDOM concentrations' values in the stations close to the inflow site in most reservoirs except Lake Moogerah and Lake Weyba. These high values of those stations are considered an indicator to the high discharge of surrounding areas and therefore this indicates that CDOM portion has originated from terrestrial materials from outside the waterbodies. While this did not occur in Lake Moogerah and Lake Weyba which may be related to algal blooms, phytoplankton and water dynamics in these lakes the precise reasons are beyond the scope of this work.

A weak relationship between $a_{CDOM}(\lambda_o)$ with DOC that was found is most likely due to the variability of CDOM sources. But this relationship has improved slightly when both the amplitude and the shape of CDOM spectrum curve were included in performing multiple linear regressions that led to obtaining a better understanding in estimating DOC concentration as discussed in chapter two.

The method of fractionating CDOM into humic and non-humic substances tested in this thesis showed that more than 87% of DOM in the collected samples are humic. These humic substances dominated on 54% - 67% of the total DOC in water for the collected samples from the study area. Nonetheless, the investigation in the relationship between CDOM fractions and DOC showed different trends such as not all DOC in CDOM can be chromophoric.

6.2.3 Objective 3 (Spectral Decomposition)

"To evaluate the potential of decomposing the measured CDOM absorption spectrum for the purpose of obtaining a better correlation estimation with DOC that can be used as an alternative to the single exponential model in DOC estimation algorithms."

In pursuing this aim I improved the estimation of the DOC and its retrieval accuracy by minimising the errors associated with using simple modelling as explained in Chapter Four. This objective focused on how CDOM fractions participate in the shape of the CDOM absorption spectrum. The simple exponential model to describe the shape of CDOM spectrum does not always give the right shape for CDOM absorption values due to some factors. One of these factors is errors that result from the interference of Chl-a absorption by some phytoplankton in the blue region with CDOM absorption. The other factor is from the passage of some small particles during the filtration process that causing attenuation in CDOM absorption measurements and it cannot be neglected. Also, CDOM absorption measurements affected by systematic errors originated from the cuvette wall, baseline shift between the reference and the sample, temperature and the instrument.

The first correction is for the baseline shift to reduce systematic errors in the CDOM absorption where 25% of the offset can be caused by the cuvette and the instrument. After that, the spectral decomposition technique was performed and tested by implementing linear and non-linear decomposition approaches in order to give the most appropriate description of the absorption spectrum. The implementation of this technique was done by fitting the sum of multi-exponential functions to the measured absorption spectrum to obtain a unique and acceptable solution.

Different slope parameter sets were tested using end-member values that were chosen carefully and can be applied for the study area and Australian inland waters. The linear technique was easier to apply and less complicated than the non-linear technique and led to a unique solution. The final results of using CDOM spectral decomposition were useful and helpful to give a good explanation to the relationship between CDOM absorption and DOC concentration on the one hand and between CDOM absorption and its sources on the other. Also, the results showed that using

the multi-components fitting model to describe the shape of CDOM spectrum that involved the major CDOM fractions was more applicable to meet the correct shape.

6.2.4 Objective 4 (Algorithm Development and Assessment)

"To parameterize and assess the contribution of the various water components beside CDOM major fractions on the simulated and modelled water reflectance spectra."

Assessing the variability in remote sensing reflectance spectra for the study area locations that results from water components were examined and explained in Chapter Five. It was implemented through obtaining simulated spectral reflectance curves ($R(0-)_{simulated}$) from running the RTE using different concentrations for water components (CDOM, Chl and TR) with a total of 18424 simulations. Water reflectance was simulated using measured per-sample CDOM-SIOPs numerically in ECOLIGHT® 5 software and then convolved with MERIS bands. The simulation showed how the influence of the other colour producing agents in the water (e.g. Chl and TR) affected the retrieval accuracy of CDOM.

Then, we selected the most appropriate exponential fitting model and developed it to give a better description by decomposing CDOM into its humic and non-humic substances as stated in chapter four. That part of the work focused to find the $R(0-,\lambda)_{optical-model}$ using the developed Gordon model but this time using measured per-sample SIOPs of CDOM fractions. The same spectral variations that were in the simulated spectra have been noticed because they caused by scattering and absorption characteristics of the water body components. The average RMSE of the optical corresponds between the two spectra derived from MERIS bands data was used to express the differences between both spectra and were relatively similar. On average, the $R(0-,\lambda)_{optical-model}$ spectra are similar in shape and height to the $R(0-)_{simulated}$.

6.2.5 Objective 5 (Algorithm Validation)

"To compare the expected errors occurring when using the simple CDOM model as opposed to a more complex CDOM multi-component model as part of a DOC retrieval algorithm."

Matrix inversion method was adopted as an inversion technique to retrieve water components under fully controlled conditions. The correlation coefficients for all retrieved components showed evidence for a reliable retrieving when using the multi-component algorithm with CDOM fractions' SIOPs inputs were much better than using the simple algorithm with per-sample CDOM-SIOPs inputs. Information acquired was exploited as an alternative for deriving DOC estimations. The multi-components model leads to 20 -25 % higher estimates, comparable to the inversion using the per-sample CDOM-SIOPs sets. The reason attributed to the distribution ratio of DOC among CDOM fractions according to their sources. Thus, a better correlation with the fractions gives a better DOC estimation.

6.3 Thesis Main Findings

The results of this study could serve to provide some useful data and information that can contribute to filling a portion of the gap in the SEQ region. A summary of what has been obtained through this thesis is in the following listed points but the main achievement that recognized in this thesis was the improvement in DOC estimation in the study area:

1. The major source of DOM/CDOM in SEQ reservoirs is from allochthonous sources and there is a significant effect from these allochthonous inputs on the CDOM absorption in these water bodies affecting the estimation of DOC.
2. The correlation between $a_{CDOM}(\lambda_o)$ and (S) is a negative relationship ranging from moderate to weak in most cases in SEQ reservoirs.
3. $a_{CDOM}(\lambda_o)$ alone is a poor predictor to estimate DOC and there is a poorly positive relationship between $a_{CDOM}(\lambda_o)$ and DOC in SEQ waterbodies even with using (S) as an additional predictive variable.

4. CDOM fractions are participating in the shape of CDOM absorption spectrum.
5. The absorbance of HPOB, HPIB and HPIN fractions were near negligible and accounting about 5% of the total absorption, but these fractions contain around 40% of the total DOC and this, in turn, led to that "**not all DOC is possible to associate with chromophoric DOM**".
6. SEQ reservoirs are humic waterbodies due to their high ratio of HA compared to *FA*.
7. Using the multi-exponential model is convenient for optical modelling and remote sensing applications.
8. Large sources of random errors affect the absorption measurement and the spectral decomposing technique assisted in reducing the effect of the random errors in the absorption measurements of CDOM samples.
9. The final results of using CDOM spectral decomposition useful and helpful to give a good explanation to the relationship between CDOM absorption and DOC concentration on the one hand and between CDOM absorption and its chemical composition on the other.
10. The estimation of DOC concentrations from water's colour is more complex and the accuracy factor is limited, due to the poor performance of the standard models and algorithms in addition to the confounding effects of both TSS and Chl-a.
11. The accurate assessment of CDOM concentration then the correct estimation of DOC by remote sensing reflectance spectra is a great challenge in the optically complex case-II waters.
12. Applying an inaccurate SIOPs for CDOM in the inversion process will lead to errors as confirmed in this thesis.
13. Including Chl-a in a multiple regression beside CDOM slope coefficient and CDOM fractions may improve DOC predictions in low coloured lakes.

14. One of the reasons for the poor CDOM-DOC relationship; CDOM in SEQ regions can transform into colourless DOM by extensive solar UV radiation due to a strong photochemical and microbiological process that leads to a weak CDOM-DOC relationship.

6.4 Research Contributions

6.4.1 Contribution from A Scientific Knowledge Perspective

The results of this study could bring a number of substantial benefits of which:

1. Describing and quantitatively demonstrating a limitation of the current approach is a valuable contribution to the field.
2. This thesis will assist to fill a part of the information gap by providing CDOM-IOPs and associated SIOPs for some SEQ reservoirs. These can be used then for validating remote sensing data in this region.
3. Improve the capability and accuracy of modelling applications.
4. This thesis contributes to developing a new method for retrieving DOC concentrations under high spatial variations from satellite remote sensing measurements.
5. Understanding the impact of CDOM fractions (HPO and HPI) on remote sensing reflectance spectrum.
6. Comprehend the relationship between CDOM and DOC and how it correlates with its sources.
7. This thesis is important for the scientific community to assist in understanding the mechanism that governs the relationship between CDOM and DOC in inland freshwaters that subject to heavy impact from the surrounding.

6.4.2 Contribution in Providing and Support National and Regional Information

Australia is not well endowed with natural lakes and contains many large artificial man-made water bodies and dams for reserving rainfall and runoff water. Therefore, Australian water quality managers always interested to have a source of data for updating their information, but unfortunately, there is a shortage in these data as stated in CSIRO's (2012) report and in SOE (Australia State of the Environment) (2011) and (2015) reports. CDOM/DOC measurement set presented in this thesis contribute to filling part of the existing gap of information coverage lack across Australia. The finding of using methods and products presented in this thesis would help in the identification of trends and spatial patterns of CDOM composition in the SEQ regions and other Australian environments. Also, the applications of retrieving the important parameters can be directly used as new approaches to developing dynamic models to quantify CDOM flux in the reservoirs. Providing SIOPs data will support gathering information to scope the operationalisation of a systematic monitoring system of NPEI[2]. Finally, monitoring DOC is critical for carbon budgets and because of this thesis we can now potentially more accurately monitor DOC in lacustrine environments.

6.5 Future Work and Recommendations

For monitoring water quality using remote sensing technique in inland freshwater areas, several interconnected issues were addressed in this thesis. This thesis could not cover all aspects related to estimating DOC from remote sensing data in case-II waters and in the study area but at least several aspects have been investigated in this thesis such as establishing CDOM fractions IOPs and SIOPs. Also, testing the existing algorithms for inland waters, applying the radiative transfer model and a semi-analytical model for estimating CDOM/DOC. However, there are some important issues that still need further investigation in the future summarize as follows:

[2] The National Plane for Environmental Information initiative

1. *Water quality information provided by fluorescence data*

As explained in chapter two organic matter in the water can either be from the allochthonous or autochthonous origin and this information can be useful for water managers to understanding their water system. It is possible to test another method to collect information on the origin and the composition of CDOM and compare it with the SPE technique that was used to isolate CDOM to its fractions in this thesis. For example, the fluorescence index (FI) by McKnight et al. (2001) to collect information on the origin of organic matter.

2. *Inversion and forward model of bio-optical properties*

The retrieved parameters inversely were not validated yet due to the unavailability of enough in situ measurements of $R(0-)$. Thus, in future studies, more in situ measurements have to be done and the same algorithm can be applied.

Before the completion, some items should be taken into account for the future works:

1. Further investigation is needed for the algorithm developed in chapter five and should be applied to more areas to check its performance for a wider scale.
2. The precision of bio-optical models depends on their parameterization of SIOPs, so we need to do a better job parameterizing model.
3. Measuring the humic and fulvic acids instead of CDOM to build a regional model.

REFERENCES

(IHSS), IHSS http://www.humicsubstances.org/isolation.html>.

Abdellah, M 2017, *In Silico Brain Imaging: Physically-plausible Methods for Visualizing Neocortical Microcircuitry*.

Aiken, GR, McKnight, DM, Thorn, K & Thurman, E 1992, 'Isolation of hydrophilic organic acids from water using nonionic macroporous resins', *Organic Geochemistry*, vol. 18, no. 4, pp. 567-73.

Aiken, J & Moore, GF, *Case 2 Anomalous Scattering and Gelbstoff Waters Flags MERIS Algorithm Theoretical Basis Document 2.8,* 2000.

Albert, A & Gege, P 2006, 'Inversion of irradiance and remote sensing reflectance in shallow water between 400 and 800 nm for calculations of water and bottom properties', *Applied Optics*, vol. 45, no. 10, pp. 2331-43.

Alvarez-Puebla, RA, Valenzuela-Calahorro, C & Garrido, JJ 2006, 'Theoretical study on fulvic acid structure, conformation and aggregation: A molecular modelling approach', *Science of The Total Environment*, vol. 358, no. 1, pp. 243-54.

Anderson, N & Stedmon, CA 2007, 'The effect of evapoconcentration on dissolved organic carbon concentration and quality in lakes of SW Greenland', *Freshwater Biology*, vol. 52, no. 2, pp. 280-9.

Anesio, AM, Hollas, C, Granéli, W & Laybourn-Parry, J 2004, 'Influence of humic substances on bacterial and viral dynamics in freshwaters', *Applied and environmental microbiology*, vol. 70, no. 8, pp. 4848-54.

Anumol, T & Snyder, SA 2015, 'Rapid analysis of trace organic compounds in water by automated online solid-phase extraction coupled to liquid chromatography–tandem mass spectrometry', *Talanta*, vol. 132, pp. 77-86.

ANZECC/ARMCANZ 2000, 'Australian and New Zealand guidelines for fresh and marine water quality', *Australian and New Zealand Environment and Conservation Council and Agriculture and Resource Management Council of Australia and New Zealand, Canberra*, pp. 1-103.

Aryal, R, Grinham, A & Beecham, S 2014, 'Tracking Inflows in Lake Wivenhoe during a Major Flood Using Optical Spectroscopy', *Water*, vol. 6, no. 8, p. 2339.

Averett, RC, Leenheer, J, McKnight, DM & Thorn, K 1994, *Humic substances in the Suwannee River, Georgia; interactions, properties, and proposed structures*, USGPO; US Geological Survey, Map Distribution.

Azam, F & Malfatti, F 2007, 'Microbial structuring of marine ecosystems', *Nature Reviews Microbiology*, vol. 5, no. 10, pp. 782-91.

Babin, M, Roesler, CS & Cullen, JJ 2008, *Real-time coastal observing systems for marine ecosystem dynamics and harmful algal blooms: Theory, instrumentation and modelling*, Unesco.

Babin, M, Stramski, D, Ferrari, GM, Claustre, H, Bricaud, A, Obolensky, G & Hoepffner, N 2003, 'Variations in the light absorption coefficients of phytoplankton, nonalgal particles, and dissolved organic matter in coastal waters around Europe', *Journal of Geophysical Research: Oceans*, vol. 108, no. C7, p. 3211.

Bai, Y, Pan, D, Cai, WJ, He, X, Wang, D, Tao, B & Zhu, Q 2013, 'Remote sensing of salinity from satellite-derived CDOM in the Changjiang River dominated East China Sea', *Journal of Geophysical Research: Oceans*, vol. 118, no. 1, pp. 227-43.

Bartley, R, Speirs, WJ, Ellis, TW & Waters, DK 2012, 'A review of sediment and nutrient concentration data from Australia for use in catchment water quality models', *Marine pollution bulletin*, vol. 65, no. 4, pp. 101-16.

Belzile, C, Roesler, CS, Christensen, JP, Shakhova, N & Semiletov, I 2006, 'Fluorescence measured using the WETStar DOM fluorometer as a proxy for dissolved matter absorption', *Estuarine, Coastal and Shelf Science*, vol. 67, no. 3, pp. 441-9.

Blondeau-Patissier, D, Brando, V, Oubelkheir, K, Dekker, A, Clementson, L & Daniel, P 2009, 'Bio-optical variability of the absorption and scattering properties of the Queensland inshore and reef waters, Australia', *Journal of Geophysical Research: Oceans (1978–2012)*, vol. 114, no. C5.

Bob, MM & Walker, HW 2001, 'Effect of natural organic coatings on the polymer-induced coagulation of colloidal particles', *Colloids and Surfaces A: Physicochemical and Engineering Aspects*, vol. 177, no. 2-3, pp. 215-22.

Boyle, ES, Guerriero, N, Thiallet, A, Vecchio, RD & Blough, NV 2009, 'Optical Properties of Humic Substances and CDOM: Relation to Structure', *Environmental science & technology*, vol. 43, no. 7, pp. 2262-8.

Brando, VE, Dekker, AG, Park, YJ & Schroeder, T 2012, 'Adaptive semianalytical inversion of ocean color radiometry in optically complex waters', *Appl Opt*, vol. 51, no. 15, pp. 2808-33.

Brando, VE, Dekker, AG, Schroeder, T, Park, YJ, Clementson, LA, Steven, A & Blondeau-Patissier, D 2008, 'Satellite Retrieval of Chlorophyll CDOM and NAP in Optically Complex Waters Using a Semi-Analytical Inversion Based on Specific Inherent Optical Properties. A Case Study for Great Barrier Reef Coastal Waters', in *Ocean Optics XIX*: *Proceedings of the Ocean Optics XIX* Barga, Italy, p. 10.

Bricaud, A, Morel, A & Prieur, L 1981, 'Absorption by Dissolved Organic Matter of the Sea (Yellow Substance) in the UV and Visible Domains', *Limnology and oceanography*, vol. 26, no. 1, pp. 43-53.

Bricaud, A, Morel, A & Prieur, L 1983, 'Optical efficiency factors of some phytoplankters', *Limnology and oceanography*, vol. 28, no. 5, pp. 816-32.

Bricaud, A, Morel, A, Babin, M, Allali, K & Claustre, H 1998, 'Variations of light absorption by suspended particles with chlorophyll a concentration in oceanic (case 1) waters: Analysis and implications for bio-optical models', *Journal of Geophysical Research-Oceans*, vol. 103, no. C13, pp. 31033-44.

Brown, M 1977, 'Transmission spectroscopy examinations of natural waters: C. Ultraviolet spectral characteristics of the transition from terrestrial humus to marine yellow substance', *Estuarine and Coastal Marine Science*, vol. 5, no. 3, pp. 309-17.

Bukata, RP, Jerome, JH, Kondratyev, AS & Pozdnyakov, DV 1995, *Optical properties and remote sensing of inland and coastal waters*, CRC press.

Bukata, RP, Jerome, John H., Kondratyev, K.Y., Pozdnyakov, D.V. 1995, *Optical properties and remote sensing of inland and coastal waters*, Y, CRC Press, Boca Raton.

Campbell, G 2010, 'Dirty Water: Remote Sensing of Water Quality in Tropical and Sub-tropical Freshwater Impoundments', The University of Queensland.

Campbell, G & Phinn, SR 2010, 'An assessment of the accuracy and precision of water quality parameters retrieved with the Matrix Inversion Method', *Limnology and Oceanography: Methods*, vol. 8, pp. 16-29.

Campbell, G, Phinn, SR & Daniel, P 2011a, 'The specific inherent optical properties of three sub-tropical and tropical water reservoirs in Queensland, Australia', *Hydrobiologia*, vol. 658, no. 1, pp. 233-52.

Campbell, G, Phinn, S & Daniel, P 2011b, 'The specific inherent optical properties of three sub-tropical and tropical water reservoirs in Queensland, Australia', *Hydrobiologia*, vol. 658, no. 1, pp. 233-52.

Campbell, IC, James, KR, Hart, BT & Devereaux, A 1992a, 'Allochthonous coarse particulate organic material in forest and pasture reaches of two south-eastern Australian streams: I. Litter accession', *Freshwater Biology*, vol. 27, no. 3, pp. 341-52.

Campbell, IC, James, KR, Hart, BT & Devereaux, A 1992b, 'Allochthonous coarse particulate organic material in forest and pasture reaches of two south-eastern Australian streams: II. Litter processing', *Freshwater Biology*, vol. 27, no. 3, pp. 353-65.

Candiani, G, Giardino, C, Brando, VE, Bartoli, M & Reverberi, F 2007, 'MERIS timeseries data to detect water quality in Subalpine lakes', in *3rd Workshop Remote Sensing of the Coastal Zone*: *Proceedings of the 3rd Workshop Remote Sensing of the Coastal Zone* Bolzano, Italy.

Carder, Kendall L & Steward, RG, Harvey, George R, Ortner, Peter B 1989, 'Marine humic and fulvic acids: Their effects on remote sensing of ocean chlorophyll', *Limnology and oceanography*, vol. 34, no. 1, pp. 68-81.

Carder, KL, Steward, RG, Harvey, GR & Ortner, PB 1989, 'Marine humic and fulvic-acids - their effects on remote-sensing of ocean chlorophyll', *Limnology and Oceanography*, vol. 34, no. 1, pp. 68-81.

Cazenave, A, Champollion, N, Benveniste, J & Chen, J 2016, *Remote Sensing and Water Resources*, vol. 55, Springer.

Chavez et al., KRB, Robert R. Bidigare, David M. Karl, Dale Hebel, Mike1 Latasa, Lisa Campbell 1995a, 'On the chlorophyll *a* retention properties of glass-fiber GF/F filters', *Limnology and oceanography*, vol. 40, no. 2, pp. 428-33.

Chavez et al., KRB, Robert R. Bidigare, David M. Karl, Dale Hebel, Mike1 Latasa, Lisa Campbell 1995b, 'On the chlorophyll a retention properties of glass-fiber GF/F filters. Authors' reply', *Limnology and oceanography*, vol. 40, no. 2, pp. 428-36.

Chen, RF, Bissett, P, Coble, P, Conmy, R, Gardner, GB, Moran, MA, Wang, X, Wells, ML, Whelan, P & Zepp, RG 2004, 'Chromophoric dissolved organic matter (CDOM) source characterization in the Louisiana Bight', *Marine Chemistry*, vol. 89, no. 1, pp. 257-72.

Chin, Y-P, Aiken, G & O'Loughlin, E 1994, 'Molecular weight, polydispersity, and spectroscopic properties of aquatic humic substances', *Environmental science & technology*, vol. 28, no. 11, pp. 1853-8.

Chow, AT, Gao, S & Dahlgren, RA 2005, 'Physical and chemical fractionation of dissolved organic matter and trihalomethane precursors: A review', *Journal of Water Supply: Research and Technology-AQUA*, vol. 54, no. 8, pp. 475-507.

Coble, PG 1996, 'Characterization of marine and terrestrial DOM in seawater using excitation-emission matrix spectroscopy', *Marine Chemistry*, vol. 51, no. 4, pp. 325-46.

Committee, ASotE 2001, *Australia, State of the Environment 2001 Inland waters theme report*, CSIRO Publishing, Melbourne.

Committee, SotE 2011, *Australia state of the environment 2011*, Independent report to the Australian Government Minister for Sustainability, Environment, Water, Population and Communities (Department of Sustainability, Environment, Water, Population and Communities, Canberra).

Cottingham, R, Delfau, KF & Garde, P 2010, 'Managing diffuse water pollution in South East Queensland'.

Croue, J-P, Korshin, GV & Benjamin, MM 2000, *Characterization of natural organic matter in drinking water*, American Water Works Association.

Croue, J, Debroux, J, Amy, G, Aiken, G & Leenheer, J 1999, 'Natural organic matter: structural characteristics and reactive properties', *Formation and control of disinfection by-products in drinking water*, pp. 65-93.

Croué, JP, Lefebvre, E, Martin, B & Legube, B 1993, 'Removal of dissolved hydrophobic and hydrophilic organic substances during coagulation/flocculation of surface waters', *Water Science and Technology*, vol. 27, no. 11, pp. 143-52.

CSIRO and Bureau of Meteorology 2015, *Climate Change in Australia Information for Australia's Natural Resource Management Regions: Technical Report*, CSIRO and Bureau of Meteorology, Australia.

Das, S, Hazra, S, Giri, S, Das, I, Chanda, A, Akhand, A & Maity, S 2017, 'Light absorption characteristics of chromophoric dissolved organic matter (CDOM) in the coastal waters of northern Bay of Bengal during winter season'.

De Deckker, P & Williams, WD 2012, *Limnology in Australia*, vol. 61, Springer Science & Business Media.

de Gruijter, J 1999, 'Spatial sampling schemes for remote sensing', in *Spatial Statistics for Remote Sensing*, Springer, pp. 211-42.

De Haan, H, De Boer, T, Kramer, H & Voerman, J 1982, 'Applicability of light absorbance as a measure of organic carbon in humic lake water', *Water Research*, vol. 16, no. 6, pp. 1047-50.

De Wit, JC, van Riemsdijk, WH & Koopal, LK 1993, 'Proton binding to humic substances. 2. Chemical heterogeneity and adsorption models', *Environmental science & technology*, vol. 27, no. 10, pp. 2015-22.

Defoin-Platel, M & Chami, M 2007, 'How ambiguous is the inverse problem of ocean color in coastal waters?', *Journal of Geophysical Research: Oceans (1978–2012)*, vol. 112, no. C3.

Dekker, AG & Hestir, EL 2012, *Evaluating the feasibility of systematic inland water quality monitorig with satellite remote sensing*, 117441, CSIRO.

Dekker, AG, Malthus, TJM & Hoogenboom, HJ 1995, 'The remote sensing of inland water quality', in FM Danson & SE Plummer (eds), *Advances in Environmental Remote Sensing*, John Wiley & Sons, UK, Chichester, pp. 123-42.

Del Castillo, CE & Miller, RL 2011, 'Horizontal and vertical distributions of colored dissolved organic matter during the Southern Ocean Gas Exchange Experiment', *Journal of Geophysical Research: Oceans*, vol. 116, no. C4.

Del Castillo, CE, Coble, PG, Morell, JM, Lopez, JM & Corredor, JE 1999, 'Analysis of the optical properties of the Orinoco River plume by absorption and fluorescence spectroscopy', *Marine Chemistry*, vol. 66, no. 1-2, pp. 35-51.

Department of Infrastructure Local Government and Planning 2017, *South East Queensland Regional Plan 2017 ShapingSEQ*, LGaP Department of Infrastructure, State of Queensland, Brisbane Qld 4000, Australia.

Dev, PJ & Shanmugam, P 2014, 'New model for subsurface irradiance reflectance in clear and turbid waters', *Optics Express*, vol. 22, no. 8, pp. 9548-66.

Doerffer, R & Schiller, H 2007, 'The MERIS Case 2 water algorithm', *International Journal of Remote Sensing*, vol. 28, no. 3, pp. 517 - 35.

Ferrari, GM & Dowell, MD 1998, 'CDOM Absorption Characteristics with Relation to Fluorescence and Salinity in Coastal Areas of the Southern Baltic Sea', *Estuarine, Coastal and Shelf Science*, vol. 47, no. 1, pp. 91-105.

Ferrari, GM, Dowell, MD, Grossi, S & Targa, C 1996, 'Relationship between the optical properties of chromophoric dissolved organic matter and total concentration of dissolved organic carbon in the southern Baltic Sea region', *Marine Chemistry*, vol. 55, no. 3-4, pp. 299-316.

Fichot, CG & Benner, R 2011, 'A novel method to estimate DOC concentrations from CDOM absorption coefficients in coastal waters', *Geophysical research letters*, vol. 38, no. 3.

Fichot, CG & Benner, R 2012, 'The spectral slope coefficient of chromophoric dissolved organic matter (S275–295) as a tracer of terrigenous dissolved organic carbon in river-influenced ocean margins', *Limnology and oceanography*, vol. 57, no. 5, pp. 1453-66.

Findlay, S & Sinsabaugh, RL 2003, *Aquatic ecosystems: Interactivity of dissolved organic matter*, Academic Press.

Gallie, E 1997, 'Variation in the specific absorption of dissolved organic carbon in Northern Ontario lakes', in *Ocean Optics XIII*, International Society for Optics and Photonics, pp. 417-23.

Gege, P 2000, 'Gaussian model for yellow substance absorption spectra'.

Gege, P 2004, 'The water color simulator WASI: an integrating software tool for analysis and simulation of optical in situ spectra', *Computers & Geosciences*, vol. 30, no. 5, pp. 523-32.

Gege, P 2005, 'The water colour simulator WASI. User manual for version 3', *DLR-Interner Bericht, No. DLR-IB*, pp. 564-1.

Gitelson, AA, Grits, YA, Etzion, D, Ning, Z & Richmond, A 2000, 'Optical properties of *Nannochloropsis* sp and their application to remote estimation of cell mass', *Biotechnology and Bioengineering*, vol. 69, no. 5, pp. 516-25.

Glass Fiber Filter, filter paper and Membrane Solutions, 2018, https://www.membrane-solutions.com/glass_fiber_disc_membrane.htm>.

Goldman, EA, Smith, EM & Richardson, TL 2013, 'Estimation of chromophoric dissolved organic matter (CDOM) and photosynthetic activity of estuarine phytoplankton using a multiple-fixed-wavelength spectral fluorometer', *Water Research*, vol. 47, no. 4, pp. 1616-30.

Gordon, HR 1973, 'Simple Calculation of the Diffuse Reflectance of the Ocean', *Applied Optics*, vol. 12, no. 12, pp. 2803-4.

Gordon, HR 2002, 'Inverse methods in hydrologic optics', *Oceanologia*, vol. 44, no. 1, pp. 9-58.

Gordon, HR & Morel, A 1983, *Remote assessment of ocean color for interpretation of satellite visible imagery : a review*, Y, Springer-Verlag, New York.

Gordon, HR, Brown, OB & Jacobs, MM 1975, 'Computed relationships between the inherent and apparent optical properties of a flat homogeneous ocean', *Applied Optics*, vol. 14, no. 2, pp. 417-27.

Gordon, HR, Brown, OB, Evans, RH, Brown, JW, Smith, RC, Baker, KS & Clark, DK 1988, 'A Semianalytic radiance model of ocean color', *Journal of Geophysical Research*, vol. 93, no. D9, pp. 10909-24.

Goslan, EH, Fearing, DA, Banks, J, Wilson, D, Hills, P, Campbell, AT & Parsons, SA 2002, 'Seasonal variations in the disinfection by-product precursor profile of a reservoir water', *Journal of Water Supply: Research and Technology-AQUA*, vol. 51, no. 8, pp. 475-82.

Grasshoff, K, Kremling, K & Ehrhardt, M 2009, *Methods of seawater analysis*, John Wiley & Sons.

Green, SA & Blough, NV 1994, 'Optical-Absorption and Fluorescence Properties af Chromophoric Dissolved Organic-Matter in Natural-Waters', *Limnology and oceanography*, vol. 39, no. 8, pp. 1903-16.

Green, SA & Blough, NV 1994, 'Optical absorption and fluorescence properties of chromophoric dissolved organic matter in natural waters', *Limnology and oceanography*, vol. 39, no. 8, pp. 1903-16.

Grunert, BK, Mouw, CB & Ciochetto, AB 2018, 'Characterizing CDOM spectral variability across diverse regions and spectral ranges', *Global Biogeochemical Cycles*, vol. 32, no. 1, pp. 57-77.

Hansell, DA & Carlson, CA 2014, *Biogeochemistry of marine dissolved organic matter*, Academic Press.

Harrison, RM 2001, *Pollution: causes, effects and control*, Royal Society of Chemistry.

Harvey, ET, Kratzer, S & Andersson, A 2015, 'Relationships between colored dissolved organic matter and dissolved organic carbon in different coastal gradients of the Baltic Sea', *Ambio*, vol. 44, no. 3, pp. 392-401.

Hayes, MH, Mylotte, R & Swift, RS 2017, 'Humin: its composition and importance in soil organic matter', in *Advances in Agronomy*, Elsevier, vol. 143, pp. 47-138.

Heavens, O 1992, 'Handbook of optical constants of solids II', *Journal of Modern Optics*, vol. 39, no. 1, pp. 189-.

Hedges, JI 1992, 'Global biogeochemical cycles: progress and problems', *Marine Chemistry*, vol. 39, no. 1-3, pp. 67-93.

Helms, JR, Stubbins, A, Ritchie, JD, Minor, EC, Kieber, DJ & Mopper, K 2008, 'Absorption spectral slopes and slope ratios as indicators of molecular weight, source, and photobleaching of chromophoric dissolved organic matter', *Limnology and oceanography*, vol. 53, no. 3, p. 955.

Hessen, D & Tranvik, LJ 2013, *Aquatic humic substances: ecology and biogeochemistry*, vol. 133, Springer Science & Business Media.

Hestir, EL, Brando, V, Campbell, G, Dekker, A & Malthus, T 2015, 'The relationship between dissolved organic matter absorption and dissolved organic carbon in reservoirs along a temperate to tropical gradient', *Remote Sensing of Environment*, vol. 156, pp. 395-402.

Hoge, FE, Vodacek, A, Swift, RN, Yungel, JK & Blough, NV 1995, 'Inherent optical properties of the ocean: retrieval of the absorption coefficient of chromophoric dissolved organic matter from airborne laser spectral fluorescence measurements', *Applied Optics*, vol. 34, no. 30, pp. 7032-8.

Hu, C, Wang, Y, Yang, Q, He, S, Hu, L & He, M 2007, 'Comparison of ocean color data products from MERIS, MODIS, and SeaWiFS: preliminary results for the East China Seas', in *Proceedings of Envisat Symposium*, pp. 23-7.

Huckins, JN, Petty, JD & Booij, K 2006, *Monitors of organic chemicals in the environment: semipermeable membrane devices*, Springer Science & Business Media.

Hwang, C, Krasner, S, Sclimenti, M, Amy, G, Dickenson, E, Bruchet, A, Prompsy, C, Filippi, G, Croué, J & Violleau, D 2001, 'Polar NOM: characterization', *DBPs, treatment, AWWA Research Foundation and American Water Works Association (USA)*.

Ibrahim, N & Aziz, HA 2014, *Trends on Natural Organic Matter in Drinking Water Sources and its Treatment*, vol. 2.

Jacobsson, J 2014, 'The Suitability of Using Landsat TM-5 Images for Estimating Chromophoric Dissolved Organic Matter in Subarctic Lakes'.

Jaffé, R, McKnight, D, Maie, N, Cory, R, McDowell, W & Campbell, J 2008, 'Spatial and temporal variations in DOM composition in ecosystems: The importance of long-term monitoring of optical properties', *Journal of Geophysical Research: Biogeosciences (2005–2012)*, vol. 113, no. G4.

Jerlov, NG 1968, *Optical oceanography*, vol. 5, Amsterdam : Elsevier, Amsterdam Amsterdam ; New York.

Jerlov, NG 1976, *Marine optics*, Y, Elsevier Scientific Pub. Co., Amsterdam New York.

Judd, KE, Crump, BC & Kling, GW 2006, 'Variation in dissolved organic matter controls bacterial production and community composition', *Ecology*, vol. 87, no. 8, pp. 2068-79.

Keith, DJ, Schaeffer, BA, Lunetta, RS, Gould, RW, Rocha, K & Cobb, DJ 2014, 'Remote sensing of selected water-quality indicators with the hyperspectral imager for the coastal ocean (HICO) sensor', *International Journal of Remote Sensing*, vol. 35, no. 9, pp. 2927-62.

Kirk, JT 1994, *Light and photosynthesis in aquatic ecosystems*, 2nd edn, Cambridge university press.

Kirk, JT 2011, *Light and photosynthesis in aquatic ecosystems*, 3rd edn, Cambridge university press.

Kirk, JTO 1976, 'Yellow substance (gelbstoff) and its contribution to attenuation of photosynthetically active radiation in some inland and coastal Southeastern Australian waters', *Australian Journal of Marine and Freshwater Research*, vol. 27, no. 1, pp. 61-71.

Kotyk, A & Slavík, J 1989, *Intracellular pH and its Measurement*, CRC Press.

Krijgsman, J 1994, 'Optical remote sensing of water quality parameters: interpretation of reflectance spectra'.

Kutser, T, Pierson, D, Tranvik, L, Reinart, A, Sobek, S & Kallio, K 2005, 'Using Satellite Remote Sensing to Estimate the Colored Dissolved Organic Matter Absorption Coefficient in Lakes', *Ecosystems*, vol. 8, no. 6, pp. 709-20.

Laanen, M 2007, 'Yellow Matters: Remote sensing of Coloured Dissolved Organic Matter in inland freshwaters', Vrije Universiteit, Amsterdam.

Laanen, M, Peters, S, Dekker, A & Van Der Woerd, H 2011, 'Assessment of the scattering by sub-micron particles in inland waters', *Journal of the European Optical Society: Rapid Publications*, vol. 6, p. 11046.

Lee, Z & Carder, KL 2002, 'Effect of spectral band numbers on the retrieval of water column and bottom properties from ocean color data', *Applied Optics*, vol. 41, no. 12, pp. 2191-201.

Lee, Z, Carder, KL & Arnone, RA 2002, 'Deriving Inherent Optical Properties from Water Color: a Multiband Quasi-Analytical Algorithm for Optically Deep Waters', *Applied Optics*, vol. 41, no. 27, pp. 5755-72.

Lee, Z, Carder, KL & Du, K 2004, 'Effects of molecular and particle scatterings on the model parameter for remote-sensing reflectance', *Applied Optics*, vol. 43, no. 25, pp. 4957-64.

Leenheer, J 1985, 'Fractionation techniques for aquatic humic substances'.

Leenheer, JA 1981, 'Comprehensive approach to preparative isolation and fractionation of dissolved organic carbon from natural waters and wastewaters', *Environmental Science and Technology*, vol. 15, no. 5, pp. 578-87.

Leenheer, JA & Croué, J-P 2003, 'Peer reviewed: characterizing aquatic dissolved organic matter', *Environmental science & technology*, vol. 37, no. 1, pp. 18A-26A.

Leenheer, JA, Croue, J-P, Benjamin, M, Korshin, GV, Hwang, CJ, Bruchet, A & Aiken, GR 2000, 'Comprehensive isolation of natural organic matter from water for spectral characterizations and reactivity testing', in *ACS symposium series*, pp. 68-83.

Liang, S 2017, *Comprehensive Remote Sensing*, Elsevier.

Linnemann, K, Gege, P, Rößler, S, Schneider, T & Melzer, A 2013, 'CDOM retrieval using measurements of downwelling irradiance', in *SPIE Remote Sensing*, International Society for Optics and Photonics, pp. 88880I-I-10.

Lyons, MB 2012, 'Mapping and monitoring the long term spatial dynamics of land cover and seagrass distribution in South East Queensland, Australia', The University of Queensland.

Ma, RH, Tang, J & Dai, J 2006, 'Bio-optical model with optimal parameter suitable for Taihu Lake in water colour remote sensing', *International Journal of Remote Sensing*, vol. 27, no. 19, pp. 4305 - 28.

MacCarthy, P, Malcolm, R, Clapp, C & Bloom, P 1990, 'An introduction to soil humic substances', *Humic Substances in Soil and Crop Sciences: Selected Readings*, no. humicsubstances, pp. 1-12.

Mannino, A, Russ, ME & Hooker, SB 2008, 'Algorithm development and validation for satellite-derived distributions of DOC and CDOM in the US Middle Atlantic Bight', *Journal of Geophysical Research: Oceans (1978–2012)*, vol. 113, no. C7.

Mannino, A, Novak, MG, Hooker, SB, Hyde, K & Aurin, D 2014, 'Algorithm development and validation of CDOM properties for estuarine and continental shelf waters along the northeastern U.S. coast', *Remote Sensing of Environment*, vol. 152, no. 0, pp. 576-602.

Marhaba, TF, Pu, Y & Bengraine, K 2003, 'Modified dissolved organic matter fractionation technique for natural water', *Journal of Hazardous Materials*, vol. 101, no. 1, pp. 43-53.

Markager, S & Vincent, WF 2000, 'Spectral light attenuation and the absorption of UV and blue light in natural waters', *Limnology and oceanography*, vol. 45, no. 3, pp. 642-50.

Massicotte, P & Markager, S 2016, 'Using a Gaussian decomposition approach to model absorption spectra of chromophoric dissolved organic matter', *Marine Chemistry*, vol. 180, pp. 24-32.

Matilainen, A, Vepsäläinen, M & Sillanpää, M 2010, 'Natural organic matter removal by coagulation during drinking water treatment: a review', *Advances in colloid and interface science*, vol. 159, no. 2, pp. 189-97.

Matsuoka, A, Hooker, SB, Bricaud, A, Gentili, B & Babin, M 2013, 'Estimating absorption coefficients of colored dissolved organic matter (CDOM) using a semi-analytical algorithm for southern Beaufort Sea waters: application to deriving concentrations of dissolved organic carbon from space', *Biogeosciences*, vol. 10, pp. 917-27.

Matsuoka, A, Bricaud, A, Benner, R, Para, J, Sempéré, R, Prieur, L, Bélanger, S & Babin, M 2012, 'Tracing the transport of colored dissolved organic matter in water masses of the Southern Beaufort Sea: relationship with hydrographic characteristics', *Biogeosciences*, vol. 9, no. 3, pp. 925-40.

McKnight, D, Aiken, G, Andrews, E, Bowles, E & Harnish, R 1993, *Dissolved organic material in dry valley lakes: A comparison of Lake Fryxell, Lake Hoare and Lake Vanda*, Wiley Online Library.

McKnight, DM, Boyer, EW, Westerhoff, PK, Doran, PT, Kulbe, T & Andersen, DT 2001, 'Spectrofluorometric characterization of dissolved organic matter for indication of precursor organic material and aromaticity', *Limnology and oceanography*, vol. 46, no. 1, pp. 38-48.

Miller, RL, Castillo, CED & McKee, BA 2007, *Remote Sensing of Coastal Aquatic Environments: Technologies, Techniques and Applications*, Springer Netherlands.

Mingos, DMP 2016, 'The Chemical Bond: Lewis and Kossel's Landmark Contribution', in PDM Mingos (ed.), *The Chemical Bond I: 100 Years Old and Getting Stronger*, Springer International Publishing, Cham, pp. 1-56.

Mirza, MA, Ahmad, N, Agarwal, SP, Mahmood, D, Khalid Anwer, M & Iqbal, Z 2011, 'Comparative evaluation of humic substances in oral drug delivery', *Results in Pharma Sciences*, vol. 1, no. 1, pp. 16-26.

Mishra, DR, Ogashawara, I & Gitelson, AA 2017, *Bio-optical Modeling and Remote Sensing of Inland Waters*, Elsevier.

Mobley, C, Boss, E & Roesler, C 2010, *Ocean optics web book*.

Mobley, CD 1994, *Light and water : radiative transfer in natural waters*, Academic Press, San Diego.

Mobley, CD 1995, 'The optical properties of water', *Handbook of optics*, vol. 1, pp. 43.1-.56.

Mobley, CD 1996, 'The Optical Properties of Water', in M Bass (ed.), *Handbook of optics CD-ROM*, 2nd edition edn, McGraw-Hill.

Mobley, CD 1999, 'Estimation of the Remote-Sensing Reflectance from Above-Surface Measurements', *Applied Optics*, vol. 38, no. 36, pp. 7442-55.

Mobley, CD & Sundman, L 2001, *Hydrolight 4.2 Technical Documentation.*, Sequoia Scientific, Inc., Redmond, WA.

Moran, XA, Gasol, JM, Arin, L & Estrada, M 1999, 'A comparison between glass fiber and membrane filters for the estimation of phytoplankton POC and DOC production', *Marine Ecology Progress Series*, vol. 187, pp. 31-41.

Morel, A 1974, 'Optical properties of pure water and pure seawater', in NG Jerlov & E Steeman Nielsen (eds), *Optical Aspects of Oceanography*, Academic Press Inc, London, pp. 1-24.

Morel, A 1991, 'Optics of marine particles and marine optics', in *Particle analysis in oceanography*, Springer, pp. 141-88.

Morel, A & Prieur, L 1977, 'Analysis of variations in ocean color', *Limnology and oceanography*, vol. 22, no. 4, pp. 709-22.

Mostofa, K, Liu, C, Wu, F, Fu, P, Ying, W & Yuan, J 2009, 'Overview of key biogeochemical functions in lake ecosystem: impacts of organic matter pollution

and global warming', in *Proceedings of 13th World Lake Conference, Wuhan, China*, pp. 1-5.

Mostofa, KM, Liu, C-q, Vione, D, Mottaleb, MA, Ogawa, H, Tareq, SM & Yoshioka, T 2013, 'Colored and chromophoric dissolved organic matter in natural waters', in *Photobiogeochemistry of Organic Matter*, Springer, pp. 365-428.

Mueller, JL, Fargion, GS, McClain, CR, Pegau, S, Zaneveld, JRV, Mitchell, BG, Kahru, M, Wieland, J & Stramska, M 2003, *Ocean Optics Protocols For Satellite Ocean Color Sensor Validation, Revision 4, Volume IV: Inherent Optical Properties: Instruments, Characterizations, Field Measurements and Data Analysis Protocols*, NASA, Greenbelt, Maryland.

Nelson, NB & Siegel, DA 2013, 'The global distribution and dynamics of chromophoric dissolved organic matter', *Annual Review of Marine Science*, vol. 5, pp. 447-76.

Neukermans, G & Fournier, G 2018, 'Optical modeling of spectral backscattering and remote sensing reflectance from Emiliania huxleyi blooms', *Frontiers in Marine Science*, vol. 5, p. 146.

Nguy-Robertson, A, Li, L, Tedesco, LP, Wilson, JS & Soyeux, E 2013, 'Determination of absorption coefficients for chlorophyll a, phycocyanin, mineral matter and CDOM from three central Indiana reservoirs', *Journal of Great Lakes Research*, vol. 39, pp. 151-60.

O'Bree, T 2007, 'Investigations of light scattering by Australian natural waters for remote sensing applications'.

Odermatt, D, Gitelson, A, Brando, VE & Schaepman, M 2012, 'Review of constituent retrieval in optically deep and complex waters from satellite imagery', *Remote Sensing of Environment*, vol. 118, no. 0, pp. 116-26.

Ogawa, H & Tanoue, E 2003, 'Dissolved organic matter in oceanic waters', *Journal of Oceanography*, vol. 59, no. 2, pp. 129-47.

Oliver, BG, Thurman, EM & Malcolm, RL 1983, 'The contribution of humic substances to the acidity of colored natural waters', *Geochimica et Cosmochimica Acta*, vol. 47, no. 11, pp. 2031-5.

Osburn, CL & Bianchi, TS 2016, 'Linking optical and chemical properties of dissolved organic matter in natural waters', *Frontiers in Marine Science*, vol. 3, p. 223.

Osburn, CL & Bianchi, TS 2017, *Linking optical and chemical properties of dissolved organic matter in natural waters*, Frontiers Media SA.

Padisák, J, Krienitz, L, Koschel, R & Nedoma, J 1997, 'Deep-layer autotrophic picoplankton maximum in the oligotrophic Lake Stechlin, Germany: origin, activity, development and erosion', *European Journal of Phycology*, vol. 32, no. 4, pp. 403-16.

Pagano, T, Bida, M & Kenny, JE 2014, 'Trends in Levels of Allochthonous Dissolved Organic Carbon in Natural Water: A Review of Potential Mechanisms under a Changing Climate', *Water*, vol. 6, no. 10, pp. 2862-97.

Page, D & Dillon, PJ 2007, *Measurement of the biodegradable fraction of dissolved organic matter relevant to water reclamation via aquifers*, CSIRO Water for a Healthy Country Flaship.

Para, J, Coble, PG, Charrière, B, Tedetti, M, Fontana, C & Sempéré, R 2010, 'Fluorescence and absorption properties of chromophoric dissolved organic matter (CDOM) in coastal surface waters of the Northwestern Mediterranean Sea (Bay of Marseilles, France)', *Biogeosciences Discussions*, vol. 7, no. 4, pp. 5675-718.

Pegau, WS, Gray, D & Zaneveld, JRV 1997, 'Absorption and attenuation of visible and near-infrared light in water: dependence on temperature and salinity', *Applied Optics*, vol. 36, no. 24, pp. 6035-46.

Pettit, RE 2004, 'Organic matter, humus, humate, humic acid, fulvic acid and humin: their importance in soil fertility and plant health', *CTI Research*.

Peuravuori, J, Lehtonen, T & Pihlaja, K 2002, 'Sorption of aquatic humic matter by DAX-8 and XAD-8 resins: Comparative study using pyrolysis gas chromatography', *Analytica Chimica Acta*, vol. 471, no. 2, pp. 219-26.

Peuravuori, J, Ingman, P, Pihlaja, K & Koivikko, R 2001, 'Comparisons of sorption of aquatic humic matter by DAX-8 and XAD-8 resins from solid-state 13 C NMR spectroscopy's point of view', *Talanta*, vol. 55, no. 4, pp. 733-42.

Philp, R 1981, 'Diagenetic organic matter in recent sediments and environments of deposition', *BMR J. Australian Geol. Geophys*, vol. 6, pp. 301-6.

Phlips, E 1995, 'Chlorophyll a, tripton, color, and light availability in Florida Bay, USA', *Mar Ecol Prog Ser*, vol. 127, pp. 223-34.

Pope, RM & Fry, ES 1997, 'Absorption spectrum (380 -700 nm) of pure water. II. Integrating cavity measurements', *Applied Optics*, vol. 36, no. 33, pp. 8710-23.

Pravin, J, Shanmugam, P & Ahn, Y 2015, 'A semi-analytical model for diffuse reflectance in marine and inland waters', *Ocean Sci. Discuss*, vol. 12, no. 4, pp. 1893-912.

Pure, IUo, Chemistry, ACCotNoO, Panico, R, Powell, WH & Richer, JC 1993, *A Guide to IUPAC Nomenclature of Organic Compounds: Recommendations 1993 (including Revisions, Published and Hitherto Unpublished, to the 1979 Edition of Nomenclature of Organic Chemistry*, Blackwell Scientific Publications.

Qin, B 2008, *Lake Taihu, China : dynamics and environmental change*, Dordrecht : Springer, Dordrecht

Dordrecht].

quality, AaNZgffamw 2000, 'Australian and New Zealand guidelines for fresh and marine water quality', *Australian and New Zealand Environment and Conservation Council and Agriculture and Resource Management Council of Australia and New Zealand, Canberra*, pp. 1-103.

Queensland, G 2017, *Queensland Government Datasets*, https://www.data.qld.gov.au/dataset>.

Queensland, Go 2014, *Business and Industry Portal: Darling Downs*.

Ratpukdi, T, Rice, JA, Chilom, G, Bezbaruah, A & Khan, E 2009, 'Rapid Fractionation of Natural Organic Matter in Water Using a Novel Solid-Phase Extraction Technique', *Water Environment Research*, vol. 81, no. 11, pp. 2299-308.

Rheinboldt, WC 1998, *Methods for solving systems of nonlinear equations*, vol. 70, Siam.

Rice, JA 2001, 'Humin', *Soil Science*, vol. 166, no. 11, pp. 848-57.

Roesler, C & Culbertson, C 2016, 'Lake transparency: a window into decadal variations in dissolved organic carbon concentrations in lakes of Acadia National Park, Maine', in *Aquatic Microbial Ecology and Biogeochemistry: A Dual Perspective*, Springer, pp. 225-36.

Roesler, CS & Perry, MJ 1995, 'In situ phytoplankton absorption, fluorescence emission, and particulate backscattering spectra determined from reflectance', *Journal of Geophysical Research: Oceans (1978–2012)*, vol. 100, no. C7, pp. 13279-94.

Roesler, CS & Barnard, AH 2013, 'Methods in Oceanography'.

Roesler, CS, Perry, MJ & Carder, KL 1989, 'Modeling in Situ Phytoplankton Absorption from Total Absorption Spectra in Productive Inland Marine Waters', *Limnology and oceanography*, vol. 34, no. 8, Hydrologic Optics, pp. 1510-23.

Rook, JJ 1974, 'Formation of Haloforms during Chlorination of natural Waters', *Water Treat. Exam.*, vol. 23, pp. 234-43.

Ruszczyński, AP & Ruszczynski, A 2006, *Nonlinear optimization*, vol. 13, Princeton university press.

Sabins, FF 2007, *Remote sensing: principles and applications*, Waveland Press.

Schroeder, T, Devlin, MJ, Brando, VE, Dekker, AG, Brodie, JE, Clementson, LA & McKinna, L 2012, 'Inter-annual variability of wet season freshwater plume extent into the Great Barrier Reef lagoon based on satellite coastal ocean colour observations', *Marine pollution bulletin*, vol. 65, no. 4-9, pp. 210-23.

Shao, T, Wang, T, Liang, X, Xu, H & Li, L 2019, 'Characterization of DOC and CDOM and their relationship in turbid waters of a high-altitude area on the western Loess Plateau, China', *Water Science and Technology*, vol. 80, no. 9, pp. 1796-806.

Shao, T, Song, K, Du, J, Zhao, Y, Ding, Z, Guan, Y, Liu, L & Zhang, B 2015, 'Seasonal Variations of CDOM Optical Properties in Rivers Across the Liaohe Delta', *Wetlands*, pp. 1-12.

Shen, Y, Chapelle, FH, Strom, EW & Benner, R 2015, 'Origins and bioavailability of dissolved organic matter in groundwater', *Biogeochemistry*, vol. 122, no. 1, pp. 61-78.

Smith, RC & Baker, KS 1981, 'Optical properties of the clearest natural waters (200-800 nm)', *Applied Optics*, vol. 20, no. 2, pp. 177-84.

Sobek, S, Tranvik, LJ, Prairie, YT, Kortelainen, P & Cole, JJ 2007, 'Patterns and regulation of dissolved organic carbon: An analysis of 7,500 widely distributed lakes', *Limnology and oceanography*, vol. 52, no. 3, pp. 1208-19.

SOE, ASotE 2011, *National Water Quality Assessment 2011*, Australia State of the Environment, Canberra.

Song, K, Zhao, Y, Wen, Z, Chong, F & Shang, Y 2017, 'A systematic examination of the relationships between CDOM and DOC in inland waters in China', *Hydrology and Earth System Sciences*, vol. 21, no. 10, p. 5127.

Spencer, RG, Bolton, L & Baker, A 2007, 'Freeze/thaw and pH effects on freshwater dissolved organic matter fluorescence and absorbance properties from a number of UK locations', *Water Research*, vol. 41, no. 13, pp. 2941-50.

Spencer, RG, Butler, KD & Aiken, GR 2012, 'Dissolved organic carbon and chromophoric dissolved organic matter properties of rivers in the USA', *Journal of Geophysical Research: Biogeosciences (2005–2012)*, vol. 117, no. G3.

Stedmon, C & Markager, S 2001, 'The optics of chromophoric dissolved organic matter (CDOM) in the Greenland Sea: An algorithm for differentiation between marine and terrestrially derived organic matter', *Limnology and oceanography*, vol. 46, no. 8, pp. 2087-93.

Stedmon, CA & Nelson, NB 2014, 'The optical properties of DOM in the ocean', in *Biogeochemistry of Marine Dissolved Organic Matter (Second Edition)*, Elsevier, pp. 481-508.

Stedmon, CA, Markager, S & Kaas, H 2000, 'Optical properties and signatures of chromophoric dissolved organic matter (CDOM) in Danish coastal waters', *Estuarine, Coastal and Shelf Science*, vol. 51, no. 2, pp. 267-78.

Stedmon, CA, & Nelson, N. B. 2014, 'The optical properties of DOM in the ocean', in *Biogeochemistry of Marine Dissolved Organic Matter*, 2nd edn, pp. 481-508.

Steelink, C 1963, 'What is humic acid?', *Journal of Chemical Education*, vol. 40, no. 7, p. 379.

Steinberg, C 2003, *Ecology of humic substances in freshwaters: determinants from geochemistry to ecological niches*, Springer.

Strömbeck, N, Candiani, G, Giardino, C & Zilioli, E 2003, 'Water quality monitoring of Lake Garda using multi-temporal MERIS data.', in *MERIS Users Workshop*: *Proceedings of the MERIS Users Workshop* Frascati, Italy, p. 6.

Sun, DY, Li, YM, Wang, Q, Lu, H, Le, CF, Huang, CC & Gong, SQ 2011, 'A neural-network model to retrieve CDOM absorption from in situ measured hyperspectral data in an optically complex lake: Lake Taihu case study', *International Journal of Remote Sensing*, vol. 32, no. 14, pp. 4005-22.

Sunwater 2005, *Sunwater 04-05 annual report*, viewed 25 May 2006, <http://www.sunwater.com.au/pdf/about/SunWater_Annual_Report.pdf>.

Tan, KH 2003, *Humic Matter in Soil and the Environment: Principles and Controversies*, Taylor & Francis.

Tanaka, K, Takesue, N, Nishioka, J, Kondo, Y, Ooki, A, Kuma, K, Hirawake, T & Yamashita, Y 2016, 'The conservative behavior of dissolved organic carbon in surface waters of the southern Chukchi Sea, Arctic Ocean, during early summer', *Scientific reports*, vol. 6, p. 34123.

Thomas, GE & Stamnes, K 2002, *Radiative transfer in the atmosphere and ocean*, Cambridge University Press.

Thurman, EM 1985, *Organic geochemistry of natural waters*, vol. 2, Springer.

Thurman, EM & Malcolm, RL 1981, 'Preparative isolation of aquatic humic substances', *Environmental science & technology*, vol. 15, no. 4, pp. 463-6.

Tranvik, LJ, Downing, JA, Cotner, JB, Loiselle, SA, Striegl, RG, Ballatore, TJ, Dillon, P, Finlay, K, Fortino, K & Knoll, LB 2009, 'Lakes and reservoirs as regulators of carbon cycling and climate', *Limnology and oceanography*, vol. 54, no. 6, pp. 2298-314.

Traub, J 2012, 'Patterns in the Variation of CDOM Spectral Slopes in the Western Lake Erie Basin', University of Toledo.

Twardowski, MS, Boss, E, Sullivan, JM & Donaghay, PL 2004, 'Modeling the spectral shape of absorption by chromophoric dissolved organic matter', *Marine Chemistry*, vol. 89, no. 1-4, pp. 69-88.

Twardowski, MS, Boss, E, Macdonald, JB, Pegau, WS, Barnard, AH & Zaneveld, JRV 2001, 'A model for estimating bulk refractive index from the optical backscattering ratio and the implications for understanding particle composition in case I and case II waters', *Journal of Geophysical Research-Oceans*, vol. 106, no. C7, pp. 14129-42.

Uyguner, CS, Bekbolet, M & Swietlik, J 2007, 'Natural organic matter: Definitions and characterization', *Advances in control of disinfection by-products, vol*.

Valentine, RL 1998, *Chloramine decomposition in distribution system and model waters*, American Water Works Association.

Van der Meer, FD & De Jong, SM 2011, *Imaging spectrometry: basic principles and prospective applications*, vol. 4, Springer Science & Business Media.

Vantrepotte, V, Danhiez, F-P, Loisel, H, Ouillon, S, Mériaux, X, Cauvin, A & Dessailly, D 2015, 'CDOM-DOC relationship in contrasted coastal waters: implication for DOC retrieval from ocean color remote sensing observation', *Optics Express*, vol. 23, no. 1, pp. 33-54.

Vinebrooke, RD & Leavitt, PR 1998, 'Direct and interactive effects of allochthonous dissolved organic matter, inorganic nutrients, and ultraviolet radiation on an alpine littoral food web', *Limnology and oceanography*, vol. 43, no. 6, pp. 1065-81.

Vodacek, A, Blough, NV, DeGrandpre, MD & Nelson, RK 1997, 'Seasonal variation of CDOM and DOC in the Middle Atlantic Bight: Terrestrial inputs and photooxidation', *Limnology and oceanography*, vol. 42, no. 4, pp. 674-86.

Walker, RE 1994, *Marine light field statistics.*, Wiley, New York.

Wells, ML & Boehme, J 2008, *The Source, Cycling, and Behavior of Chromophoric Dissolved Organic Matter in Coastal Waters*, DTIC Document.

Wershaw, RL 1999, 'Molecular aggregation of humic substances', *Soil Science*, vol. 164, no. 11, pp. 803-13.

Widder, E, In, B & Archer, S 2001, 'BIO-OPTICAL MODELS', *Nature, London*, vol. 267, no. 788, p. 793.

Winn, NT 2008, 'Modeling Dissolved Organic Carbon (DOC) in Subalpine and Alpine Lakes With GIS and Remote Sensing', Miami University.

Woźniak, B 2007, *Light absorption in sea water*, New York, NY : Springer, New York, NY.

Wurl, O 2009, *Practical guidelines for the analysis of seawater*, CRC press.

Yang, W, Matsushita, B, Chen, J, Yoshimura, K & Fukushima, T 2013, 'Retrieval of Inherent Optical Properties for Turbid Inland Waters From Remote-Sensing Reflectance', *IEEE Transactions on Geoscience and Remote Sensing*, vol. 51, no. 6, pp. 3761-73.

Yee, LF, Abdullah, MP, Abdullah, A, Ishak, B & Abidin, KNZ 2009, 'Hydrophobicity characteristics of natural organic matter and the formation of THM', *The Malaysian Journal of Analytical Sciences*, vol. 13, no. 1, pp. 94-9.

York, R & Bell, NG 2020, 'Molecular Tagging for the Molecular Characterization of Natural Organic Matter', *Environmental science & technology*, vol. 54, no. 6, pp. 3051-63.

Yoro, SC, Panagiotopoulos, C & Sempéré, R 1999, 'Dissolved organic carbon contamination induced by filters and storage bottles', *Water Research*, vol. 33, no. 8, pp. 1956-9.

Zepp, RG & Schlotzhauer, PF 1981, 'Comparison of photochemical behavior of various humic substances in water: III. Spectroscopic properties of humic substances', *Chemosphere*, vol. 10, no. 5, pp. 479-86.

Zepp, RG, Baughman, GL & Schlotzhauer, PF 1981, 'Comparison of photochemical behavior of various humic substances in water: I. Sunlight induced reactions of aquatic pollutants photosensitized by humic substances', *Chemosphere*, vol. 10, no. 1, pp. 109-17.

Zhang, M, Dong, Q, Cui, T, Xue, C & Zhang, S 2014, 'Suspended sediment monitoring and assessment for Yellow River estuary from Landsat TM and ETM + imagery', *Remote Sensing of Environment*, vol. 146, no. 0, pp. 136-47.

Zhang, Y, Qin, B, Zhu, G, Zhang, L & Yang, L 2007, 'Chromophoric dissolved organic matter (CDOM) absorption characteristics in relation to fluorescence in Lake Taihu, China, a large shallow subtropical lake', in B Qin, et al. (eds), *Eutrophication of Shallow Lakes with Special Reference to Lake Taihu, China*, Springer Netherlands, vol. 194, ch 5, pp. 43-52.

Zhang, Y, Ma, R, Duan, H, Loiselle, S & Xu, J 2014, 'A spectral decomposition algorithm for estimating Chlorophyll-a concentrations in Lake Taihu, China', *Remote Sensing*, vol. 6, no. 6, pp. 5090-106.

Zhang, Y, Qin, B, Liu, M, Zhu, G, Gong, Z & Li, Y 2011, 'Modelling the spectral absorption of tripton using exponential and hyperbolic models', *International Journal of Remote Sensing*, vol. 32, no. 14, pp. 3917-33.

Zhang, YL, Liu, ML, Wang, X, Zhu, GW & Chen, WM 2009, 'Bio-optical properties and estimation of the optically active substances in Lake Tianmuhu in summer', *International Journal of Remote Sensing*, vol. 30, no. 11, pp. 2837-57.

Zsolnay, Á 2003, 'Dissolved organic matter: artefacts, definitions, and functions', *Geoderma*, vol. 113, no. 3–4, pp. 187-209.

Appendix (A) - Average SIOPs for all the study locations extracted using; left) bio-optical modelling; right) ECOLIGHT® simulation

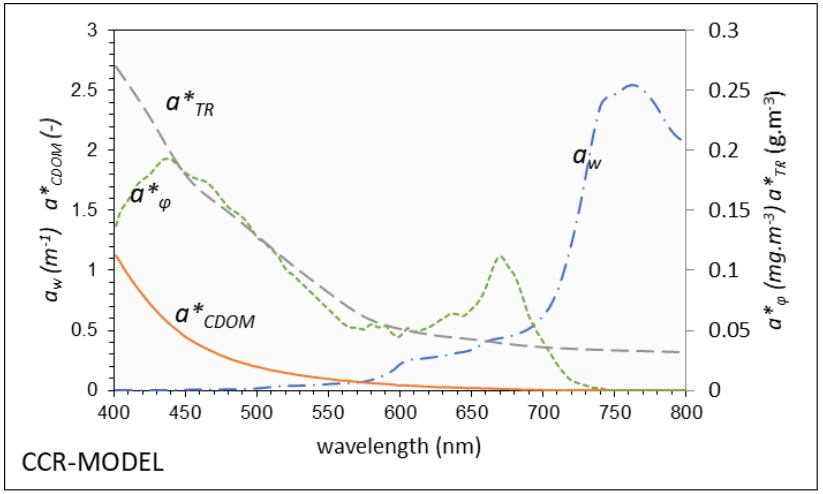

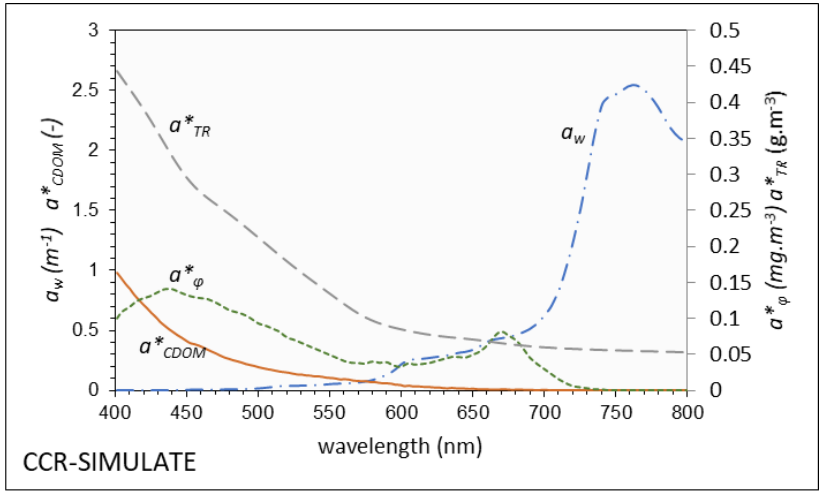

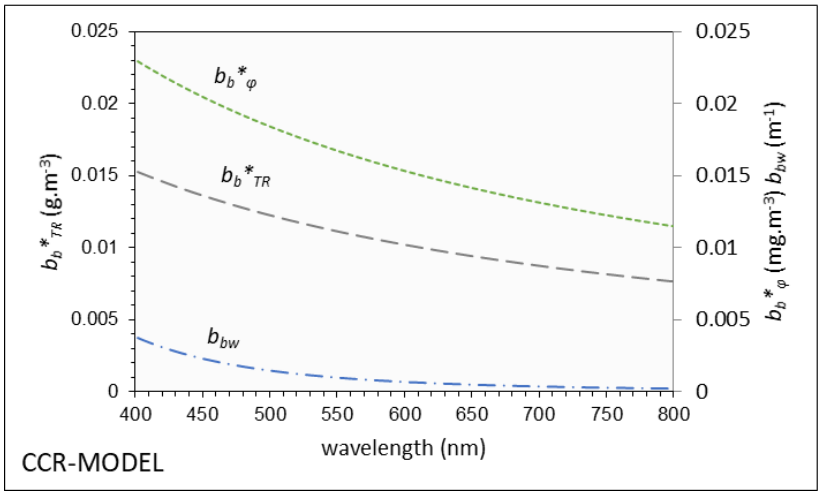

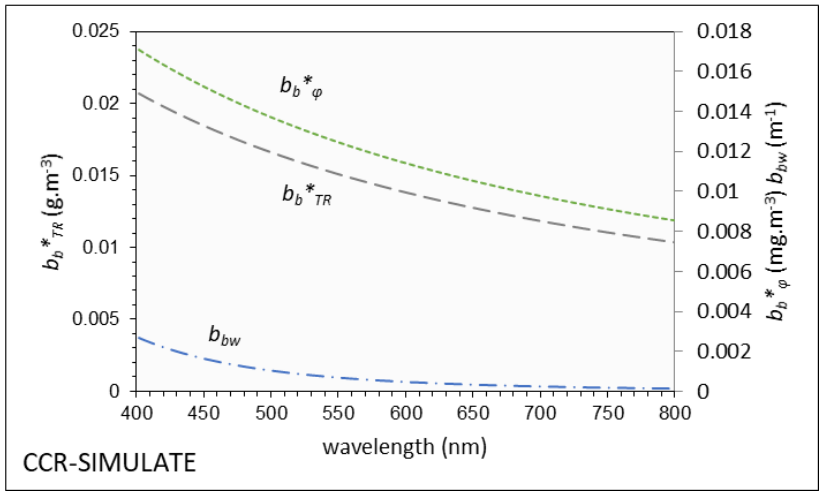

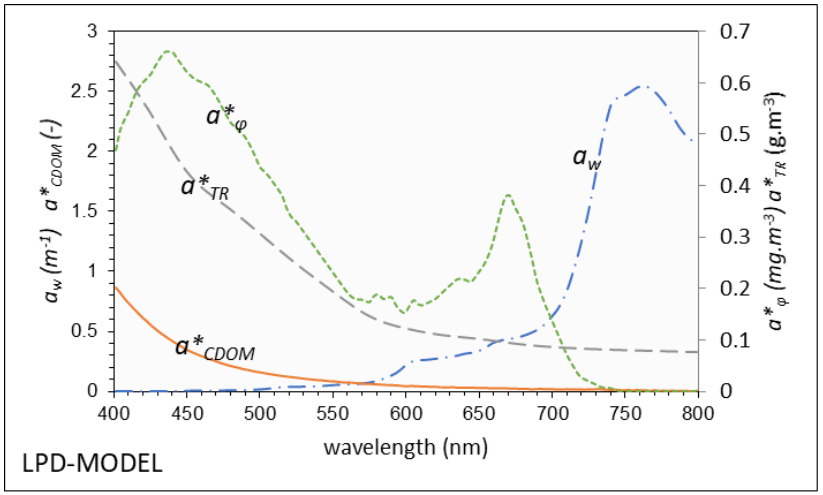
LPD-MODEL
wavelength (nm)
a_w (m^{-1}) a^*_{CDOM} (-)
a^*_{φ} ($mg.m^{-3}$) a^*_{TR} ($g.m^{-3}$)
a^*_{φ}
a^*_{TR}
a_w
a^*_{CDOM}

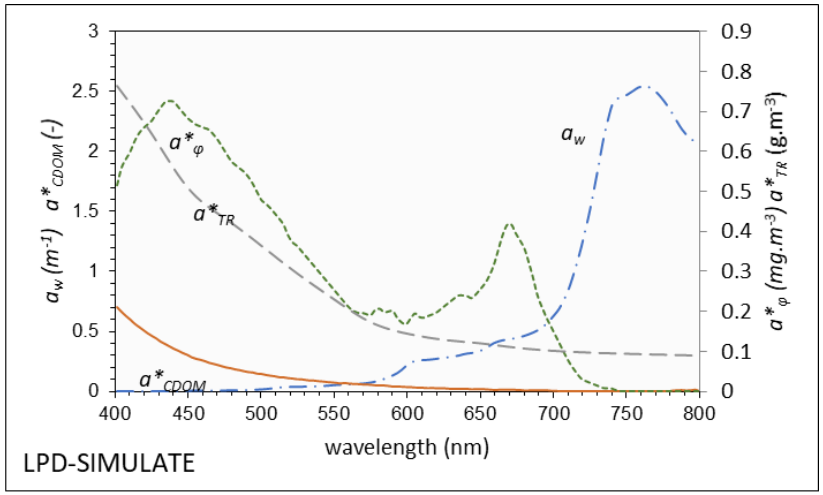
LPD-SIMULATE
wavelength (nm)
a_w (m^{-1}) a^*_{CDOM} (-)
a^*_{φ} ($mg.m^{-3}$) a^*_{TR} ($g.m^{-3}$)
a^*_{φ}
a^*_{TR}
a_w
a^*_{CDOM}

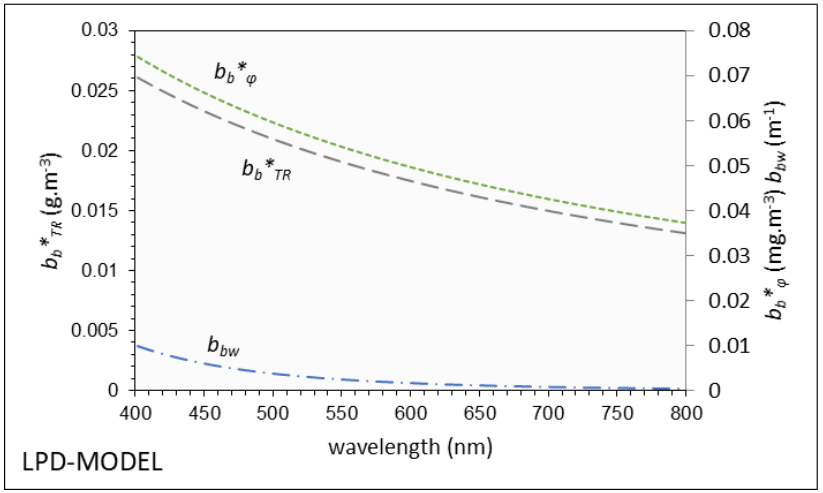
LPD-MODEL
wavelength (nm)
$b_b{}^*_{TR}$ ($g.m^{-3}$) b_{bw} (m^{-1})
$b_b{}^*_{\varphi}$ ($mg.m^{-3}$) b_{bw} (m^{-1})
$b_b{}^*_{\varphi}$
$b_b{}^*_{TR}$
b_{bw}

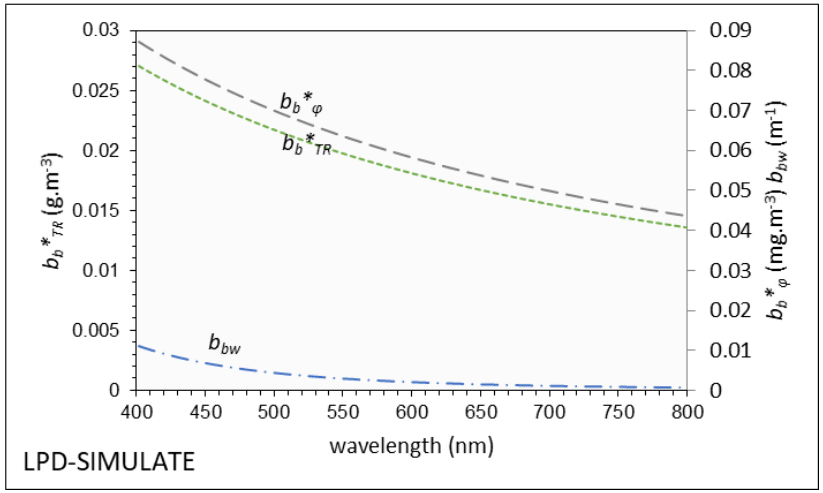
LPD-SIMULATE
wavelength (nm)
$b_b{}^*_{TR}$ ($g.m^{-3}$) b_{bw} (m^{-1})
$b_b{}^*_{\varphi}$ ($mg.m^{-3}$) b_{bw} (m^{-1})
$b_b{}^*_{\varphi}$
$b_b{}^*_{TR}$
b_{bw}

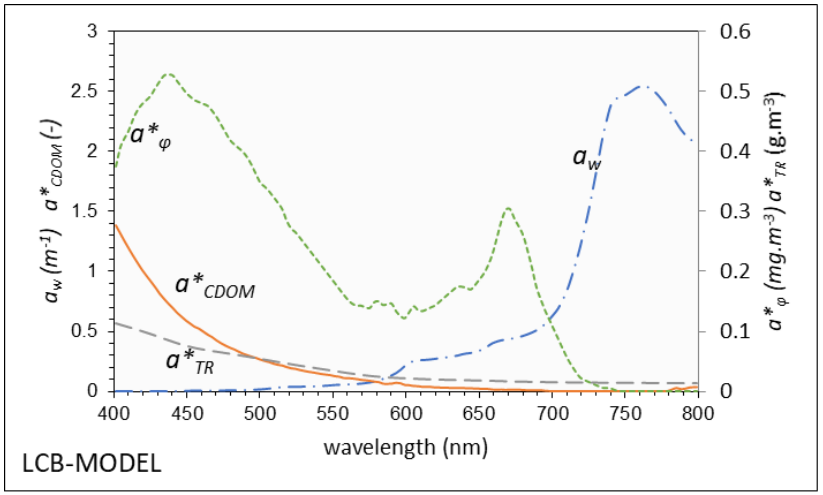
a_w (m^{-1}) a^*_{CDOM} (-)
a^*_φ (mg.m^{-3}) a^*_{TR} (g.m^{-3})
a^*_φ
a_w
a^*_{CDOM}
a^*_{TR}
wavelength (nm)
LCB-MODEL

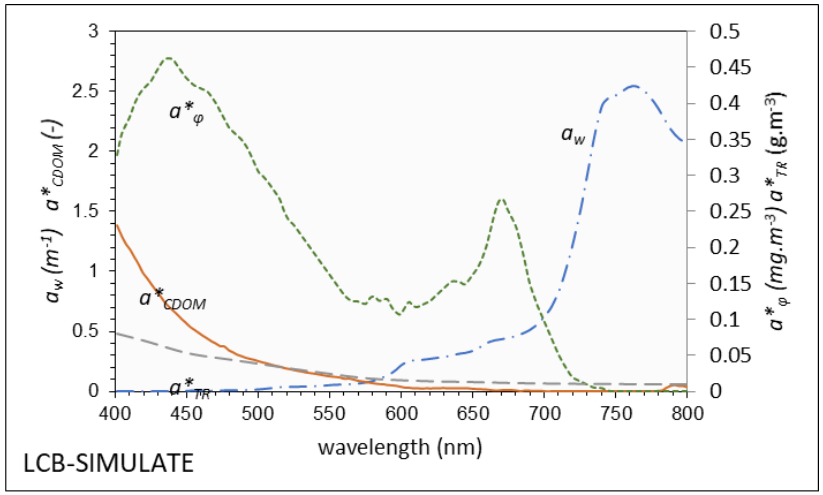
a_w (m^{-1}) a^*_{CDOM} (-)
a^*_φ (mg.m^{-3}) a^*_{TR} (g.m^{-3})
a^*_φ
a_w
a^*_{CDOM}
a^*_{TR}
wavelength (nm)
LCB-SIMULATE

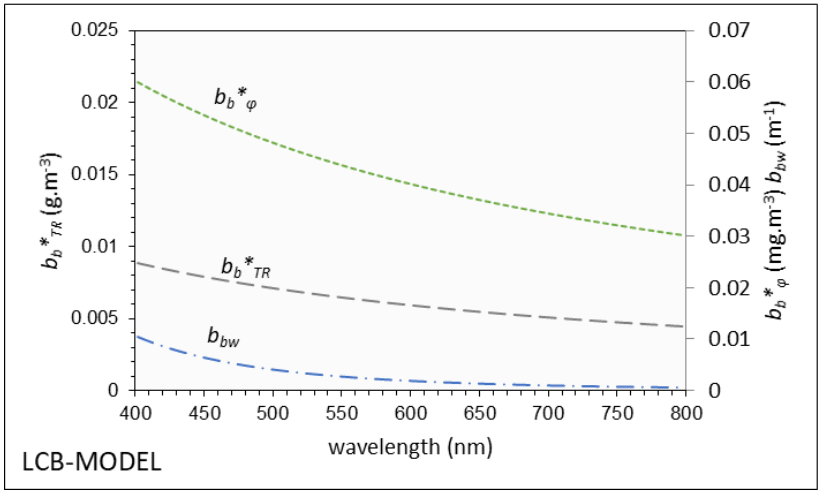
$b_b{}^*_{TR}$ (g.m^{-3})
$b_b{}^*_\varphi$ (mg.m^{-3}) b_{bw} (m^{-1})
$b_b{}^*_\varphi$
$b_b{}^*_{TR}$
b_{bw}
wavelength (nm)
LCB-MODEL

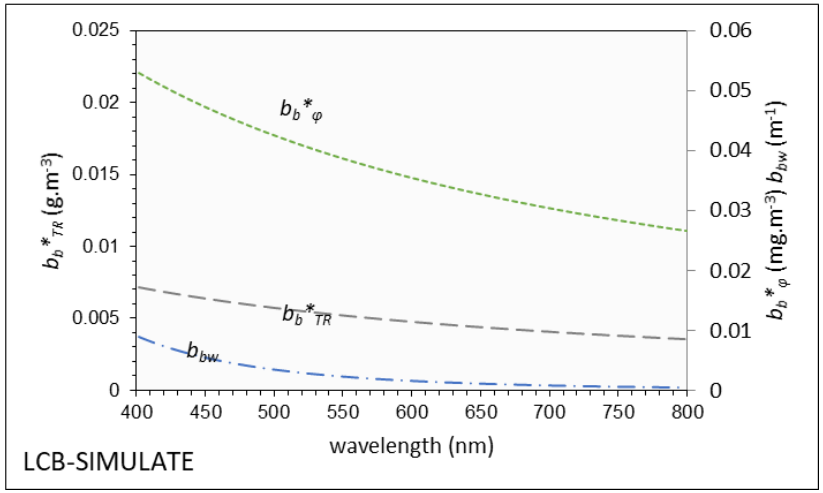
$b_b{}^*_{TR}$ (g.m^{-3})
$b_b{}^*_\varphi$ (mg.m^{-3}) b_{bw} (m^{-1})
$b_b{}^*_\varphi$
$b_b{}^*_{TR}$
b_{bw}
wavelength (nm)
LCB-SIMULATE

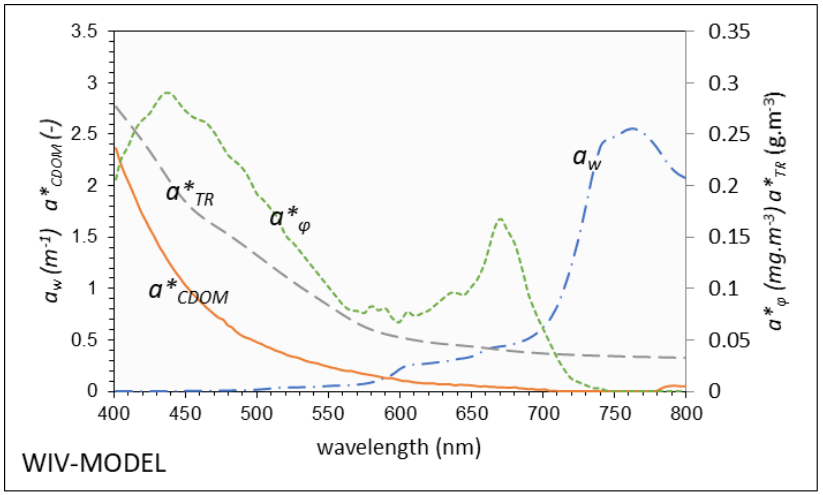
WIV-MODEL
wavelength (nm)
a_w (m^{-1}) a^*_{CDOM} (-)
a^*_{φ} ($mg.m^{-3}$) a^*_{TR} ($g.m^{-3}$)
a^*_{TR}
a^*_{φ}
a^*_{CDOM}
a_w

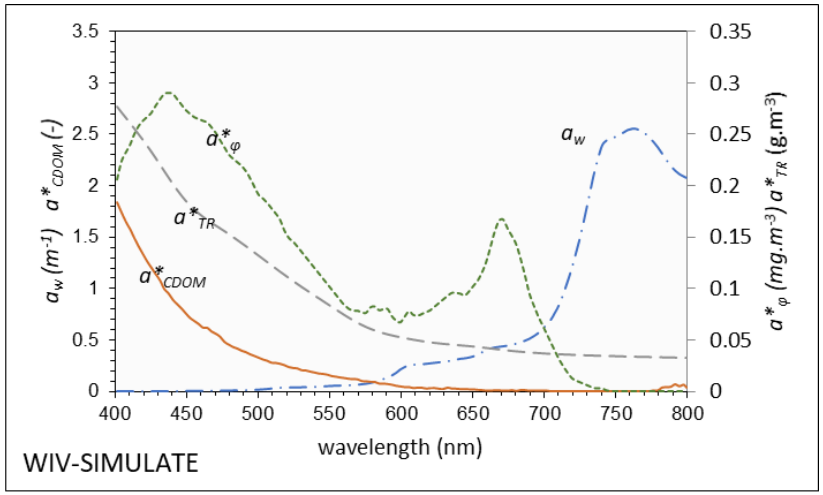
WIV-SIMULATE
wavelength (nm)
a_w (m^{-1}) a^*_{CDOM} (-)
a^*_{φ} ($mg.m^{-3}$) a^*_{TR} ($g.m^{-3}$)
a^*_{φ}
a^*_{TR}
a^*_{CDOM}
a_w

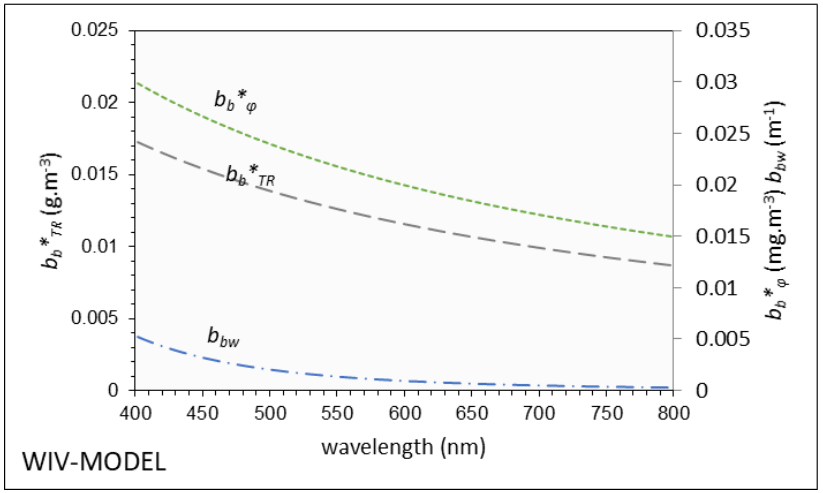
WIV-MODEL
wavelength (nm)
$b_b{}^*_{TR}$ ($g.m^{-3}$) b_{bw} (m^{-1})
$b_b{}^*_{\varphi}$ ($mg.m^{-3}$) b_{bw} (m^{-1})
$b_b{}^*_{\varphi}$
$b_b{}^*_{TR}$
b_{bw}

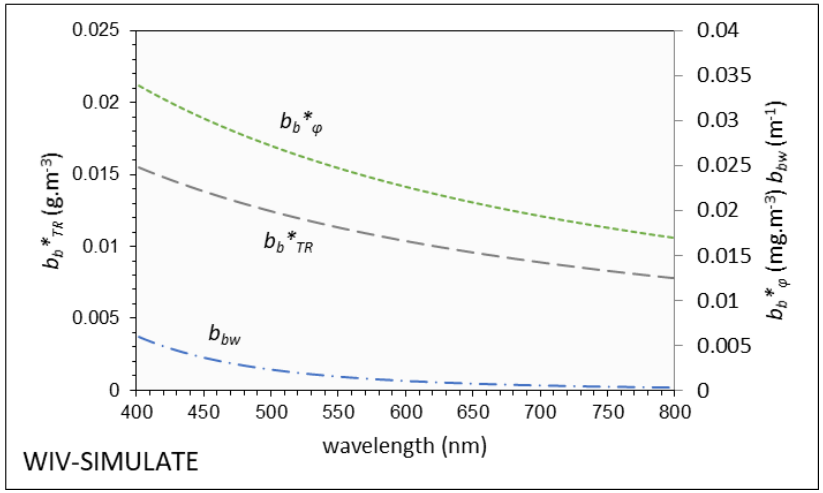
WIV-SIMULATE
wavelength (nm)
$b_b{}^*_{TR}$ ($g.m^{-3}$) b_{bw} (m^{-1})
$b_b{}^*_{\varphi}$ ($mg.m^{-3}$) b_{bw} (m^{-1})
$b_b{}^*_{\varphi}$
$b_b{}^*_{TR}$
b_{bw}

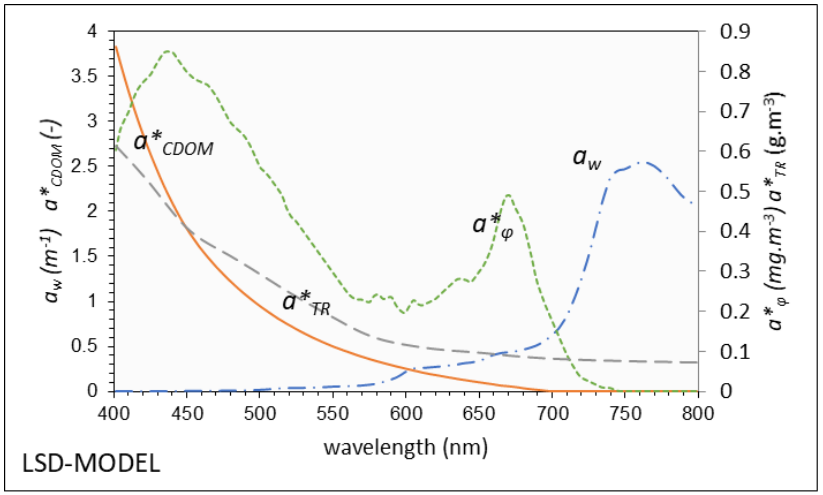
a_w (m^{-1}) a^*_{CDOM} (-)
a^*_{φ} ($mg.m^{-3}$) a^*_{TR} ($g.m^{-3}$)
a^*_{CDOM}
a^*_{TR}
a^*_{φ}
a_w
wavelength (nm)
LSD-MODEL

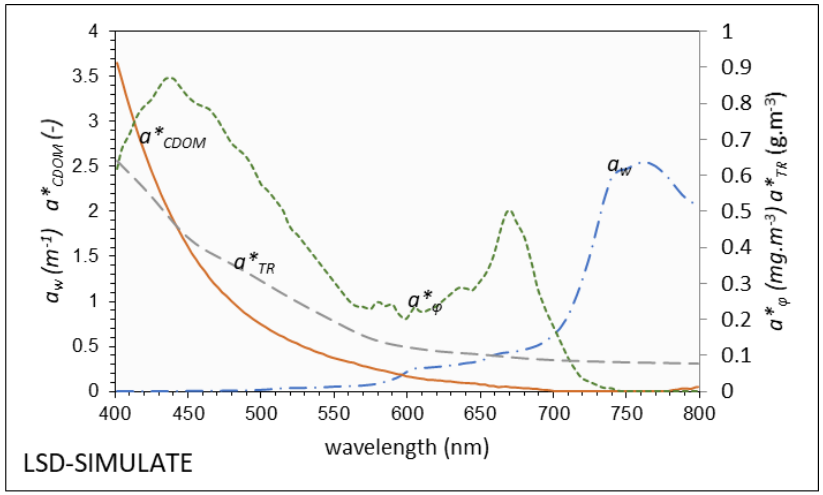
a_w (m^{-1}) a^*_{CDOM} (-)
a^*_{φ} ($mg.m^{-3}$) a^*_{TR} ($g.m^{-3}$)
a^*_{CDOM}
a^*_{TR}
a^*_{φ}
a_w
wavelength (nm)
LSD-SIMULATE

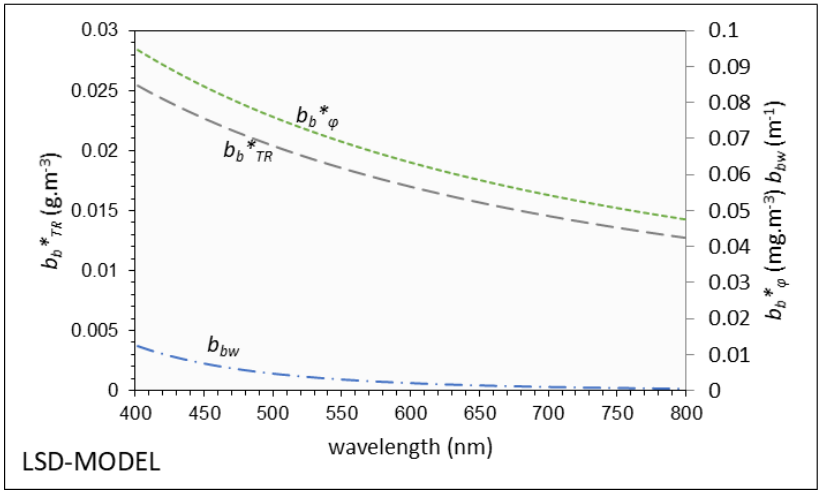
$b_b{}^*_{TR}$ ($g.m^{-3}$)
$b_b{}^*_{\varphi}$ ($mg.m^{-3}$) b_{bw} (m^{-1})
$b_b{}^*_{\varphi}$
$b_b{}^*_{TR}$
b_{bw}
wavelength (nm)
LSD-MODEL

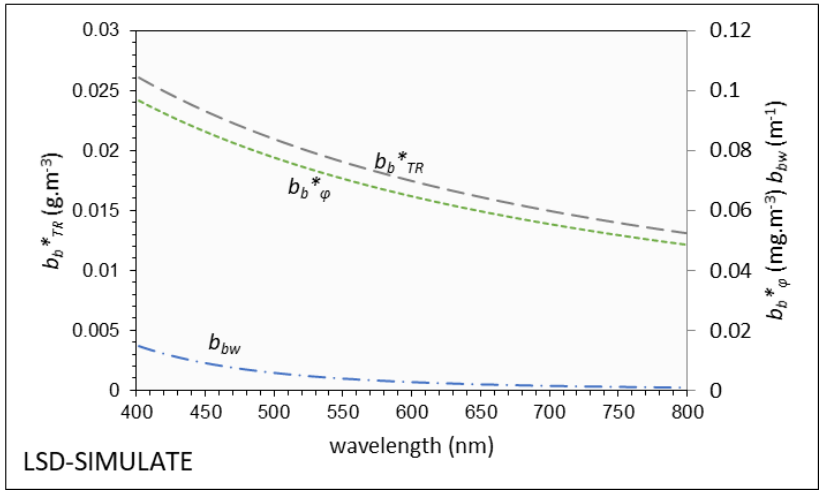
$b_b{}^*_{TR}$ ($g.m^{-3}$)
$b_b{}^*_{\varphi}$ ($mg.m^{-3}$) b_{bw} (m^{-1})
$b_b{}^*_{TR}$
$b_b{}^*_{\varphi}$
b_{bw}
wavelength (nm)
LSD-SIMULATE

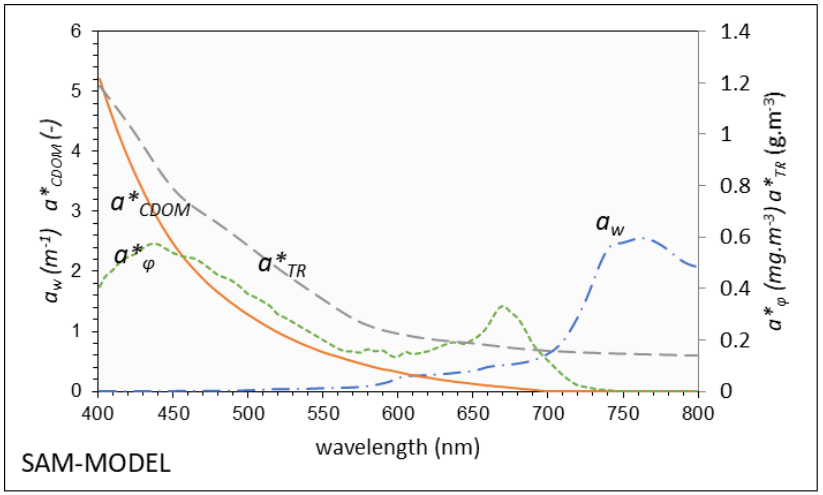
a_w (m^{-1}) a^*_{CDOM} (-)
a^*_{φ} ($mg.m^{-3}$) a^*_{TR} ($g.m^{-3}$)
a^*_{CDOM}
a^*_{φ}
a^*_{TR}
a_w
wavelength (nm)
SAM-MODEL

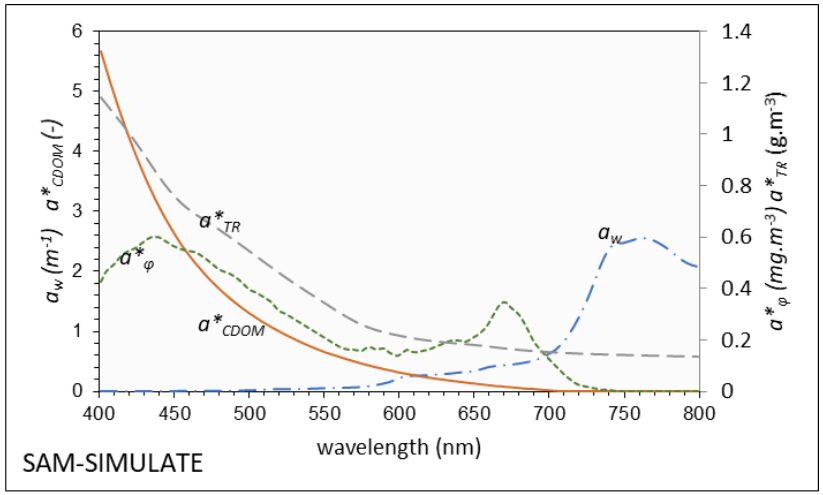
a_w (m^{-1}) a^*_{CDOM} (-)
a^*_{φ} ($mg.m^{-3}$) a^*_{TR} ($g.m^{-3}$)
a^*_{TR}
a^*_{φ}
a^*_{CDOM}
a_w
wavelength (nm)
SAM-SIMULATE

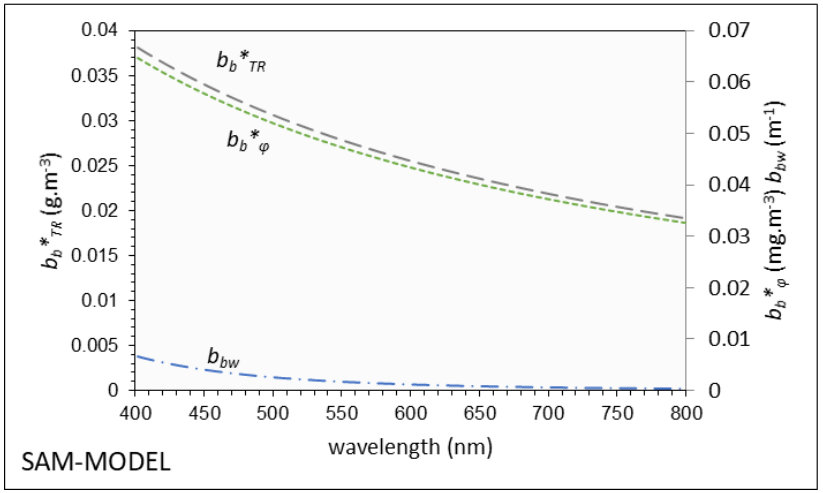
$b_b{}^*_{TR}$ ($g.m^{-3}$) b_{bw} (m^{-1})
$b_b{}^*_{\varphi}$ ($mg.m^{-3}$) b_{bw} (m^{-1})
$b_b{}^*_{TR}$
$b_b{}^*_{\varphi}$
b_{bw}
wavelength (nm)
SAM-MODEL

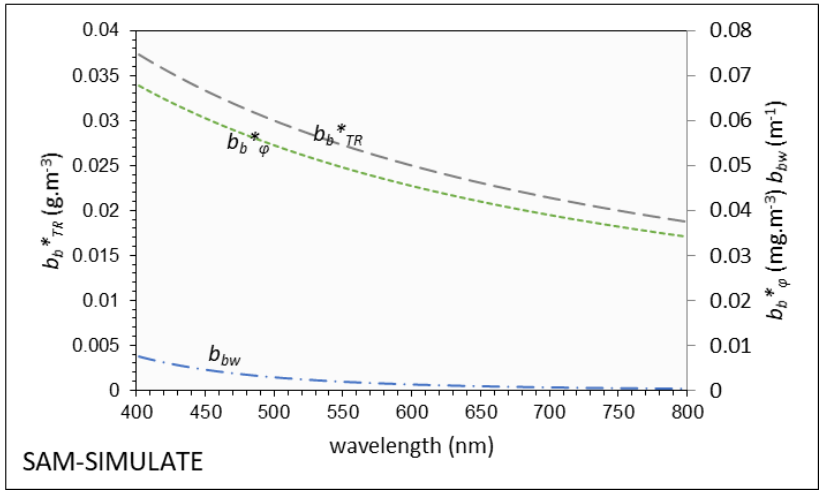
$b_b{}^*_{TR}$ ($g.m^{-3}$) b_{bw} (m^{-1})
$b_b{}^*_{\varphi}$ ($mg.m^{-3}$) b_{bw} (m^{-1})
$b_b{}^*_{\varphi}$
$b_b{}^*_{TR}$
b_{bw}
wavelength (nm)
SAM-SIMULATE

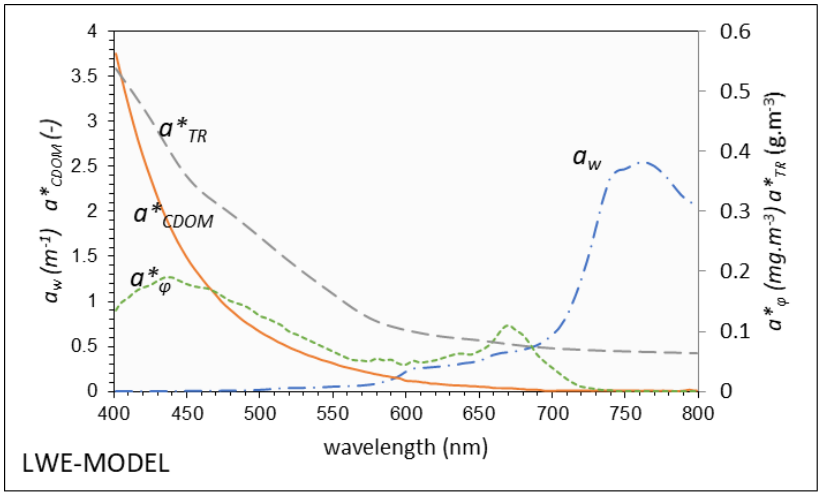
LWE-MODEL
wavelength (nm)
a_w (m^{-1}) a^*_{CDOM} (-)
a^*_φ ($mg.m^{-3}$) a^*_{TR} ($g.m^{-3}$)
a^*_{TR}
a^*_{CDOM}
a^*_φ
a_w

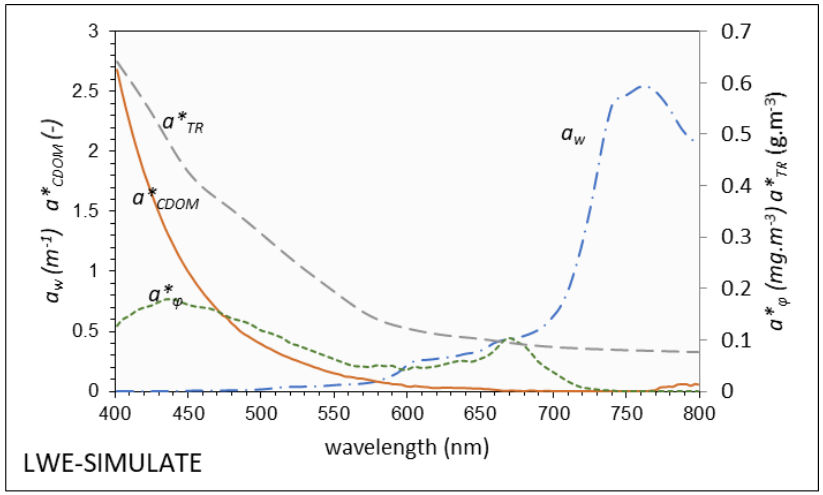
LWE-SIMULATE
wavelength (nm)
a_w (m^{-1}) a^*_{CDOM} (-)
a^*_φ ($mg.m^{-3}$) a^*_{TR} ($g.m^{-3}$)
a^*_{TR}
a^*_{CDOM}
a^*_φ
a_w

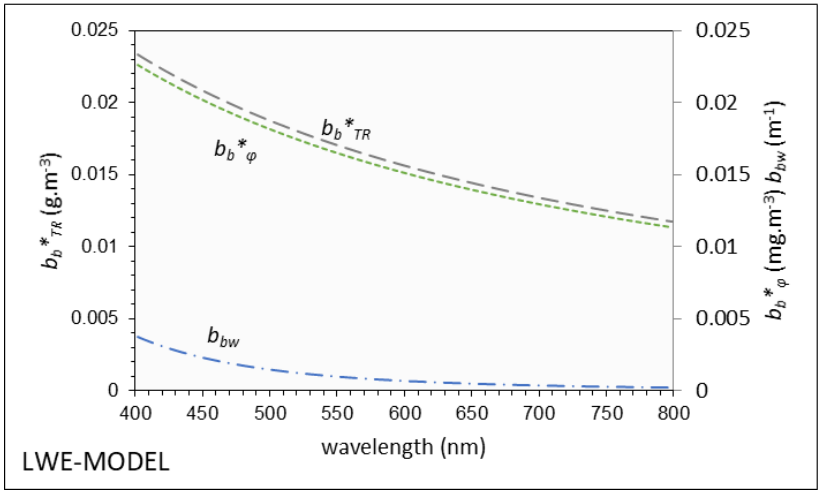
LWE-MODEL
wavelength (nm)
$b_b{}^*_{TR}$ ($g.m^{-3}$) b_{bw} (m^{-1})
$b_b{}^*_\varphi$ ($mg.m^{-3}$) b_{bw} (m^{-1})
$b_b{}^*_{TR}$
$b_b{}^*_\varphi$
b_{bw}

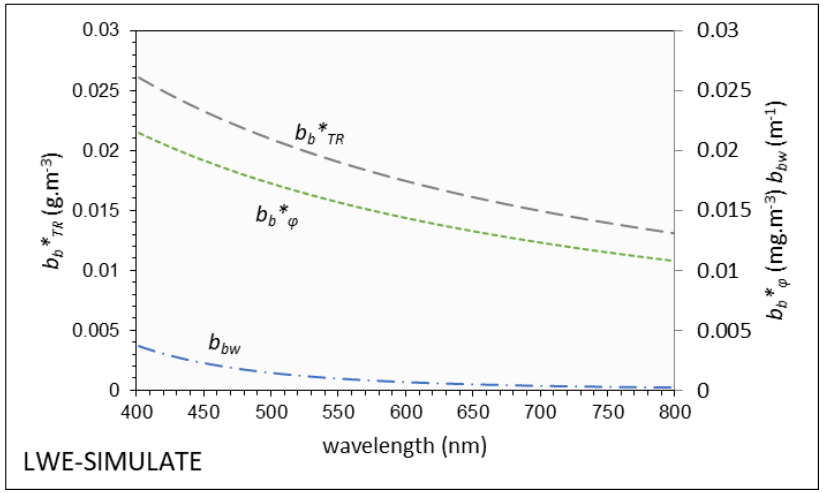
LWE-SIMULATE
wavelength (nm)
$b_b{}^*_{TR}$ ($g.m^{-3}$) b_{bw} (m^{-1})
$b_b{}^*_\varphi$ ($mg.m^{-3}$) b_{bw} (m^{-1})
$b_b{}^*_{TR}$
$b_b{}^*_\varphi$
b_{bw}

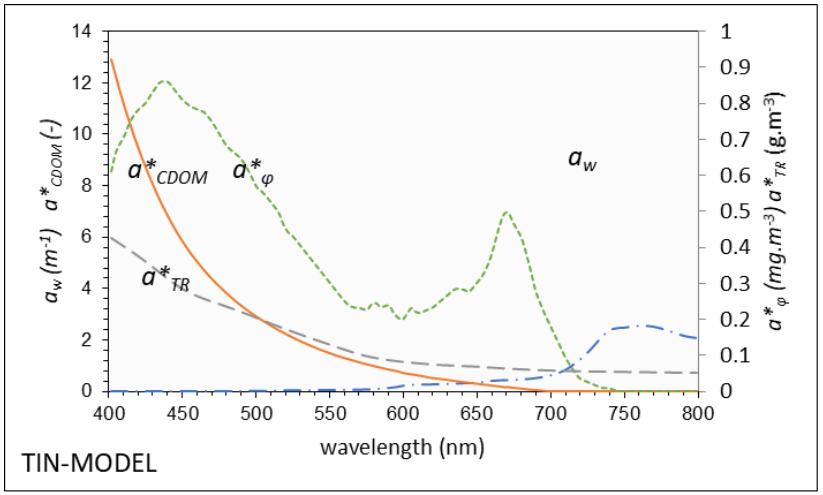
a_w (m^{-1}) a^*_{CDOM} (-)
a^*_{φ} ($mg.m^{-3}$) a^*_{TR} ($g.m^{-3}$)
a^*_{CDOM}
a^*_{φ}
a_w
a^*_{TR}
wavelength (nm)
TIN-MODEL

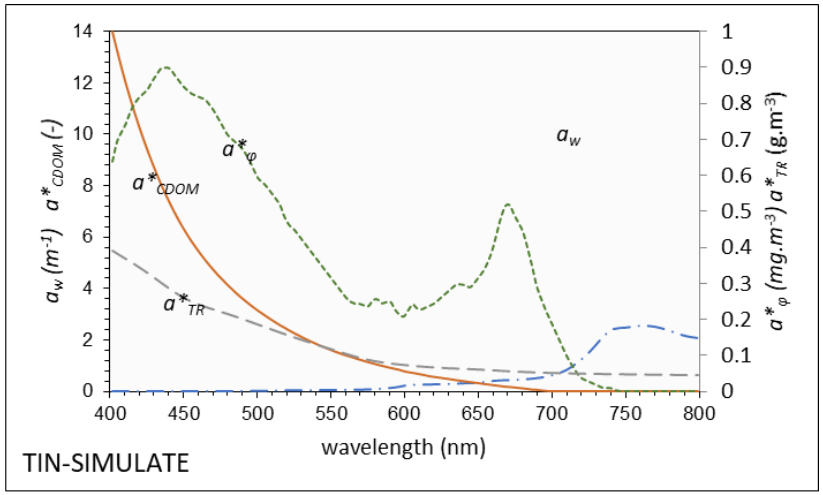
a_w (m^{-1}) a^*_{CDOM} (-)
a^*_{φ} ($mg.m^{-3}$) a^*_{TR} ($g.m^{-3}$)
a^*_{φ}
a^*_{CDOM}
a_w
a^*_{TR}
wavelength (nm)
TIN-SIMULATE

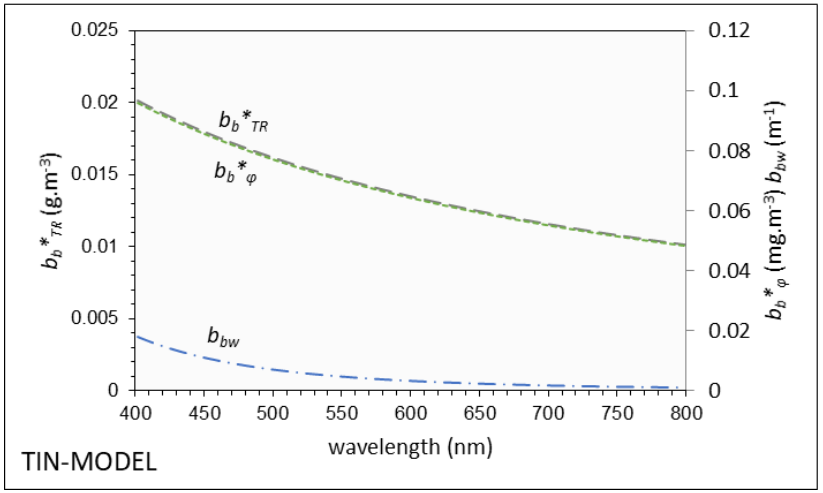
$b_b{}^*_{TR}$ ($g.m^{-3}$) $b_b{}^*_{\varphi}$ ($mg.m^{-3}$) b_{bw} (m^{-1})
$b_b{}^*_{TR}$
$b_b{}^*_{\varphi}$
b_{bw}
wavelength (nm)
TIN-MODEL

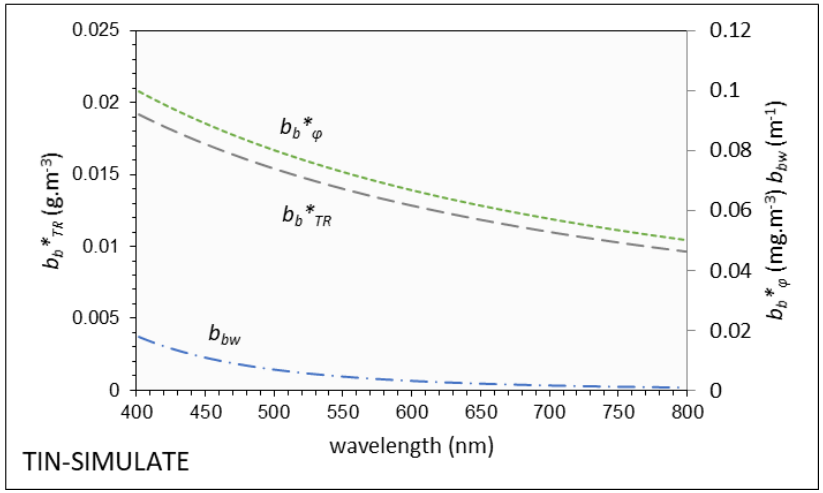
$b_b{}^*_{TR}$ ($g.m^{-3}$) $b_b{}^*_{\varphi}$ ($mg.m^{-3}$) b_{bw} (m^{-1})
$b_b{}^*_{\varphi}$
$b_b{}^*_{TR}$
b_{bw}
wavelength (nm)
TIN-SIMULATE

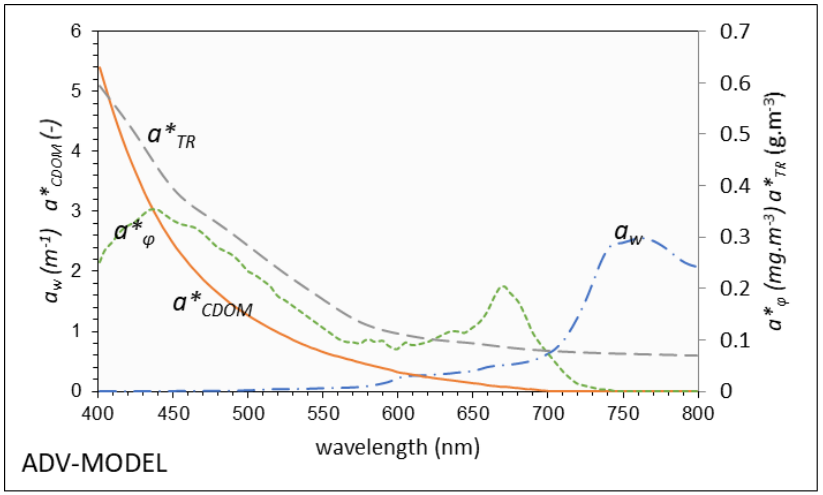
ADV-MODEL
wavelength (nm)
a_w (m^{-1}) a^*_{CDOM} (-)
a^*_{φ} ($mg.m^{-3}$) a^*_{TR} ($g.m^{-3}$)
a^*_{TR}
a^*_{φ}
a^*_{CDOM}
a_w

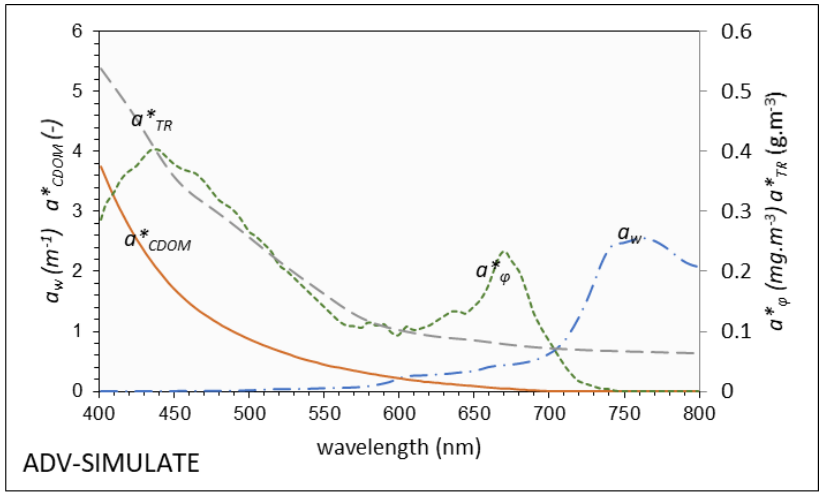
ADV-SIMULATE
wavelength (nm)
a_w (m^{-1}) a^*_{CDOM} (-)
a^*_{φ} ($mg.m^{-3}$) a^*_{TR} ($g.m^{-3}$)
a^*_{TR}
a^*_{CDOM}
a^*_{φ}
a_w

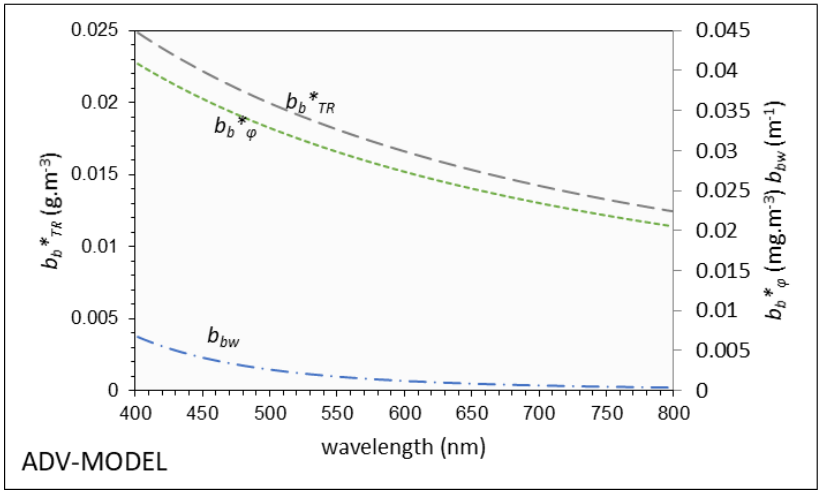
ADV-MODEL
wavelength (nm)
$b_b{}^*_{TR}$ ($g.m^{-3}$) b_{bw} (m^{-1})
$b_b{}^*_{\varphi}$ ($mg.m^{-3}$) b_{bw} (m^{-1})
$b_b{}^*_{TR}$
$b_b{}^*_{\varphi}$
b_{bw}

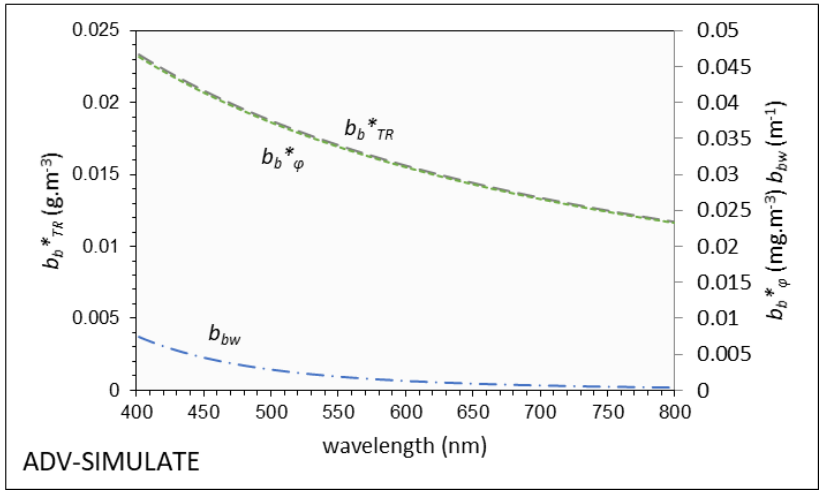
ADV-SIMULATE
wavelength (nm)
$b_b{}^*_{TR}$ ($g.m^{-3}$) b_{bw} (m^{-1})
$b_b{}^*_{\varphi}$ ($mg.m^{-3}$) b_{bw} (m^{-1})
$b_b{}^*_{TR}$
$b_b{}^*_{\varphi}$
b_{bw}

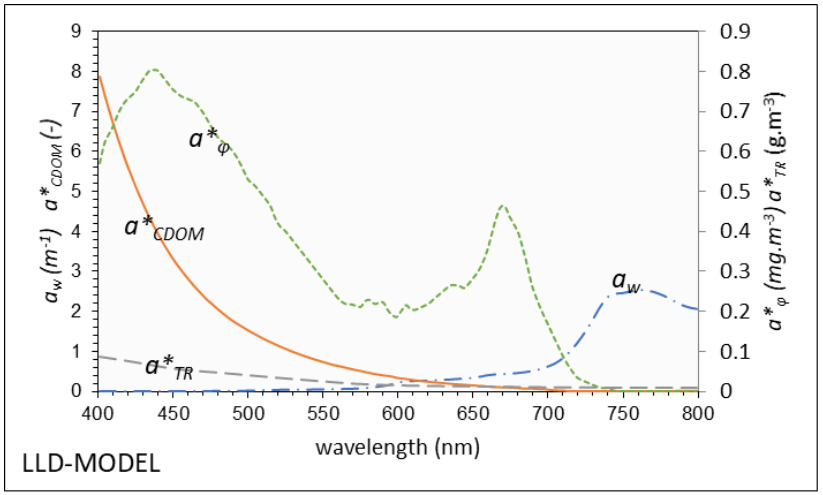
LLD-MODEL
wavelength (nm)
a_w (m^{-1}) a^*_{CDOM} (-)
a^*_{φ} ($mg.m^{-3}$) a^*_{TR} ($g.m^{-3}$)
a^*_{φ}
a^*_{CDOM}
a_w
a^*_{TR}

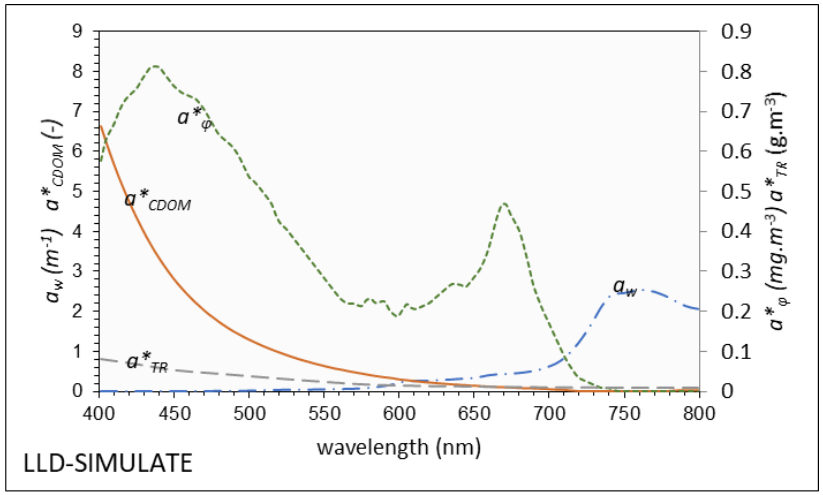
LLD-SIMULATE
wavelength (nm)
a_w (m^{-1}) a^*_{CDOM} (-)
a^*_{φ} ($mg.m^{-3}$) a^*_{TR} ($g.m^{-3}$)
a^*_{φ}
a^*_{CDOM}
a_w
a^*_{TR}

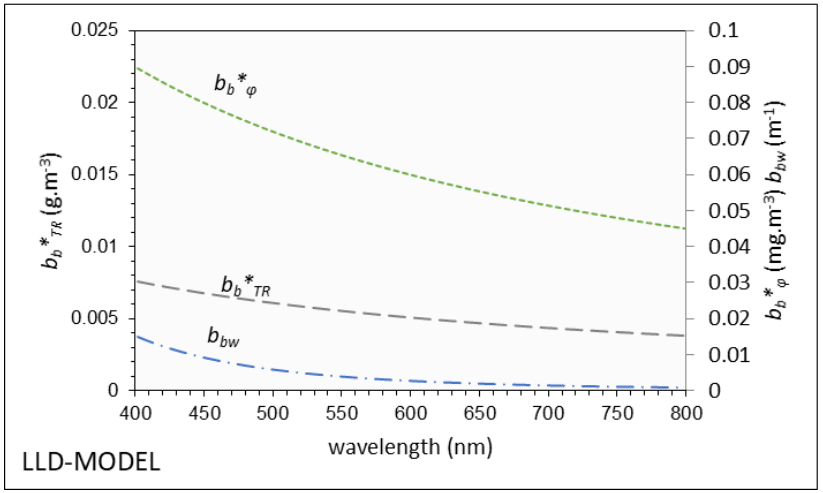
LLD-MODEL
wavelength (nm)
$b_b{}^*_{TR}$ ($g.m^{-3}$) b_{bw} (m^{-1})
$b_b{}^*_{\varphi}$ ($mg.m^{-3}$) b_{bw} (m^{-1})
$b_b{}^*_{\varphi}$
$b_b{}^*_{TR}$
b_{bw}

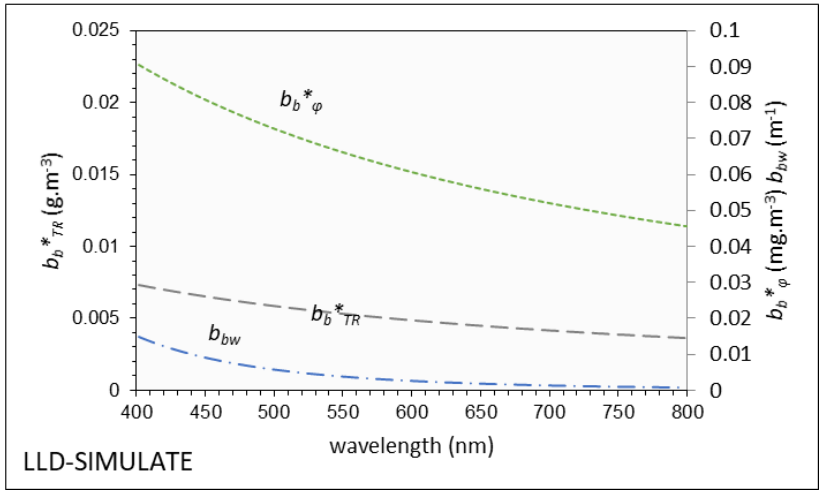
LLD-SIMULATE
wavelength (nm)
$b_b{}^*_{TR}$ ($g.m^{-3}$) b_{bw} (m^{-1})
$b_b{}^*_{\varphi}$ ($mg.m^{-3}$) b_{bw} (m^{-1})
$b_b{}^*_{\varphi}$
$b_b{}^*_{TR}$
b_{bw}

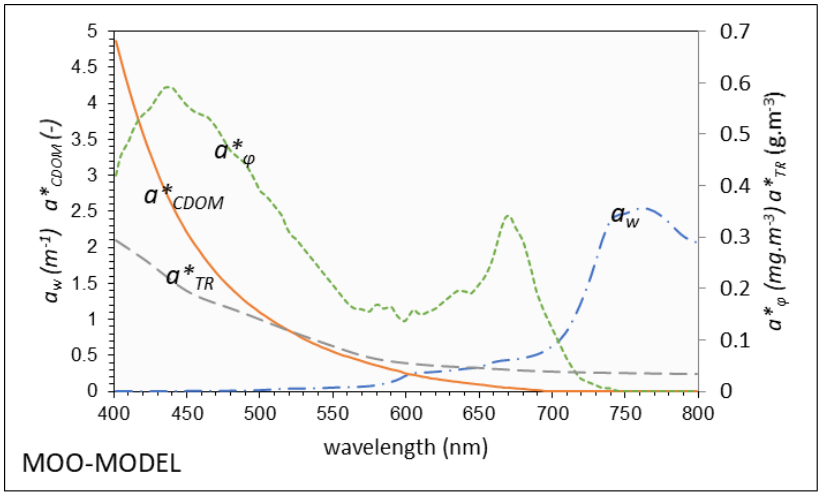
a_w (m^{-1}) a^*_{CDOM} (-)
a^*_{φ} ($mg.m^{-3}$) a^*_{TR} ($g.m^{-3}$)
a^*_{φ}
a^*_{CDOM}
a^*_{TR}
a_w
wavelength (nm)
MOO-MODEL

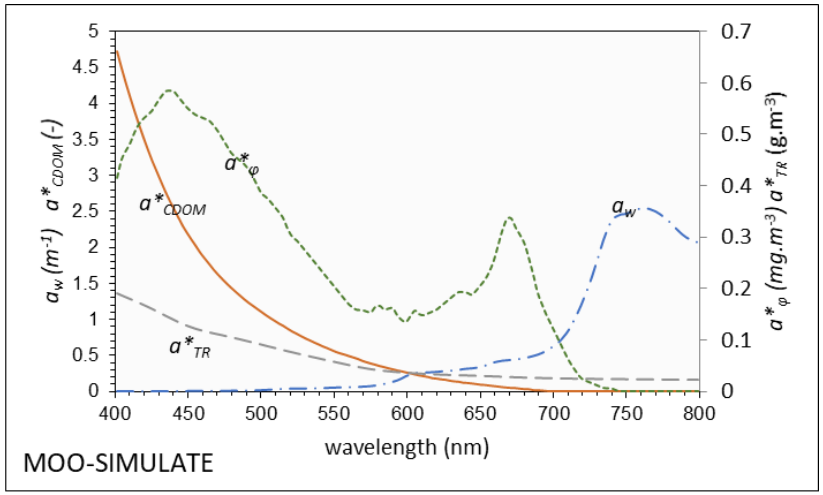
a_w (m^{-1}) a^*_{CDOM} (-)
a^*_{φ} ($mg.m^{-3}$) a^*_{TR} ($g.m^{-3}$)
a^*_{φ}
a^*_{CDOM}
a^*_{TR}
a_w
wavelength (nm)
MOO-SIMULATE

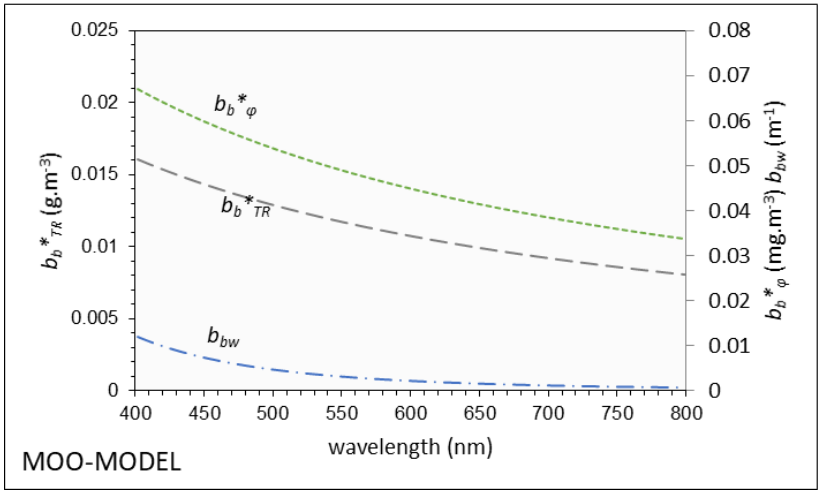
$b_b{}^*_{TR}$ ($g.m^{-3}$)
$b_b{}^*_{\varphi}$ ($mg.m^{-3}$) b_{bw} (m^{-1})
$b_b{}^*_{\varphi}$
$b_b{}^*_{TR}$
b_{bw}
wavelength (nm)
MOO-MODEL

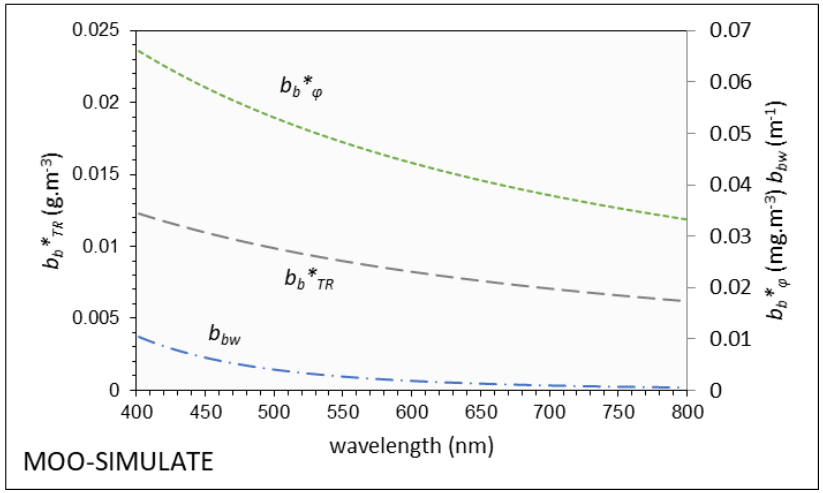
$b_b{}^*_{TR}$ ($g.m^{-3}$)
$b_b{}^*_{\varphi}$ ($mg.m^{-3}$) b_{bw} (m^{-1})
$b_b{}^*_{\varphi}$
$b_b{}^*_{TR}$
b_{bw}
wavelength (nm)
MOO-SIMULATE

Appendix (B) - The laboratory analysis results for measuring the absorption spectrum curves to the six isolated fractions and their total absorption curves within selected wavelengths from 350 nm to 700 nm.

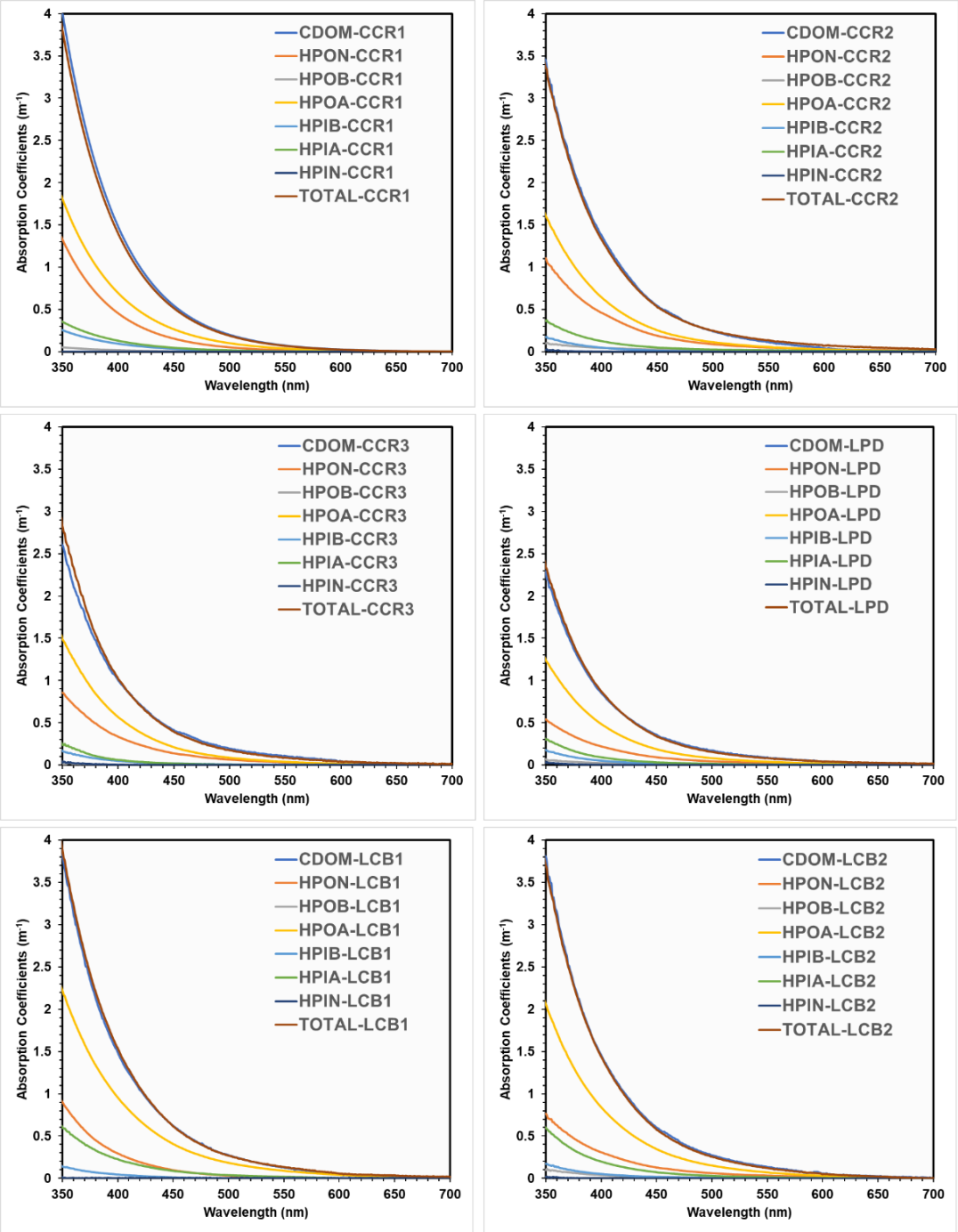

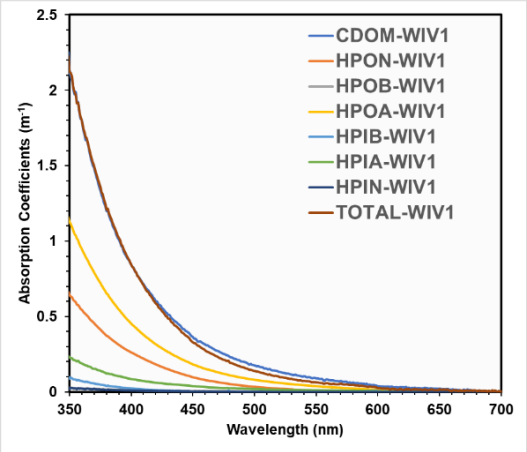
CDOM-WIV1
HPON-WIV1
HPOB-WIV1
HPOA-WIV1
HPIB-WIV1
HPIA-WIV1
HPIN-WIV1
TOTAL-WIV1
Absorption Coefficients (m-1)
Wavelength (nm)

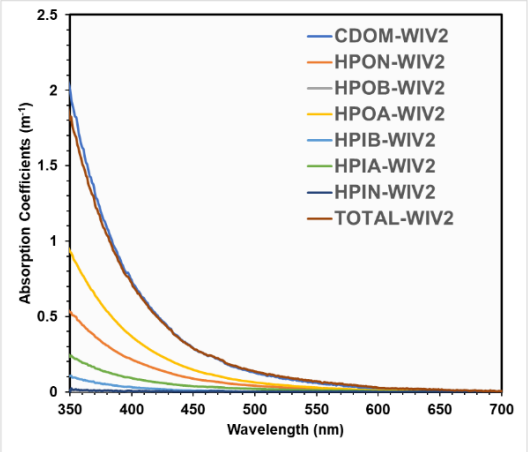
CDOM-WIV2
HPON-WIV2
HPOB-WIV2
HPOA-WIV2
HPIB-WIV2
HPIA-WIV2
HPIN-WIV2
TOTAL-WIV2
Absorption Coefficients (m-1)
Wavelength (nm)

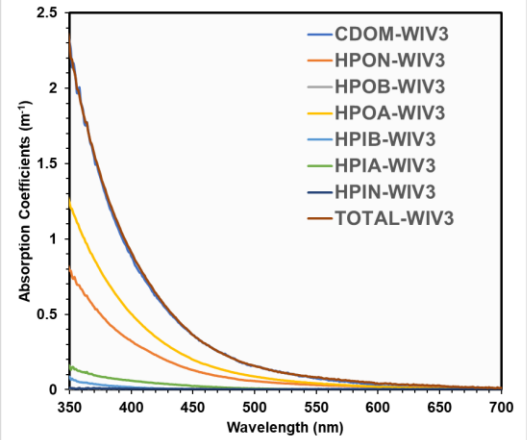
CDOM-WIV3
HPON-WIV3
HPOB-WIV3
HPOA-WIV3
HPIB-WIV3
HPIA-WIV3
HPIN-WIV3
TOTAL-WIV3
Absorption Coefficients (m-1)
Wavelength (nm)

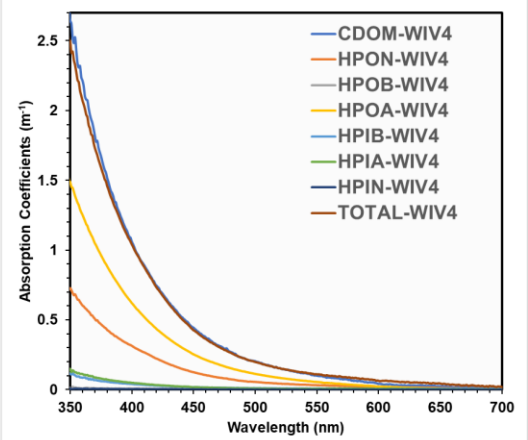
CDOM-WIV4
HPON-WIV4
HPOB-WIV4
HPOA-WIV4
HPIB-WIV4
HPIA-WIV4
HPIN-WIV4
TOTAL-WIV4
Absorption Coefficients (m-1)
Wavelength (nm)

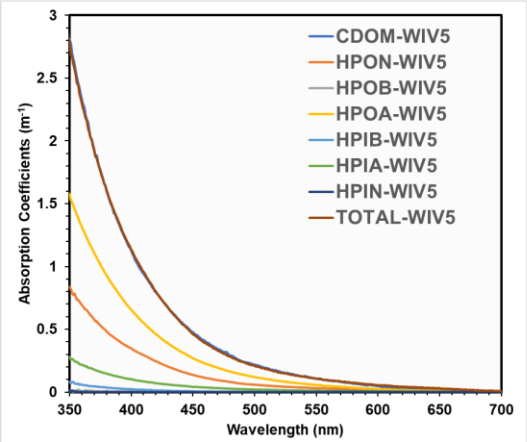
CDOM-WIV5
HPON-WIV5
HPOB-WIV5
HPOA-WIV5
HPIB-WIV5
HPIA-WIV5
HPIN-WIV5
TOTAL-WIV5
Absorption Coefficients (m-1)
Wavelength (nm)

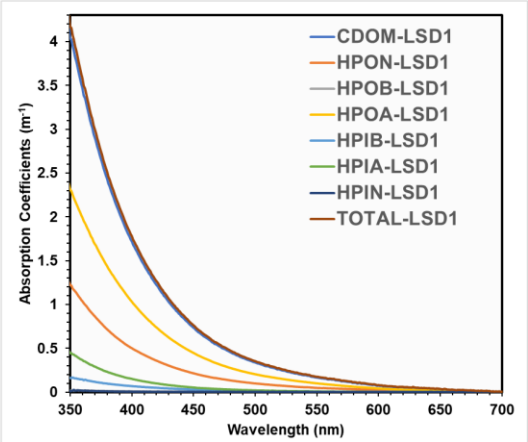
CDOM-LSD1
HPON-LSD1
HPOB-LSD1
HPOA-LSD1
HPIB-LSD1
HPIA-LSD1
HPIN-LSD1
TOTAL-LSD1
Absorption Coefficients (m-1)
Wavelength (nm)

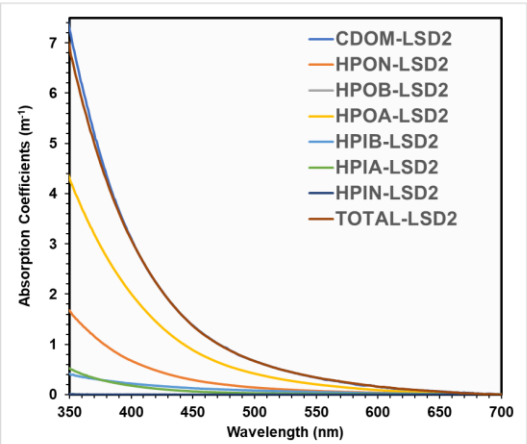
CDOM-LSD2
HPON-LSD2
HPOB-LSD2
HPOA-LSD2
HPIB-LSD2
HPIA-LSD2
HPIN-LSD2
TOTAL-LSD2
Absorption Coefficients (m-1)
Wavelength (nm)

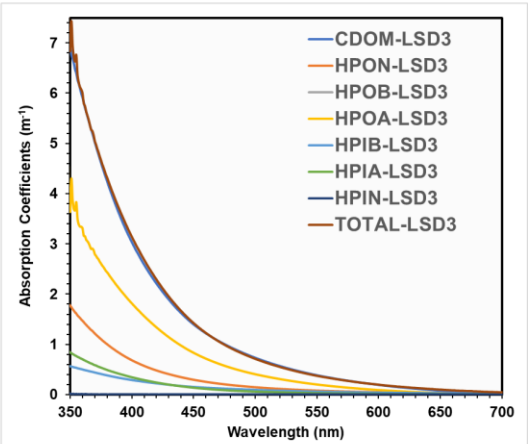
CDOM-LSD3
HPON-LSD3
HPOB-LSD3
HPOA-LSD3
HPIB-LSD3
HPIA-LSD3
HPIN-LSD3
TOTAL-LSD3
Absorption Coefficients (m-1)
Wavelength (nm)

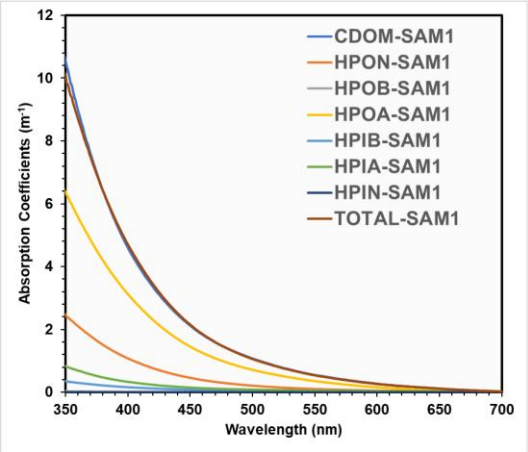
CDOM-SAM1
HPON-SAM1
HPOB-SAM1
HPOA-SAM1
HPIB-SAM1
HPIA-SAM1
HPIN-SAM1
TOTAL-SAM1
Absorption Coefficients (m-1)
Wavelength (nm)

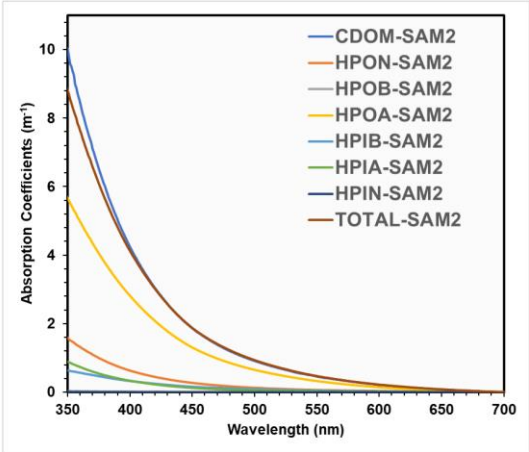
CDOM-SAM2
HPON-SAM2
HPOB-SAM2
HPOA-SAM2
HPIB-SAM2
HPIA-SAM2
HPIN-SAM2
TOTAL-SAM2
Absorption Coefficients (m-1)
Wavelength (nm)

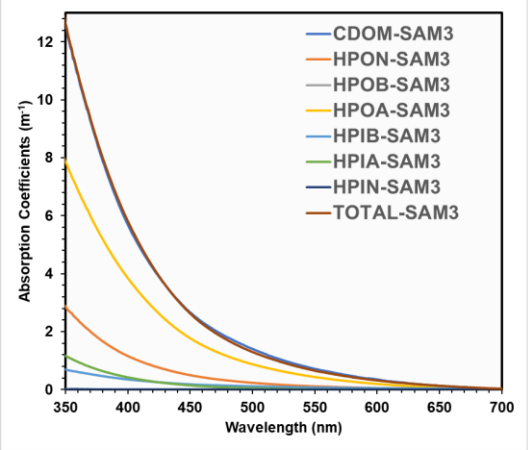
CDOM-SAM3
HPON-SAM3
HPOB-SAM3
HPOA-SAM3
HPIB-SAM3
HPIA-SAM3
HPIN-SAM3
TOTAL-SAM3
Absorption Coefficients (m-1)
Wavelength (nm)

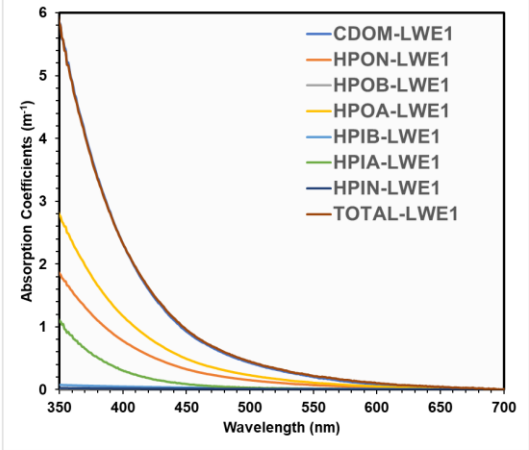
CDOM-LWE1
HPON-LWE1
HPOB-LWE1
HPOA-LWE1
HPIB-LWE1
HPIA-LWE1
HPIN-LWE1
TOTAL-LWE1
Absorption Coefficients (m-1)
Wavelength (nm)

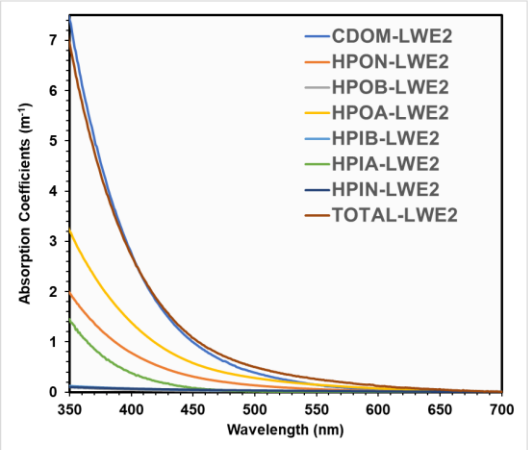
CDOM-LWE2
HPON-LWE2
HPOB-LWE2
HPOA-LWE2
HPIB-LWE2
HPIA-LWE2
HPIN-LWE2
TOTAL-LWE2
Absorption Coefficients (m-1)
Wavelength (nm)

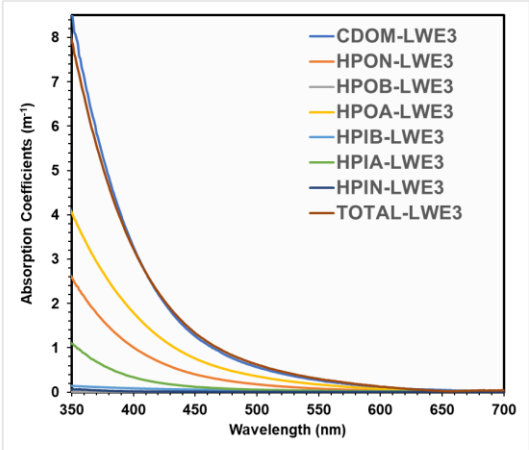
CDOM-LWE3
HPON-LWE3
HPOB-LWE3
HPOA-LWE3
HPIB-LWE3
HPIA-LWE3
HPIN-LWE3
TOTAL-LWE3
Absorption Coefficients (m-1)
Wavelength (nm)

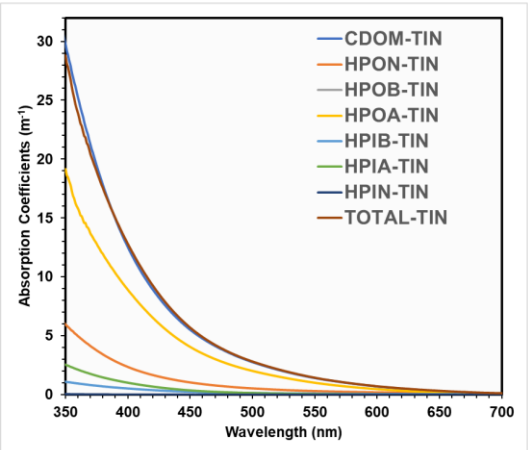
CDOM-TIN
HPON-TIN
HPOB-TIN
HPOA-TIN
HPIB-TIN
HPIA-TIN
HPIN-TIN
TOTAL-TIN
Absorption Coefficients (m-1)
Wavelength (nm)

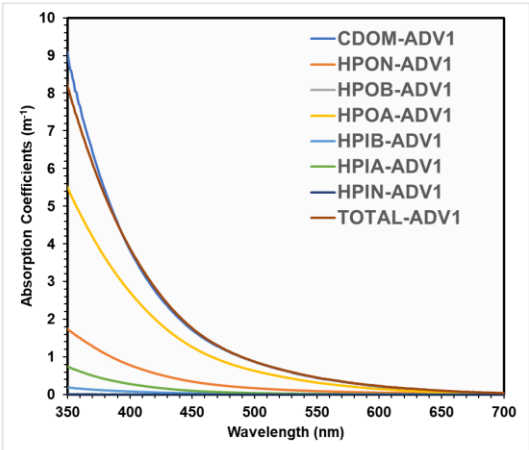
CDOM-ADV1
HPON-ADV1
HPOB-ADV1
HPOA-ADV1
HPIB-ADV1
HPIA-ADV1
HPIN-ADV1
TOTAL-ADV1
Absorption Coefficients (m-1)
Wavelength (nm)

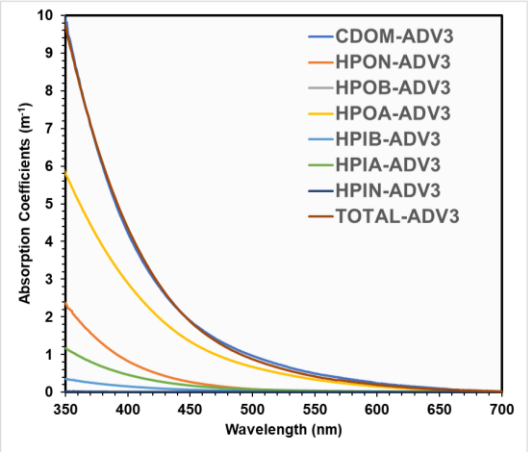
Absorption Coefficients (m-1)
Wavelength (nm)
CDOM-ADV3
HPON-ADV3
HPOB-ADV3
HPOA-ADV3
HPIB-ADV3
HPIA-ADV3
HPIN-ADV3
TOTAL-ADV3

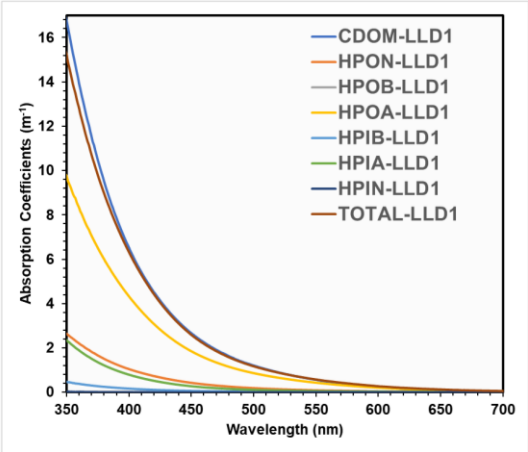
Absorption Coefficients (m-1)
Wavelength (nm)
CDOM-LLD1
HPON-LLD1
HPOB-LLD1
HPOA-LLD1
HPIB-LLD1
HPIA-LLD1
HPIN-LLD1
TOTAL-LLD1

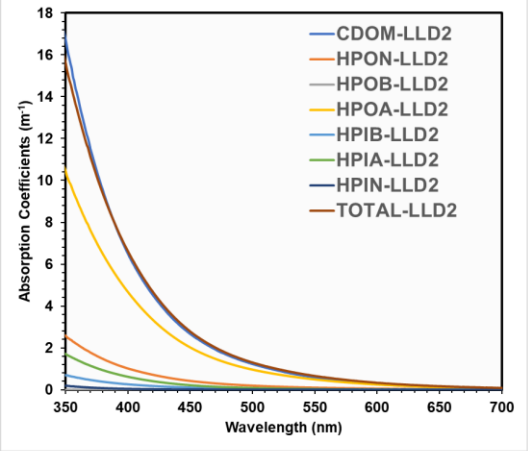
Absorption Coefficients (m-1)
Wavelength (nm)
CDOM-LLD2
HPON-LLD2
HPOB-LLD2
HPOA-LLD2
HPIB-LLD2
HPIA-LLD2
HPIN-LLD2
TOTAL-LLD2

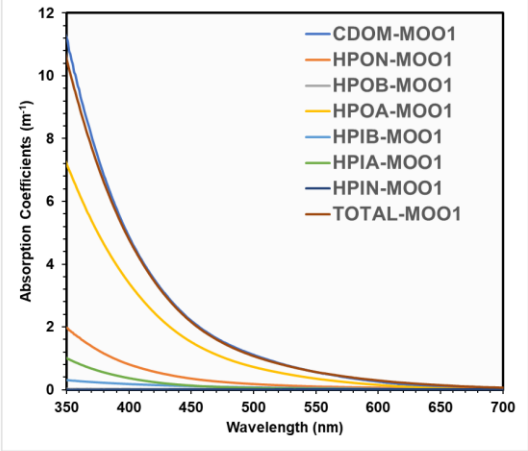
Absorption Coefficients (m-1)
Wavelength (nm)
CDOM-MOO1
HPON-MOO1
HPOB-MOO1
HPOA-MOO1
HPIB-MOO1
HPIA-MOO1
HPIN-MOO1
TOTAL-MOO1

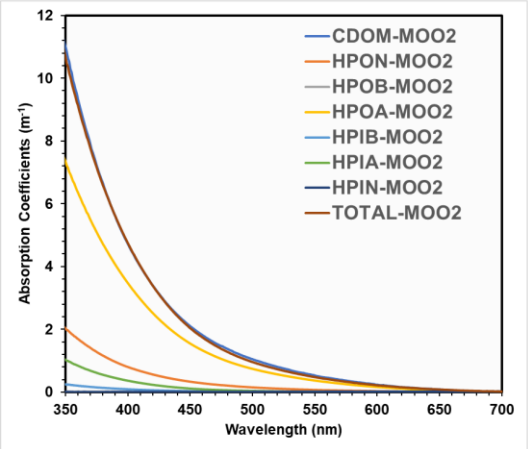
Absorption Coefficients (m-1)
Wavelength (nm)
CDOM-MOO2
HPON-MOO2
HPOB-MOO2
HPOA-MOO2
HPIB-MOO2
HPIA-MOO2
HPIN-MOO2
TOTAL-MOO2

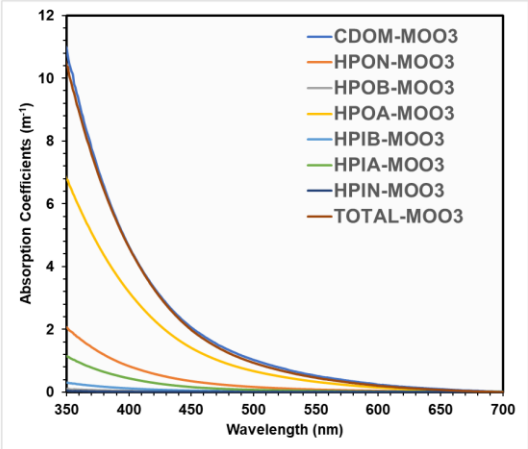
Absorption Coefficients (m-1)
Wavelength (nm)
CDOM-MOO3
HPON-MOO3
HPOB-MOO3
HPOA-MOO3
HPIB-MOO3
HPIA-MOO3
HPIN-MOO3
TOTAL-MOO3